Unflattened Radiotherapy beams; characterisation, optimisation and application

David John Paynter

Submitted in accordance with the requirements for the degree of
Doctor of Philosophy

The University of Leeds
School of Medicine

December 2019

The candidate confirms that the work submitted is his own, except where work which has formed part of jointly-authored publications has been included. The contribution of the candidate and the other authors to this work has been explicitly indicated below. The candidate confirms that appropriate credit has been given within the thesis where reference has been made to the work of others.

The work in Chapter 3 the thesis has appeared in publication as follows:
Beam characteristics of energy-matched flattening filter free beams. *Medical Physics.* **41**(5). Paynter, D., Weston, S.J., Cosgrove, V.P., Evans, J.A. and Thwaites, D.I. 2014.

I was responsible for the collecting and analysing of the data and writing of the text.
The contribution of the other authors was that of a normal student supervisor relationship.
Full copyright clearance has been produced for the publication of this work in the thesis.
License number 4638660107461.

The work in Chapter 4 of the thesis has appeared in publication as follows:
Characterisation of flattening filter free (FFF) beam properties for initial beam set-up and routine QA, independent of flattened beams. *Phys Med Biol.* **63**(1), p015021. Paynter, D., Weston, S.J., Cosgrove, V.P. and Thwaites, D.I. 2017.

I was responsible for the collecting and analysing of the data and writing of the text.
The contribution of the other authors was that of a normal student supervisor relationship.

This research was performed in accordance with ethical principles that have their origin in the Declaration of Helsinki and is consistent with the International Conference on Harmonization (ICH)/Good Clinical Practice (GCP) guidelines. The work was performed as part of service development and therefore did not require ethics approval.

The technical specifications of the linear accelerator used to produce the Monte Carlo model in chapter are subject to a Non-Disclosure Agreement with Elekta Instrument AB Stockholm. In order for the work to be reproduced the investigator would be required to contact the above party to obtain technical specifications.

Table of Contents

Acknowledgements 7
Abstract 8
List of Abbreviations 9
List of Tables 11
List of Figures 12
1. Introduction 1
1.1. Overview of Radiotherapy 1
1.2. Linear accelerator design 1
1.2.1. FFF implementations 5
1.3. Clinical aims of radiotherapy 5
1.4. Intensity Modulated Radiotherapy 6
1.5. Monte Carlo simulation 6
1.6. Scope of Work 7
1.6.1. Cyberknife and Tomotherapy 8
2. Literature review 9
2.1. Second Cancer induction following radiotherapy 12
2.2. Monte Carlo studies on FFF Linacs 14
2.2.1. Beam Quality 14
2.2.2. Beam Penumbra 15
2.2.3. FFF with Varian Linacs 16
2.2.4. Out of field dose and radiation protection considerations 18
2.3. Empirical measurements on FFF Linacs 20
2.3.1. Varian accelerators 20
2.3.2. Elekta Accelerators 22
2.3.3. MV portal imaging with FFF 25
2.4. Treatment planning studies on FFF Linacs 26
2.4.1. Treatment planning system benchmarking 26
2.4.2. Head and Neck planning studies 27
2.4.3. Prostate planning studies 30
2.4.4. Stereotactic Ablative Radiotherapy planning studies 31
2.4.5. Treatment planning studies on other sites 35

2.4.6. Summary of treatment planning study findings 36
2.5. Guidelines for FFF beams 36
2.6. Summary of findings 37
3. Characteristics of FFF beams 39
3.1. Introduction 39
3.2. Method 40
3.2.1. Implementation 40
3.2.2. Profiles and PDDs 41
3.2.3. Output Factors 42
3.2.4. Head leakage 42
3.2.5. Radiation Protection 44
3.3. Results 45
3.3.1. Profiles 45
3.3.2. PDDs 50
3.3.3. Output Factors 52
3.3.5. Head leakage 54
3.3.6. Radiation Protection 54
3.4. Discussion 56
3.5. Conclusion 59
4. Characterisation of FFF beam properties for initial beam set-up and routine QA, independent of Flattened Beams 61
4.1. Introduction 61
4.2. Method 62
4.3. Results 63
4.3.1. Profile symmetry 63
4.3.2. Profile flatness 65
4.3.3. Beam energy 66
4.3.5. Penumbra 68
4.3.6. Field size 69
4.4. Discussion 69
4.5. Conclusion 72
5. Monte Carlo modelling of an FFF Linac with energy matching 73
5.1. Introduction 73
5.2. Producing the MC model 73

5.2.1. Measured data 73
5.2.2. Geometry 74
5.2.4. PDD and profile calculation 77
5.2.5. Benchmarking 77
5.2.6. Electron beam characteristics 77
5.2.7. Field size calibration 78
5.3. Results 79
5.3.1. Electron beam characteristics 79
5.3.2. Field size calibration 82
5.3.3. Benchmarking 85
5.4. Discussion 99
5.5. Conclusion 101
6. Pre-Clinical evaluation of matched FFF treatments on Elekta Linacs 103
6.1. Introduction 103
6.2. FFF beams for hypofractionated SABR treatments for lung and other sites 103
6.2.1. SABR lung fractionations 103
6.2.2. Method 103
6.2.3. Results 107
6.2.4. Discussion 120
6.3. Standard fractionated treatments 126
6.3.1. Head and Neck 2Gy/# 126
6.4. Conclusion 131
7. Summary and future work 133
8. References 137
Appendix A 147
Appendix B 148
Appendix C 149

Acknowledgements

I would like to thank my wife Samantha for the support and encouragement she has given me during this project. I would also like to thank my supervisory team David Thwaites, Vivian Cosgrove, Steven Weston, Tony Evans and Steven Sourbron for their support and assistance in completing this work. Finally I would like to thank everyone in the Leeds Teaching Hospitals radiotherapy department in helping to facilitate the completion of this project.

Abstract

The goal of this thesis was to investigate flattening filter free (FFF) beams produced by medical linear accelerators for radiotherapy applications, from their initial setup through to their clinical implementation. This was split into four sections that comprise the main experimental chapters of this thesis. The characteristics of FFF beams both matched (by tuning beam quality to the equivalent cFF beam) and unmatched were compared to conventional flattening filter (cFF) beams. The characterisation of FFF beams highlighted inconsistencies with the current parameters used for the description and quality assurance (QA) of cFF beams. New methods suitable for the QA of both cFF and FFF beams were investigated and proposed. The use of Monte Carlo (MC) modelling was investigated to determine how to model an FFF beam and facilitate further investigations. Treatment planning studies were performed for lung stereotactic ablative radiotherapy (SABR), pelvic SABR and Head and Neck volumetric modulated arc therapy (VMAT). The planning work concluded that clinically acceptable plans were achievable through the use of FFF beams and provides a solid basis for clinical implementation. The work overall provides a comprehensive set of practical data and methods to support the use of FFF beams in clinical practice.

List of Abbreviations

3DCRT	3D Conformal Radiotherapy
AAA	Analytic Anisotropic Algorithm
AXB	Acuros XB
CAX	Central Axis
CTE	Commissioning Through Evaluation
cFF	Conventional Flattening Filter
Dmax	Depth of maximum dose
DVH	Dose Volume Histogram
EGS	Electron Gamma Shower
EPID	Electronic Portal Imaging Device
FFF	Flattening Filter Free
FSD	Focus to Surface Distance
FWHM	Full Width Half Maximum
GUI	Graphical User Interface
GTV	Gross Tumour Volume
HVL	Half Value Layer
H&N	Head and Neck
HDRM	High Dose Rate Mode
IMRT	Intensity Modulated Radiotherapy
LINAC	Linear Accelerator
MFFF	Matched Flattening Filter Free
MU	Monitor Unit
MLC	Multi Leaf Collimator
NTCP	Normal Tissue Complication Probability
OAR	Organ At Risk
PDD	Percentage Depth Dose
PTV	Planning Target Volume
QA	Quality Assurance
RMS	Route Mean Squared
RMSD	Route Mean Squared Deviation
SSD	Source to Surface Distance
SABR	Stereotactic Ablative Radiotherapy
TVL	Tenth Value Layer

TPR	Tissue Phantom Ratio
TPS	Treatment Planning System
TCP	Tumour Control Probability
UFFF	Unmatched Flattening Filter Free
VMAT	Volumetric Modulated Arc Therapy

List of Tables

Table 1: Potential advantages and disadvantages of FFF beams 38
Table 2: Bending magnet and gun current values for the beams studied 41
Table 3: Leakage measurements for 3 modes of operation, Flattening Filter (cFF), Unmatched Flattening Filter Free (UFFF) and Energy Matched Flattening Filter Free (MFFF), in patient and non patient planes (expressed as a % of an open 10cm x 10cm beam). 55
Table 4: Doserate survey results from around the FFF linear accelerator bunker for Flattening Filter (cFF), Unmatched Flattening Filter Free (UFFF) and Energy Matched Flattening Filter Free (MFFF) 56
Table 5: Relationship between beam energy, profile CAX and beam 'flatness' 66
Table 6: Measured difference in mm between inflection method and current 'gold standard' penumbra measurement methods for flat (cFF), unmatched flattening filter free (UFFF) and matched flattening filter free (MFFF) beams. 67
Table 7: Difference in calculated field size for 6MV unmatched Flattening filter Free (UFFF) and matched Flattening Filter free (MFFF) beams based on 50% field sizes following from the 55% inflection point method compared to measured 50% field size for cFF beam. 70
Table 8: The relationship between the focal spot size of the electron beam and the profile penumbra in the direction of the MLCs. 82
Table 9: The calibration for the jaw aperture size to match measured data at isocentre. 84
Table 10: The calibration for the MLC aperture size to match measured data at isocentre 85
Table 11: Description of conformality constraints for lung SABR treatments. 105
Table 12: Average results for the five patients planned for the FFF planning comparison. Stated VMAT delivery times are reported by the treatment planning system, 3DCRT times are delivery times as reported by the record and verify system. 107
Table 13: Average results for the three patients planned for the FFF planning comparison. Stated delivery times are reported by the treatment planning system. 110
Table 14: DVH prameters for 7 patients with PTV in close proximity to OARs, planned with FFFcompared to the parameters obtained using a 3DCRT technique with a cFF beam. Stated delivery times are reported by the treatment planning system. 115
Table 15: DVH parameters for 7 patients with metastatic disease in the pelvis planned with FFF SABR against the OAR constraints, including one patient with two PTVs to be treated concurrently 118
Table 16: DVH values obtained for two patients planned with both cFF and FFF beams. Patient 1 refers to a patient with the high dose region in close proximity to optical OARs, patient 2 refers to a patient with a large high dose region. Red text highlights OAR doses that exceed dosimetric aim. 130

List of Figures

Figure 1: Diagram of Elekta Linear accelerator. 2
Figure 2: Diagram of the effect of removing the flattening filter on the beam profile 3
Figure 3: A 25cm x 25cm 6MV cFF beam (above) and a 25cm x 25cm 6MV FFF beam (below) measured at 100cm SSD and a depth of 10cm in water 10
Figure 4: A 3cm x 3cm cFF beam (above) and a 3cm x 3cm FFF beam (below) measured at 100cm SSD at a depth of 10cm in water. 11
Figure 5: 20cm x 20cm FFF profile taken at 100cm SSD at a depth of maximum dose in water. The inflection points use for normalisation are marked by vertical lines. 16
Figure 6: Positions for the measurements in the patient plane. Circles represent a constant radius from the isocentric position 43
Figure 7: Positions for the non-patient plane leakage measurements. 43
Figure 8: Barrier doserate measurement positions 44
Figure 9: A comparison of profile shape with differing beam energies for a 10cm x 10cm field at 100cm SSD measured at a depth of maximum dose in water. 46
Figure 10: A comparison of the change in profile shape with increasing field size for 6MV cFF (above) and FFF (below) beams at 100cm SSD and a depth of 10cm in water. 47
Figure 11: A comparison of the change of profile shape with varying depth in water (1.5cm, 10cm, 20cm) for 6MV cFF (above) and FFF (below) beams at 100cm SSD with a field size of 10cm x 10cm. 48
Figure 12: A comparison of the penumbra for 6MV beams taken at 100cm SSD and a deth of maximum dose. The 3cm x 3cm fields (above) the measured penumbra was 2.7mm for each mode and for the 25cm x 25cm field (below) the penumbra was 3.1mm for each mode. 49
Figure 13: 6MV (above) and 10MV (below) PDD difference plots for matched flattening filter free (dashed) and unmatched flattening filter free (solid) compared to the associated (reference) cFF beam (dotted) measured at 100cm SSD. 50
Figure 14: The variation of PDD10 (left) and PDD20 (right) for field sizes of 3cm x 3cm to 30cm x 30cm at 100cm SSD. 6MV (above) 10MV (below) 51
Figure 15: Output factors at 100cm SSD and 10 cm deep in water with varying field size for 6MV (above) and 10MV (below) beams for cFF, matched flattening filter free and unmatched flattening filter free modalities. 53
Figure 16: Diagram of electron transport system of an Elekta Linear accelerator. Steering coils operate radially (2R) and cross-plane (2T) to the plane of the electron beam path. 62
Figure 17: The effect of adjusting 2T bending magnet current on profile shape and CAX position for 6MV FFF beams (above) and cFF beams (below) taken at 100cm SSD at a depth of maximum dose in water. 64
Figure 18: Profile central axis shift with changing 2T steering currents for a 6MV FFF beam at 100cm SSD and at a depth of maximum dose in water. 65
Figure 19: Top: Change in 6MV FFF inplane Profile flatness for a 1% change in PDD at 100cm SSD and 10cm deep in water. Bottom: Profile shift for a 1% change in PDD at 100cm SSD and 10cm deep in water. 66
Figure 20: Depiction of second derivative determining the position of inflection for 6MV cFF (above) and FFF (below) beams for a 20cm x 20cm profile taken at 100cm SSD and 10cm in water. 68
Figure 21: Inflection point normalised 25cm x 25cm in-plane profile measured at 100SSD and 10cm deep in water. 69
Figure 22: Diagram of the modelled ionisation chamber in the linear accelerator, this component was constructed of 21layers with up to 3 cones. 74
Figure 23: Figure of linear accelerator head as modelled in EGS/BEAMnrc 76
Figure 24: Diagram of angular spread parameter for Monte Carlo modelling 78

Figure 25: Impact of nominal accelerating potential on a 20cm x 20cm profile shape (above) at 100cm SSD and a depth of maximum dose in water and a 10cm x 10cm PDD at 100cm SSD (below). 80
Figure 26: Impact of angular spread parameter on a 20cm x 20cm profile shape (above) at 100cm SSD and a depth of maximum dose in water and a 10cm x 10cm PDD at 100cm SSD (below). 81
Figure 27: The relationship between the required move of the jaw in the model in to move 1cm at isocentre with respect to field size. 83
Figure 28: The relationship between the required move of the mlc in the model in to move 1cm at isocentre with respect to field size. 84
Figure 29: Benchmarking results for the 10cm x 10cm Monte Carlo calculated profiles (blue) against measured data profiles (red). The red circles mark where the difference between the profiles is greater than a global 1%/1mm gamma tolerance. The displayed profiles are (a) at a depth of maximum dose collimated by the jaws (b) at a depth of maximum dose collimated by the MLC (c) at a depth of 20cm collimated by the jaws (d) at a depth of 20cm collimated by the MLC. 86
Figure 30: Benchmarking results for the 20cm x 20cm Monte Carlo calculated profiles (blue) against measured data profiles (red). The red circles mark where the difference between the profiles is greater than a global 1%/1mm gamma tolerance. The displayed profiles are (a) at a depth of maximum dose collimated by the jaws (b) at a depth of maximum dose collimated by the MLC (c) at a depth of 20cm collimated by the jaws (d) at a depth of 20cm collimated by the MLC. 87
Figure 31: Benchmarking results for the 3cm x 3cm Monte Carlo calculated profiles (blue) against measured data profiles (red). The red circles mark where the difference between the profiles are greater than a global 1%/1mm gamma tolerance. The displayed profiles are (a) at a depth of maximum dose collimated by the jaws (b) at a depth of maximum dose collimated by the MLC (c) at a depth of 20cm collimated by the jaws (d) at a depth of 20cm collimated by the MLC. 88
Figure 32: A 3cm x 3cm field calculated (blue) 10cm offset from the central axis in the MLC direction compared to measured data (red) at 100cm SSD and a depth of maximum dose in water. 89
Figure 33: A benchmarked 3cm x 3cm Monte Carlo profile collimated by the jaws with the thickness of the primary collimator increased. 90
Figure 34: The impact or increasing and decreasing the thickness of the filter plate on the out of field dose 91
Figure 35: The impact of changing the electron transport cutoff energy on the out of field dose (above) comparing the cutoff energies of 512keV and 700keV (below) comparing the 512keV Monte Carlo profile against measured data. 92
Figure 36: Comparison of Monte Carlo calculated profile with straight jaw edge (blue) compared to measured data (red). 93
Figure 37: Profiles measured with semiflex3D (red) compared to Monte Carlo (blue) for field sizes of 3cm x 3cm (upper) and 10cm x 10cm (lower) at the depth of maximum dose (left) and at 20cm deep (right). 94
Figure 38: Back-up collimation settings (a) original model (b) corrected model 95
Figure 39: Benchmarking results for the 3cm x 3cm Monte Carlo calculated profiles (blue) against measured data profiles (red) at 100cm SSD. The red circles mark where the difference between the profiles are greater than a global 1%/1mm gamma tolerance. The displayed profiles are (above) at a depth of 10cm in water collimated by the jaws (below) at a depth of 10cm in water collimated by the MLC. 96
Figure 40: Benchmarking results for the 10cm x 10cm Monte Carlo calculated profiles (blue) against measured data profiles (red) at 100cm SSD. The red circles mark where the difference between the profiles are greater than a global 1%/1mm gamma tolerance. The displayed profiles are (above) at a depth of 10cm in water collimated by the jaws (below) at a depth of 10cm in water collimated by the MLC. 97

Figure 41: Benchmarking results for the 20cm x 20cm Monte Carlo calculated profiles (blue) against measured data profiles (red) at 100cm SSD. The red circles mark where the difference between the profiles are greater than a global 1%/1mm gamma tolerance. The displayed profiles are (above) at a depth of 10cm in water collimated by the jaws (below) at a depth of 10cm in water collimated by the MLC. 98
Figure 42: Transaxial slices of the three different techniques for one of the patients investigated. (a) 3DCRT treatment plan, (b) cFF VMAT plan, (c) FFF VMAT plan, (d) DVHs for PTV (blue), right lung (yellow), left lung (green) for each of the treatment techniques (a)solid line (b) dashed line (c) dotted line. 109
Figure 43: Transaxial slices of the two different with FFF VMAT (b) compared to 3DCRT (a). 112
Figure 44: Transaxial slice for the two techniques of one 60in8# plan sparing the spinal cord for patient 7. 116
Figure 45: Transaxial slice of the plan treating two PTVs concurrently 119
Figure 46: The relationship between OAR overlap and the dose to 95% of the PTV 122
Figure 47: Dose in cGy/MU with respect to off axis distance for 40cm x 40cm 6MV FFF and cFF beams taken at 100cm SSD at a depth of maximum dose 124
Figure 48: Three of the possible GTV locations within one respiratory cycle 125
Figure 49: Example of a modulated segment and an open segment, the outer contour represents the PTV and the inner contours represent the ITV and GTV. The shaded areas show the beam aperture. 126
Figure 50: Transaxial slices from two of the planning cases comparing the dose distribution between the two modes of delivery. Upper left FFF, Upper right cFF, Lower left cFF, lower right FFF. Above: a plan with a 70Gy PTV close to optical OARs. Below: a plan with a large high dose region with lower dose elective region to the right hand side of the patient. 129

1. Introduction

1.1. Overview of Radiotherapy

There were over 280,000 cases of cancer diagnosed in 2012 in the UK, this has risen by 2% per annum and is predicted to reach 360,000 by 2030. Of the cases diagnosed with cancer approximately 50% will have radiotherapy as part of their treatment (Independent Cancer Taskforce, 2015). Radiotherapy is the use of ionising radiation to induce cell death in tumour cells. This is achieved through the use of radioisotopes, x-ray beams and particle beam therapies. With an increase in demand for radiotherapy, additional capacity is required, which can be achieved through increased treatment machine provision, extended treating hours, or through efficiency improvements utilising improved treatment delivery technology such as Flattening Filter Free (FFF) beams and techniques such as those covered in section 1.4.

1.2. Linear accelerator design

The majority of external beam radiotherapy is delivered using C-arm linear accelerators (LINACS). These Linacs accelerate electrons to high energies (in the region of 4-25MeV) which are diverted towards the patient to treat with an electron beam or directed so that they strike an x-ray target producing bremsstrahlung radiation. These energies are sufficient to penetrate to the required depths within the body. The linear accelerator is mounted as part of a rotating gantry so that the beam can be directed from any direction around the patient. The main components of an Elekta linear accelerator with Agility head (Cosgrove et al., 2009) are briefly described and shown (Figure 1) below (Podgorsak and International Atomic Energy Agency., 2005).

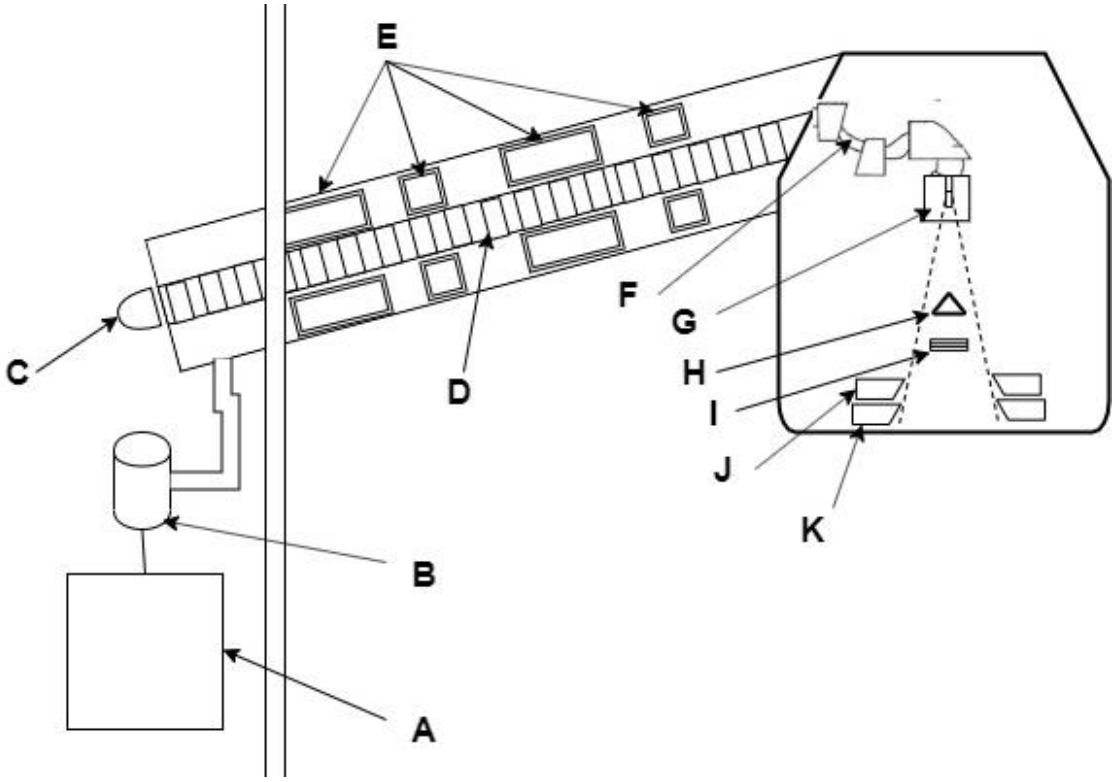

Figure 1: Diagram of Elekta Linear accelerator.

- The pulse forming network generates a high voltage pulse (A) that is used to provide power to a magnetron (B) and an electron gun (C).
- The magnetron (B) produces the high frequency microwaves that are injected into the waveguide (D).
- The electron gun (C) provides a pulse of electrons that are accelerated into the travelling waveguide (D).
- The travelling waveguide (D) accelerates the electrons produced by the electron gun (C). These electrons are focussed along the waveguide by two sets of focussing magnetic coils and steered by two sets of steering coils (E). The electrons exit the travelling waveguide into the flight tube (F) with the required energy for the radiotherapy treatment. The excess energy from the microwave is terminated in an RF load or can be recycled through a coupling waveguide back into the travelling waveguide.
- The flight tube (F) contains a set of three bending magnets in a slalom with a total angle of bend of 112° that focus the electron beam onto the target or exit window and act as an energy selector. The magnetic field is adjusted by setting the bending currents, bending coarse and bending fine. Bending coarse applies the current to all three bending magnets and bending fine applies the current to the final bending magnet only.

- For the production of MV photons used for radiotherapy the high energy electron beam is focussed to be incident on a tungsten target (G). The electrons decelerate creating Bremsstrahlung radiation. In order to conserve momentum the radiation is produced with a forward directional bias. The higher the beam energy the greater the forward bias.
- The radiation emitted that is not directed towards the treatment area is collimated by a fixed size primary collimator to reduce the dose outside of the treatment area.
- Beyond the primary collimator is the flattening filter (H); this conical filter attenuates the centre of bremsstrahlung radiation and results in a flattened beam profile. For FFF machines this conical filter is replaced by a flat filter plate (Figure 2).By removing the flattening filter a source of attenuation within the beam is removed, increasing the intensity (dose rate) of the treatment beam.

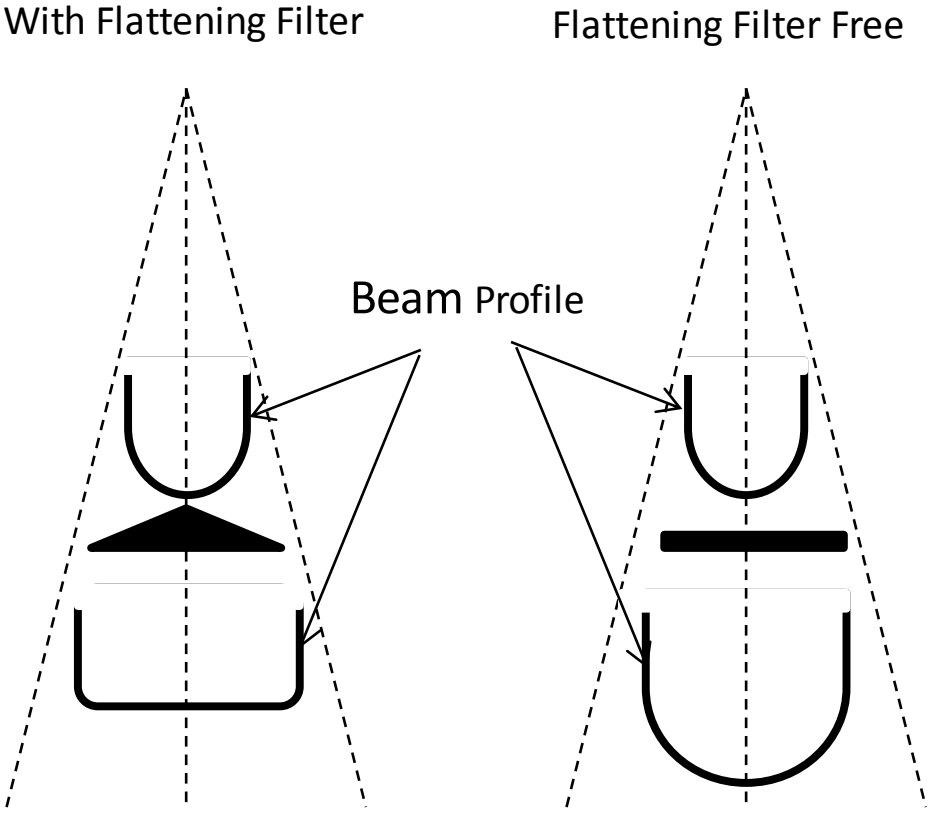

Figure 2: Diagram of the effect of removing the flattening filter on the beam profile

- Once the beam has passed though the filter it passes through the monitor chamber (I). The monitor chamber contains three ionisation chambers. Two for measuring the amount of radiation delivered and a segmented ion chamber for measuring beam asymmetry in both the radial and transverse directions and for measuring the difference

between the outer and inner parts of the beam, which is used as a surrogate for energy changes of the beam.

- An LED optical system uses visible light to form the light field to demonstrate the beam position. The optical system also has an infra red camera that is used to track the Multi leaf collimator (MLC) positions (J). The optical system floods the MLCs with ultra violet light that causes the ruby reflectors on the MLC leaf tips to fluoresce in the infra red spectrum.
- The MLC on the Agility head contains 160 tungsten leaves arranged in 80 pairs. Each leaf has a projected size at 100cm from the x-ray target of 0.5cm. The leaves are used to collimate the beam and can be used to create irregular shapes, these irregular shapes are required for the delivery of Intensity Modulated Radiotherapy (IMRT), which will be covered in a following section.
- Below the MLC are two tungsten diaphragms (K) that collimate the beam perpendicular to the MLC travel direction, these are often referred to as 'jaws'
- The beam exits the treatment head through a fixed aperture that is sealed with a Mylar window. This has crosshairs marked on it that identify the position of the central axis of the beam.

The above description is of an Elekta linear accelerator, the other major manufacturer of Linacs is Varian. In the Varian design the microwaves are produced by a klystron and rather than a travelling waveguide system a standing waveguide is used. Details of the head design differ (Mohan et al., 2008), the leaf positions are determined through an optical encoding system rather than the optical system used in Elekta machines.

C-arm Linacs have traditionally used a flattening filter to produce a uniform beam profile (conventional flattening filter (cFF) flattened beam) in order to simplify plan calculations and deliver uniform doses across individual beams. With the advent of IMRT (covered in section1.4) and inverse planning the flattening filter is no longer required, as beam profile variations can be compensated for by the MLCs. With the removal of the flattening filter a large source of attenuation (and scatter) in the beam path is removed, increasing the efficiency of the Linac and increasing the available doserate for FFF beams. The use of Linacs for cFF treatments is well established including the Quality Assurance (QA) tests required for maintaining the beams within clinical tolerances. The use of FFF beams in clinical practice with respect to C-arm Linacs is not well established, with commercially available clinical systems only available since 2011 (Varian TrueBeam) and 2013 (Elekta VersaHD). These two manufacturers have implemented FFF

through different approaches, therefore in order to ensure safe clinical use an appropriate system of beam characterisation and QA needs to be investigated.

1.2.1. FFF implementations

There have been two approaches to the implementation of FFF beams. The differences in these approaches have significant impact on the properties of the beam such that two beams referred to as 6/10MV FFF differ depending on the implementation used. One approach is to remove the flattening filter and use the same settings for producing the MV beam. This implementation results in a beam with a softer spectrum and reduced penetration. This 'unmatched' approach is the implementation deployed with the Varian TrueBeam Linacs. The second approach is to additionally change the settings such that the accelerating potential is increased in order to produce a FFF beam that more closely matches the penetration of the associated cFF beam. This approach has been deployed with the Elekta VersaHD Linacs. The differences between these approaches are investigated in Chapter 3

1.3. Clinical aims of radiotherapy

The aim of radiotherapy is to damage tumour cells. The mechanism for this is that the ionisation within cells produced by the radiotherapy treatment creates free radicals, and these free radicals cause chemical interactions within the cell resulting in DNA damage. Cells contain mechanisms for repairing this chemical damage, but if sufficient damage to the DNA within the nucleus can be accumulated, cell death can be induced. A dose of 1Gy results in approximately 1000 single strand breaks and 40 double strand breaks in the nucleus of a cell. Higher radiation doses increase this number and reduce the possibility of the cell repair mechanisms being successful. This relationship between increasing dose and a reduction in the survival of cells is characterised by the linear quadratic model.

$$\textbf{Equation 1: } S = \exp[-(\alpha D + \beta D^2)]$$

Where S is the surviving fraction of cells, D is the dose delivered and α and β are constants relating to the type of tissue being irradiated.

The relationship between these constants is often referred to as the α/β ratio. Tissues with a low α/β are typically normal tissues and are more sensitive to the linear component of the model requiring lower doses per fraction with more effective cell repair mechanisms. Tissues with a high α/β ratio are less sensitive to fraction size and represent tissues with fast growth such as tumour cells (Mayles et al., 2007).

As radiation damages both tumour cells and normal healthy cells, it is important that treatments conform closely to the target volume and do not irradiate normal tissues more than is required. Conformality, to match high dose volumes to the target and minimise doses to nearby organs at risk (OAR) has been a driving force in developments in radiotherapy delivery technology and treatment techniques. This has developed from 2D planning on a patient outline to 3D conformal radiotherapy (3DCRT) planning using the patient's CT dataset and to the current state of the art IMRT (Brahme et al., 1982) and Volumetric Modulated Arc Therapy (VMAT) (Teoh et al., 2011) with on treatment imaging.

1.4. Intensity Modulated Radiotherapy

Treating areas of Planning Target Volume (PTV) with high dose radiotherapy often requires the ability to reduce dose to OARs in close proximity to the treated volume. A method of achieving this is by the application of a non-uniform dose profile applied at multiple beam angles that when combined in superposition produces a dose distribution with the required shape in 3D (Brahme et al., 1982). The technique of using non-uniform radiation fluence to produce the type of desired dose distributions is referred to as IMRT. With the advent of MLCs that can shape the radiation beam and computer algorithms that can determine the required radiation fluence to produce the desired dose distribution, IMRT has become routinely provided in most radiotherapy centres. Further developing on IMRT is the delivery of VMAT where the gantry is in constant rotation with both the MLCs moving and the dose rate increasing or decreasing to provide the desired radiation fluence. The advantages of VMAT over IMRT are an increased flexibility to deliver the dose from multiple angles and the reduction of treatment delivery times (Teoh et al., 2011). With the increased prevalence of these techniques it is no longer necessary for the photon fluence from the linear accelerator to be uniform and therefore treating without the flattening filter in the beam path becomes a possibility. IMRT techniques take longer to treat than 3DCRT, this has the potential to introduce problems with patient immobilisation and movement during treatment, VMAT techniques reduce this treatment time and the use of FFF beams with VMAT delivery can potentially reduce treatment times further.

1.5. Monte Carlo simulation

Monte Carlo simulation can be a powerful tool for investigating the stochastic processes of radiation beam interactions and characteristics. An appropriately benchmarked Monte Carlo simulation can be used for investigations that might otherwise prove difficult practically either by their implementation or through access to a dedicated research Linac (Cranmer-Sargison et al., 2012; Muir et al., 2011; Titt et al., 2006b). The first Monte Carlo publication was in 1949

(Metropolis and Ulam, 1949) and described a statistical method for mathematically solving physics problems (Seco and Verhaegen, 2013). The premise of Monte Carlo is that when the probability of each of the interactions is known to sufficient precision then after a sufficient number of random interactions are modelled; the modelled results approach the true result. For radiation physics these are interaction cross sections for radiation with matter. There are a number of Monte Carlo codes available (EGSnrc, GEANT, PENELOPE, MCNPX) (Agostinelli et al., 2003; Baro et al., 1995; Waters et al., 2007; Rogers, D. W. O. and Bielajew, 1984). The Electron Gamma Shower (EGS) code was first developed in 1978. It has undergone many developments from the EGS3 code to EGSnrc that is openly available today. The EGSnrc code has a specific user code BEAMnrc (Rogers, D.W. et al., 1995) that was developed between 1990 and 1996. This additional code was specifically developed for the modelling of Linacs and will be used for the Monte Carlo work in this thesis.

1.6. Scope of Work

Given the increasing availability and use of FFF beams, the aim of this thesis is to investigate FFF beams from the initial characterisation through to the final implementation in the clinical setting, to provide new knowledge to underpin the basis of their use. This is done through answering a number of research questions.

- What are the properties of FFF beams and do these properties differ between the two implementations?
- Can suitable definitions be determined in order to characterise and QA all radiotherapy photon beams, cFF and both implementations of FFF?
- Can existing Monte Carlo packages be used to accurately model FFF beams?
- How can FFF beams be implemented in the clinic and are they suitable for a range of treatment sites?

This will be done through the following chapters;

1. A literature review of current publications and their findings with respect of FFF beams, identifying gaps and required information to support clinical use.
2. The characterisation of the two implementations of FFF beams by the two main manufacturers of Linacs.
3. The setup and quality assurance of FFF beams and proposed new suitable definitions of beam parameters.
4. The Monte Carlo modelling of FFF beams and how this can be achieved.

5. The implementation of FFF beams in a clinical setting including feasibility studies for different treatment sites and dose fractionations.

1.6.1. Cyberknife and Tomotherapy

Predating the implementation of FFF on conventional c-arm linear accelerators there exist two commercially available radiotherapy treatment machines that utilise FFF beams. The Cyberknife system (Accuray Inc., Sunnyvale, California, USA) is a 6MV linear accelerator mounted on a robotic arm with 6 degrees of freedom. The system has a maximum field size of 60mm resulting in radiotherapy beam profiles comparable to a cFF beam. The beam operates with a maximum doserate of 1000MU/minute. The system is designed for radiosurgical treatments and is not included in the scope of this work (Adler et al., 1997).

The second commercially available system is TomoTherapy (TomoTherapy Inc., Madison, WI, USA). This system uses a 6MV linear accelerator mounted on a rotating gantry similar to a CT scanner. The maximum field size of the beam is 40cm x 5cm and therefore the profile shape only differs from that of a conventional cFF beam in the lateral direction (Jeraj et al., 2004). The output of the radiation beam is 1000MU/min. Due to the fan shaped beam used on the TomoTherapy system the treatments are delivered by helically irradiating the patient through a combination of rotating the gantry and moving the treatment couch.

Each of these systems whilst sharing some characteristics with the FFF beams produced by conventional c-arm linear accelerators deliver their treatments in a significantly different manner and therefore are not included in the scope of this work.

2. Literature review

Radiotherapy Linacs produce an x-ray beam that is forward peaked when the electron beam interacts with the target. This forward peaked distribution is conventionally directed to be incident on an attenuating flattening filter to produce a flat photon beam. Until recently, almost all Linacs used in radiotherapy utilise a flattening filter, where the aim of their design is such that the beam profile would be flat at a depth of 10cm in water (Dalaryd et al., 2010; Mesbahi, 2007; Khan, 2003), in order to help ensure a uniform coverage of the target. An example of a cFF 25cm x 25cm beam and its FFF equivalent are shown in Figure 3.

With the improvements in computer technology more complex dose calculations can be performed and this has led to treatments such as IMRT, VMAT, radiosurgery and stereotactic ablative radiotherapy (SABR). With the increase of these advanced techniques there has been an increased interest in the operation of Linacs with the flattening filter removed. There are a number of reasons behind this interest. The flattening filter attenuates a large proportion of the beam incident on it thereby reducing the efficiency of the linear accelerator. The removal of the flattening filter results in an increase of the available doserate of the beam. Radiosurgery generally uses small fields (< 5cm x 5cm) and large doses per fraction requiring high numbers of monitor units per beam. Due to the small beam widths, FFF small fields have a comparable profile with the flattening filter removed as when it is present (Mesbahi, 2007) as well as having an increased doserate that may increase the treatment delivery speed. IMRT uses the MLC to produce non-uniform beam fluence. Therefore it is not a requirement that the beam has a uniform profile before the modulation procedure.

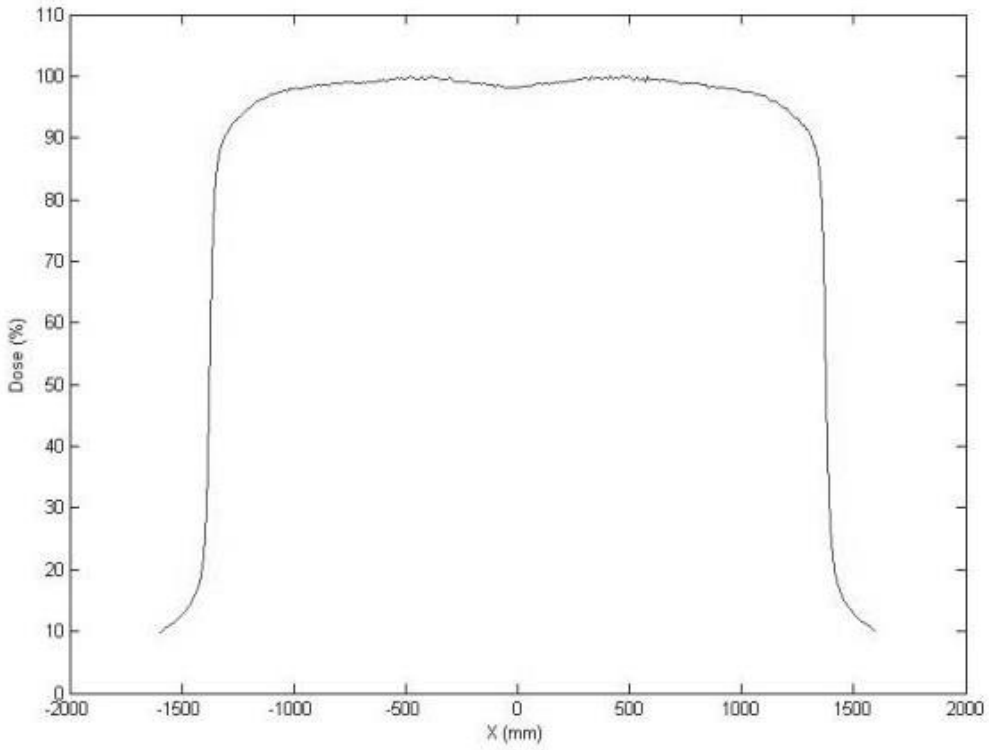

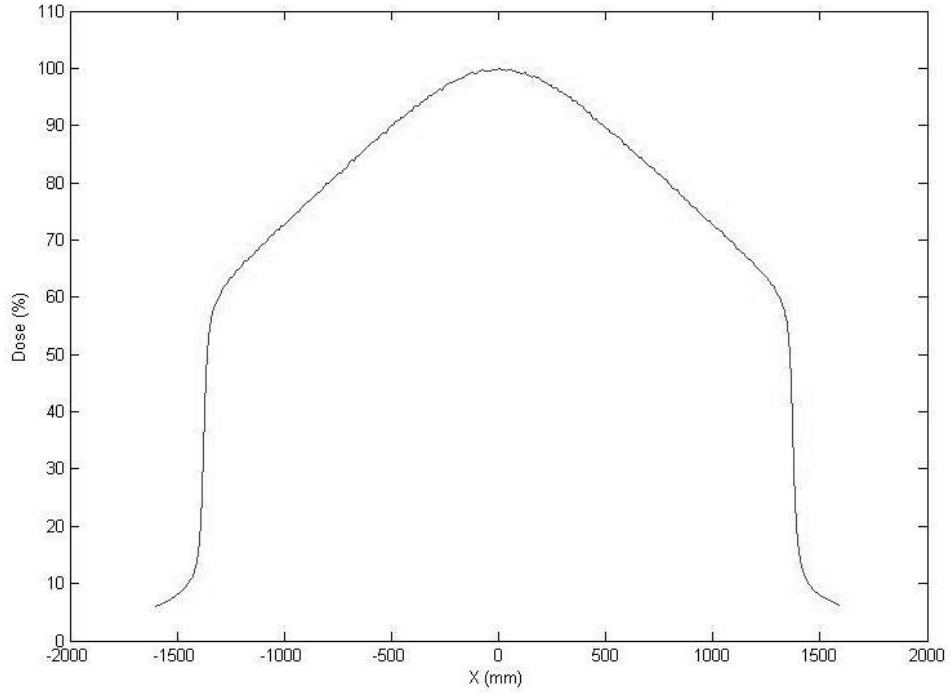

Figure 3: A 25cm x 25cm 6MV cFF beam (above) and a 25cm x 25cm 6MV FFF beam (below) measured at 100cm SSD and a depth of 10cm in water

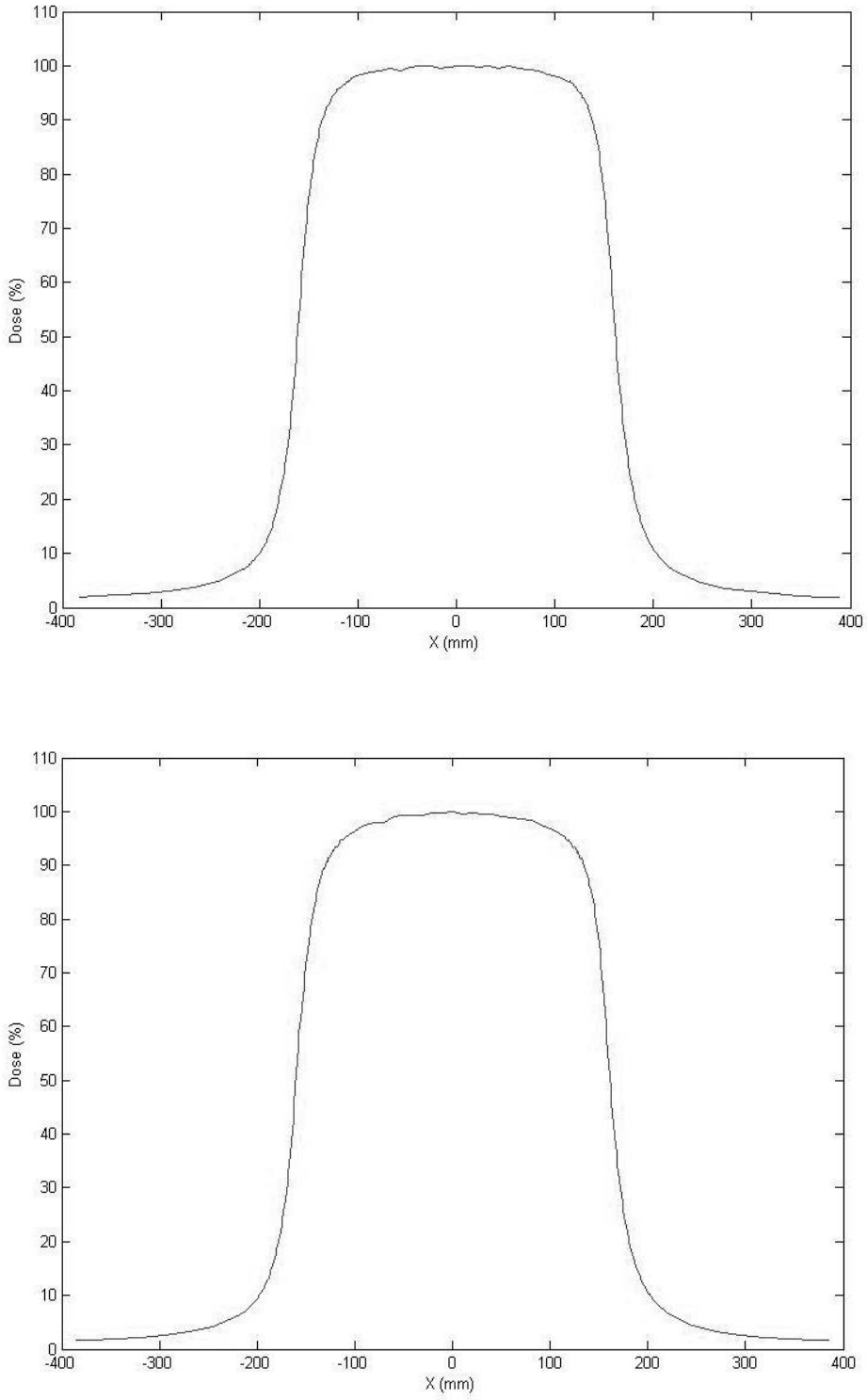

Figure 4: A 3cm x 3cm cFF beam (above) and a 3cm x 3cm FFF beam (below) measured at 100cm SSD at a depth of 10cm in water.

In addition, there have been a number of Monte Carlo studies that have demonstrated that the flattening filter is the dominant source of scattered radiation in the linear accelerator treatment head (Dalaryd et al., 2010; Titt et al., 2006a). The scatter produced in the treatment head increases the complexity of modelling off-axis fields which are frequently used in IMRT treatments and SABR treatments. The flattening filter also produces a variation in beam quality with off-axis distance, due to the variation in beam-hardening effects caused by the conically shaped flattening filter. This produces a treatment beam with variable energy spectra as you move away from the central-axis. The removal of the flattening filter could potentially result in improved dose calculations for IMRT plans due to the simplification of off-axis calculations compared to delivery with the flattening filter in situ (Cashmore, 2008) and the reduction in scatter from the treatment head may reduce the unwanted out-of-field dose.

Thirdly, the softer spectrum of the FFF beam has been used as an indication that FFF beams could prove beneficial for MV imaging and portal dosimetry (Tyner et al., 2009). This softer spectrum would improve the low contrast resolution of MV imaging and have the potential to increase the sensitivity of portal imaging through greater attenuation of the low energy photons contained in the beam.

2.1. Second Cancer induction following radiotherapy

With improved radiotherapy treatments resulting in greater cancer control and increased long term survival rates, the risk of developing second primary malignancies due to the irradiation of normal tissue has become an area of concern (Hall, 2006; Dorr and Herrmann, 2002). The cumulative incidence of second primary cancers could be as high as 20% of patients receiving radiotherapy treatment (Tubiana, 2009). A study by Brenner et al. (2000) concluded that following radiotherapy to treat prostate cancer the relative risk of developing a second malignancy was 6% higher than those who were treated surgically, this increases to 15% and 34% following 5 years and 10 years survival, respectively. In absolute terms, the estimated risk of developing a radiation-associated second malignancy was 1 in 290 for all prostate carcinoma patients treated with radiotherapy, increasing to 1 in 70 for long term survivors (> 10 years). The majority of the increased risk was carcinomas of the bladder, rectum and lung. The use of FFF treatments can reduce the whole body dose to the patient and reduce the out of field dose, potentially reducing the risk of these incidences.

IMRT treatments can increase the number of monitor units delivered by a factor of 2-10 (Klein et al., 2006; Mansur et al., 2007) compared to 3D conformal treatment approaches. This increase

will also increase peripheral dose from leakage through the linear accelerator head. This could be reduced through the removal of the flatting filter.

The majority of second cancers are located within the margins of the radiotherapy treatment field. However, second cancers can still be located in the periphery of the patient (Chofor et al., 2010). A study by Dorr and Herrmann (2002) looked at where second cancers occurred following radiotherapy. The findings were that 50% of new tumours occurred in the margins of the previous radiotherapy treatment, where the margin is defined as the distance -2.5cm inside the nominal field edge to 5cm outside the nominal field edge. This is compared to 10% of second tumours located in the field and 10% in the adjacent area (5cm to 20cm from the field). The study also found that 30% of the tumours were located at distances greater than 20cm from the field. The dose delivered to 58% of the sites was less than 6Gy, demonstrating the importance peripheral doses can have in radiotherapy treatments.

The sources that contribute to peripheral doses, distant from the site of treatment are head leakage, head scatter and phantom scatter i.e. scatter within the patient from the primary treatment area. It may be possible to reduce the first two sources through the removal of the flattening filter from the treatment head as the interaction of the photon beam with the flattening filter causes additional scatter. Phantom scatter will vary as a function of the mean energy of the primary photon beam. Removal of the flattening filter will have an effect on this.

Out of field dose has been linked to the induction of secondary cancers following radiotherapy treatment. A reduction in out of field dose could potentially reduce the incidence of radiation induced second cancers. Titt et al. (2006a) stated that out of field doses were reduced with the flattening filter removed whereas Kry et al. (2010) reported that out of field doses were comparable near the treatment site and were reduced by 30% at distances greater than 20cm from the treatment site, this reduction is as a result of the reduced head leakage when using FFF beams. A reduction in peripheral doses was also observed by Dobler et al. (2017) when delivering head and neck VMAT.

Cashmore et al. (2011), Murray et al. (2015), Bouchta et al. (2018) and Moret et al. (2018) performed studies looking at the risk of second cancer induction following radiotherapy with both FFF and cFF beams. The study by Cashmore et al. (2011) was performed on an Elekta Precise linear accelerator with an MLCi treatment head whereas the studies by Murray et al. (2015) and Moret et al. (2018) were performed on an Elekta Synergy model with an Agility treatment head. The study by Bouchta et al. (2018) was performed on a Varian TrueBeam. All Elekta studies used

energy matched FFF beams, with Murray et al. (2015) and Moret et al. (2018) matching at 10cm deep as per the current matching advice for Elekta FFF. Cashmore et al. (2011) stated that the match was performed at both 10cm deep but also as a Tissue Phantom Ratio (TPR) TPR20/10 match. The study by Bouchta et al. (2018) used unmatched FFF beams. The sites investigated were paediatric cranial IMRT (Cashmore et al., 2011), paediatric cranial VMAT (Moret et al., 2018; Bouchta et al., 2018) and prostate 3DCRT, VMAT & SABR (Murray et al., 2015). Plans were produced in the Xio Treatment Planning System (TPS) version 4.34.02 (Cashmore et al., 2011), Monaco version 3.3 (Murray et al., 2015), Oncentra External Beam version 4.5.2 (Moret et al., 2018) and Eclipse verson 11 (Bouchta et al., 2018) each with a 2mm dose grid. Cashmore et al. (2011) optimised the plans for 6MV cFF and then re-optimised with the same parameters for FFF. The other studies optimised all plans individually. All studies found that plan quality was comparable with cFF and FFF beams. Two studies measured doses in anthropomorphic phantoms, the anthropomorthic paediatric phantom (CIRS Inc, VA, USA) (Cashmore et al., 2011) and the Rando phantom (The Phantom Laboratory, USA) (Murray et al., 2015). Each study found that peripheral doses were reduced with the use of FFF beams, by up to 70% (Cashmore et al., 2011), 55% (Murray et al., 2015), 25.6% (Bouchta et al., 2018) and 25% (Moret et al., 2018). Although this relative reduction is large, the change in absolute risk of cancer induction was determined to be 0.0023 per 10000 (Murray et al., 2015). The absolute risk for this cohort of patients was low as it factored life expectancy into the calculation, had the calculation of absolute risk been evaluated for paediatric patients the absolute risk would have been greater.

2.2. Monte Carlo studies on FFF Linacs

A number of studies have been performed on the operation of a linear accelerator without the flattening filter in situ. A large proportion of these studies have been performed via Monte Carlo methods such that the authors do not need a working FFF machine to perform the investigations.

2.2.1. Beam Quality

Xiong and Rogers (2008) performed a study comparing the beam quality specifiers $\%dd(10)_x$ and TPR^{20}_{10} in terms of the Spencer-Attix water to air restricted mass collision stopping power-ratio. Current dosimetry standards and protocols use a correction factor relating to these beam quality specifiers to determine the dose to water measured with an ionisation chamber. It was proposed that the change in spectrum caused by the removal of the flattening filter could result in differences between the appropriate calibration factor for a measured beam quality. The Monte Carlo software used for the study was BEAMnrc/EGSnrc, the 9 Linacs modelled had been verified in prior studies. The stopping power ratios calculated agreed closely with the relationship used

in TG-51 for $\%dd(10)_x$ to the stopping power ratio for the beams with a flattening filter. The largest deviation from the relationship used in TG-51 was a route mean square deviation (RMSD) of 0.0028. For beams without the flattening filter the maximum RMSD was 0.0041. The change in k_Q would be a maximum of 0.2% if the TG-51 relationship was modified for the FFF beams. When comparing the stopping power ratio to TPR measurements for cFF and FFF beams the stopping power ratio can differ by between 0.4-1% for the same TPR value. This demonstrates that TPR may not be as suitable a beam quality measure for Linacs operating without a flattening filter. The work published by the IPEM working party (Budgell et al., 2016) proposed a new factor when calibrating FFF beams, this factor of 0.997 corrects the TPR value for the softer photon spectrum when using FFF beams.

Ceberg et al. (2010) performed a Monte Carlo simulation using the BEAMnrc/EGSnrc software package. The study suggested a new beam quality specifier that may be more appropriate for FFF beams. Although $\%dd(10)_x$ can be used with acceptable deviations for FFF beams, TPR cannot (Ceberg et al., 2010). The subsequent work published as part of the IPEM working party (Budgell et al., 2016) provides a correction factor that corrects for this change in spectrum allowing TPR to be used as a beam specifier. Ceberg et al. (2010) propose that the mean energy of the beam and the coefficient of variation could be more appropriate measures of beam quality. The mean energy and coefficient of variation was determined from phase space files produced by the BEAMnrc/EGSnrc software. The authors did not indicate how these values could be measured in an empirical method. The relationship between the stopping power ratio and the mean energy and coefficient of variation was determined to be:

Equation 2: $$\left(\bar{L}/\rho\right)_{air}^{water} = b_1 + b_2\bar{\mu} - b_3\bar{\mu}^2 + b_4\bar{\mu}^3 - b_5 c_v$$

Where μ is the mean energy, c_v is the coefficient of variation and b_x are coefficients.

The stopping power ratios were calculated from the data produced using EGSnrc/BEAMnrc and compared to data previously measured by Xiong and Rogers (2008). The maximum deviation from the calculated stopping power ratio and those determined previously was 0.13%.

2.2.2. Beam Penumbra

The profiles of FFF beams are significantly different than cFF beams for field sizes of greater than $4cm^2$. This is problematic when comparing beam penumbra as the 80%-20% dose values used for cFF beams are not appropriate as the 80% dose may be located within the FFF beam profile. Ponisch et al. (2006) proposed a method for measuring the penumbra of an FFF beam that

normalises the profile to a cFF profile. The normalisation points used are the inflection points of the profiles (Figure 5).

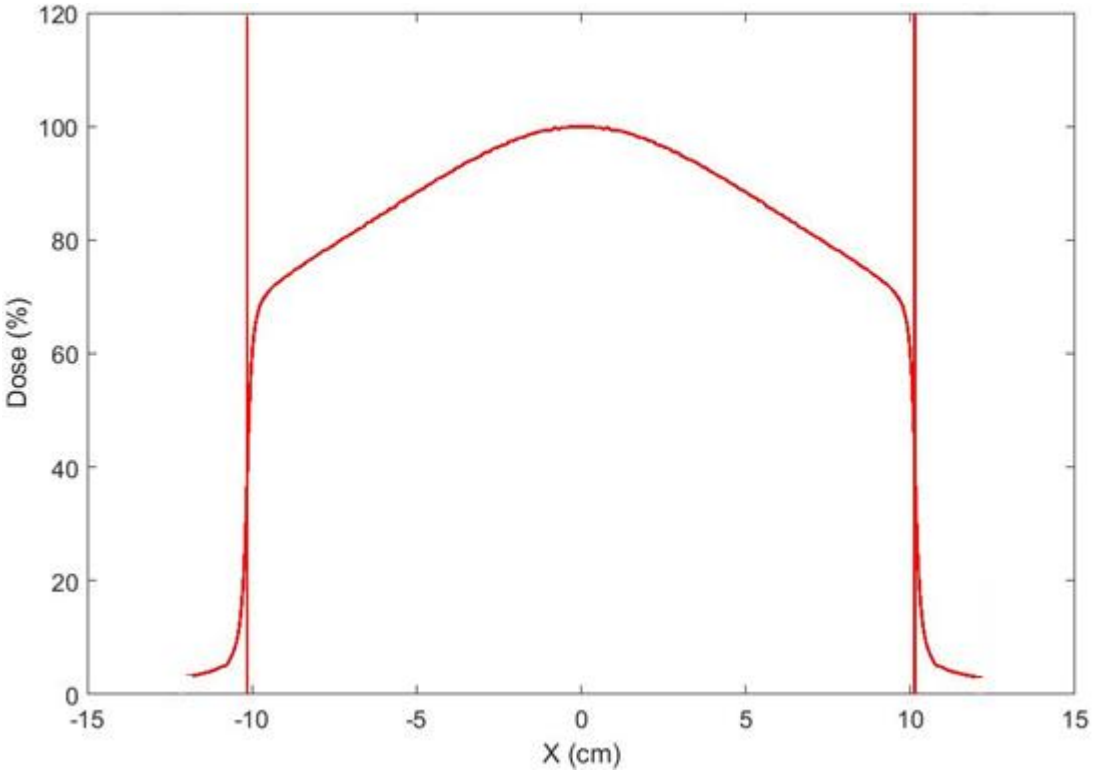

Figure 5: 20cm x 20cm FFF profile taken at 100cm SSD at a depth of maximum dose in water. The inflection points use for normalisation are marked by vertical lines.

The penumbra of the FFF beam is measured as the distance between the 80% and 20% of the normalised dose. The normalised dose is given by:

$$\textbf{Equation 3: } D_n = \frac{D_u}{D_f} D_{CAX}$$

Where D_n is the normalised dose, D_u is the dose at the inflection point on the FFF beam, D_f is the dose at the inflection point of the cFF beam and D_{CAX} is the dose at the central axis for the FFF beam.

This normalisation method is not universally adopted throughout the literature but as accepted guidelines on the beam parameters of FFF beams are not yet agreed, this method will be used in this thesis for determining the penumbra of an FFF beam.

2.2.3. FFF with Varian Linacs

There have been many papers produced comparing the beams of cFF and FFF beams using Monte Carlo simulations of Varian Linacs (Ponisch et al., 2006; Kry et al., 2010; Titt et al., 2006c;

Titt et al., 2006a; Vassiliev et al., 2006a; Tsiamas et al., 2011). The FFF mode of a Varian linear accelerator does not support the re-tuning of the electron beam before it is incident on the target. Therefore, the FFF beam produced has a lower mean energy than the cFF beam. For the 6MV beam a flat 2mm copper filter is positioned where the flattening filter would have been located. The purpose of this is to remove contamination electrons that may have penetrated the target through normal use or target damage, whilst also producing sufficient secondary electrons for the monitor chambers to respond. The 18MV beam has a thicker target and so no filtration is required for the photon beam (Kry et al., 2010). The 18MV beam was produced on a prototype machine and has not been released clinically and there are no specifications from the manufacturer that provide information on whether a filter plate is included in the clinical implementation of FFF beams for Varian machines. The Monte Carlo software used for the studies were either BEAMnrc/EGSnrc (Titt et al., 2006a; Vassiliev et al., 2006a; Tsiamas et al., 2011) or MCNPX (Ponisch et al., 2006; Kry et al., 2010; Titt et al., 2006c; Titt et al., 2006a; Mesbahi, 2007).

Conventional Linacs have been designed to operate with a flattening filter; the beam stability is controlled by a series of feedback servos and the dose delivered to the patient is monitored through ionisation chambers. It is important to ensure that these mechanisms still function correctly for FFF beams. Titt et al. (2006c) performed a study to determine whether the softer photon spectrum of the FFF beam would result in sufficient changes in backscatter to the ionisation chambers to alter their function. The Monte Carlo code used for this study had previously been benchmarked against an earlier backscatter study with the linear accelerator operating in normal mode. The Monte Carlo simulation agreed with measurements to within <1%. The findings of the study were that for fields larger than 2cm x 2cm at 18MV the change in the backscatter to the ionisation chambers was lower than the uncertainty in the Monte Carlo calculations demonstrating that no significant change occurs and the ionisation chambers would work in the same manner as for a cFF beam.

The effect on the percentage depth doses (PDD) was studied in each of the Monte Carlo studies. The PDDs were noted to have a shape more closely resembling a 4MV cFF beam for a 6MV FFF beam and a 15MV cFF beam for the 18MV FFF beam (Vassiliev et al., 2006a). This is due to the softer spectrum caused by the higher proportion of low energy photons in the FFF beam that would have otherwise been attenuated by the flattening filter. A comparison of the penumbra for cFF and FFF beams showed that the penumbra could be reduced by up to 1mm with the use of a cFF beam when compared with the normalisation method proposed by Ponisch et al. (2006).

It was reported by Titt et al. (2006a) that the penumbrae of FFF and cFF beams were comparable, however, no explanation as to how the penumbrae were defined for FFF beams was provided.

The removal of the flattening filter removes a significant source of photon attenuation and therefore increases the maximum doserate available. The increase in doserate has been reported as a factor of 2 times (Titt et al., 2006a), 2.3 (Mesbahi, 2007), 1.9 (Tsiamas et al., 2011) and has been reported as up to 5.45 times (Vassiliev et al., 2006a). The increase in doserate has a possibility of decreasing treatment delivery time, especially for stereotactic radiosurgery where large doses per fraction are typically required.

It was noted by Titt et al. (2006a) that the shape of the profiles were more consistent with increasing depth as the off-axis softening is reduced in the FFF mode of operation. Without the flattening filter in place the variation of energy spectra with off-axis distance is decreased (Vassiliev et al., 2006a). This reduces a variation of 0.33MeV over the range of a 10cm x 10cm to 40cm x 40cm field for a cFF beam to a variation of 0.02MeV for FFF beams (Mesbahi, 2007). This reduction is expected as the flattening filter acts as a differential attenuator across the beam, attenuating more of the low energy photons closer to the beam central axis.

Zavgorodni (2013) and Tsiamas et al. (2011) performed a Monte Carlo study into the feasibility of using large electron beam divergence parameters on the target to produce an FFF beam that more closely represented a cFF beam. This work used electron beam divergences of up to 20° to produce this 'flattened' FFF beam. The subsequent Monte Carlo studies into the characteristics of the Flat-flattening filter free beams (F4) showed that they maintained some of the characteristics of FFF beams such as reduced variation of profile with increasing depth in water, reduced out-of-field doses and reduced output factor variation. Tsiamas et al. (2011) concluded that divergences of or near 14° caused the electron beam to interact with the primary collimator impacting on the doserate to the edge of the profile. They concluded that divergences of 5-10° produce fields flat enough for IMRT treatments without compromising the peripheral dose or increased doserate.

2.2.4. Out of field dose and radiation protection considerations

Kry et al. (2009) performed a Monte Carlo study to investigate how the change in the beam parameters affects the shielding requirements for a linear accelerator vault. The tenth value layer (TVL), the thickness of attenuating material that reduces the radiation level by a factor of one tenth of the initial level, and the equilibrium TVL, the depth where the radiation directional and spectral distributions are practically independent of thickness, were determined for

Portland concrete and the patient-scattered radiation was also determined. The shielding calculations assumed that the linear accelerator would operate exclusively in FFF mode and each patient would receive an IMRT treatment.

When the linear accelerator was operating without a flattening filter the first and equilibrium TVL was reduced by an average of 12%, reflecting the reduced effective energy in Varian FFF conditions. The amount of patient scatter was less at an angle of <60° and more for angles >60°. If the linear accelerator was operating at only 6MV FFF, the required thickness of primary barrier was determined to be 20% thinner and secondary barriers 10% thinner compared to that required for a cFF 6MV beam. For the linear accelerator operating with both 6MV and 18MV FFF modes, the primary barrier would be 9% thinner and secondary barrier 20% thinner. However, the implementation of the FFF mode for Elekta Linacs is different to the method used by Varian. The electron beam incident on the target can be tuned on an Elekta linear accelerator so that the percentage depth dose at 10cm deep in water for the photon beam produced matches that of the cFF beam (ELEKTA, 2010). Therefore, the conclusions of Kry et al. (2009) regarding bunker shielding are unlikely to translate to a bunker housing a 'matched' FFF linear accelerator.

Fewer Monte Carlo studies have been carried out on the Elekta implementation of a FFF mode. This may be because the model cannot be easily benchmarked against data of a linear accelerator operating in flattening filter mode as a new incident electron beam spectra needs to be derived.

Almberg et al. (2012) performed a Monte Carlo study on an Elekta Synergy linear accelerator equipped with an MLCi head. The work was performed using the EGS/BEAMnrc Monte Carlo user code. This work investigated FFF beams with and without energy matching to an associated cFF beam. The paper found that with both types of FFF beam the out of field dose was reduced by up to 40% but with a greater reduction of out of field dose near the treatment volume when using an energy match FFF beam. The model was a development of an existing Monte Carlo model on a cFF beam with the filter replaced by a 2mm stainless steel plate. As with Varian Linacs the purpose of this plate is to remove contamination electrons and also act as a source of secondary electrons so that the ionisation chamber servo systems can operate correctly. The authors did not benchmark the model against measured FFF data and instead stated that the cFF model had been benchmarked.

2.3. Empirical measurements on FFF Linacs

2.3.1. Varian accelerators

Prototype conventional Linacs have been developed to run in a mode where the flattening filter is not present in the beamline. The beam parameters of these Linacs have been published by a number of authors from different sites (Ponisch et al., 2006; Hrbacek et al., 2010; Kry et al., 2007a; Vassiliev et al., 2006b; Stathakis et al., 2009).

The backscatter to the ionisation chambers was found to be comparable with the FFF beam compared to the cFF (Zhu et al., 2006). This confirms the results of previous Monte Carlo studies (Titt et al., 2006c). The dose-rates measured for FFF beams were reported to increase by a factor of 1.99 (Stathakis et al., 2009) to 2.26 (Hrbacek et al., 2010) compared to cFF beams at 6MV and 3.62 (Stathakis et al., 2009) to 4.03 (Hrbacek et al., 2010) compared to cFF beams at 10MV. As with the reported increase in doserate observed from Monte Carlo studies this is expected as the flattening filter acts as an attenuator in the beam reducing the doserate.

The in-air output ratio changes less with field-size for FFF beams compared to cFF beams (Zhu et al., 2006), this is expected as the flattening filter is the dominant source of scatter within the treatment head with head scatter as the dominant cause of in-air output ratio changes with respect to field size. The surface dose for FFF beams was measured to be 10% higher than for cFF beams. Also, the depth of maximum dose (d_{max}) was closer to the patient surface for FFF beams (Hrbacek et al., 2010; Vassiliev et al., 2006b; Stathakis et al., 2009). The increased surface and shallower d_{max} is a result of the higher proportion of low energy photons in the FFF beam. The variation of the depth of maximum dose varies less with field size for FFF beams so that a 40cm x 40cm field has a depth of maximum dose deeper than that for a cFF beam (Hrbacek et al., 2010; Vassiliev et al., 2006b). This is due to the reduction in head-scatter associated with FFF beams. The profiles of FFF beams are closely matched to cFF beams for field sizes smaller than 4cm x 4cm. The measured PDDs for a 6MV FFF beam more closely resembled that of a 4MV cFF beam with the 18MV profile being more closely matched to that of a 15MV cFF beam (Vassiliev et al., 2006b). The penumbrae for 6MV FFF beams were 0.3mm sharper than cFF for depths up to 12cm but for depths over that the cFF beams had a sharper penumbra when compared to FFF. The penumbrae for 10MV FFF beams were sharper for all depths with the largest difference of 0.6mm at the depth of maximum dose (Hrbacek et al., 2010). Other authors stated a reduction of penumbrae of 0.6mm for a 6MV beam and 0.9mm with an 18MV beam (Ponisch et al., 2006).

The collimator exchange effect describes how the output of an Xcm x Ycm treatment field differs from a Ycm x Xcm field, due to the different location in the treatment head of the X and Y diaphragms. The effect is reduced in FFF beams, being 1.8% for cFF beams at 6MV and 1.2% for FFF beams. The values are 2.4% for cFF and 1.5% for FFF at 10MV (Hrbacek et al., 2010). This is likely a result of the reduction in head scatter for FFF beams.

The measured leakage through the MLC from an FFF beam has been reported as being reduced compared to cFF beams: by 0.29% at 6MV and 0.16% at 18MV (Ponisch et al., 2006). This reduction is due to the softer energy spectrum of the FFF beams.

Neutron production in high Z materials within the linear accelerator head can contribute to both patient and operator dose. The flattening filter is a significant source of neutron production and the effect of the removal of the flattening filter on the number of neutrons produced in an 18MV photon beam has been studied (Kry et al., 2007a). The number of neutrons produced for each MU was 20% lower with the flattening filter removed.

Lang et al. (2012b) performed a study on the effects of FFF beams on the collection efficiency of ionisation chambers used to measure dose. The collection efficiency was determined using a two voltage technique (Lillicrap et al., 1990). The change in collection efficiency with respect to dose per pulse changed by 0.8% from the highest dose per pulse measured (1.7mGy per pulse) to the lowest dose per pulse (0.4mGy per pulse), the conclusion was that the tested air vented ionisation chambers could be used for relative dosimetry without the need for collection efficiency to be accounted for. Measurements on matched 6 and 10 MV FFF beams at St James's University Hospital, Leeds yield a change in collection efficiency of 0.3% from 10cm deep to 20cm deep in water for 6MV FFF and 0.6% for 10MV FFF. The impact on the measured TPR results in a change of dosimetric calibration factor of 0% for 6MV FFF beams and <0.1% for 10MV FFF beams.

Many of the quality assurance parameters that are used for cFF beams such as beam flatness and current penumbra definitions are not appropriate for FFF beams, mainly due to the normalisation of the beams to the central axis as part of the definition. Fogliata et al. (2012b) proposed new normalisation and parameters such as unflatness and in-profile slope to characterise the FFF beams. The normalisation parameters were field-size dependent and were determined through measurements on beam profiles of unmatched FFF beams (Fogliata et al., 2012b). At this stage no proposal for clinically relevant tolerances were made by the author.

Further studies into the quality assurance of FFF beams on Varian accelerators have been performed by Clivio et al. (2014). These studies compiled data from 3 different TrueBeam machines that used the analysis parameters proposed by Fogliata et al. (2012b) to determine the stability of FFF beams over a year and determine reference levels for the QA of these FFF beams. The measurements were performed with ion chambers, the Starcheck (PTW,Freiberg) detector array and the electronic portal image detector (EPID) panel. The findings of the study suggest that the proposed slope parameter is susceptible to the positioning of the measurement device. The peak position parameter was also susceptible to variation depending on the resolution of the measuring device. Based on this study the tolerances for these measurement parameters were found to be a change from baseline of 0.04 for the unflatness value, 0.1%/mm for the slope and 1mm for the peak position. This investigation has not been performed on 'matched' FFF beams such as those produced by the VersaHD linear accelerator (Elekta AB, Sweden). Further work by Fogliata et al. (2016b) confirmed that the normalisation parameters defined in the earlier work were consistent across two additional TrueBeam Linacs. The work did conclude that the slope parameter previously described was susceptible to large variations, on average 6.3% between the different machines. The suggestion was made that the parameter be used as part of the assessment of peak position only.

2.3.2. Elekta Accelerators

The tuning method employed on Elekta Linacs produces a harder photon spectrum than that produced in the Varian FFF operation and so may change a number of the properties that have been previously associated with FFF beams. The recommendation of how the beam should be tuned was not agreed when much of the published material was produced. This results in discrepancies between the ways that the FFF mode has been implemented in the literature.

The characteristics of operating an Elekta linear accelerator without a flattening filter and without any tuning of the beam energy have been published by a number of authors (Dalaryd et al., 2010; Cashmore, 2008; Georg et al., 2010; Kragl et al., 2009). Some publications reported on FFF beams that had been tuned so that the TPR^{20}_{10} matched that of the cFF beam (Dalaryd et al., 2010; Georg et al., 2010; Kragl et al., 2009). The associated increase in dose-rate with the removal of the flattening filter has been reported as 1.76 (Dalaryd et al., 2010) and 2.3 (Cashmore, 2008) compared to the cFF doserate for a 6MV beam and 2.66 (Dalaryd et al., 2010) for a 10MV beam. These results are consistent with the findings on Varian Linacs and are as a result of removing a large source of attenuation from the treatment beam.

The ability of the linear accelerator to function safely in clinical mode depends on the ionisation chambers within the head to have sufficient response to automatically control or 'servo' the beam effectively. The number of monitor units (MU) recorded by the chambers was accurate down to 2MU (Cashmore, 2008) demonstrating that the chambers can respond to the increased dose-rate associated with the flattening filter beam without additional modification for sensitivity. The response of the ion chamber is consistent with FFF as a result of adding the flat filter plate which helps to remove contamination electrons as well as produce sufficient secondary electrons to produce a signal in the ion chamber.

The beam steering on an Elekta linear accelerator is controlled by a feedback mechanism in the monitor chambers. This feedback loop ensures that the beam is incident on the flattening filter at the correct position to ensure a symmetrical beam profile. The beam steering showed half the variation for the same bending current with an FFF beam compared to a cFF beam (Cashmore, 2008), producing a more stable beam. This stability would be expected as the symmetry of the beam is no longer affected by the position at which the beam is incident on the flattening filter. When beam segments are delivered with IMRT, low monitor units delivered per segment are avoided to ensure that beam start-up variations do not affect the intended treatment. With the flattening filter removed, the beam is much more stable at delivering low MUs. A variation in symmetry of 0.3% for FFF beams compared to 1.5% for cFF was observed (Cashmore, 2008). The energy of the photon beam in an Elekta linear accelerator is controlled by comparing the response of the inner and outer ion chambers in the monitor chamber; this is possible due to the variation of energy across the beam profile caused by the flattening filter. With the flattening filter removed, the beam energy does not vary in this way (Cashmore, 2008). The energy can still be monitored via this method due to the profile shape of the FFF beams, with a higher intensity on the central axis compared to the periphery that is dependent on the energy of the electrons striking the target.

As discussed previously, the softer spectrum of the FFF beam results in a decrease of the proportion of leakage radiation. When the beam energy is not tuned, the leakage value was measured to have reduced by 44-69% (Cashmore, 2008; Kragl et al., 2011) for a 6MV FFF beam. No data has been published on the effect of tuning the radiation beam on the leakage radiation.

The softer spectrum produced by the FFF beam results in a PDD that is closer to a 5MV cFF beam from an Elekta linear accelerator when the FFF beam has not been tuned. This is harder than the PDD of an FFF beam produced on a Varian linear accelerator where the PDD was more closely matched to a 4MV cFF beam.

The variation in the beam spectra with off-axis distance has been measured. The variation of mean energy across the beam was reduced by 14% (Dalaryd et al., 2010) for the 6MV FFF beam and 8% (Dalaryd et al., 2010) for the 10MV FFF beam. This is consistent with the reduction in Varian accelerators and is as a result of the flattening filter producing differential beam hardening across the profile of the beam.

The variation of the half value layer (HVL), the thickness of attenuating material that reduces the radiation level by a factor of one half of the initial level, with off-axis distance has also been studied. The HVL varied by less than 5% (Kragl et al., 2009) for FFF beams and 11% (Kragl et al., 2009) for cFF beams. The change in profile for the FFF beams gave a reduction of the penumbra by 0.5mm (Cashmore, 2008). This reduction is comparable to those reported for Varian Linacs. The head scatter from the photon beam is an important parameter for determining the output factor used in the dose calculation. The variation of head scatter over a range of field sizes (4cm x 4cm to 40cm x 40cm) was 3% (Cashmore, 2008) for an FFF beam compared to 9% for an associated cFF beam. The total scatter demonstrated a comparable effect to the head scatter with a variation of 8% (Cashmore, 2008) for the FFF beams over a range of field sizes compared with the variation of 15% for a cFF beam. This demonstrates that the other component of total scatter (phantom scatter) does not increase for FFF beams when compared to cFF beams.

With the removal of the flattening filter from the beam path there is an increased number of low energy photons present in FFF beams, however, the removal of the filter also reduces the number of contaminant electrons produced as the beam passes though the filter. Cashmore (2016) looked at the surface dose of a matched 6MV FFF beam compared to a 6MV cFF beam and an unmatched 10MV FFF beam compared to a 10MV cFF beam on an Elekta Synergy model. The 6MV FFF beam showed an increased surface dose of 3.4% for a 3cm x 3cm field but this value decreased to a reduced surface dose of 7.1% for a 40cm x 40cm field. The crossover point for this relationship was at a field size of 10cm x 10cm. The unmatched 10MV FFF beam shows an increase of 10% for smallest field sizes that decreases to a reduced surface dose of 5% at 40cm x 40cm. The crossover point for the unmatched 10MV FFF beam is at a field size of 25cm x 25cm. With the use of wedges both FFF beams showed a decrease in surface dose when compared to the associated cFF beams. With changing SSD the 6MV FFF beam showed similar surface doses to the 6MV cFF beam but for the 10MV unmatched FFF beam the cFF beam showed a large reduction in surface dose when compared to the FFF beam at SSDs over 60cm.

Normalisation parameters for VersaHD FFF profiles were evaluated by Fogliata et al. (2016b). These normalisation parameters are the same as proposed in their earlier work with Varian

machines (Fogliata et al., 2012b) as discussed in the previous section (section 2.3.1). The work does not propose any clinical tolerances for these parameters.

2.3.3. MV portal imaging with FFF

Tyner et al. (2009) performed a study to investigate the effect of the removal of the flattening filter on an a-Si EPID. The linear accelerator used in the investigation was an Elekta Precise model with an MLCi beam shaping device and an Elekta iViewGT a-Si EPID. The FFF beam was not tuned to the 6MV cFF beam, resulting in a softer spectrum than the 6MV beam, whereas the current Elekta guidelines for FFF operation is that the beam should be matched so that the percentage depth dose at 10cm deep in water matches that of the cFF 6MV beam.

An additional 3mm of copper build-up was added to the EPID panel, this additional build-up material ensures that the response of the EPID varies by less than 2.5% for an air gap range of 30-60cm from the exit surface of the patient to the detector. The variation of EPID response with field size reduced with the flattening filter removed. The variation of response from the detector with increasing dose increased with the linear accelerator operating in FFF mode, resulting in an improvement in the detection of small dose deviations, possibly improving portal dosimetry for FFF beams.

The response of the EPID with increasing phantom thickness varies by 14% over 30cm with the FFF beam compared to 7% with the cFF beam. This increase in variation is due to the softer photon spectrum in the FFF beam and would result in better contrast of MV images. The variation of response with off-axis distance was consistent when operating in FFF mode. This consistency could result in the possibility of patient specific verification of IMRT treatments being easier to implement by simplifying the calibrations required. As the results recorded in this study used an additional 3mm of Cu build-up added to the EPID the device would be considered a modified medical device. With the release of the VersaHD by Elekta a new design of EPID panel was introduced that is suitable for FFF beams, this new panel has a faster readout time of 80 lines per pulse compared to the previous 12 lines per pulse so that the panel no longer saturates at high doserates.

Work on an EPID device of a Varian TrueBeam was performed by Nicolini et al. (2013). The study found that in order for the panel response not to saturate for the dose-rates of both unmatched 6 & 10MV FFF beams the panel needed to be deployed at a distance of 150cm SSD. Appropriate gain correction was also required in order for the profile shape measured on the EPID to match profiles measured with an ion chamber. The study looked at using the panel for pre-treatment

QA of VMAT and found that plans passed with over 95% of points passing a gamma index of 2% and 2mm. Gamma analysis is a metric used in radiotherapy to compare one dose distribution to another. Each reference point is compared to points on the distribution to be evaluated and a metric calculated based on the dose deviation and distance to agreement. This metric is explained further in the publication by Low et al. (1998).

2.4. Treatment planning studies on FFF Linacs

A possible benefit of FFF beams is the increased dose rate available through the removal of the flattening filter resulting in a reduction of treatment times for patients, reducing the risk of intra-fraction movement errors and improving patient throughput. The increase in dose-rate may not, however, result in faster delivery times for IMRT treatments as the degree of beam modulation required may increase such that the delivery time could instead be extended.

The softer spectrum of unmatched FFF beams has been proposed as a method of improving coverage at the periphery of lung tumours. Vassiliev et al. (2018) performed a study on the impact of unmatched FFF beams produced by a Varian linear accelerator on the coverage at the periphery of lung tumours. The study used a Monte Carlo model produced in EGS/BEAMnrc to calculate the dose to a phantom containing lung and tumour. The model used the phase space file provided by Varian for the TrueBeam 6MV FFF beam above the jaws and modelled the remainder of the linear accelerator as a Varian 2100C with millennium MLC. The calculation grid was set to 1mm voxels for plans with a Gross Tumour Volume (GTV) of diameter 5cm and 3cm and voxels of 0.5mm for plans with a GTV of 1cm. Each plan consisted of 7 coplanar beams normalised to give 50Gy to the PTV. The Monte Carlo doses were also compared to doses calculated with the Analytic Anisotropic Algorithm (AAA) (Sievinen et al., 2005) and Acuros XB (AXB) (Bush et al., 2011) dose algorithms used in the commercially available TPS.

The Monte Carlo calculation showed that for each GTV size the use of 6MV FFF compared to 6MV cFF improved the surface coverage of the GTV by up to 4% of the prescription dose. This improved coverage is likely a result of the softer spectrum of the FFF beam resulting in a more rapid build-up of dose moving from the lung to GTV boundary. Comparing the Monte Carlo to the commercial algorithms showed that they underestimated this difference by up to a factor of 2.

2.4.1. Treatment planning system benchmarking

In order for treatment planning studies to be considered reliable, the algorithm used for the study should be evaluated to ensure that the doses calculated are correct. Cashmore et al. (2012)

looked at the ability of a modified virtual source model and XVMC in the Monaco TPS to calculate the dose of an FFF beam produced by an Elekta Synergy linear accelerator. The work showed that the profiles calculated matched the measured data in water to within 1% and that measurements of the calculated IMRT plans passed with a 2%/2mm gamma criteria using a Delta4 detector.

Lang et al. (2012c) found that for the TrueBeam linear accelerator the dose calculated on the Eclipse TPS version 8.9 passed verifications with a result of 99% of points passing a gamma analysis tolerance of 3% and 3mm. These measurements were performed with a range of radiation devices including Delta4, Gafchromic film, Arccheck, matrix and point dose measurements with ion chambers. These results are comparable to the results described by Nicolini et al. (2013) when performing verification measurements with the EPID system.

These studies demonstrate that the commercially available treatment planning systems can calculate the dose deposited from FFF beams to sufficient accuracy for clinical use.

2.4.2. Head and Neck planning studies

Standard fractionation regimes of approximately 2Gy per fraction are not generally considered to benefit from the increased dose-rate of FFF beams as much as hypofractionated regimes with large doses per fraction. Head and Neck (H&N) treatments are often in close proximity to multiple OARs and require high degrees of modulation to produce a treatment plan. The gantry rotation speed and the speed of leaf travel in MLCs is thought to prevent the linear accelerator from utilising the high dose-rates of FFF beams.

Fu et al. (2004) performed a study to determine the change in plan delivery time for IMRT treatments of the nasopharynx with the removal of the flattening filter. This is the earliest study into FFF treatments for H&N and uses a prototype system. The treatment delivery time is determined by the beam on time, the leaf travel time and the verification and recording time. The study modelled a BJ-6B linear accelerator (Beijing Medical Equipment Institute) with the MLC devices of a number of different vendors including Varian, Elekta and Siemens. For the Elekta machine there is no information as to whether the beam had been tuned. This is unlikely as the paper was published prior to the manufacturer's recommendation of beam tuning (ELEKTA, 2010).

Plans were produced for 10 nasopharynx cases and 10 prostate cases. The treatment volume for the nasopharynx cases had a median size of 132cm^2. This volume is significantly smaller than the median volume treated in St. James's University Hospital, Leeds. The relatively small size may

result in plans with less modulation and therefore fewer segments reducing the leaf travel time and leaf position verification time for the treatment, compared to plans with larger volumes. The plans produced have all been normalised so that 95% of the PTV receives the 70Gy prescription dose, however, there appears to be no attempt to remove hotspots. This could be due to the clinical protocol in use at the centre. The plan with the smallest hotspots still has over 30% of the PTV receiving a dose of over 110%. This would not be acceptable in the clinical protocol used in St. James's University Hospital, Leeds. The lack of modulation to remove hotspots could result in the delivery times not being representative of clinical practices elsewhere. However, the study found that the average beam-on time was reduced by 43% with the flattening filter removed, despite the number of segments in the plans increasing by 1-2%. The overall treatment time was not reduced by a significant amount (0.7-1.4mins for a 10-20min slot) (Fu et al., 2004).

A further pre-clinical study on FFF for H&N treatments has been performed by Lechner et al. (2013). This treatment planning study compared IMRT and VMAT plans delivered with both cFF and FFF 10MV beams. The 10MV beams used were TPR matched as described in previous studies (Kragl et al., 2009). The machines used for this study were Elekta Synergy Linacs equipped with MLCi treatment heads. The plans were produced in Monaco v3.2 and were produced for 6 head and neck cases. The plan quality was comparable for both cFF and FFF beams. The study found that higher MU (up to 34%) and more segments were required to compensate for the non-uniform fluence of the FFF beams.

Since the commercial release of a linear accelerator for the delivery of FFF beams further investigations have been performed into the feasibility of FFF treatments for H&N treatments (Zhuang et al., 2013; Nicolini et al., 2012; Yan et al., 2016; Lechner et al., 2013; Gasic et al., 2014; Jia et al., 2018). These studies have all been performed with unmatched FFF beams of the TrueBeam linear accelerator and the Eclipse TPS (Varian Medical Systems, Palo Alto, CA). The Eclipse TPS has been verified to calculate FFF beams sufficiently accurately for clinical use (Nicolini et al., 2013). The version of the Eclipse TPS has not been consistent with versions 8.6 (Nicolini et al., 2012), 10 (Yan et al., 2016; Jia et al., 2018) and 11 (Gasic et al., 2014) being used. The grid size used for these studies were 2mm (Zhuang et al., 2013; Gasic et al., 2014; Jia et al., 2018) and 2.5mm (Yan et al., 2016; Nicolini et al., 2012). For each of these studies the plans were optimised and then normalised. The normalisation was so that 95% of the PTV was covered with 95% of the prescription dose (Zhuang et al., 2013; Nicolini et al., 2012; Yan et al., 2016) and Jia et al. (2018) normalising such that 95% of the PTV received 100% of the prescription dose as

with Fu et al. (2004). No information is provided as to how the plans produced by Gasic et al. (2014) were normalised. This normalisation method is not what is performed at St. James's University Hospital, Leeds as it changes the doses to the OARs and affects the size of hotspots after the optimisation has been completed.

The findings of these studies demonstrates the variation in treatment volumes and treatment planning among different institutes with different conclusions on the plan quality when comparing cFF to FFF plans. PTV coverage was found to be equivalent in two of the five studies (Nicolini et al., 2012; Yan et al., 2016), the PTV coverage was found to be less homogenous in three of the studies (Zhuang et al., 2013; Gasic et al., 2014; Jia et al., 2018) and two studies (Zhuang et al., 2013; Jia et al., 2018) also found the maximum dose to the PTV to be higher and the coverage less conformal for FFF beams. The study by Jia et al. (2018) also allowed up to 1% of the PTV to receive a dose of 110% of the prescription dose that would not be clinically acceptable at St James's University Hospital, Leeds. In terms of OAR dose, two of the studies found FFF beams improved the OAR sparing (Nicolini et al., 2012; Yan et al., 2016) by up to 9% (Yan et al., 2016). One study found that doses to some of the OARs increased with FFF plans (Zhuang et al., 2013). Jia et al. (2018) reported that no significant difference was found.

The delivery efficiency of the FFF plans was commented on by each author with all authors stating that an increased number of MU was required for the FFF deliveries, 20% higher (Nicolini et al., 2012), 11% (Jia et al., 2018) and 30% higher (Zhuang et al., 2013). This increase in MU would be expected. Delivering away from the central axis, the dose per MU drops, requiring more MU to deliver the same dose when compared to cFF beams. Despite this increase in MU, the treatment delivery time was found to be comparable (Zhuang et al., 2013; Gasic et al., 2014; Jia et al., 2018) with the plans optimised by Nicolini et al. (2012) such that the same gantry speed was used for both cFF and FFF deliveries.

A study on an Elekta linear accelerator was performed by Dobler et al. (2017) using matched 6MV FFF beams. The study was performed on an Elekta Synergy linear accelerator with Agility MLC and the treatment plans were produced using Oncentra External Beam version 4.5 (Elekta AB, Sweden). The doserate of the 6MV FFF beam was 1700MU/min, which is higher than the manufacturer's recommended doserate of 1400MU/min ± 10%. Plans were produced for both IMRT and VMAT with both cFF and FFF beams. However, the plans were optimised with the cFF beams and the same parameters used for the FFF beam. This could result in the FFF plans not being fully optimised.

The study found that all plans produced were clinically acceptable with comparable PTV coverage and OAR doses. The exception was that the dose to the brainstem was 7% higher for FFF deliveries but still acceptable. Had the plans been fully optimised for the FFF beam this could potentially have been further reduced. The delivery times were comparable for both cFF and FFF beams demonstrating that gantry rotation and MLC travel speeds are the limiting factors rather than doserate. The study did find that peripheral doses were 18% lower with the FFF beam, which is consistent with the reduced head leakage demonstrated by FFF beams.

2.4.3. Prostate planning studies

Prostate treatment volumes are smaller than H&N volumes and have fewer organs at risk. For these reasons the prostate may be a more appropriate site for FFF treatments and a number of studies have been performed to investigate this (Vassiliev et al., 2007; Stathakis et al., 2009; Lechner et al., 2013; Gasic et al., 2014; Yan et al., 2016). With the exception of one pre-clinical study (Lechner et al., 2013) and one clinical study by Treutwein et al. (2017) these studies used unmatched FFF beams and two of the studies were performed on pre-clinical prototype machines (Vassiliev et al., 2007; Stathakis et al., 2009). The studies on the matched FFF beams used a 10MV FFF beam matched to a TPR20/10 value rather than the final clinical implementation of the beam being matched to the dose at 10cm deep in water (Lechner et al., 2013) and a 6MV FFF matched beam (Treutwein et al., 2017). The Lechner et al. (2013) study was performed on a prototype Elekta Synergy linear accelerator with an MLCi treatment head as opposed to the clinical implementation of a VersaHD linear accelerator with an Agility treatment head. Each of the plans was performed using the Monaco TPS version 3.2. The study by Treutwein et al. (2017) was performed on an Elekta Synergy machine with Agility head and planned using Oncentra External Beam version 4.5. Both studies concluded that the plan quality was comparable to cFF plans but required 34% (Lechner et al., 2013) and 10% (Treutwein et al., 2017) more MU to deliver, the difference in additional MU could be a result of the differing energies used in each study. The study by Treutwein et al. (2017) also concluded that treatment delivery was 8% faster with the FFF beam when compared to the cFF beam and peripheral doses were reduced.

Each of the studies on unmatched FFF beams used the Eclipse TPS, the studies performed after the clinical release of FFF used versions 10 (Yan et al., 2016) and 11 (Gasic et al., 2014) to model the unmatched 6 and 10MV FFF beams from a TrueBeam. The pre-clinical studies also investigated an unmatched 18MV FFF beam (Vassiliev et al., 2007; Stathakis et al., 2009). The pre-clinical study by Vassiliev et al. (2007) found that the number of MUs delivered with FFF

beam was half that of the cFF beam for 6MV and was reduced by a factor of 2.6 for the 18MV FFF beam. The reduction in MUs would reduce the amount of leakage radiation and dose outside the treatment field. The author suggests that the reduction in MU could result in reduced treatment delivery times, however no information on the number of segments per field was provided. The author states that the FFF treatments had a better conformity index than the cFF 6MV plans, whereas the 18MV plans had a worse conformity index. The doses to critical organs such as the rectum and femoral heads were reduced for the 6MV FFF treatment and comparable for the remaining organs. The doses to the organs at risk increased with the 18MV FFF beam. The author indicates that this may not be representative of the plan quality achievable as the optimisation was not altered for the FFF beams and the same parameters were used for both cFF and FFF beams.

The study performed by Stathakis et al. (2009) concluded that there was no change in plan quality through the use of an FFF photon beam but that benefits may be from a reduced number of MUs in the treatment delivery reducing the delivery time and peripheral dose through head leakage. The reduced MU in each of these clinical studies is due to the calibration of the machine such that 1MU delivered more than 1cGy to the dose specification point in contrast to the calibration of the cFF beam.

The two studies on the clinical implementation of unmatched FFF beams found that the PTV coverage of the FFF plans was equivalent to the cFF plans. One of the studies found that the FFF plans had improved OAR sparing with the exception of the maximum dose to the rectum (Yan et al., 2016) whilst the other study found that the OAR doses were dosimetrically equivalent (Gasic et al., 2014). In contrast to the pre-clinical studies Yan et al. (2016) found that an increase of MU of 30% was required for the FFF plans when compared to the cFF plans (Yan et al., 2016), this increase is comparable to the 34% increase (Lechner et al., 2013) found in the pre-clinical evaluation of FFF plans for TPR matched FFF beams. The treatment delivery times were found to be equivalent in one study (Yan et al., 2016) and 4.9% faster in another (Gasic et al., 2014) highlighting that the method in which the plans are produced can result in differing optimisation outcomes.

2.4.4. Stereotactic Ablative Radiotherapy planning studies

The increased dose-rate available through the use of FFF beams has resulted in many studies being performed on hypofractionated treatments such as stereotactic ablative radiotherapy (SABR). These treatments require large numbers of MU in order to deliver the high doses per

fraction. This can lead to long treatment times increasing patient discomfort and have the potential to increase the amount of intrafraction motion.

The only treatment study on a matched FFF beam was performed by Kragl et al. (2011) where the peripheral doses were assessed for both 3DCRT SABR treatments to the lung. This study found a reduction in peripheral doses for the FFF plans when compared to the cFF plans. The study was performed on a prototype Synergy linear accelerator with an MLCi2 treatment head, rather than the clinically released VersaHD. The beams were energy matched to the TPR value rather than the dose at 10cm deep in water. No comparison of the plan quality between the modes of delivery was performed as part of this study.

As with previous sites the majority of the literature focuses on unmatched FFF beams produced by the TrueBeam linear accelerator. The energies used were 6MV FFF (Gasic et al., 2014; Lang et al., 2013; Tambe et al., 2016; Hrbacek et al., 2014; Lu et al., 2015) and 10MV FFF (Gasic et al., 2014; Prendergast et al., 2012; Tambe et al., 2016; Lang et al., 2013; Hrbacek et al., 2014; Lu et al., 2015; Navarria et al., 2013; Scorsetti et al., 2011; Reggiori et al., 2012a). The planning system used for these studies was Eclipse versions 8.9 (Hrbacek et al., 2014), 10 (Lu et al., 2015) and 11 (Gasic et al., 2014; Tambe et al., 2016). The sites investigated were lung (Gasic et al., 2014; Prendergast et al., 2012; Lang et al., 2013; Tambe et al., 2016; Hrbacek et al., 2014; Lu et al., 2015; Navarria et al., 2013; Scorsetti et al., 2011; Tyler and Dowdell, 2018), abdomen (Lang et al., 2013), brain (Fiorentino et al., 2017) and liver (Reggiori et al., 2012a; Ogata et al., 2017).

The majority of these studies that compared the FFF beams to cFF found that plans with both beams were clinically acceptable and equivalent with one study noting that, although PTV coverage and OAR sparing was equivalent (Gasic et al., 2014; Prendergast et al., 2012; Tambe et al., 2016; Lang et al., 2013), the 6MV FFF plans were more conformal than the 6MV cFF and 10MV FFF plans (Hrbacek et al., 2014). Lu et al. (2015) compared the two beam types in terms of Tumour control probability (TCP) and normal tissue complication probability (NTCP) using an in-house code written in MATLAB 7.0 (Mathworks, Natick, MA). This study found that the TCP of the 6MV FFF and 10MV FFF plans were comparable but that the NTCP of the lungs and chest wall were lower for the 6MV FFF plans compared to the 10MV FFF plans. The comparison performed by Prendergast et al. (2012) compared IMRT cFF plans to VMAT FFF plans, making it difficult to determine if the results are impacted by the change in delivery technique as well as the beam type. Gasic et al. (2014) commented that each plan was only optimised once and therefore more optimal plans may have been possible.

The delivery efficiency of FFF beams compared to cFF for these plans demonstrated that FFF beams had reduced treatment delivery times when compared to cFF beams. This reduction in beam-on time was reported as 52% (Hrbacek et al., 2014), and 55% (Tambe et al., 2016) faster for 6MV FFF compared to 6MV cFF. In the case of 10MV FFF this reduction in beam-on time improves to 59% (Hrbacek et al., 2014) and 61% (Tambe et al., 2016). Lang et al. (2013) concluded that for treatments over 1000MU or 4Gy per fraction, 6MV FFF had an delivery efficiency improvement over 6MV cFF and for treatments over 2000MU or 10Gy, 10MV FFF had a delivery efficiency improvement over 6MV FFF.

An improvement in efficiency of 10MV FFF compared to 6MV FFF with increasing dose was also found by Lu et al. (2015) with 10MV FFF deliveries being 32-44% faster than 6MV FFF with fraction sizes increasing from 12Gy to 34Gy. Prendergast et al. (2012) concluded that 10MV FFF deliveries were faster than cFF deliveries; however this study was comparing FFF VMAT treatments to cFF IMRT treatments and included intrafraction imaging. The amount of intrafraction imaging varied and 84% of cFF plans received intrafraction imaging whereas only 24% of FFF treatment received intrafraction imaging. Hrbacek et al. (2014) found this reduction in treatment time was achieved despite an increase in MU of 25% for 6MV FFF plans and 21% for 10MV FFF plans when compared to cFF plans. Lu et al. (2015) also found that 10MV FFF plans required 5-6% less MU than an associated 6MV FFF plan.

Retrospective studies into the clinical outcomes of unmatched FFF lung SABR treatments were performed by Navarria et al. (2013) and Scorsetti et al. (2011) with Fiorentino et al. (2017) analysing the impact of FFF beams on brain metastases. Two of these studies found that the FFF plans had an earlier radiological response when compared to cFF plans (Navarria et al., 2013; Scorsetti et al., 2011). These studies were comparing earlier studies of 3DCRT to VMAT it is unclear if this earlier response is as a result of the FFF beams or the treatment technique employed.

Nakano et al. (2018) investigated the effects of FFF beams on non-small cell lung cancer cells. The study used an ARTISTE-TM linear accelerator (Siemens, Erlangen, Germany) to deliver 6MV cFF and 7MV FFF beams. The doses to the in-vitro cells were calculated with the Xio treatment planning system. The study found that the increased doserate of the FFF beams had no effect on cell survival. These findings suggest that the earlier response reported previously by Navarria et al. (2013) and Scorsetti et al. (2011) was as a result of the change in treatment technique rather than the change to FFF beams.

The study by Fiorentino et al. (2017) did not compare to cFF beams and looked at the clinical outcomes of 45 patients who received radiotherapy with FFF beams. The study found that the acute and late toxicities were acceptable and that FFF deliveries were feasible and safe for treatment of these brain metastases. The mean follow up time of this study was 12 months and therefore longer follow up is required to determine efficacy of treatment. However, this would not provide insight into whether FFF beams were beneficial when compared to cFF beams without a clinical trial.

A study into the robustness of treating lung SABR with FFF was investigated by Tyler and Dowdell (2018). This study compared 3DCRT and VMAT with 10MV FFF beams with the isocentre placement at either the centre of the PTV or on the patient midline. The plans were then copied and recalculated 1-2mm offset to determine if isocentre placement or beam modality had an impact on the robustness of the treatment plan. The study found that with 3DCRT the delivery efficiency was improved with the isocentre placed at the centre of the PTV. This is due to the increased fluence of the FFF beam on the central axis relative to off-axis. This same improvement in delivery efficiency was not seen when delivering VMAT treatments. The impact of isocentre shifts on plan robustness was comparable for both 3DCRT and VMAT deliveries with both midline isocentres and isocentres within the PTV. This is likely a result of the profile shape of small fields delivered with FFF beams being comparable to those of cFF beams.

Breath-hold treatments provide the potential to reduce the volume of PTVs and therefore normal lung irradiation in lung SABR treatments. This technique increases treatment times when delivering with cFF beams to approximately 30mins when using IMRT. Boda-Heggemann et al. (2013) performed a study where 10MV FFF beams were used for the same technique. This reduced the delivery time for the beam to 8minutes and the treatment time to 15mins. This is a significant reduction in treatment time when compared to cFF IMRT. The use of 10MV FFF beams has the added advantage of increased dose-rate over 6MV FFF beams (2200MU/min compared to 1400MU/min). However, with 10MV FFF the build-up to maximum dose within the GTV would be deeper when compared to 6MV FFF potentially reducing coverage/efficacy.

The feasibility of planning FFF SABR to the liver was investigated by Reggiori et al. (2012b). The study looked at VMAT SABR delivering 75Gy in 3fractions using an unmatched 10MV FFF beam from a Varian TrueBeam. There was no statistically significant difference between the cFF and FFF plans in terms of plan quality. As with other FFF planning studies, the authors noted that an increased number of MU were required for the FFF plans. In this study the average increase in MU for FFF compared to cFF was 9%. Despite this increase of MU the beam-on time reduced

from 8.2minutes±1minute to 2.2minutes±0.2minutes (73%) for the FFF plans, this reduction is greater than the reduction of approximately 60% seen when treating lung SABR with 10MV FFF.

Another study looking at the optimal leaf margin around the PTV for liver SABR was performed by Ogata et al. (2017). This study also used 10MV cFF and FFF beams delivered with a TrueBeam and calculated with the Eclipse TPS version 11.0.31. The study used 7 to 9 coplanar 3DCRTbeams with leaf margins ranging from -3mm to +5mm and found that for a given leaf margin the dose distributions were comparable for both modes of delivery and OAR sparing was equivalent. The exception was that the FFF plans were less homogenous than the cFF plans but this is clinically acceptable for SABR deliveries. The author concluded that to deliver optimum plans a leaf margin of 0 or -1mm should be used. The authors did not report on the delivery times for this treatment and do not state why 3DCRT was used rather than VMAT when VMAT has been demonstrated to be superior for other SABR sites.

2.4.5. Treatment planning studies on other sites

Spruijt et al. (2013a) performed an investigation to determine if FFF beams could be used for the treatment of breast radiotherapy. The plans were produced to deliver 50Gy in 25 fractions to the whole breast PTV with an integrated boost region to receive 68.75Gy in 25 fractions. Plans were produced with the Eclipse TPS and version 8.9.08 for unmatched 10MV FFF and 10MV cFF beams delivered by a Varian TrueBeam linear accelerator. The study found that equivalent plan quality was delivered with both FFF and cFF beams. The out of field dose was found to be on average 10% lower for FFF beams. The treatment times were reduced by 31% for FFF beams compared to cFF but required twice the MU.

Kumar et al. (2017) investigated the effect of unmatched FFF beams at both 6MV and 10MV compared to cFF beams for cervix patients. The plans were delivered with a TrueBeam linear accelerator and planning using Eclipse version 10. Plans were normalised such that 95% of the PTV received 100% of the prescription dose. This differs from the protocols here that require 95% of the PTV to receive 95% of the prescription dose. This difference could result in plans with higher OAR doses and higher maximum doses within the PTV. The study found that all plans produced were clinically acceptable, but found the FFF plans inferior in terms of homogeneity, conformality and bladder and rectal OAR doses. The FFF plans were also found to require more MU, 20.5% for 6MV FFF and 43.7% for 10MV FFF, when compared to associated cFF plans. This increase in MU would be expected as more MU is required to deliver the same dose away from the central axis. With cervix plans typically treating large volumes this increase would be more

than for sites with smaller PTVs. The increased proportion with 10MV FFF is also expected as the profile is more peaked than the 6MV FFF profile increasing this off axis difference.

2.4.6. Summary of treatment planning study findings

Studies into the validation of the dose calculation algorithms through verification measurements have demonstrated that both unmatched and matched implementation of FFF beams can be modelled with sufficient accuracy for clinical use on the Eclipse and Monaco TPS. The majority of publications are studies relating to unmatched FFF beams with few studies into matched FFF beams. The studies of matched FFF beams have been matched to the TPR20/10 value of the associated cFF beams; this is not consistent with the final implementation of matched FFF beams that are matched to the percentage depth dose value at 10cm deep in water for a 10cm x 10cm field with an SSD of 100cm.

The conclusions with respect to the plan quality of FFF beams when compared to cFF beams are not consistent; this is the case for studies of the same sites with the same implementation of FFF beams and the same planning system. However, FFF beams have consistently demonstrated a requirement for more MU in order to deliver a plan compared to the associated cFF beam, this increase ranges from 9% to 34%. The increase is independent of whether the FFF beams are matched or unmatched and is a result of the reduction in dose delivered per MU as the distance from the central axis increases. This decreasing dose per MU is a result of the peaked profile shape of FFF beams. Despite this increase in MU it is noted that the treatment beam-on times are equivalent or shorter for FFF beams. With increasing MU the delivery times decrease such that for all hypofractionated treatments there is a reduction of beam on time of up to 70%.

2.5. Guidelines for FFF beams

The implementation of FFF beams by early adopters of the technology has preceded much of the now available guidance and recommendations. The American Association of Physicists in Medicine (AAPM) published their review of the current status of FFF beams in 2015 (Xiao et al., 2015). The UK Institution of Physics and Engineering in Medicine (IPEM) published their guidelines in 2016 (Budgell et al., 2016). Dosimetry protocols for determining the absorbed doses in radiotherapy have been set up for the use of cFF beams. The validity of these protocols for application to FFF beams has been reviewed by a number of authors (Budgell et al., 2016; de Prez et al., 2018; Lye et al., 2016). Lye et al. (2016) performed a Monte Carlo study and found differences of 0.2%. De Prez et al. (2018) performed measurements on an Elekta VersaHD linear accelerator and found the differences between the correction factors for cFF and FFF beams for

TPR20/10 based protocols to be less than 0.19% and for D10cm based protocols less than 0.42%. The results of both of these studies shows a similar magnitude to the k_{fff} correction factor proposed in Budgell et al. (2016) of 0.997 for the absorbed dose from FFF beams.

2.6. Summary of findings

This review of the literature has highlighted areas for investigation with respect to FFF beams, where necessary information required to underpin and optimise characterisation, quality assurance and clinical use of FFF beams is missing. The implementations that have been adopted by the two main manufacturers' means FFF beams are either unmatched or matched in beam quality to their equivalent cFF beam, such that an FFF beam of a given nominal (stated) energy has different properties depending on the machine it is delivered on. The potential advantages of FFF beams are highlighted in Table 1. Research work to characterise these differences is required and will form the basis of chapter 3 of this thesis.

The literature has highlighted that certain parameters used to characterise cFF radiotherapy beams are not suitable for FFF beams. Some work has been performed to determine new parameters for the characterisation of FFF beams. A study to determine parameters that can be used for both FFF and cFF beams is required and will form the basis of chapter 4 in this thesis.

A number of Monte Carlo studies have been performed on FFF beams, some of these studies have been performed on prototype machines that do not match the final implementation of FFF beams by the respective manufacturers. More recent studies on FFF machines have almost all been with respect to the Varian TrueBeam linear accelerator and have used a 'golden' phase space file provided by the manufacturer rather than being a full Monte Carlo simulation. There is a lack of studies in the literature of the matched FFF implementation by Elekta on the VersaHD linear accelerator and a Monte Carlo model of this implementation will be included in this work (chapter 5).

Since the clinical release of FFF, many studies have been performed on the use of FFF beams for clinical treatment. The majority of these studies correspond to the unmatched (Varian) implementation of FFF beams and systematic studies into the matched (Elekta) implementation are required. A range of relevant planning studies is presented in chapter 6.

Table 1: Potential advantages and disadvantages of FFF beams

Advantages of FFF beams	**Disadvantages of FFF beams**
Increased doserates from 600MU/min to 1400MU/min for 6MV FFF and 2400MU/min for 10MV FFF have the potential to reduce treatment times, especially for hypo fractionated treatments.	Treatment planning systems have been developed for use with cFF beams, do current assumptions still apply to modelling FFF beams?
Reduced spectral changes away from the central axis have the potential to improve modelling of FFF beams.	FFF profiles are non-uniform, does this require additional modulation and therefore increase treatment delivery times and reduce calculation accuracy?
With the removal of the flattening filter the beams are potentially more stable to symmetry changes.	Not all current QA metrics can be applied to FFF beams, can beams be quality assured without normalising to cFF beams or comparing to 'golden' datasets?
The removal of the flattening filter reduces the head leakage and head scatter with the potential to reduce peripheral doses and reduce incidences of secondary cancer induction.	

3. Characteristics of FFF beams

3.1. Introduction

With the increase in Intensity Modulated Radiotherapy (IMRT) treatments in radiotherapy there has been an improvement in treatment plan quality but often with an increase in treatment delivery time (Palma et al., 2008). This is due to the segmented treatment deliveries requiring more Monitor Units relative to conventional conformal planning techniques. The use of IMRT is not dependant on a flat beam profile, as the beam fluence can be modulated to the required distribution by the MLCs. The use of FFF beams is becoming more wide-spread as the increased dose-rate available through the removal of the flattening filter has been shown to reduce treatment delivery times whilst maintaining plan quality (Spruijt et al., 2013b; Mancosu et al., 2012; Reggiori et al., 2012a; Scorsetti et al., 2011; Vassiliev et al., 2007).

There have been a range of studies in the literature into the beam characteristics of FFF photon beams with comparison to cFF beams (Cashmore, 2008; Dalaryd et al., 2010; Georg et al., 2010; Kragl et al., 2009; Ponisch et al., 2006; Hrbacek et al., 2010; Kry et al., 2009; Kry et al., 2007b; Vassiliev et al., 2006b; Stathakis et al., 2009). At the time of this work, this was the first study of the beam characteristics of the final High Dose-Rate Mode (HDRM) configuration implemented by Elekta (Elekta AB, Stockholm, Sweden), where the FFF beams have been matched to the cFF beam by increasing the beam energy. The configuration includes a new filter plate design and is implemented on a Linac with an Agility MLC head. To 'match' the beam energies between FFF and cFF beams, requires tuning the accelerator parameters so that the percentage depth dose (PDD) matches the cFF beam at a depth of 10cm for a 10cm x 10cm field. For both cFF and matched FFF 6 MV beams, this PDD value is matched to within 1% of 67.5% at 10cm deep in water at an SSD of 100cm. Existing literature on FFF characteristics largely relates to the Varian TrueBeam accelerators that implement FFF beams in an 'unmatched' mode, whereby FFF beams are produced by removing the flattening filter without any subsequent change in beam energy or PDD matching (Ponisch et al., 2006; Hrbacek et al., 2010; Kry et al., 2009; Kry et al., 2007b; Vassiliev et al., 2006b; Stathakis et al., 2009). There is some work by Kragl et al. (2009) that has considered FFF beams on Elekta machines matching the TPR20/10 value to the associated cFF beam. The work presented here compares matched (energy tuned) FFF beams (Elekta implementation) to cFF beams and unmatched FFF beams (FFF beams produced by removing the flattening filter but without any further changes to the accelerating parameters, equivalent to the Varian implementation). The comparison with the unmatched FFF beam seeks to examine the differences between the two implementations of FFF beams.

3.2. Method

3.2.1. Implementation

All work was carried out as part of a pilot implementation project. An Elekta Synergy linear accelerator with Agility MLC was modified to enable FFF deliveries. This involved: an update to the Synergy control system to Integrity v3.1; installation of a new dose control card to allow dose rates of up to 2200MU per min; and replacement of the conical flattening filter with a flat disk made of 2mm thick stainless steel. The disk is designed to remove electron contamination and produce sufficient secondary electrons for the monitor chamber to function consistently.

For an 'unmatched' FFF beam, no additional tuning or modification of the beam properties were made in that the same power conditions for the magnetron and waveguide were used as for the cFF beam and the current through the slalom bending magnet system was also left unchanged. This would be consistent with the methodology to produce an FFF beam reported by others (Georg et al., 2011; Hrbacek et al., 2010; Georg et al., 2010; Kragl et al., 2009; Cashmore, 2008; Vassiliev et al., 2006b; Ponisch et al., 2006) and the same as the final implementation of FFF beams on Varian TrueBeam Linacs. However, the Elekta implementation (now commercially available on the Versa HD) supports energy tuning of the beam, by alteration of the power conditions and gun current to increase the mean electron energy incident on the target and changing the bending magnet currents to adjust the electron energy selection window. Therefore, these parameters were modified so that the resulting PDD of the matched FFF beam was matched to within 1% at 10cm deep in water in a 10cm x 10cm field at 100cm source to surface distance (SSD) to the standard cFF beam. International dosimetry protocols such as AAPM TG-51 (Almond et al., 1999) use 10cm deep as a reference point for calibration. It was therefore decided to use this specific reference for the point of beam matching.

The nominal energies used in this study are 6MV and 10MV. The 'unmatched' beams were set up on the Elekta Synergy Linac by keeping the accelerator parameters the same as for the cFF beam. Typical central axis dose rates increase from 580cGy/min at the isocentre for the cFF beam to 1300 cGy/min for the FFF 6MV (6MV FFF) and 2000cGy/min for the FFF 10 MV (10MV FFF) beam. The bending coarse, bending fine and gun current values for the energy selection of the beams are shown in Table 2, power conditions were fully optimised for each accelerating potential. Bending course adjusts the bending current across all the slalom magnets of the Linac head and, bending fine controls current through the final magnet of the slalom system, the relationship between these two parameters affects the focusing of the electron beam once

through the slalom onto the target. The removal of the flattening filter results in an increased dose per pulse for both FFF beams compared with cFF beams.

Table 2: Bending magnet and gun current values for the beams studied

	Energy			
	6MV/6MV 'unmatched' FFF	6MV 'matched' FFF	10MV/10MV 'unmatched' FFF	10MV 'matched' FFF
Bending coarse	41	48	62	71
Bending fine	1.95	2.30	3.2	2.8
Gun current	7.39/7.32	7.20	7.09/7.01	6.90

3.2.2. Profiles and PDDs

Profiles and PDDs were measured at an SSD of 100cm using an MP3-M plotting tank (PTW GmbH, Freiburg, Germany). A 60008 photon diode (PTW GmbH, Freiburg, Germany) was used for profile measurements as it has a small sensitive volume with circular diameter of 1mm and thickness 2.5µm that can be used for high resolution scans and minimise the gradient effect across the active region. A 31010 semiflex ion chamber (PTW GmbH, Freiburg, Germany) was used for PDD measurements as it has a small collection volume of 0.125cc and does not over respond to scatter with depth, as the photon diode can. The over response is a result of the mass energy absorption coefficient increasing dramatically for silicon (the active component of the diode) relative to water at low photon energies. The profiles used for penumbra measurements were obtained with a resolution of 0.1mm in the penumbral region so that the inflection point of the profiles could be accurately determined with a function developed in Mathworks MATLAB 2010b. The function used applies a Canny edge detection algorithm to find the inflection point. The Canny function was used as it smooths the data with a Gaussian function to remove noise from the profile. With sufficiently long dwell times at each measurement point this results in few false inflection points being determined. The code written then allows the user to visualise the locations of the inflection points, discount the false inflection points and select the correct points. Once the function has determined the inflection points the penumbras are determined using the normalisation method proposed by Ponisch et al. (2006) (Equation 3). This method involves normalising the FFF profiles against the cFF profiles at the inflection points and the 80% to 20% of the normalisation dose is used for the penumbra measurements. Profiles were obtained at depths of dmax (1.5cm for 6MV, 2.2cm for 10MV), 5.0cm, 10.0cm, 15.0cm and

20.0cm for square field sizes of 3cm x 3cm, 5cm x 5cm, 10cm x 10cm, 15cm x 15cm, 20cm x 20cm, 25cm x 25cm, 30cm x 30cm and 40cm x 40cm the largest field size available for the Agility head.

For the same range of field sizes a central axis PDD with a depth-resolution of 1mm down to a depth of 25cm was obtained to investigate the effect of field size on the PDD. The PDD at the depth of D_{max}, 10cm and 20cm were compared over the same field sizes as the profiles and the three beam types.

3.2.3. Output Factors

Output factors were measured using the PTW water tank and a semiflex 0.125cc ion chamber for the same field sizes as the profiles and PDDs for 5cm x 5cm and larger, and a photon diode for field sizes of 4cm x 4cm and smaller. Both detectors were used for the 5cm x 5cm field so that the response of the two detectors could be normalised. The measurements were performed at 100cm focus to surface distance (FSD) and a depth of 10cm. This is consistent with the measurement geometry required for commissioning the beam data of a Monaco treatment planning system (Elekta AB, Sweden).

3.2.4. Head leakage

Head leakage values at 1m from the X-ray source are required to be below 0.1% of the value of an open 10cm x 10cm field at 100SSD.The head leakage is measured as one part of the radiation protection critical examination of a linear accelerator installation. Leakage measurements were performed using a 23332 rigid stem 0.6cc ionisation chamber (PTW GmbH, Freiburg, Germany) operating at a potential of 300V, with the supplied Perspex build-up cap. The head leakage measurements were performed at the locations specified in the IEC documentation (IEC, 1998). Leakage measurements were performed in the patient plane at 1 metre distance from the target (Figure 6) and in the other conventional planes around the accelerator head at the same distances from the electron and photon beam central axes (Figure 7), with the linear accelerator operating in FFF mode. The measurements performed were for a 1000MU delivery with the MLC in a closed position.

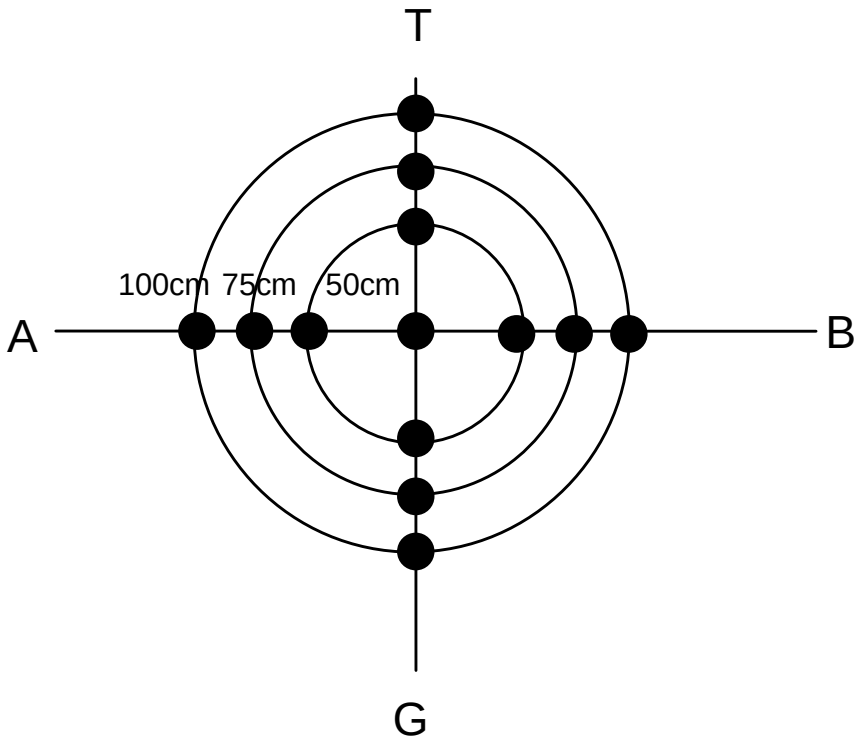

Figure 6: Positions for the measurements in the patient plane. Circles represent a constant radius from the isocentric position

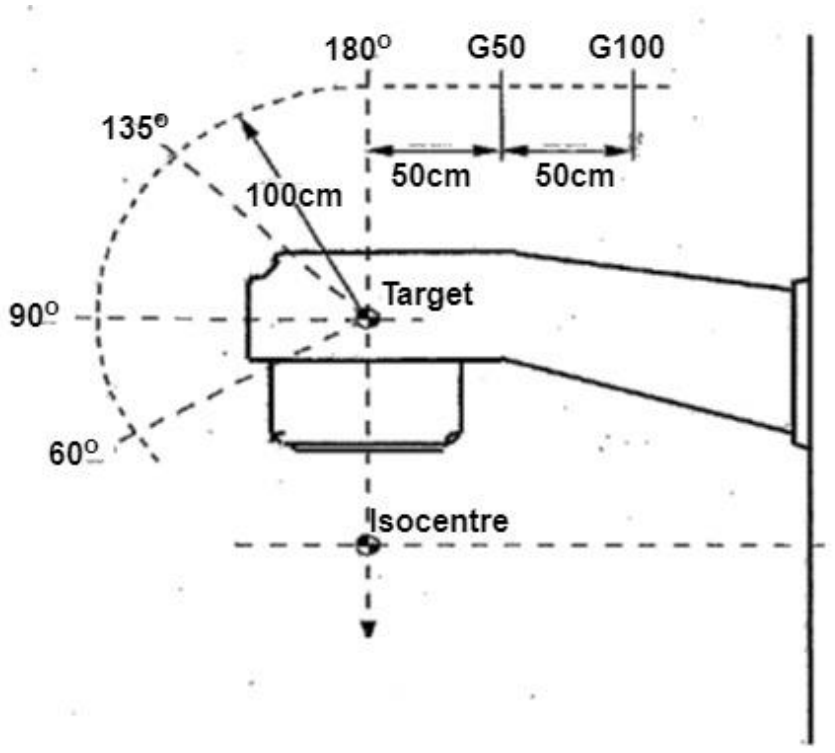

Figure 7: Positions for the non-patient plane leakage measurements.

The reading recorded at each of the positions was expressed as a percentage of the reading obtained at the isocentric position of a 10cm x 10cm reference field.

3.2.5. Radiation Protection

Radiation protection measurements on the leakage through primary and secondary barriers are performed as part of the critical exam of all Linacs. A number of measurements were performed to determine the dose-rate beyond the primary and secondary barriers and the dose-rate through the maze. The locations for the dose-rate measurements are depicted in Figure 8 by dots.

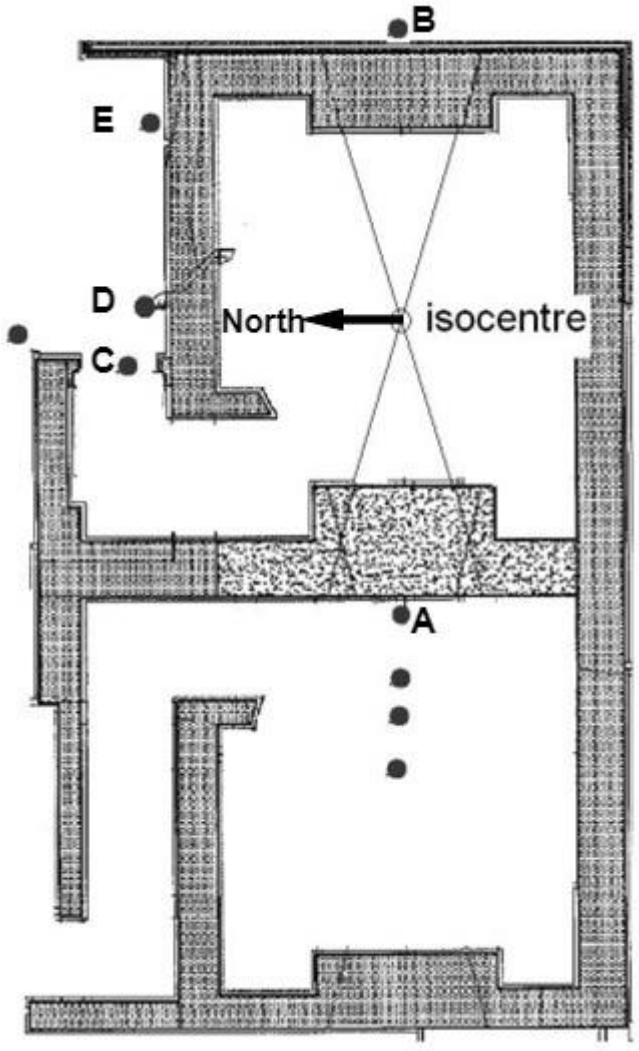

Figure 8: Barrier doserate measurement positions

The accelerator bunker was designed to a specification to contain a linear accelerator delivering a maximum photon energy of 15MV. Dose constraints are, as specified by UK Ionising Radiation

Regulations (2017) (Health and Safety Executive, 2018), to be within 1mSv per year for staff working with radiation and 0.3mSv per year for members of the public. The room was designed with the (North) side wall primary barrier constructed from 1.7m thick high-density concrete (magnetite, 3.8g/cm^3) and the (South) side wall primary barrier constructed from 2.5m thick standard concrete (density 2.35g/cm^3). The north side barrier was designed so that the instantaneous dose rate beyond the barrier would be less than 7.5µSv/hr, the requirement for an area to not be designated as controlled. The south side wall is adjacent to a second bunker, designated as a controlled radiation area allowing an instantaneous doserate of over 7.5µSv/hr. The instantaneous dose rate beyond the south side primary barrier, inside the adjacent bunker, was designed to be within 11.3µSv/hr (the specification of the room). Instantaneous dose rate in all other areas beyond the bunker is designed to be less than 7.5µSv/hr in line with recommended national guidelines (Health and Safety Executive, 2018).

Measurements were performed with a 40cm x 40cm field (the largest available) at the highest dose-rate available for the selected beam, with the gantry and collimator angles selected in order to maximise the dose-rate in each case. For all measurements, except the primary barrier, a 30cm x 30cm phantom of solid water was positioned at isocentre and used to simulate patient scatter. The dose-rate was measured with a Thermo Scientiffic SmartION Survey Meter MINI 2120 (Thermo Fischer Scientiffic, Waltham, USA) calibrated against Cs-137.

3.3. Results

3.3.1. Profiles

The inhomogeneity in an FFF beam varies as the nominal energy of the beam changes, with a higher energy beam having a more pronounced peak. The change in profiles for a 10cm x 10cm field with varying energy is shown in Figure 9, each profile has been normalised to the inflection point.

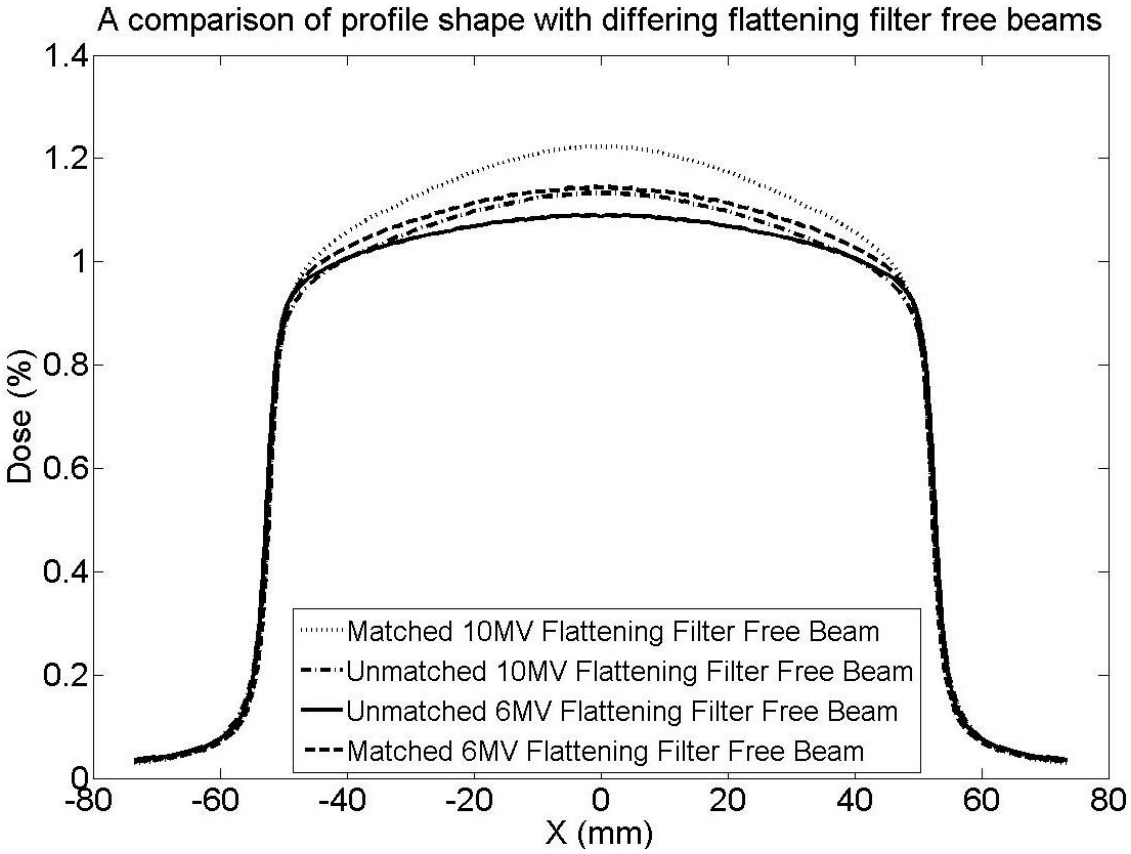

Figure 9: A comparison of profile shape with differing beam energies for a 10cm x 10cm field at 100cm SSD measured at a depth of maximum dose in water.

The inhomogeneity of the forward-peaked radiation is also a function of field size with the amplitude of the forward peaking increasing with greater field size. This effect is more pronounced with FFF beams with higher energy. Thus the shape of the FFF profile is less consistent with field size than the case for the equivalent cFF beam (Figure 10). The matched FFF beams are more forward peaked than the FFF beams without matching.

With FFF beams, there is less variation of beam quality across the beam with depth in water when compared to the differential hardening produced across the cFF beam profiles by the flattening filter. Thus, the shape of the profile with depth is more consistent for FFF beams than cFF beams (Figure 11). No significant difference was noted between the behaviour of the profiles of the matched and unmatched FFF beams as depth was changed.

The change in penumbra between an FFF beam and the equivalent cFF beam was found to be negligible when using the method proposed by Ponisch et al. (2006). This can be seen in Figure 12. The penumbra measured was the same within the experimental error of ±0.4mm for the 3 modes of operation.

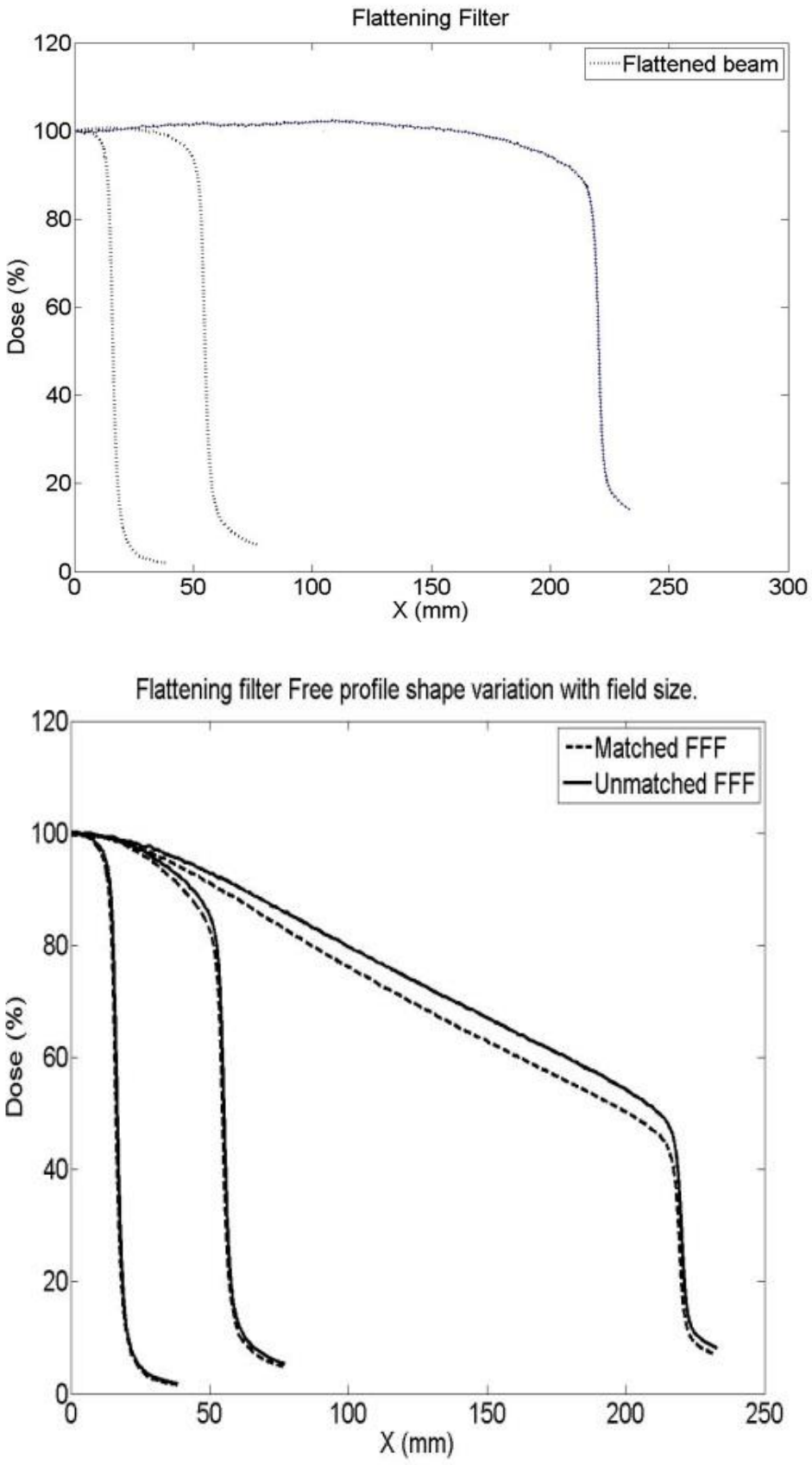

Figure 10: A comparison of the change in profile shape with increasing field size for 6MV cFF (above) and FFF (below) beams at 100cm SSD and a depth of 10cm in water.

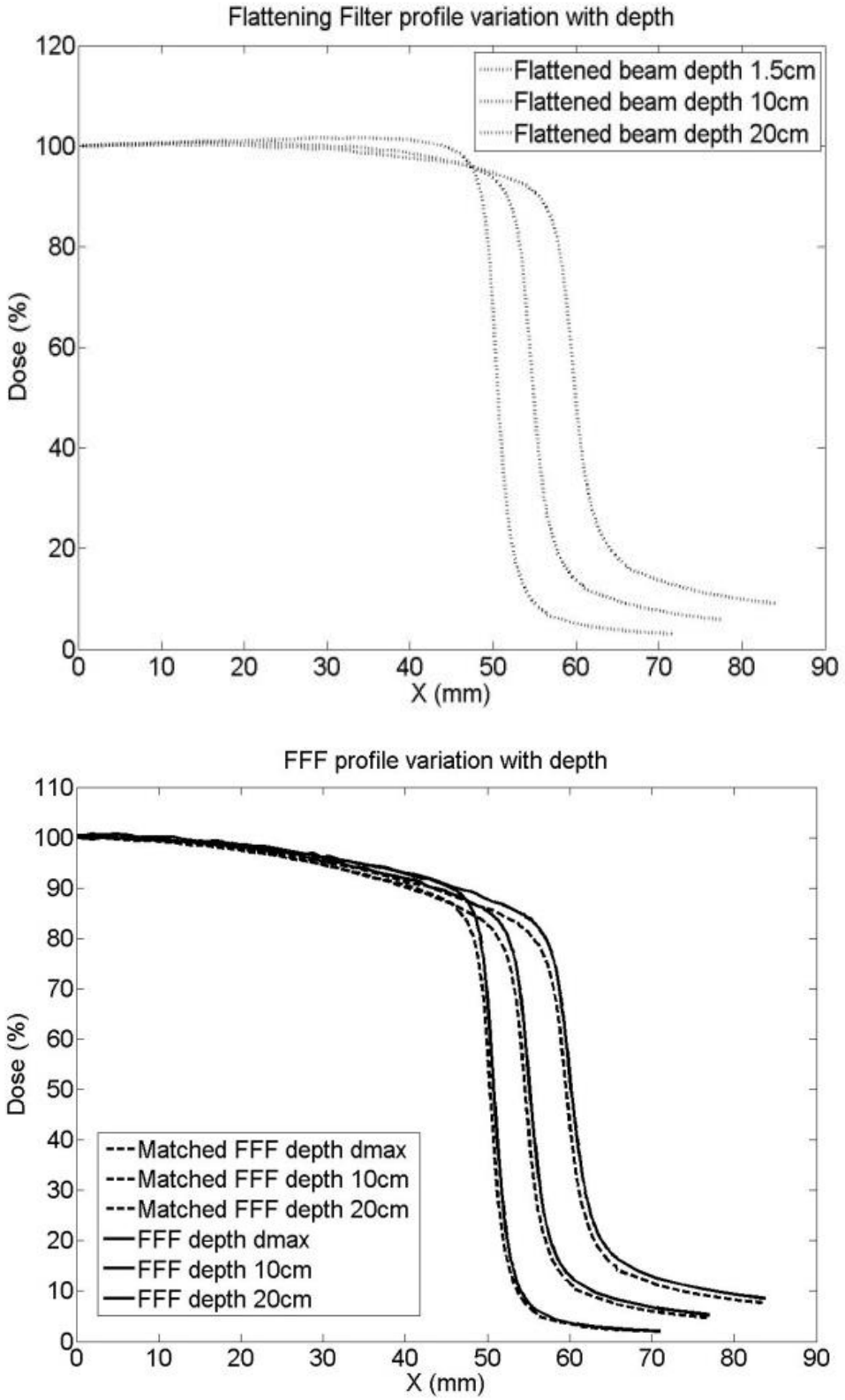

Figure 11: A comparison of the change of profile shape with varying depth in water (1.5cm, 10cm, 20cm) for 6MV cFF (above) and FFF (below) beams at 100cm SSD with a field size of 10cm x 10cm.

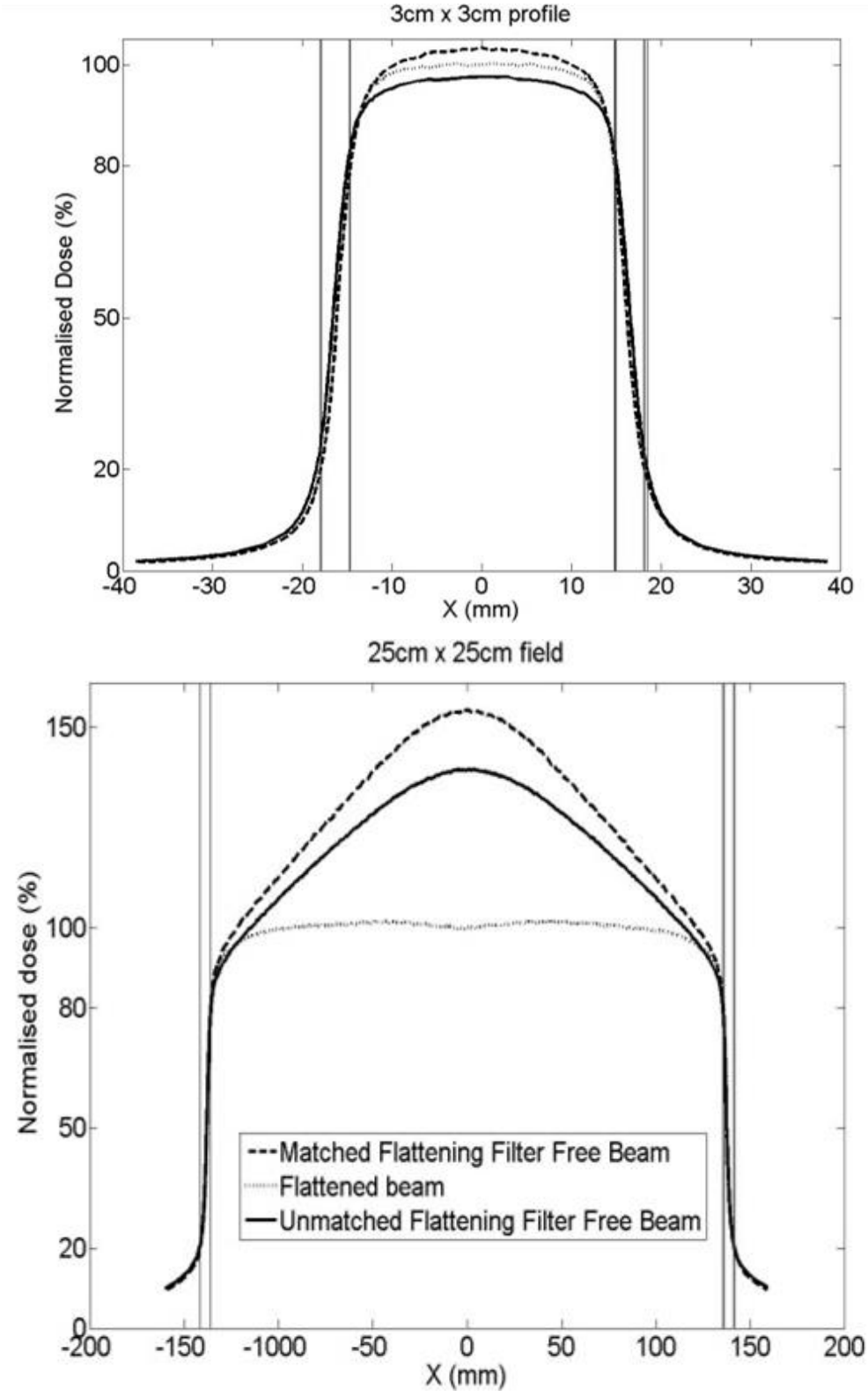

Figure 12: A comparison of the penumbra for 6MV beams taken at 100cm SSD and a deth of maximum dose. The 3cm x 3cm fields (above) the measured penumbra was 2.7mm for each mode and for the 25cm x 25cm field (below) the penumbra was 3.1mm for each mode.

3.3.2. PDDs

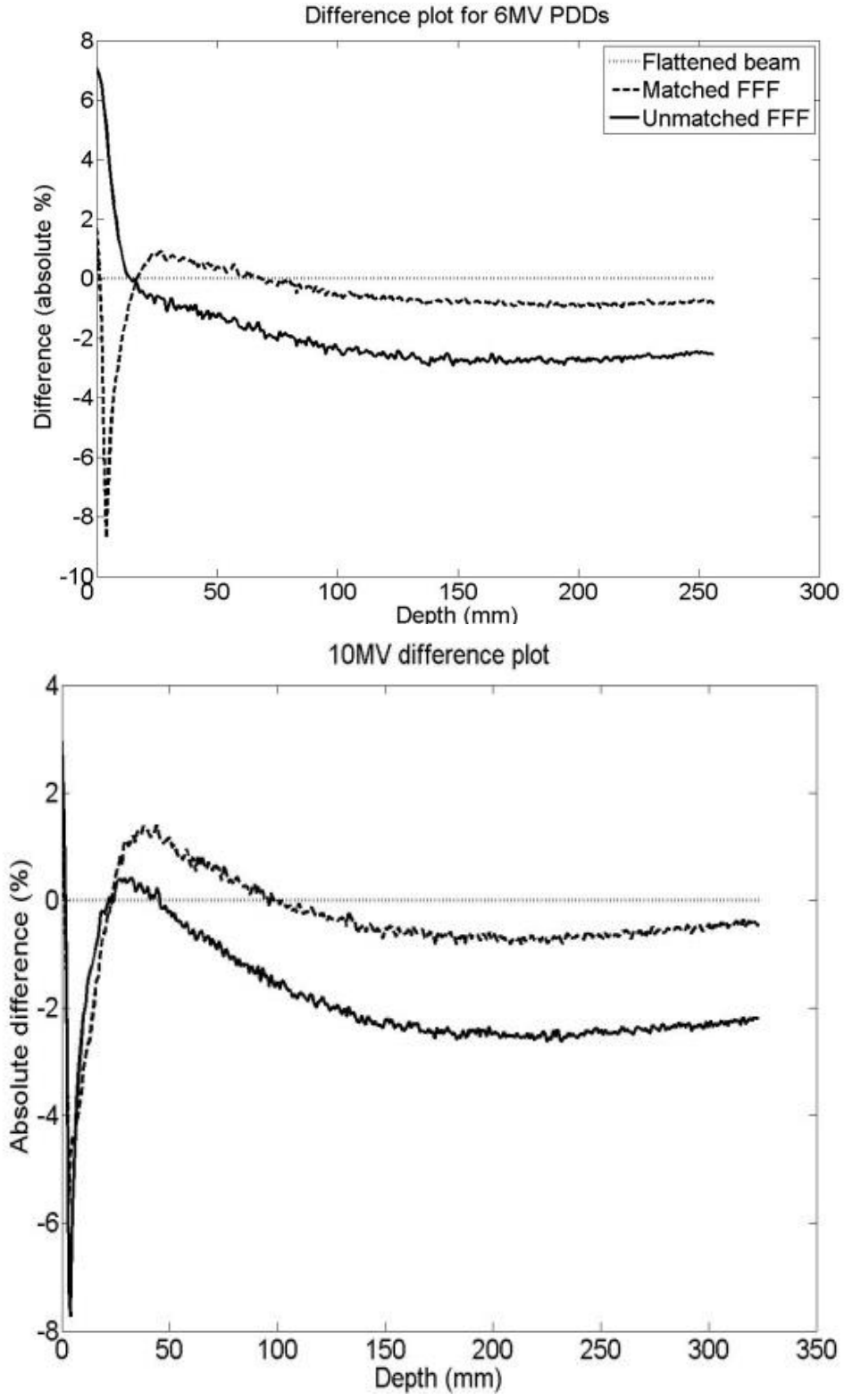

Figure 13: 6MV (above) and 10MV (below) PDD difference plots for matched flattening filter free (dashed) and unmatched flattening filter free (solid) compared to the associated (reference) cFF beam (dotted) measured at 100cm SSD.

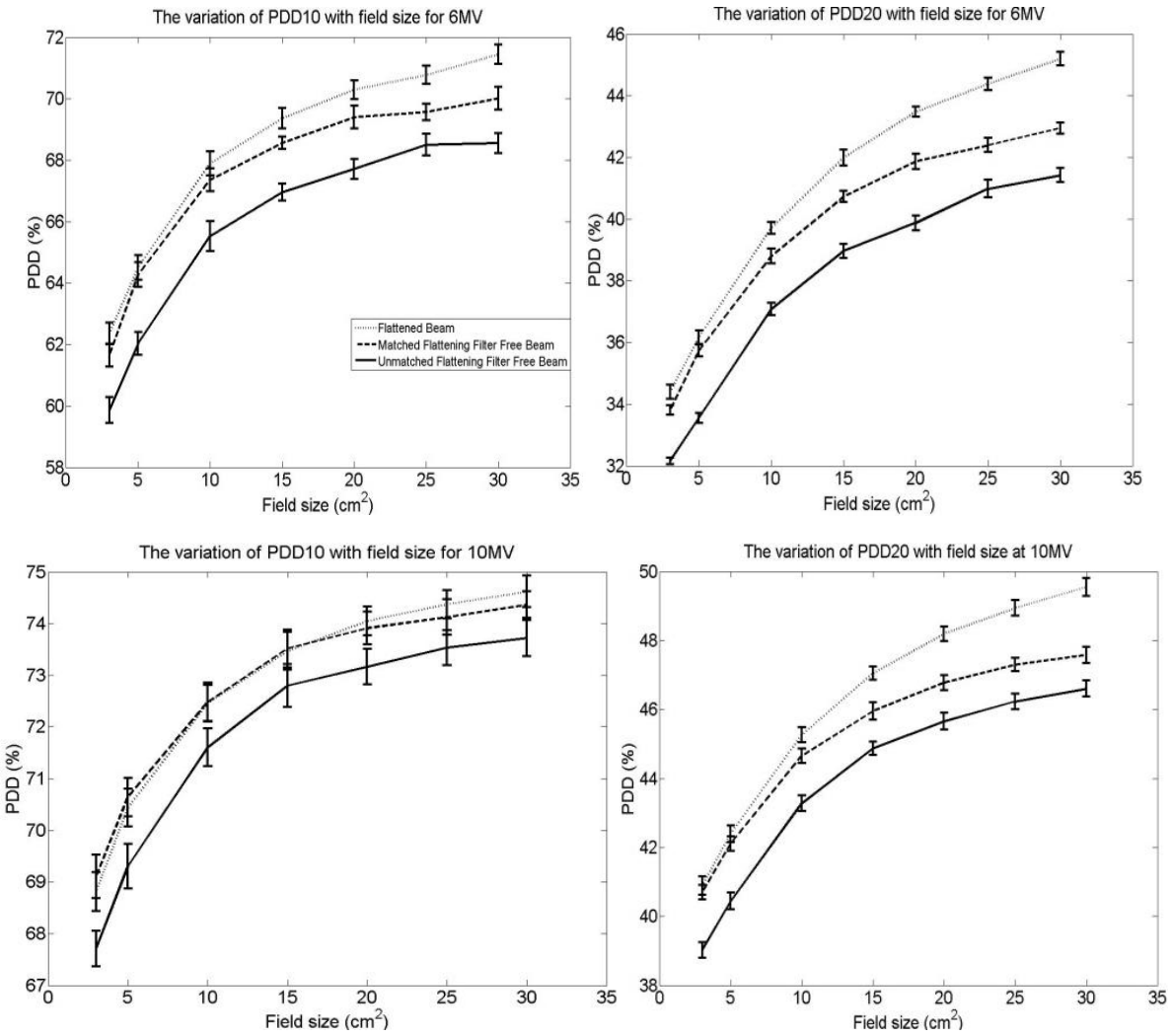

Figure 14: The variation of PDD10 (left) and PDD20 (right) for field sizes of 3cm x 3cm to 30cm x 30cm at 100cm SSD. 6MV (above) 10MV (below)

The effect on the PDD of removing a flattening filter is to increase the quantity of low energy photons in the spectrum, as compared to the equivalent cFF beam. This effect is especially prevalent on the central axis due to the removal of the attenuation caused by the flattening filter, which results in the unmatched FFF beams having a PDD resembling that of a 4MV cFF beam. Matching the FFF beam at 10cm results in the PDD becoming more comparable to the associated cFF beam (Figure 13). The change in PDD between the matched and unmatched FFF beams with respect to field size and energy is shown in Figure 14. The depth of maximum dose is more constant with field size for FFF beams due to the reduction in head scatter compared to cFF beams, which results in the depth of maximum dose being deeper for a matched FFF beam than that of a cFF beam for field sizes greater than 10cm x 10cm. The variation of PDD10 and PDD20 is reduced with FFF beams compared with cFF beams for both 6MV and 10MV beams (Figure 14).

3.3.3. Output Factors

The output factors are shown in Figure 15 and vary less with field size for both types of FFF beams when compared to the cFF beams. This is due to the reduction in head scatter with the removal of the flattening filter, which is the dominant source of this variation. The output factors are expressed in MU/cGy as is the protocol at this institute.

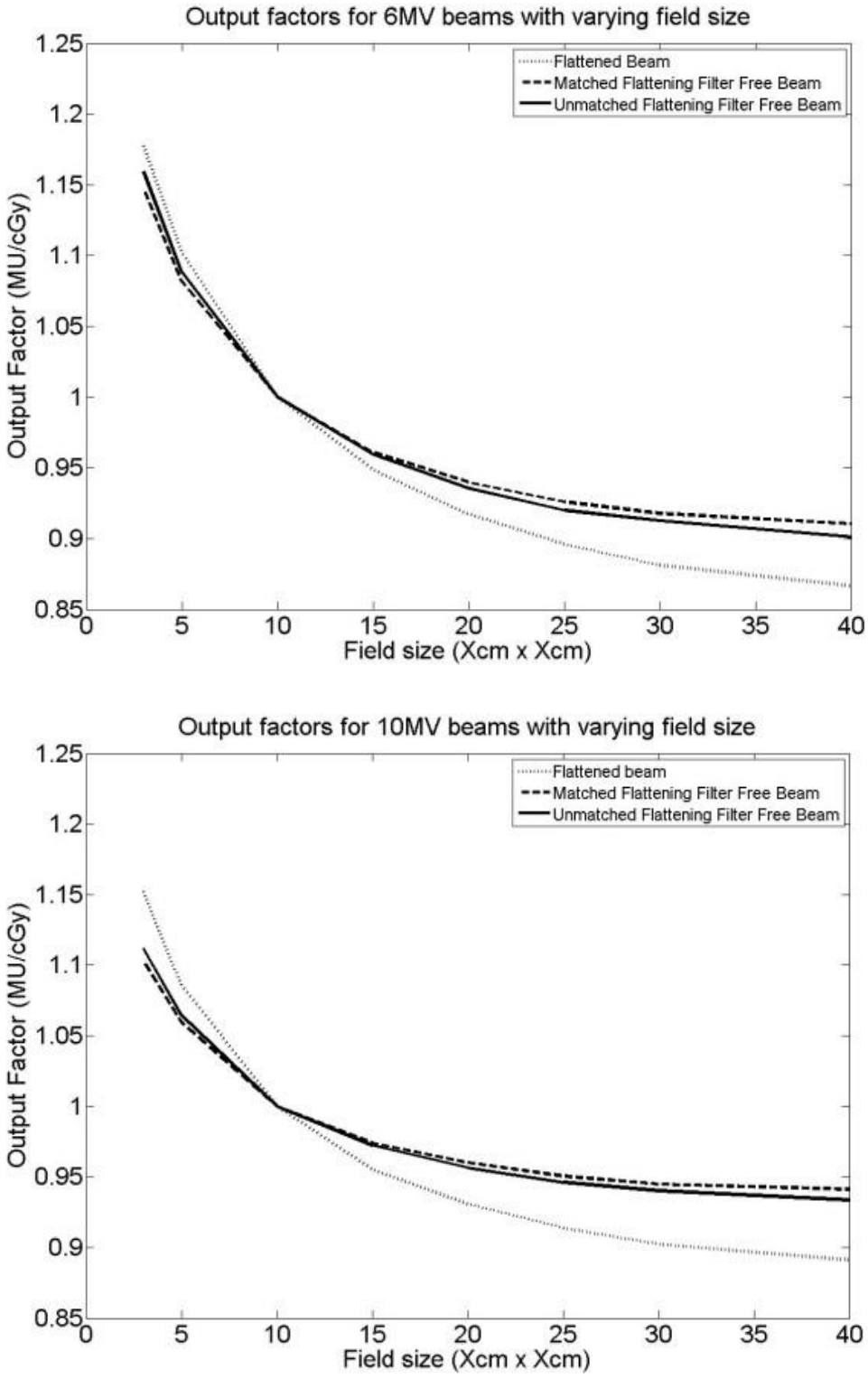

Figure 15: Output factors at 100cm SSD and 10 cm deep in water with varying field size for 6MV (above) and 10MV (below) beams for cFF, matched flattening filter free and unmatched flattening filter free modalities.

3.3.5. Head leakage

The removal of the flattening filter as a dominant source of scatter has a major effect on the leakage through the treatment head. A reduction of at least 50% in leakage radiation is measured for both the patient plane beyond 50cm and the non-patient plane. This reduction is consistent for FFF beams both with and without matching (Table 3).

3.3.6. Radiation Protection

The environmental survey of the areas surrounding the Linac bunker demonstrates that the dose-rate through the primary barrier increases more than two-fold when operating the linear accelerator in FFF mode. The changes in measured values did not change the designation of any area within the UK radiation protection legislation requirements at this centre, or require any changes in practical protection measures. At the primary barriers for the 6MV FFF and the 10MV 'unmatched' FFF beams, the increase in instantaneous dose-rate is less than the proportional increased output of the machine. For the 10MV matched FFF the increase in instantaneous dose-rate is greater than the proportional increased output of the machine (Table 4). For the secondary barriers the increased dose-rate is less than proportional to the output from the machine for all modes.

Table 3: Leakage measurements for 3 modes of operation, Flattening Filter (cFF), Unmatched Flattening Filter Free (UFFF) and Energy Matched Flattening Filter Free (MFFF), in patient and non patient planes (expressed as a % of an open 10cm x 10cm beam).

Energy	Circle radius/cm	Target direction			Gun direction			Cross plane B			Cross plane A		
		cFF	UFFF	MFFF	cFF	UFFF	MFFF	cFF	UFFF	MFFF	cFF	UFFF	MFFF
6MV	50	0.009	0.004	0.003	0.018	0.01	0.009	0.014	0.007	0.006	0.015	0.007	0.006
	75	0.008	0.003	0.003	0.028	0.011	0.009	0.015	0.008	0.006	0.016	0.007	0.006
	100	0.008	0.003	0.003				0.018	0.011	0.008	0.015	0.007	0.005

Energy	Circle radius/cm	Target direction			Gun direction			Cross plane B			Cross plane A		
		cFF	UFFF	MFFF	cFF	UFFF	MFFF	cFF	UFFF	MFFF	cFF	UFFF	MFFF
10MV	50	0.014	0.006	0.006	0.036	0.013	0.013	0.023	0.009	0.009	0.024	0.009	0.009
	75	0.01	0.003	0.003	0.04	0.012	0.011	0.023	0.008	0.007	0.023	0.007	0.007
	100	0.01	0.003	0.003				0.028	0.009	0.009	0.023	0.006	0.006

6MV	60°	90°	135°	180°	G50	G100	10MV	60°	90°	135°	180°	G50	G100
cFF	0.034	0.026	0.03	0.034	0.025	0.015	cFF	0.019	0.022	0.024	0.038	0.031	0.018
UFFF	0.011	0.006	0.007	0.013	0.011	0.006	UFFF	0.01	0.011	0.014	0.018	0.013	0.007
MFFF	0.011	0.006	0.007	0.011	0.008	0.004	MFFF	0.01	0.01	0.014	0.015	0.01	0.005

Table 4: Doserate survey results from around the FFF linear accelerator bunker for Flattening Filter (cFF), Unmatched Flattening Filter Free (UFFF) and Energy Matched Flattening Filter Free (MFFF)

Energy	Output cGy/min	Dose-rate µSv/hr					
		(A) Primary barrier (LA01)	(B) Primary Barrier Outside Walkway (G90)	Primary Barrier Ceiling - Plant room B1 (G180)	(C) Door - floor level (G270 + phantom)	(D) Dosimetry Cable "rat hole". (G270 + phantom)	(E) Changing room (G270 + phantom)
6MV cFF	580	0.2			1.7	0.4	
6MV MFFF	1400	0.2			2.9	1.1	0.1
6MV UFFF	1300	0.2			2.7	1.1	
10MV cFF	505	1.7			1.4	0.2	
10MV MFFF	2000	(i) Wall 8.8 (ii)1m from wall 3.9 (iii) 2m from wall 2.7 (iv) Iso 1.7	0.1	0	2.6	1.3	0.1
10MV UFFF	1400	3.7			2.7	1.1	

3.4. Discussion

The general findings are consistent with those of other authors (Ponisch et al., 2006; Cashmore, 2008; Kragl et al., 2009; Georg et al., 2010) when comparing cFF beams to FFF beams without matching. The major difference for the matched FFF modality is that the increase in beam energy has no detrimental effect on the previously reported beneficial effects of FFF beams such as an increased dose-rate of up to 4 times that of a cFF beam to reduce treatment times, less beam shape variation with depth and a reduction of treatment head leakage by approximately 50%.

For these matched beams, the increase of beam energy produces a PDD more similar to the equivalent cFF beam, potentially making the transition from a cFF beam to a FFF beam more consistent with current clinical practice. This increase in energy also has the potential to reduce local scatter around the periphery of the target volume, which may have a clinical effect, as 50% of radiation induced secondary cancers are reported to occur in the region from 2.5cm within the PTV to 5cm outside of the PTV (Dorr and Herrmann, 2002).

Differences in forward bias of the FFF modalities are a direct result of the forward bias of the bremsstrahlung production in the target in order to conserve momentum, now not mitigated by the flattening filter. The forward peaking increases with increasing beam energy and so a change in beam energy could be inferred from the change in the magnitude of the beam peak. Further work should be performed to determine the validity of this as a measure of beam energy.

The penumbra measured using the normalisation method proposed by Ponisch et al. (2006) demonstrated that there was no major difference between the cFF and both FFF modalities. This method measured penumbra with an error of ± 0.4 mm demonstrating its suitability for clinical use. The method requires that both cFF and FFF beam profiles are taken in order to determine the penumbra of an FFF beam. Fogliata et al. (2012b) proposed a method for profile normalisation on Varian TrueBeam accelerators that would not require the use of the inflection point but instead used empirically derived factors verified over 3 TrueBeam machines and later produced information for the use on Elekta Linacs (Fogliata et al., 2016a). A number of other FFF beam parameters were discussed including symmetry, unflatness and slope parameters. Further investigation into penumbra specification and measurement that is independent of cFF beams is required for FFF beams; as future Linacs may not have the option of a cFF beam such as for the Elekta MRI Linac (Smit et al., 2014).

The FFF beams operated at a maximum pulse repetition frequency of 400Hz. This corresponds to an interval of 2.5ms between pulses. This differs from the Varian TrueBeam which has a pulse interval of 2.8ms and drops a pulse every 4-5 pulses (Lang et al., 2012a). The maximum dose per pulse (DPP) for the Elekta FFF beams was 0.83mGy/pulse. The variation in ion collection efficiency over the range of DPP was <1% for the semiflex ion chamber and is therefore acceptable for relative measurements (Lang et al., 2012a; Budgell et al., 2016).

The difference in the PDD for cFF and unmatched FFF beams is noticeable due to the increased proportion of low energy photons along the central axis of the beam. This reduces the effective energy of the beam and may result in reduced plan quality for treatment sites located at depth in the patient. The matched FFF beam differs from the cFF beam less in terms of PDD, and would be expected to produce similar dose distributions at depth to the cFF beam in a homogeneous

medium. The depth of maximum dose is shallower for the FFF beam than for the equivalent cFF beam, but varies less with field size, e.g. by 1mm over the range of field sizes measured for the FFF beams and 5mm for the cFF beam. The variation of the PDD at 10cm and 20cm in water varies less with field size for the FFF beams than the cFF beams, with the difference between the two FFF modalities over the range of field sizes being within the experimental error. The PDD changes less with increasing field size for FFF beams as a result of the reduction in head scatter compared to the cFF beam. The reduced variation of output factor over a range of field sizes may serve to simplify planning system calculations. The effect of this on plan accuracy will be investigated further in future work.

The head leakage when operating the linear accelerator in FFF modes is reduced by >50% compared to a cFF beam, the difference between the beams with and without matching was within experimental error and demonstrates that the reduction in head leakage is as a result of the removal of the flattening filter, the dominant source of such scatter. This agrees with the finding of other authors with respect to 'unmatched' FFF beams (Cashmore, 2008). The increased energy of the matched beam did not result in a higher proportion of leakage radiation when compared to the FFF beam without matching. The reduction in head leakage has the potential to reduce the amount of out of field dose received by the patient, providing that the modulation for FFF beams does not counter this. Further studies are required to determine the number of monitor units required to deliver a comparable plan with a FFF beam when compared to a cFF beam. FFF beams demonstrate a reduction in head leakage and collimator scatter but can contain more low energy photons than cFF beams, thereby increasing the phantom scatter. This effect has been modelled by Kry et al. (2010) for unmatched FFF beams, showing an increased dose in the region of 3cm - 15cm out of field. The matching of an FFF beam would increase the average energy of the beam potentially reducing this effect. This again requires further work.

The radiation protection measurements of the dose-rates through the primary and secondary barriers demonstrated that the increase in MU/min for the FFF beam results in an increase in dose-rate through the barriers. For both of the 6MV FFF beams and the unmatched 10MV FFF beam the increase was less than the proportional increased output of the machine. This is due to the softer spectrum of the FFF beams resulting in a greater degree of relative attenuation through the barrier. For the matched 10MV FFF beam the increase was more than the proportional output. This is due to the tuning of the beam requiring the maximum photon energy produced to be approximately 13MV, close to the 15MV cFF category of the barrier. These results are not in agreement with Kry et al. (2009) who performed a Monte Carlo study and concluded that less shielding would be required for a linear accelerator delivering only FFF

beams. The difference in conclusion is due to the differences in radiation protection guidelines between the countries of the two authors. In the United Kingdom a threshold instantaneous dose-rate is also used whereas Kry et al. (2009) has used the time averaged dose-rate, assuming no increase in machine workload would result from the use of FFF beams.

The change in profile shape with field size demonstrates how FFF beams could be used clinically. For field sizes < 5 cm x 5 cm, the beam profiles are relatively flat and there is little variation in profile shape with field size. These fields could be used in a similar manner to conventional 3D conformal therapy (3DCRT) fields when the beams are on the central axis. With the benefit of increased dose-rate from FFF beams, these smaller beams offer potential in reducing the treatment time required for SABR (Georg et al., 2011; Lang et al., 2013; Fu et al., 2004).

For larger field sizes the expectation is that the beam would have to be modulated to achieve the desired dose distribution. A number of authors have performed studies on the treatment of prostate and larger head and neck target volumes with the majority concluding that a decrease in treatment delivery time is achievable with at least comparable plan quality when using unmatched FFF beams (Spruijt et al., 2013b; Mancosu et al., 2012; Reggiori et al., 2012a; Scorsetti et al., 2011; Vassiliev et al., 2007). Lechner et al. (2013) performed a planning study on an Elekta Synergy platform with an MLCi head and FFF capability. This study concluded that a decrease in treatment time was achievable when delivering prostate and head and neck treatments with IMRT but that the delivery time increased for VMAT deliveries. Further studies are required to determine if the increased leaf speed of the Agility head would be able to decrease delivery time with VMAT delivery on matched FFF beams.

The differences in profile shape and relative off-axis softening for FFF beams compared to conventional cFF beams may cause difficulties in modelling FFF beams in treatment planning systems, as several assumptions in beam modelling algorithms would no longer be relevant (e.g. scatter kernels). The reduced variation of the profile shape with depth has the possibility to simplify dose calculations; the impact of the shape change of profiles and the dosimetric accuracy of planning systems requires further investigation.

3.5. Conclusion

The purpose of this chapter was to answer the research question “What are the properties of FFF beams and do these properties differ between the two implementations?” this has been achieved and the conclusion is summarised below;

The matching of an FFF beam to a cFF beam at a depth of 10cm in water by increasing the FFF beam energy does not reduce any of the reported benefits of FFF beams. Conversely, there are

a number of benefits resulting from matching the FFF beam, e.g. the depth of maximum dose is located deeper and the beam quality and penetration more closely resemble the cFF beams currently used in clinical practice, making dose distributions in water more alike. Highlighted in this work is the fact that some conventional specifications and methods for measurement of beam parameters such as penumbra are not relevant and further work is required to address this situation with respect to 'matched' FFF beams and to determine methods of measurement that are not reliant on an associated cFF beam.

4. Characterisation of FFF beam properties for initial beam set-up and routine QA, independent of Flattened Beams

4.1. Introduction

The use of FFF beams has become more prevalent in clinical treatment delivery following the commercial availability of Linacs fitted with both conventional flattened (cFF) and FFF beam energies. For the VersaHD FFF implementation (Elekta AB, Sweden), the beam energy is retuned so that the Percentage Depth Dose (PDD) at 10cm deep in water, for a 10 cm x 10 cm beam, is matched to that of the associated cFF beam energy matched FFF beam (Paynter et al., 2014). This ability to adjust the PDD means that it is possible to both energy match the FFF beam to the cFF beam and also match the beams across a group of Linacs. This can improve service continuity and patient management in the event of planned or unplanned equipment down-time in a centre with multiple FFF enabled Linacs.

In order to use a single beam energy model for multiple Linacs, a process to match beam data across the Linacs is required; in addition, regular quality assurance (QA) will be required to ensure that the energies remain matched. Previous authors have used a system of empirically derived values to characterise and QA FFF beams from Varian and Elekta Linacs (Fogliata et al., 2016a; Fogliata et al., 2012b). This chapter develops on previous work (Paynter et al., 2014) to propose methods for matching beams on Elekta VersaHD Linacs and a framework for routine QA. Insight is gained in understanding how changes to the beam delivery system can affect beam characteristics.

The standard definition of penumbra for cFF beams is the distance between the points on the beam edge that mark 80% and 20% of the central axis dose normalised to 100%. This method is not appropriate for FFF beams as the 80% of maximum dose can be located within the in-field region of the FFF profile. Previously, a number of authors have proposed methods for measuring the penumbra and field size of FFF beams (Fogliata et al., 2012b; Ponisch et al., 2006; Budgell et al., 2016).These have been based on methods that determine an inflection point in the FFF field edge and require reference to the profile of the standard, cFF beam at the equivalent energy. As FFF beams become more prevalent for routine clinical treatment, FFF-only Linacs are becoming a commercial reality, as is already the case for Cyberknife (Adler et al., 1997), Tomotherapy (Jeraj et al., 2004) and MR Linacs (Smit et al., 2014). Therefore, a method to characterise, evaluate and QA FFF beam profiles without reference to a cFF profile is presented and investigated.

4.2. Method

This work was performed on energy matched FFF 6MV beams, where the percentage depth dose (PDD) has been matched to that of a cFF 6MV beam at 10cm deep in water. The work was carried out on one VersaHD Linac and one Elekta Synergy, each equipped with Agility collimators. The characterisations of these beams has been discussed previously in chapter 3 and published (Paynter et al., 2014). During the commissioning of the VersaHD Linac, the beam delivery parameters were adjusted so that the 6MV and 6MVFFF beams matched the previously commissioned Synergy with Agility FFF system. To do this, the beam energy was altered and the effect on both the PDD and profile shape evaluated. The beam steering was then adjusted by altering the 2R and 2T steering coil currents (Figure 16) in the Linac control system to investigate the effect of steering errors on the profiles. In addition, the profile shape was adjusted using the coarse and fine bending magnet currents.

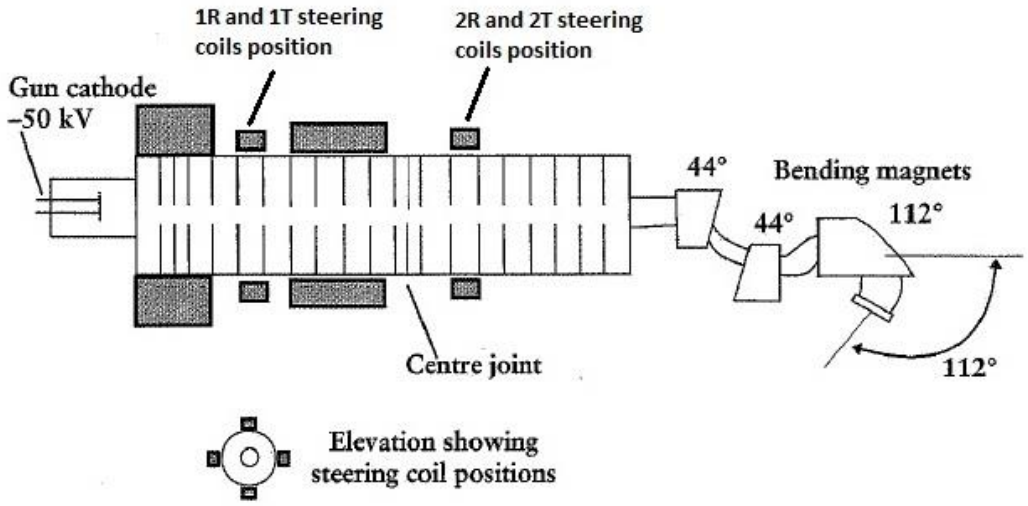

Figure 16: Diagram of electron transport system of an Elekta Linear accelerator. Steering coils operate radially (2R) and cross-plane (2T) to the plane of the electron beam path.

Profile and PDD measurements were taken at 100cm SSD in a PTW MP3 plotting tank (PTW, GmbH) controlled by the PTW Mephysto MC^2 software. A 60008 photon diode (PTW GmbH, Freiburg, Germany) was used for profile measurements and a 31010 semiflex chamber (PTW GmbH, Freiburg, Germany) used for PDD measurements. The bending coarse, bending fine and steering currents were systematically altered in order to induce errors in the beam to investigate their effect on the treatment beam characteristics.

Other manufacturers' implementations of FFF beams do not support energy matching. Instead, the beam that would have been incident on the flattening filter is not further modified when the filter is removed (Vassiliev et al., 2006b), resulting in a lower quality beam.

This alternative type of unmatched FFF beam was simulated in this work by not modifying the beam delivery parameters after the flattening filter was removed (Paynter et al., 2014).

To determine the penumbra of the FFF beam profiles, a development on the inflection point method is proposed that does not require reference to the equivalent cFF beam profile. To investigate how to best utilise the inflection point, the extracted points were normalised systematically to 50%, 55% and 60% and the penumbra taken as the distance between the 80% and 20% points. Analysis was carried out to determine the optimum normalisation to give agreement with current methods where cFF beams are available. The method was evaluated against standard methods for cFF beams where the distance between the points of 80% and 20% of maximum dose is directly measured. The method was also evaluated against the approach proposed by Ponisch et al. (2006) for FFF beams, where the FFF profile is normalised against the inflection point of the flat profile (Equation 4) and the measurement between the 80% and 20% points of the normalised profile is used as the measure of penumbra. These methods will be considered as the 'gold standard' for analysis of penumbra.

Equation 4: $$D_n = \frac{D_u}{D_f} D_{CAX}$$

where D_n is the normalised dose, D_u is the dose at the FFF inflection point, D_f is the dose at the cFF inflection point and D_{CAX} is the dose on the central axis of the cFF beam.

The suitability of this method for the determination of field size for cFF beams and FFF beams has also been evaluated by measuring between the standard 50%-50% points of the normalised profiles.

Penumbra was further analysed at 10MV, i.e. with reference to a cFF 10MV beam; an unmatched FFF beam whereby the flattening filter was removed from the beam without any further beam energy matching; and, an FFF beam energy matched at 10cm deep in water tank to the cFF 10MV FFF beam.

4.3. Results

4.3.1. Profile symmetry

The profile symmetry in the in-plane direction can be measured using the conventional method of maximum ratio between opposite points within the central 80% of the field size (Equation 5) as used for cFF beams,

Equation 5: $$symmetry = \left(\frac{D_x}{D_{-x}}\right)_{max} . 100\%$$

where D is dose and x is the distance from the central axis.

However, the effect of changes in cross-plane steering on the symmetry is insensitive to being measured in this way for FFF beams. Instead, the cross-plane symmetry can be measured by determining the central axis deviation of the beam as steering errors result in the beam shifting rather than a symmetry change (Figure 17), this shift is also present in-plane when there is an energy change. By obtaining two profile scans at collimator (col) 0 and col 180 it is possible to locate the centre of rotation situated at the midpoint between the individual central axis positions of each measurement and the central axis deviation from this point. Figure 18 shows that a linear relationship exists between the steering current applied by the Linac control system and the central axis deviation of the beam. Deviations in central axis (CAX) of more than 1mm can result in a rapid reduction in doserate and/or beam termination due to waveguide vacuum failure caused by the electron beam impinging on the travelling waveguide structure.

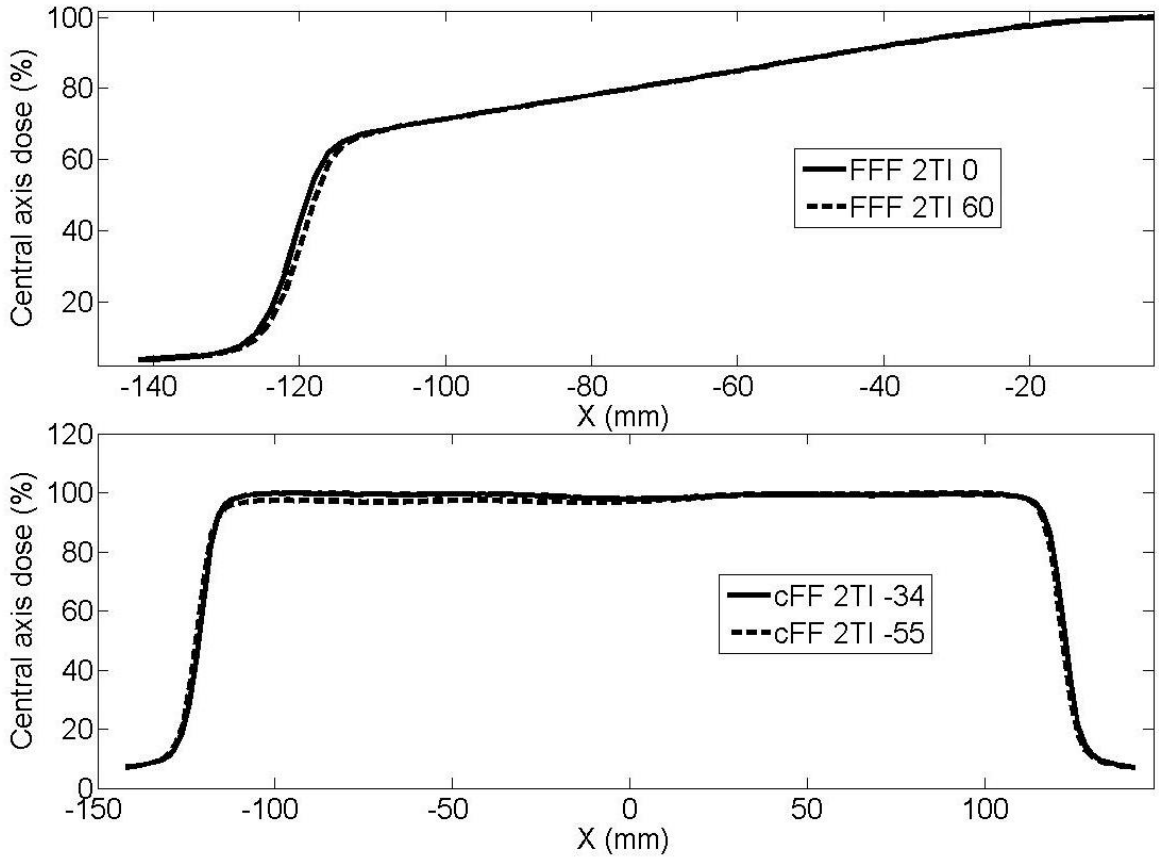

Figure 17: The effect of adjusting 2T bending magnet current on profile shape and CAX position for 6MV FFF beams (above) and cFF beams (below) taken at 100cm SSD at a depth of maximum dose in water.

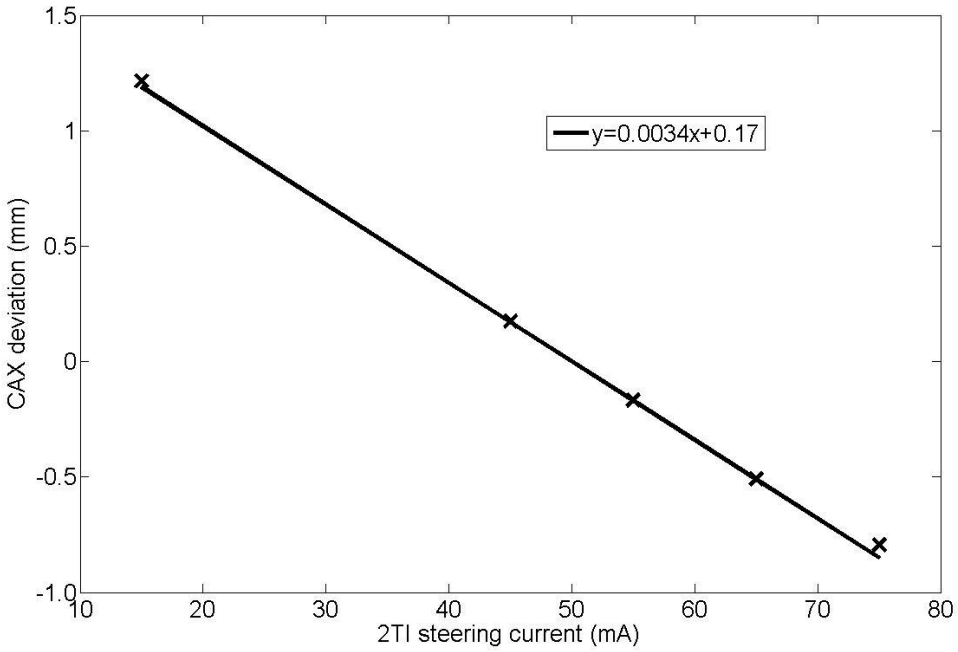

Figure 18: Profile central axis shift with changing 2T steering currents for a 6MV FFF beam at 100cm SSD and at a depth of maximum dose in water.

4.3.2. Profile flatness

As the beam energy increases the FFF beam shape changes so that the central peak becomes more pronounced. A 2% change in PDD corresponds to a 4% change in the 'flatness' of the beam. Flatness is described as the ratio of the maximum and minimum dose within the central 80% of the field size Equation 6.

Equation 6: $$\boldsymbol{flatness = \frac{D_{max}}{D_{min}}.100\%}$$

This means that the profile shape is more sensitive to an energy change than the PDD (Figure 19). The central peak can be altered by adjusting the ratio of bending coarse to bending fine currents with a minimal effect on PDD.

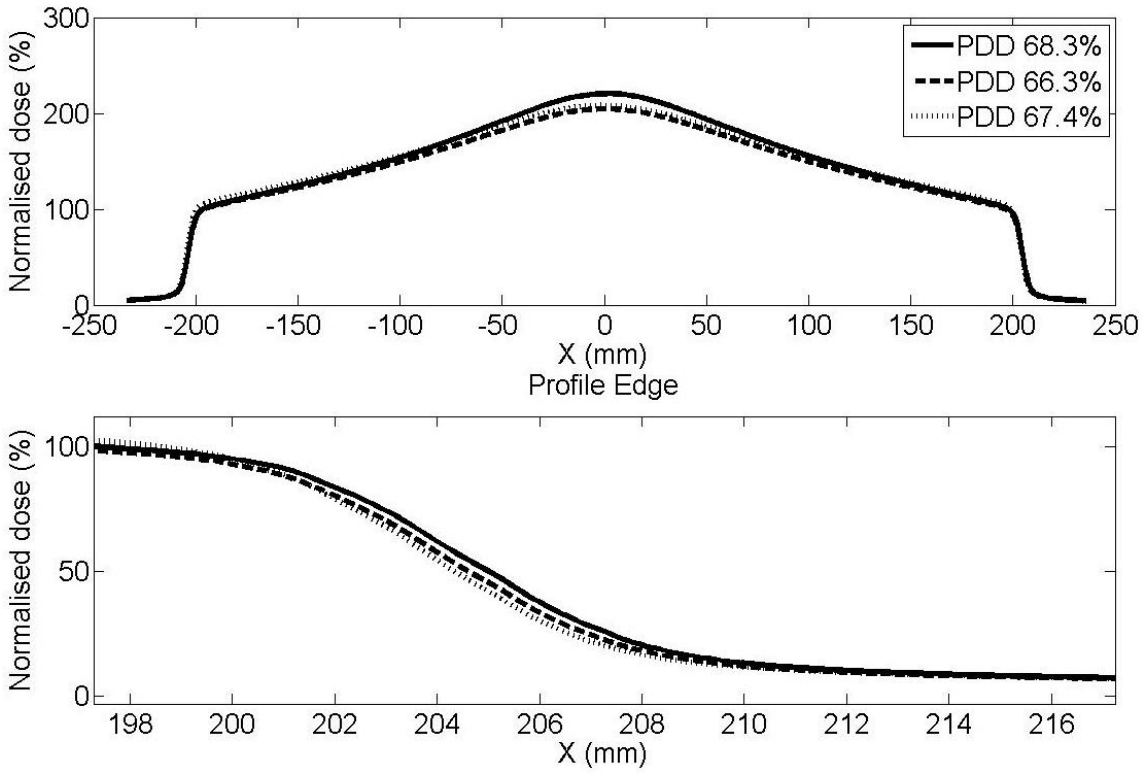

Figure 19: Top: Change in 6MV FFF inplane Profile flatness for a 1% change in PDD at 100cm SSD and 10cm deep in water. Bottom: Profile shift for a 1% change in PDD at 100cm SSD and 10cm deep in water.

4.3.3. Beam energy

The beam energy (quality) of FFF beams can be measured using the same methods currently used for cFF beams (eg PDD at a specified depth, TPR). However, care should be taken as a change in the beam energy can off-set the central axis in the in-plane direction due to a change in the electron path through the beam steering slalom, Table 5 shows that a 2% change in PDD results in a 1mm CAX shift and a 4% change in profile 'flatness' (Figure 19).

Table 5: Relationship between beam energy, profile CAX and beam 'flatness'

PDD10 (10 cm x 10 cm)(%)	CAX G-T (mm)	Symmetry G-T (%)	'Flatness' (%)
66.4	-0.50	100.40	167.72
67.3	0.29	100.26	170.68
68.4	0.89	100.34	171.69

Table 6: Measured difference in mm between inflection method and current 'gold standard' penumbra measurement methods for flat (cFF), unmatched flattening filter free (UFFF) and matched flattening filter free (MFFF) beams.

Difference from 'gold standard' 6MV profile Dmax (mm)							
Inflection point (%)	Jaw direction			MLC direction			Average
	cFF	UFFF	MFFF	cFF	UFFF	MFFF	
50	0.447	0.436	0.414	0.704	0.464	0.664	0.537
55	0.036	0.064	0.043	0.106	0.243	0.071	0.105
60	0.103	0.114	0.129	0.224	0.457	0.250	0.235
Difference from 'gold standard' 10MV Dmax (mm)							
Inflection point (%)	Jaw direction			MLC direction			Average
	cFF	UFFF	MFFF	cFF	UFFF	MFFF	
50	0.646	0.671	0.686	0.817	0.871	0.743	0.758
55	0.117	0.079	0.079	0.189	0.171	0.121	0.128
60	0.140	0.064	0.064	0.246	0.079	0.193	0.129
Difference from 'gold standard' 6MV 20cm deep (mm)							
Inflection point (%)	MLC direction			Jaw direction			Average
	cFF	UFFF	MFFF	cFF	UFFF	MFFF	
50	2.727	2.236	1.514	2.510	2.943	1.507	2.142
55	0.211	0.436	0.371	0.180	0.429	0.250	0.335
60	1.284	1.450	1.136	1.090	1.421	0.914	1.202
Difference from 'gold standard' 10MV 20cm deep (mm)							
Inflection point (%)	MLC direction			Jaw direction			Average
	cFF	UFFF	MFFF	cFF	UFFF	MFFF	
50	2.096	2.507	2.014	2.007	2.421	1.679	2.126
55	0.560	0.471	0.086	0.393	0.436	0.114	0.300
60	0.681	0.693	0.457	0.629	0.571	0.471	0.564

4.3.5. Penumbra

The profiles were analysed using software developed in house, which locates the inflection point of the profiles (Figure 20) using the Canny edge detection algorithm (Canny, 1986). This algorithm was used because it helps to remove noise from the profile when locating the edges. Any false inflection points are often located away from the true inflection point and the software allows the user to manually select the correct inflection points used for the analysis by rejection of incorrect positions. The inflection points are then normalised to the pre-defined values of 50, 55 and 60% for all beam types and the penumbra extracted as the distance between 80 and 20% profile points based on each normalisation. The values were chosen as it is often assumed that the inflection point lies at 50% of maximum dose for flat beams, this value was then iteratively altered to 60% and 55% to achieve the best match to current methods. For the FFF modalities the penumbral values determined are compared against the method published by Ponisch as this method has been used in previous papers (Ponisch et al., 2006; Cashmore, 2008; Paynter et al., 2014)**.** The cFF beam penumbra is compared to the standard 80%-20% (CAX value normalised to 100%) method. The difference in measured penumbra averaged over field sizes from 3cm x 3cm to 40cm x 40cm is shown in Table 6.

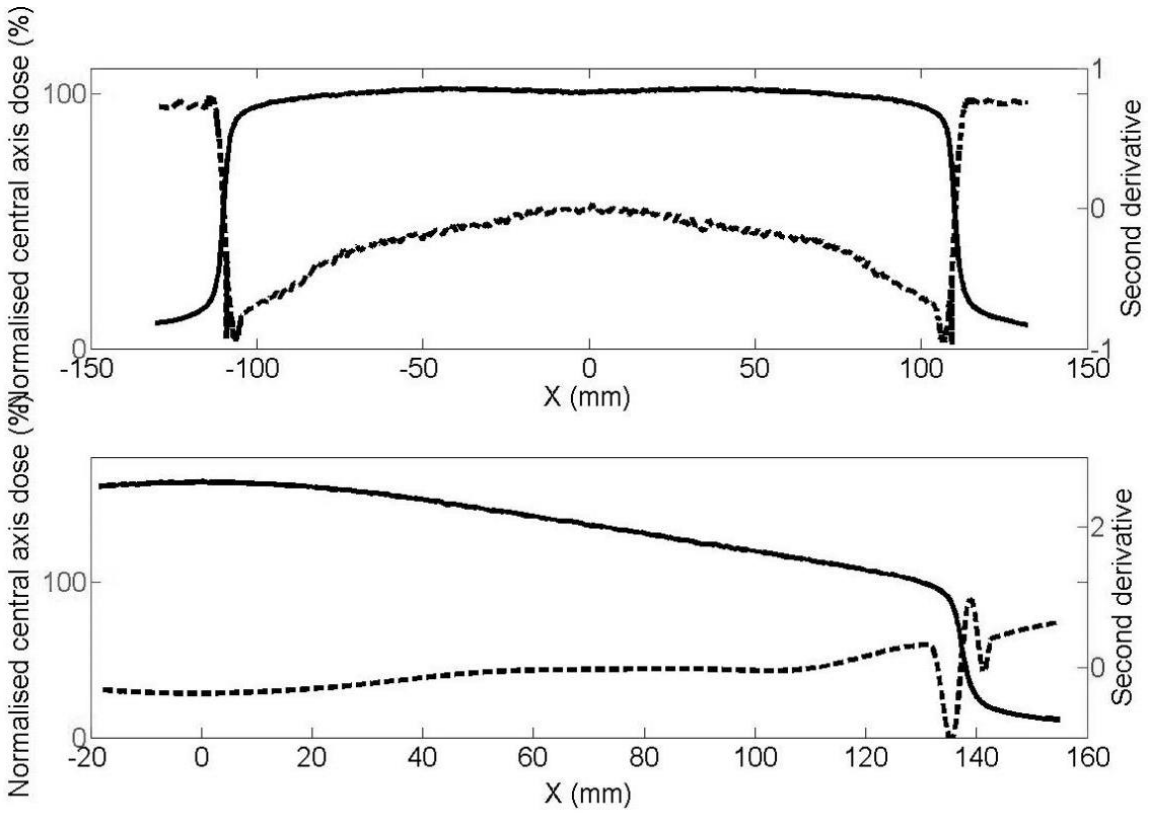

Figure 20: Depiction of second derivative determining the position of inflection for 6MV cFF (above) and FFF (below) beams for a 20cm x 20cm profile taken at 100cm SSD and 10cm in water.

4.3.6. Field size

The field size is determined using the same in-house programme, with the inflection points normalised to 55%. This was used because this value was observed to achieve the best agreement for the penumbra analysis compared to cFF (standard) beams (Table 6). The field size was still determined as the distance between the 50% points. This method was evaluated for both the FFF beams and the traditional cFF beams (Figure 21). The results are shown in Table 7.

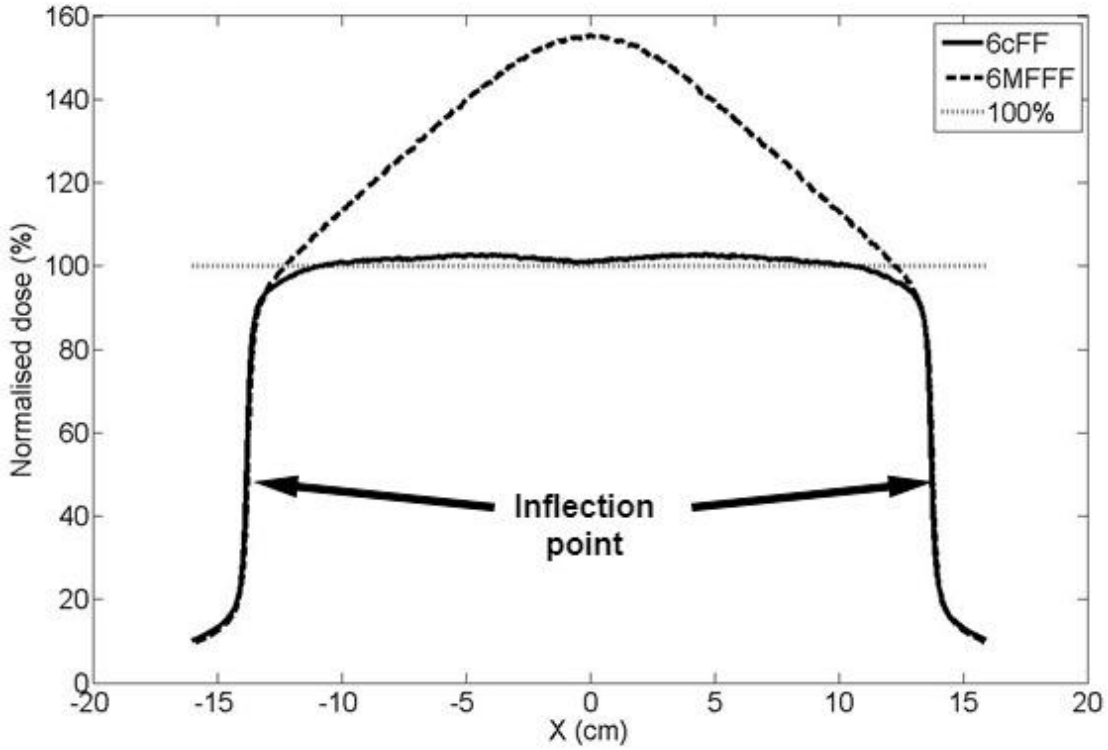

Figure 21: Inflection point normalised 25cm x 25cm in-plane profile measured at 100SSD and 10cm deep in water.

4.4. Discussion

For FFF beams a change of steering current in the 2T direction moves the beam rather than affecting the symmetry of the profile (Figure 18). This change in behaviour with respect to the symmetry in the cross-plane provides some problems with routine QA of FFF beams compared to conventional cFF beams. The position in-plane of the electron beam entering the bending magnet system affects the angle that it subsequently exits the system and onto the target. There is an optimum path the electrons can travel through the bending magnets, and an in-plane off-set either side of this can lead to the beam striking the target at a non-perpendicular angle This does not occur in the same way in the cross-plane direction. Translational off-sets of the

electron beam in the cross-plane direction do not lead to an angular change in trajectory when arriving at the target. Using measurement points a set distance left and right of the central beam axis would not show any symmetry change for an FFF beam with a steering change as the infield profile shape does not change in the cross-plane direction (Figure 17). One method for avoiding this is to compare the central axis deviation to that of a cFF beam where the central axis is fixed by the position of the flattening filter. The problem associated with this method is that whilst effective for current Linacs that have both cFF and FFF modes, a new method is required if only FFF beams were available on a given Linac. The acquisition of 2 profiles with a difference in collimator rotation of 180° allows the centre of rotation to be deduced, removing the setup uncertainty. This centre of rotation can then be used to determine the central axis deviation without the need for a cFF beam.

Table 7: Difference in calculated field size for 6MV unmatched Flattening filter Free (UFFF) and matched Flattening Filter free (MFFF) beams based on 50% field sizes following from the 55% inflection point method compared to measured 50% field size for cFF beam.

Square field size (cm^2)	Difference from CFF Field size compared to UFFF at depth of maximum dose (mm)		Difference from CFF Field size compared to MFFF at depth of maximum dose (mm)	
	Jaw Direction	MLC Direction	Jaw Direction	MLC Direction
3 x 3	0.4	0.5	0.4	0.3
10 x 10	-0.2	-0.2	0.4	0.4
20 x 20	-0.2	-0.6	-0.4	-0.5
40 x 40	-0.5	0.2	-0.5	0.0

Square field size (cm^2)		Difference from CFF Field size compared to UFFF at depth of 20cm in water (mm)		Difference from CFF Field size compared to MFFF at depth of 20cm in water(mm)	
		Jaw Direction	MLC Direction	Jaw Direction	MLC direction
3 x 3		-0.5	0.2	-0.4	0.0
10 x 10		0.5	-0.1	0.1	-0.4
20 x 20		-0.2	0.1	0.3	0.0
40 x 40		1.6	1.5	1.0	1.0

The shape of the profile can be adjusted by changing the ratio of bending coarse and bending fine currents. The bending coarse value affects the energy selection of the bending magnet system whilst the bending fine affects the position that the beam strikes the target. By altering the ratio of these values, the angle at which the electron beam strikes the target can be altered. This can be used to broaden or narrow the forward bias of the bremsstrahlung having the effect of producing a flatter (lower energy) or more peaked (higher energy) profile whilst having a minimal impact on the PDD.

After measuring the beam energy it is important to ensure that the beam steering is within tolerance for both the symmetry and CAX position as the latter can be altered when adjusting beam energy.

The method of normalising the inflection points of the FFF profiles has been discussed by previous authors (Fogliata et al., 2016a; Georg et al., 2011; Fogliata et al., 2012b; Ponisch et al., 2006). However the method used has been to normalise against a cFF profile so that the penumbras can be measured, whereas the approach and results presented here are from normalising the inflection points to a fixed value. The results show that normalising to a nominal 55% value results in measured differences in penumbra of less than 0.5mm for both FFF and cFF beams (Figure 21, Table 6). It is therefore suggested that this method could be utilised for all types of MV photon radiation beams. As the technique does not need reference to any other beam, it can be applied to FFF beams without the need to measure a linked cFF beam, or where no such cFF beam is provided.

The field size of FFF beams and of cFF beams can be determined by normalising the inflection point to 55% and then measuring field size between the same 50% of maximum dose points, as in currently used methods (Figure 21). This produces a measure of field size that is within 0.6mm of the field size measured using 50% maximum of a flat beam for all field sizes with the exception of 40cm x 40cm at 20cm deep. This new definition could be used to define field size for all types of MV radiation beam (Table 7).

The methods have only been applied to matched FFF beams implemented on Elekta Linacs and further work is required to determine their suitability for unmatched FFF beams produced by other manufacturers. However, with the consistency demonstrated between matched FFF and unmatched FFF beams, it is anticipated that the methods described would be applicable to other manufacturers' unmatched FFF beams.

4.5. Conclusion

The purpose of this chapter was to address the research question “Can suitable definitions be determined in order to characterise and QA all radiotherapy photon beams, cFF and both implementations of FFF?”. The finding of this chapter are such that new proposed methods are presented that make it possible to independently carry out characterisation, set up and QA measurements on beam energy, flatness, symmetry and field size of an FFF beam without the requirement for an equivalent cFF beam of the same energy. The methods proposed can also be used to carry out this QA for cFF beams, resulting in universal definitions and methods for MV beams. This is presented for matched FFF beams such as those produced by an Elekta linear accelerator, but is anticipated to apply to unmatched FFF beams produced by other manufacturers’.

5. Monte Carlo modelling of an FFF Linac with energy matching

5.1. Introduction

Monte Carlo modelling can be a powerful tool in the assessment of parameters that are otherwise difficult to measure experimentally. Monte Carlo models have previously been produced for clinical Linacs with FFF beams. In these models, the flattening filter component has been removed from an existing benchmarked Monte Carlo model of a Varian linear accelerator, delivering a conventionally flattened beam (cFF) (Dalaryd et al., 2010, Xiong and Rogers, 2008, Ceberg et al., 2010). However, other implementations of FFF beams , e.g. as supported on the VersaHD (Elekta AB, Sweden), include modification of the beam energy. For example, the FFF depth-dose beam characteristics at 10cm depth can be matched with the original cFF beam with a 10cm x 10cm field in water. This chapter investigates with a Monte Carlo model the techniques that can be used to aid matching that are analogous to practical investigations into the effect of beam focussing on the beam-shape characteristics of FFF beams (Paynter et al., 2017).

5.2. Producing the MC model

All Monte Carlo simulations for this work were performed with the Electron Gamma Shower (EGSnrc) user code supplied by the National Research Council Canada (Rogers, D.W.O et al., 2015). The BEAMnrc user code addition to EGSnrc contains predefined geometries that aid in the simulation of radiotherapy Linacs. The beams were simulated to be incident upon a 40cm x 40cm x 40cm water phantom using the Dosxyz user code (Walters et al., 2015) addition to EGS/BEAMnrc. This simulates the conditions of measuring data within a water filled plotting tank.

5.2.1. Measured data

In order to develop a Monte Carlo model that can be used for investigations, accurate measured data is required to validate the modelled beams. Therefore, beam data was measured at standard reference conditions, with a Source-to-surface distance (SSD) of 100cm in an MP3-M plotting tank (PTW, Freiburg). A PTW 60008 photon diode was used in order to reduce the volume averaging effect when measuring the profiles and for increased resolution in the penumbra region (Metcalfe et al., 1993). Silicon diodes over-respond to low energy scatter and therefore are not suitable for Percentage Depth-Dose (PDD) measurements. Therefore, the PDDs were measured using a PTW 31010 semiflex ion chamber at a measurement increment of 1mm.

5.2.2. Geometry

EGS/BEAMnrc contain a number of pre-defined geometries that can be customised to model a specific Linac. The geometries used for modelling the Elekta synergy accelerator with an Agility head were FLATFILT, SLABS, MIRROR, MLCE and MLCQ. These will be described in more detail below. The geometry of the linear accelerator was modelled in EGS/BEAMnrc using technical diagrams and specifications provided by Elekta (Elekta AB, Sweden) as part of a non-disclosure research agreement.

The FLATFILT component module was used to model the x-ray target, primary collimator, flattening filter and ion chamber. It was selected for these components as it is a flexible module that can be used to model both simple and complex geometries composed of multiple materials. This is achieved by creating stacked, truncated co-axial cones of which the user can define the radius at the top and bottom of each section. The complexity of these component modules varied. For example, the ion chamber was constructed of 21 layers, each of which contained up to 3 cones (Figure 22). The filter plate consisted of a single layer.

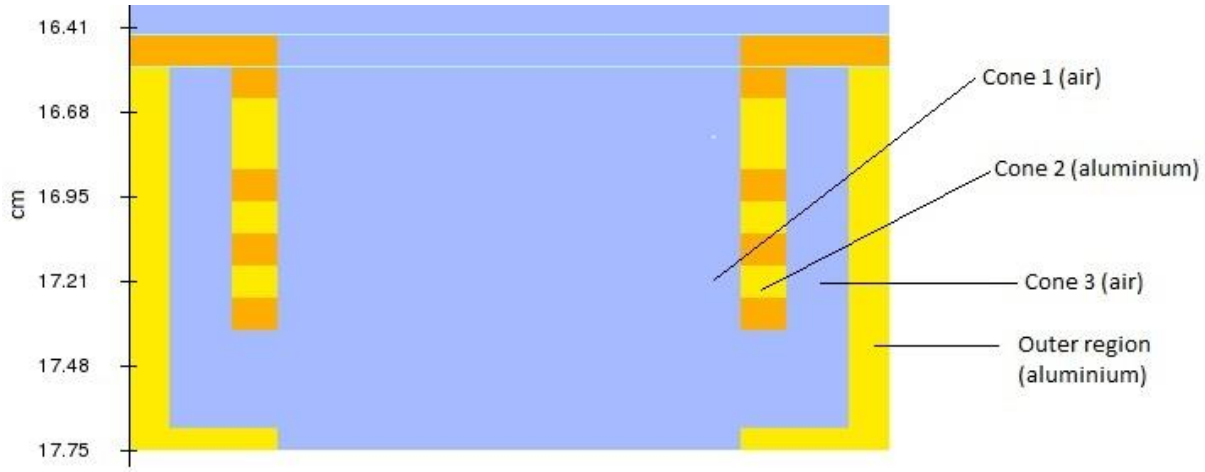

Figure 22: Diagram of the modelled ionisation chamber in the linear accelerator, this component was constructed of 21layers with up to 3 cones.

The SLABS component module allows the user to specify uniform layers of materials of varying thickness. It was used to model the backplate for the ion chamber and the exit-window of the Linac head.

The MIRROR component module was used to model the field lamp mirror, an angled mirror found in Linacs to project a light-field that is co-incident with the radiation field.

The MLCE component module allows the modelling of MLC leaves with curved ends, and a step rather than tongue and groove design. It was used for modelling the 180 leaf collimator in the

Agility head. The sides of each leaf in the leaf bank can be angled perpendicular to its direction of travel so that it focuses at a specific point within the accelerator head that does not match the beam divergence. By focussing the leaves like this, interleaf leakage is reduced without the need for 'tongue-and-groove' leaf edge design. The Agility head has diaphragms, or 'jaws', blocks of tungsten that provide bulk shielding of the radiation beam these are orthogonal to the MLC leaves. These have a curved end to define the beam edge rather than focussed as in previous Elekta Linacs (Cosgrove et al., 2009). For this reason the jaws were most conveniently modelled as two very large leaves with the MLCQ component module. This module allows the modelling of curved jaw ends without the additional focussing or step of the MLCE module.

The interaction cross-sections used for the materials were from the 700icru pegs file provided as part of the EGS/BEAMnrc package. The pegs file includes the interaction cross-section data for the component materials modelled in the linear accelerator. The 700 denotes the minimum energy in keV that the electron interactions will be modelled. The photon cross section data extends down to a minimum energy of 10keV. The areas not specified in the model were considered to be air (a predefined material in the pegs file). A schematic of the modelled accelerator is shown in Figure 23.

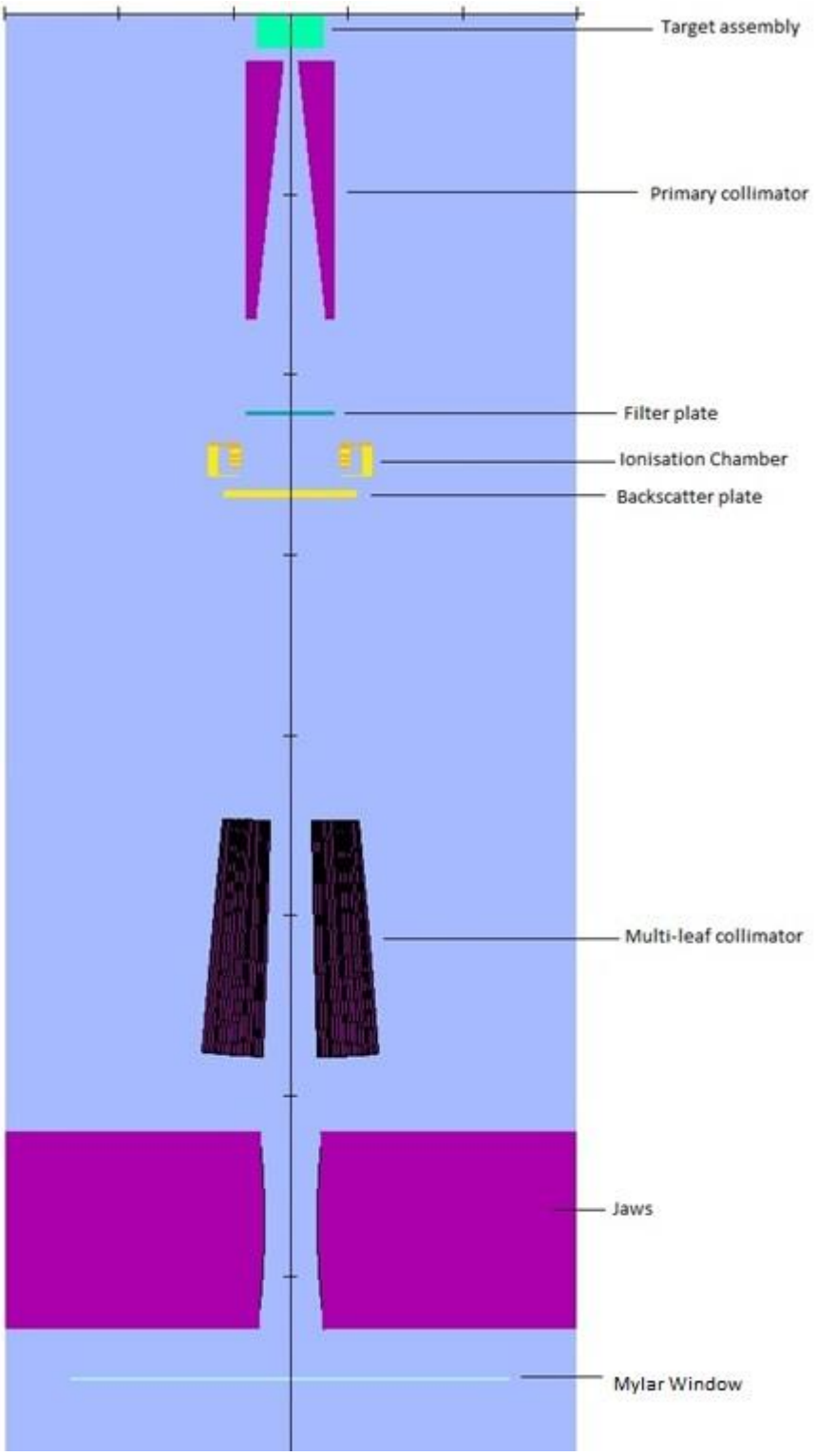

Figure 23: Figure of linear accelerator head as modelled in EGS/BEAMnrc

5.2.4. PDD and profile calculation

The PDD and profiles produced with the Monte Carlo model were calculated in the DOSXYZnrc user code. The phantom simulated in this code was a 40cm x 40cm x 40cm water box surrounded by air. The phantom was split so that profiles could be obtained at depths of dmax, 5cm, 10cm, and 20cm. The areas between these 'scoring layers' were modelled as larger voxels to increase calculation efficiency. This is achieved by having the parameter HOWFARLESS on in the user code. HOWFARLESS stops modelling the path of an electron or photon if it does not have sufficient energy to escape its current scoring voxel and deposits its entire remaining energy in that voxel.

For each calculation a full BEAMnrc simulation was used as the source, this method negates the need to calculate a phase space file of the particle fluence at the end of the accelerator and instead tracks particles from striking the target though the accelerator into the phantom to produce the required histories for the measurement. Profiles and PDDs were calculated with a 2mm resolution. The number of histories modelled into the water phantom for a PDD and profile was 6104000000. Directional bremsstrahlung splitting was used so that bremsstrahlung photons traveling in a direction that would be within a radius 1.5 times the field size from the isocentre are split 2000 times to reduce the calculation time. The number of histories used was selected to result in a local error on the Monte Carlo profiles of 0.3% inside the field and 3% outside the field for a field size 10cm x 10cm at 100SSD and at a depth of dmax.

5.2.5. Benchmarking

In order to benchmark the Monte Carlo profiles against the measured data a graphical user interface (GUI) was written in Matlab that normalised and displayed the plotting tank data against the profiles extracted from the Dosxyz Monte Carlo files. The GUI was designed to extract the field size and determine the penumbra using the methods proposed in chapter 4. The two profiles could also be compared with a 1D global gamma analysis (Low et al., 1998) that highlights the regions of the profile that exceed a global 1%, 1mm tolerance.

5.2.6. Electron beam characteristics

In order to model the FFF beam produced by the accelerator, an appropriate electron beam incident on the target must be defined. The characteristics of the electron beam can substantially influence the characteristics of the photon beam exiting the accelerator (Sheikh-Bagheri and Rogers, 2002). EGS/BEAMnrc has a number of pre-defined source models that can be modified by the user to produce the required electron beam characteristics. The source used for this work was ISOURC=19 an electron beam striking the target with a Gaussian distribution in X and Y, parallel or with angular spread. This source can be circular or elliptical in shape. The

source requires that both spectra parameters and geometric factors need to be set in order to model the electron beam striking the target.

The energy spectrum of the electron beam was iteratively altered in order to produce PDDs that matched the measured data collected on the linear accelerator. This was performed with a field size of 10cm x 10cm at 100cm source to surface distance (SSD).Once a good match to the PDD at this field size was obtained, additional field sizes ranging from 3cm x 3cm to 20cm x 20cm were modelled and compared to measured data.

The dimensions of the focal spot for the electron beam were investigated in order to match the measured penumbra of the photon beam profiles. The focal spot is the physical location that the electron beam strikes the target. The focussing of the focal spot is determined by the electron beam transport system in the Linac. The full width half maximum (FWHM) parameters that define the physical size of the electron beam were iteratively adjusted in both the MLC leaf and jaw directions in order to obtain the best match of penumbra across the previously defined range of field sizes. These parameters affect the penumbra of the photon beam and need to be modelled correctly in order to match measured data (Sheikh-Bagheri and Rogers, 2002).

The ISOURC=19 source can model the electron beam striking the target in parallel or with the electrons striking the target with a mean angular spread (Figure 24) (Paynter et al., 2017).

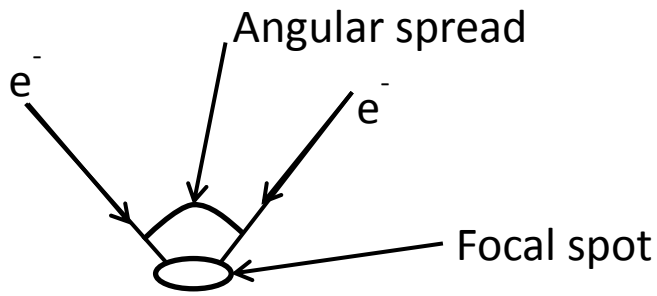

Figure 24: Diagram of angular spread parameter for Monte Carlo modelling

5.2.7. Field size calibration

Field sizes were defined in the model, from 3cm x 3cm up to a maximum of 20cm x 20cm. For each field size, the Monte Carlo profile data were compared to the measured data. The MLC and jaw aperture size in the Monte Carlo model was iteratively adjusted to match the measured field size. The final Monte Carlo aperture settings that matched the field size of the measured profiles were used to create a calibration for the jaw and MLC settings that would predict the required aperture size within the Linac head to produce the required field size at isocentre.

5.3. Results

5.3.1. Electron beam characteristics

The electron beam energy was iteratively adjusted from 6MeV to 8MeV, with varying increments in order to match the measured PDD. Iteratively changing the energy of the incident electron beam on the target affects both the beam profile and PDD dose distributions. Therefore, modifying this single parameter will either achieve matching of the profile or the PDD for a given 6MV FFF beam. Figure 25 demonstrates the impact of electron beam energy on the profile shape and PDD.

However, it was found that by changing the angular divergence of the electron beam on the target, the profiles can be further optimised without altering the associated PDD. Once an acceptable PDD match was obtained, the angular divergence of the electron beam striking the target was iteratively adjusted, starting from 0°, i.e. (an electron beam with all the electrons travelling parallel to each other), to an angular divergence of 2°.The iterative analysis indicated a Gaussian energy distribution around 8MeV provides an acceptable PDD distribution for a matched 6MV FFF beam on a Versa HD linear accelerator with an angular divergence of 1.3° (Figure 26).

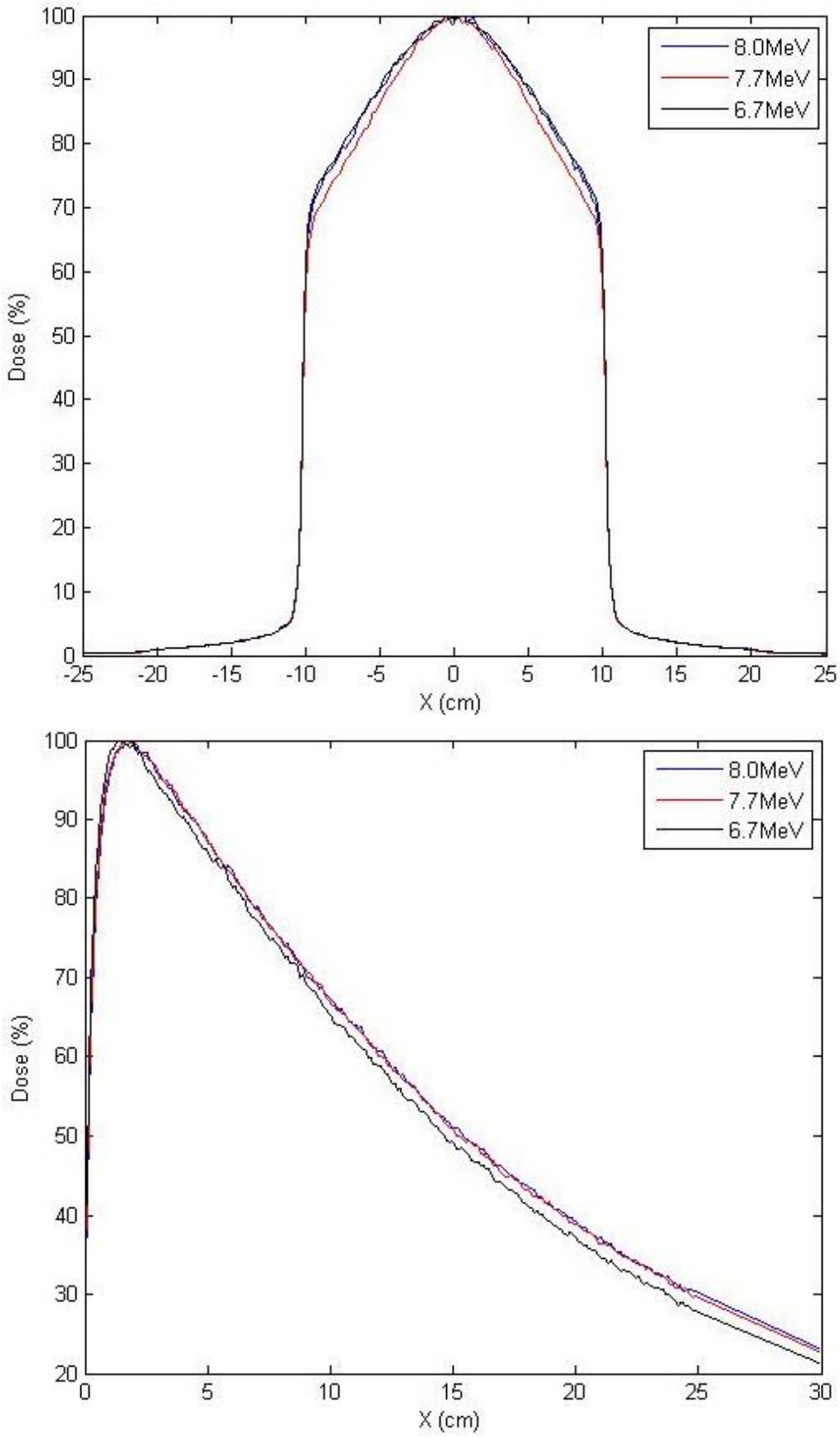

Figure 25: Impact of nominal accelerating potential on a 20cm x 20cm profile shape (above) at 100cm SSD and a depth of maximum dose in water and a 10cm x 10cm PDD at 100cm SSD (below).

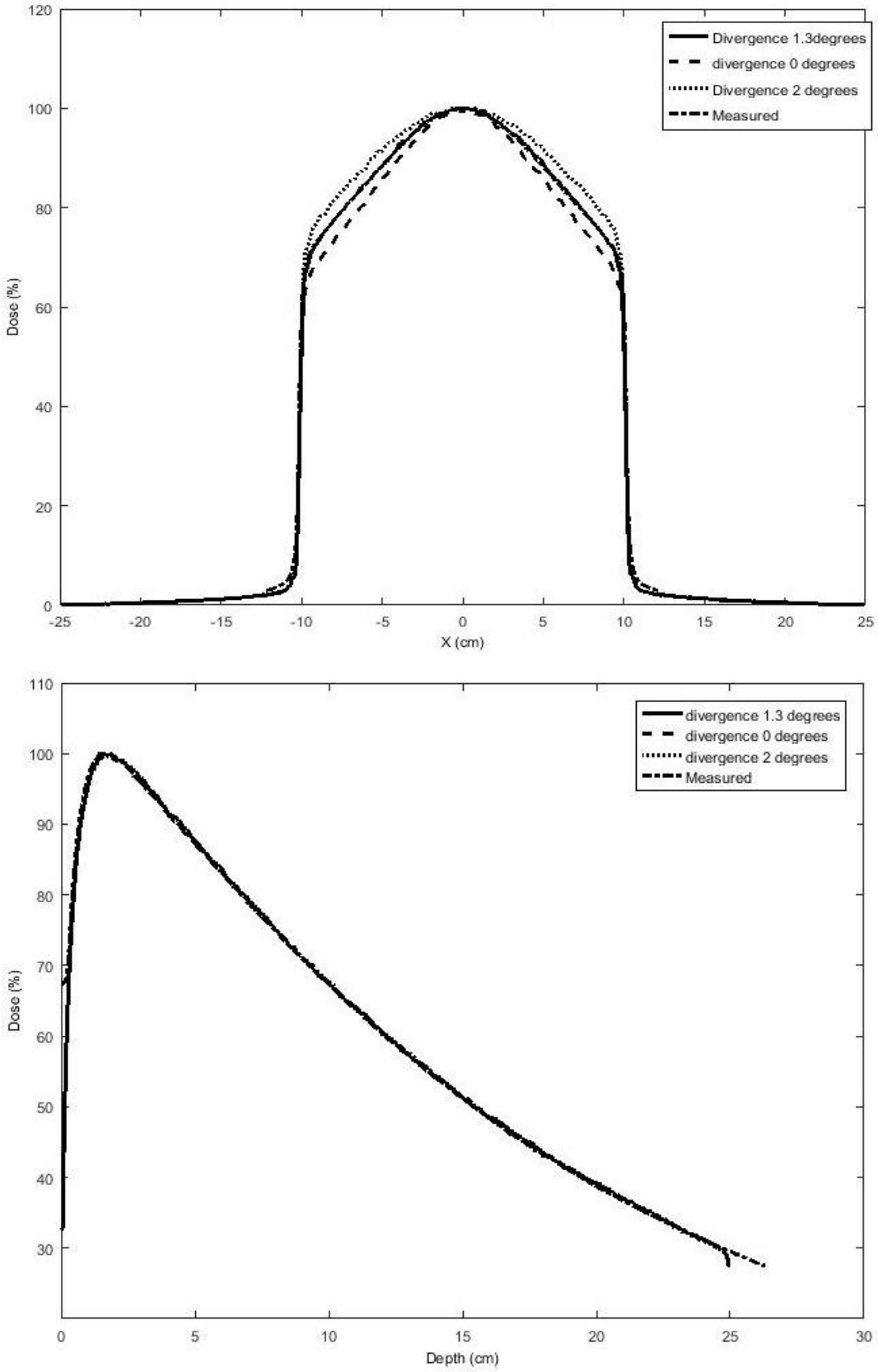

Figure 26: Impact of angular spread parameter on a 20cm x 20cm profile shape (above) at 100cm SSD and a depth of maximum dose in water and a 10cm x 10cm PDD at 100cm SSD (below).

The focal spot size was systematically altered from a circle of full width half maximum of 0.1cm in both the MLC and jaw directions. The best match to measured data was found to be with an elliptical spot size of 0.17cm in the MLC direction and 0.08cm in the jaws direction. The results for the MLC penumbra investigations are shown in Table 8.

Table 8: The relationship between the focal spot size of the electron beam and the profile penumbra in the direction of the MLCs.

Focal spot size (cm)	Calculated penumbra (mm)	Difference from measured penumbra (mm)
0.14	4.3	0.2
0.18	4.8	-0.3
0.16	4.3	0.2
0.17	4.55	-0.05

5.3.2. Field size calibration

The relationship between the distance the jaw needs to be retracted to form the aperture at the level of the aperture in order to match measured data at isocentre is displayed in Figure 27. The relationship can be fitted with a power relationship to predict the required move in the Monte Carlo model to achieve a 1cm change in field size at isocentre (Equation 7).

Equation 7: $y = 0.4375x^{1.0374}$

Where *y* is the aperture size and *x* is the required distance from the central axis.

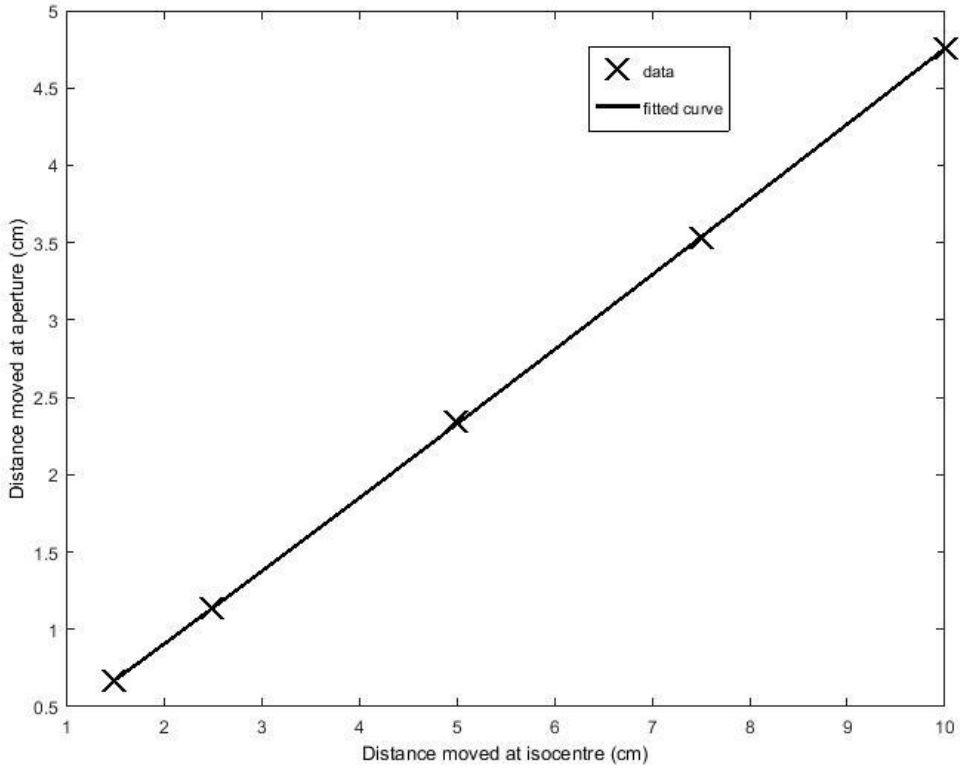

Figure 27: The relationship between the required move of the jaw in the model in to move 1cm at isocentre with respect to field size.

A plot of the relationship between the distance moved at the level of the aperture by the MLC in the model and the radiation field size, as defined at isocentre is displayed in Figure 28(Equation 8).

Equation 8: $y = 0.3283x^{1.0356}$

Where *y* is the aperture size and *x* is the required distance from the central axis.

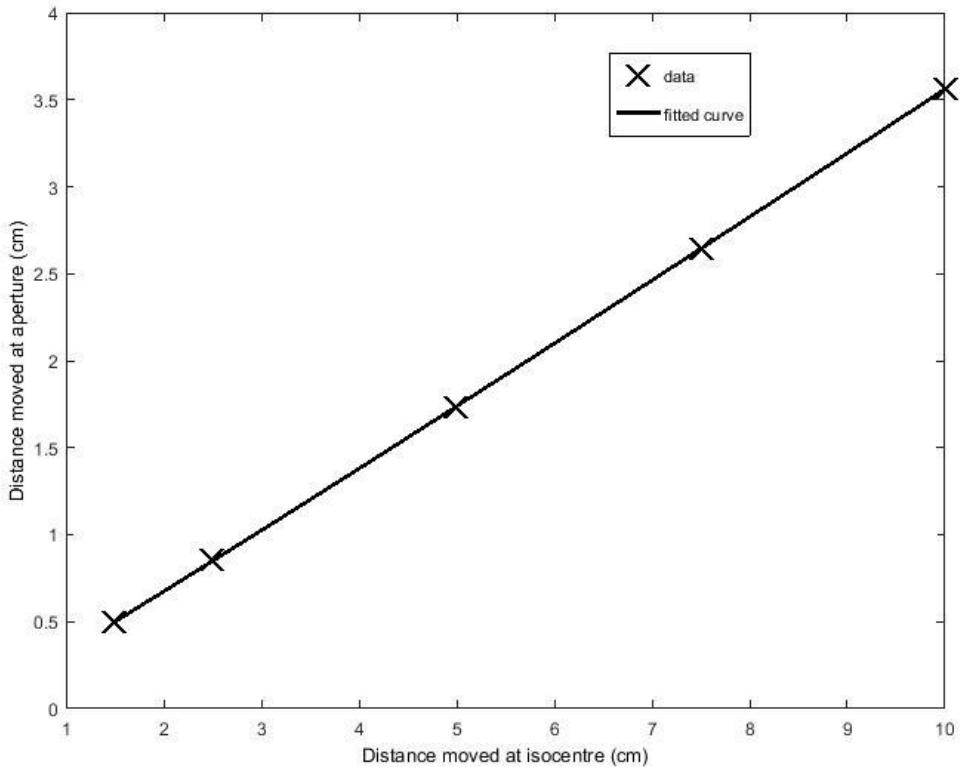

Figure 28: The relationship between the required move of the mlc in the model in to move 1cm at isocentre with respect to field size.

For each of the relationships a fit was produced that could be used to determine the location of the MLC/Jaw from the central axis without the need to iteratively adjust to match with measured data. The predicted location based on the fit with the residual error in field size is shown in Table 9 for the jaw location and Table 10 for the MLC location.

Table 9: The calibration for the jaw aperture size to match measured data at isocentre.

Location from central axis (cm)	1.5	2.5	5	7.5	10
Required aperture location (cm)	0.6630	1.1370	2.3385	3.5265	4.7580
Predicted aperture location (cm)	0.6663	1.1319	2.3232	3.5381	4.7685
Error in predicted field size (mm)	0.07	-0.11	-0.33	0.25	0.22

Table 10: The calibration for the MLC aperture size to match measured data at isocentre

Location from central axis (cm)	1.5	2.5	5	7.5	10
Required aperture location (cm)	0.4976	0.8533	1.7350	2.6445	3.5610
Predicted aperture location (cm)	0.4996	0.8480	1.7383	2.6454	3.5635
Error in predicted field size (mm)	0.06	-0.16	0.09	0.02	0.07

For each fit the predicted movement would result in a field-size error at isocentre of less than 0.5mm.

5.3.3. Benchmarking

The investigations above demonstrated the most appropriate electron beam parameters needed to match measured data were a Gaussian energy distribution centred on 8 MeV with an angular divergence of 1.3°. Using these parameters the Monte Carlo calculated data was compared to the measured data at a range of field sizes. The calculations were performed on the 'Medical Advanced Research Computer 1' cluster (University of Leeds). Each benchmarking calculation took 1247hrs of CPU time (3days real time), this time was reduced by completing the calculations in parallel utilising multiple CPU cores at once.

In Figure 29, the benchmarked profiles show good agreement of both field size, penumbra and in field dose. The gamma failures greater than a global 1%/1mm are in the region of the out of field dose and noise in the Monte Carlo calculated profiles at depth.

Figure 30 shows the benchmarking of a 20cm x 20cm field. The failures of the global 1%/1mm gamma analysis criteria are as a result of noise in the Monte Carlo profiles. The out of field doses meet the gamma analysis criteria.

Figure 31 shows the benchmarking results of the 3cm x 3cm field, the gamma failures are in the region of the out of field doses with the field size, penumbra and infield dose meeting the 1%/1mm criteria.

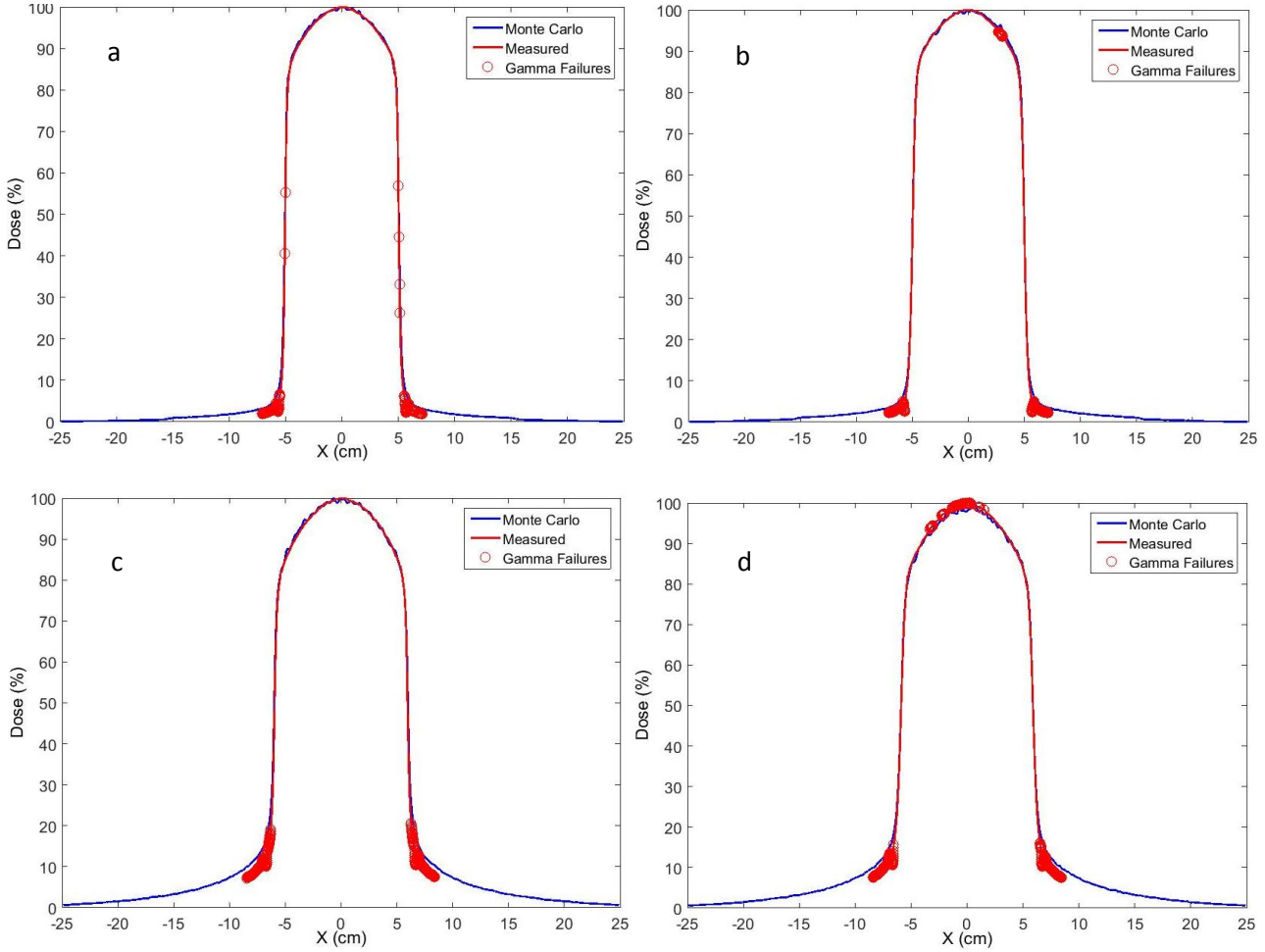

Figure 29: Benchmarking results for the 10cm x 10cm Monte Carlo calculated profiles (blue) against measured data profiles (red). The red circles mark where the difference between the profiles is greater than a global 1%/1mm gamma tolerance. The displayed profiles are (a) at a depth of maximum dose collimated by the jaws (b) at a depth of maximum dose collimated by the MLC (c) at a depth of 20cm collimated by the jaws (d) at a depth of 20cm collimated by the MLC.

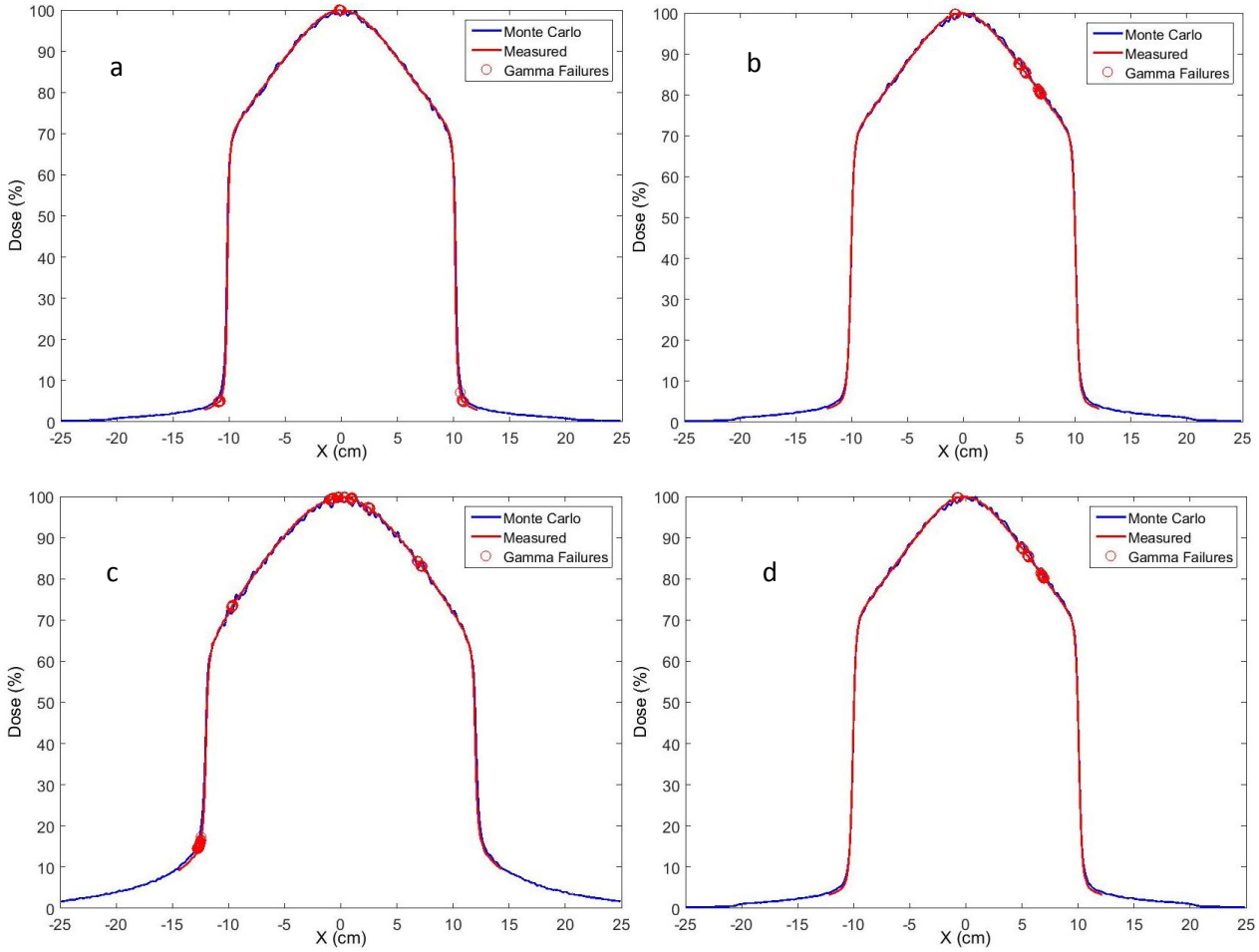

Figure 30: Benchmarking results for the 20cm x 20cm Monte Carlo calculated profiles (blue) against measured data profiles (red). The red circles mark where the difference between the profiles is greater than a global 1%/1mm gamma tolerance. The displayed profiles are (a) at a depth of maximum dose collimated by the jaws (b) at a depth of maximum dose collimated by the MLC (c) at a depth of 20cm collimated by the jaws (d) at a depth of 20cm collimated by the MLC.

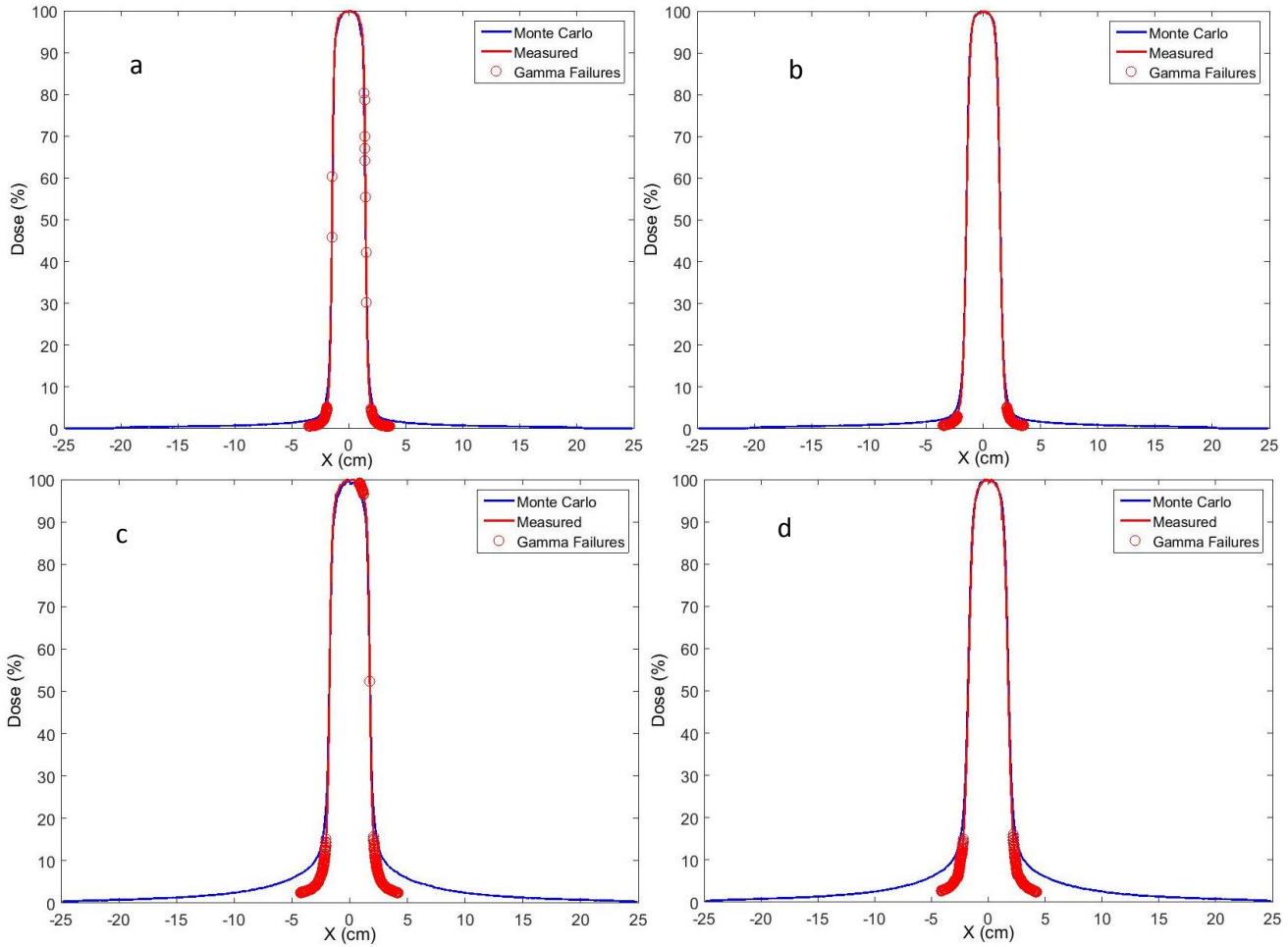

Figure 31: Benchmarking results for the 3cm x 3cm Monte Carlo calculated profiles (blue) against measured data profiles (red). The red circles mark where the difference between the profiles are greater than a global 1%/1mm gamma tolerance. The displayed profiles are (a) at a depth of maximum dose collimated by the jaws (b) at a depth of maximum dose collimated by the MLC (c) at a depth of 20cm collimated by the jaws (d) at a depth of 20cm collimated by the MLC.

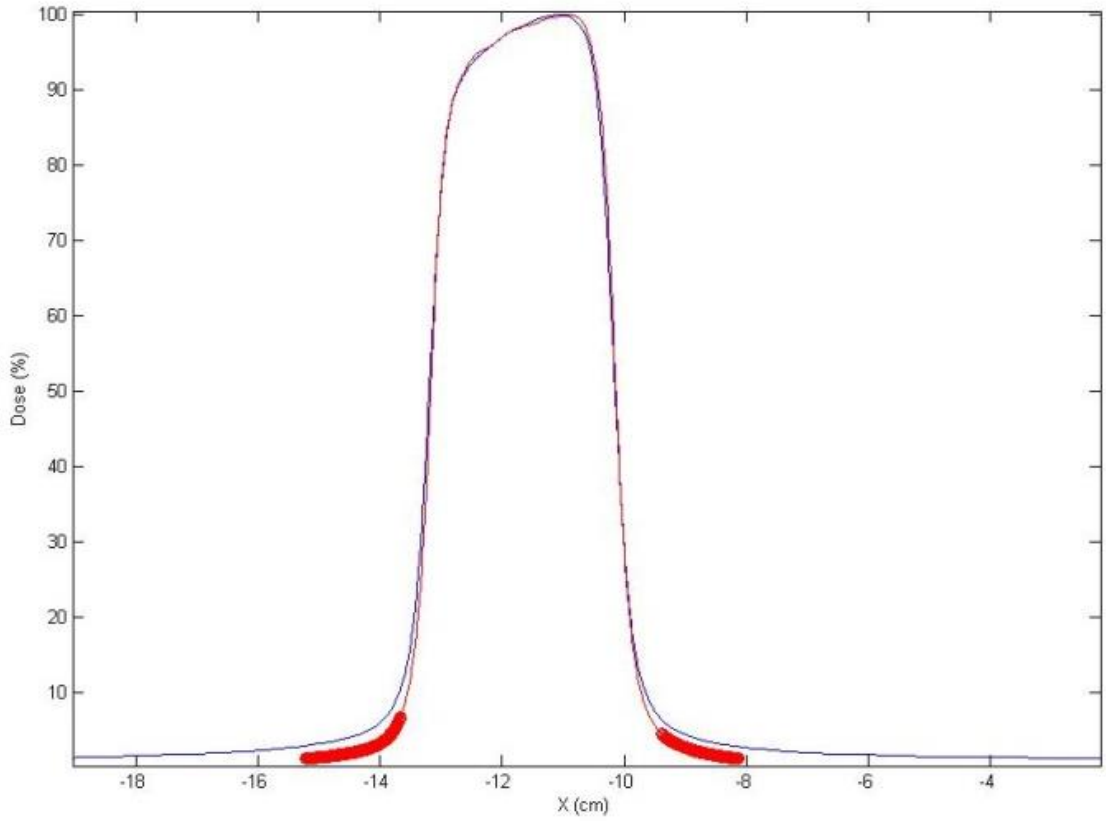

Figure 32: A 3cm x 3cm field calculated (blue) 10cm offset from the central axis in the MLC direction compared to measured data (red) at 100cm SSD and a depth of maximum dose in water.

Figure 32 shows a 3cm x 3cm field calculated 10cm off the beam central axis and compared to an equivalent measured profile. The in-field and penumbra match show good agreement with measured data. The out of field dose discrepancy is consistent with the on-axis 3cm x 3cm profiles.

5.3.3.1. Out of field dose: investigation of model parameters

The benchmarking results demonstrated that the model had less agreement with measurements for the out of field dose for small field sizes. Further investigations were performed in order to help in determining the cause of this discrepancy and improve the Monte Carlo model. The parameters systematically adjusted to investigate this discrepancy were the thickness of the primary collimator, the thickness of the filter plate and the minimum electron energy modelled in the Monte Carlo simulation. The depth selected for these investigations was a depth in water of 10cm, which was selected as the mid-point between the dmax measurements and 20cm measurements in the benchmarking and to eliminate any uncertainty at performing the measurements at dmax. The same behaviour was observed for profiles

collimated by the jaws and the MLCs therefore the investigations were performed with the field collimated by the jaws only.

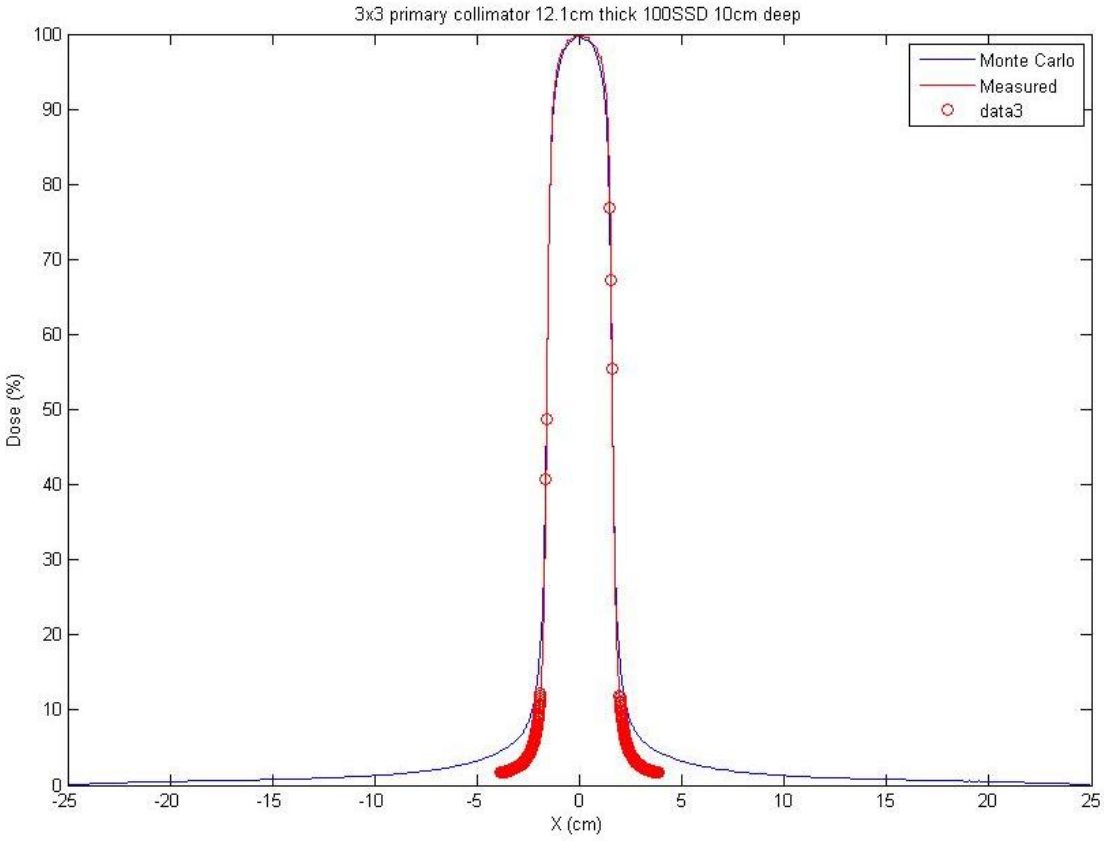

Figure 33: A benchmarked 3cm x 3cm Monte Carlo profile collimated by the jaws with the thickness of the primary collimator increased.

Figure 33: Shows that adjusting the primary collimator thickness in the MC model from the original 12.0cm thickness to 12.1cm to reduce the out of field dose had a negligible impact on the benchmarking of a 3cm x 3cm field at a depth of 10cm.

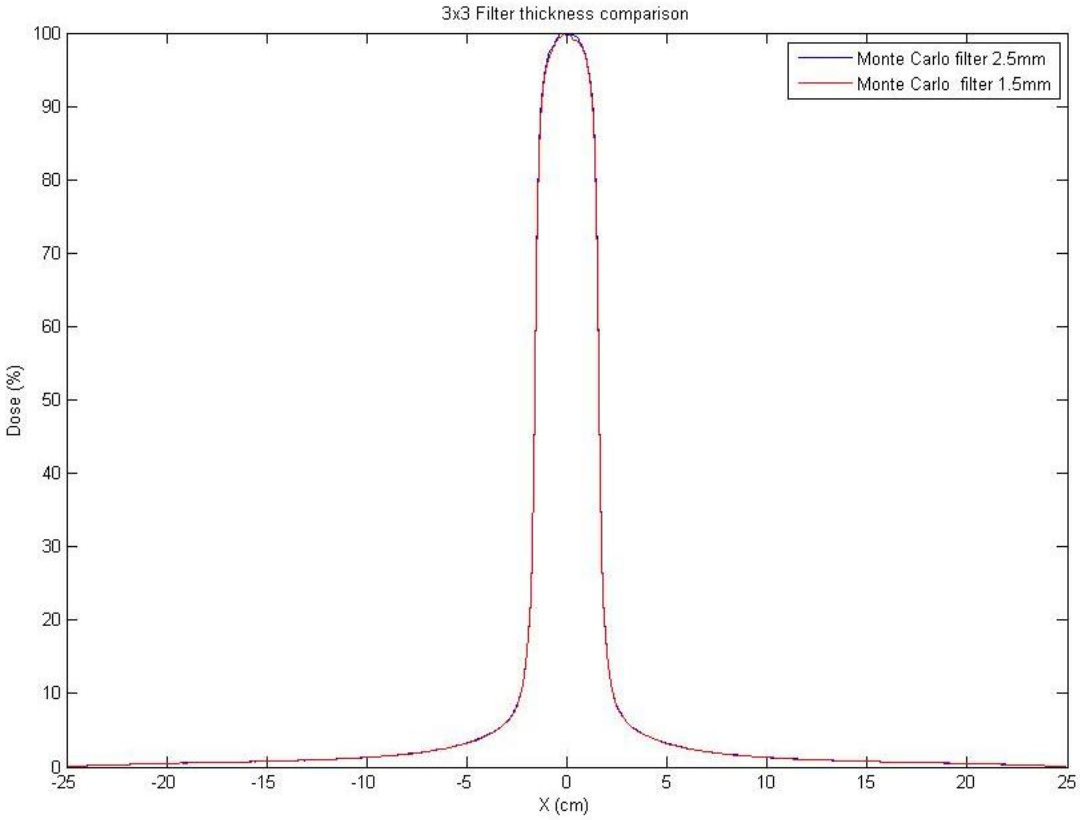

Figure 34: The impact or increasing and decreasing the thickness of the filter plate on the out of field dose

Figure 34 shows that by both increasing and decreasing the thickness of the filter plate by 0.5mm the impact on the profiles is negligible and is not the source of the out of field discrepancy.

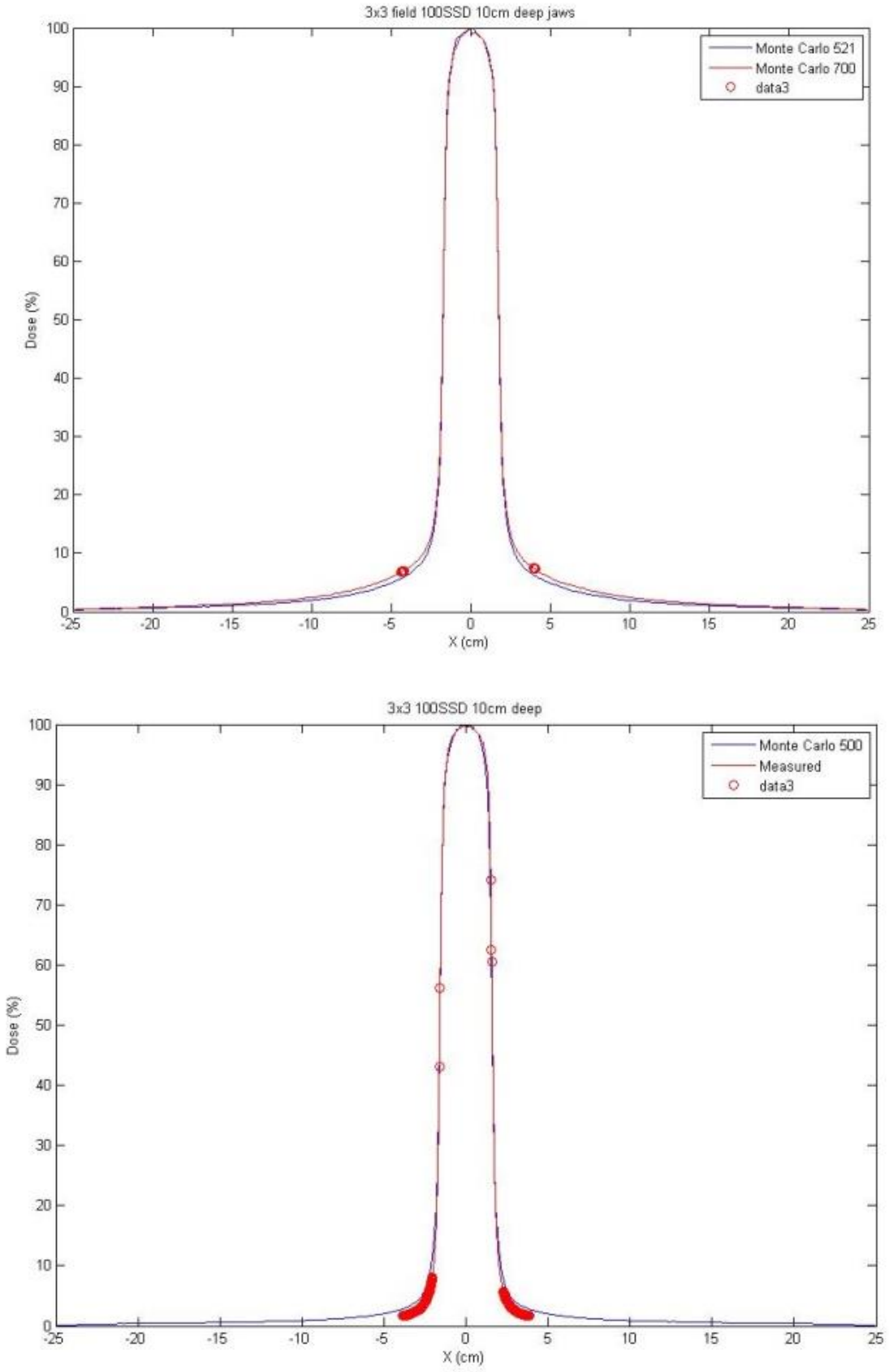

Figure 35: The impact of changing the electron transport cutoff energy on the out of field dose (above) comparing the cutoff energies of 512keV and 700keV (below) comparing the 512keV Monte Carlo profile against measured data.

Figure 35 shows that by modelling lower energy electrons the out of field dose decreases relative to the infield dose. This reduction was not significant enough to impact on the benchmarking to measured data.

The out of field dose near the field-edge is related to the transmission of the radiation through the leaf/jaw tips. Both the leaves and jaw tips in the Agility head are curved and therefore the effect of reducing this curvature to the extreme where the jaws have a straight edge was modelled. This altered the penumbra of the beam but did not affect the out of field dose (Figure 36).

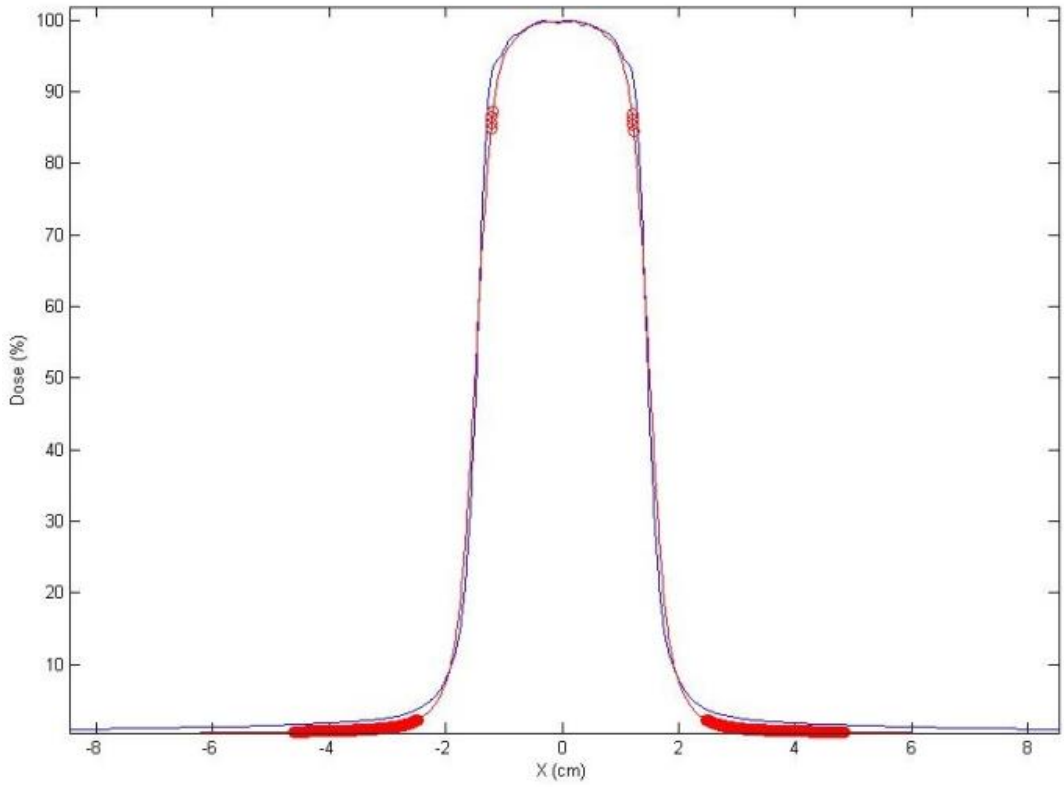

Figure 36: Comparison of Monte Carlo calculated profile with straight jaw edge (blue) compared to measured data (red).

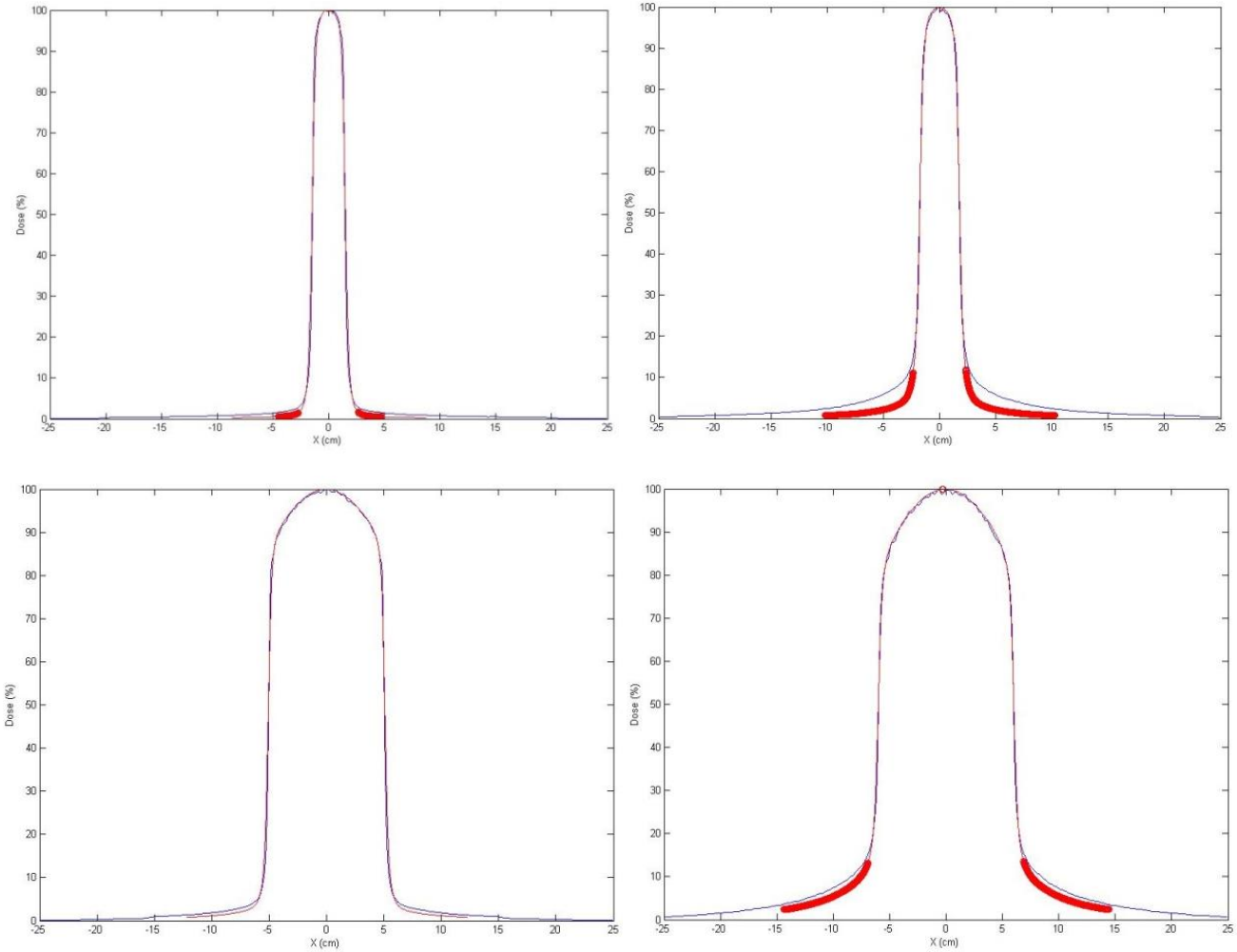

Figure 37: Profiles measured with semiflex3D (red) compared to Monte Carlo (blue) for field sizes of 3cm x 3cm (upper) and 10cm x 10cm (lower) at the depth of maximum dose (left) and at 20cm deep (right).

In order to determine whether the discrepancies observed were as a result of the original diode profile measurements performed on the Linac, further measurements were performed with a semiflex3D (PTW, Freiberg), a small ionisation chamber with active volume of 0.07cm^3. The comparisons (Figure 37) demonstrate that the measurements are not the source of the discrepancy. The semiflex3D measurements were performed so that the profiles extended further from the field edge. The agreement improves further out of field. This highlighted that the leaf/jaw tip modelling could be the cause of the issue.

5.3.3.2. Out of field dose: Investigation of back-up collimation settings.

Later detailed discussion of the results with the thesis assessors then prompted a re-investigation of any other likely causes of the out-of-field dose differences, including going back to the basic Linac settings in the model. A discrepancy was discovered in the Monte Carlo model. This discrepancy relates to the position of the MLCs out of the field. In the model described previously in this chapter the MLC leaves not being used to shape any field did not appropriately close when positioned underneath the jaw (Figure 38). They remained set at the nominal field size, resulting in extra transmission and scatter dose out of field. The result of this would be that modelled beams have higher doses out of field than measured, as seen in the profile figures earlier in section 5.3.3 and that these effects would be proportionally greater in small fields, as also observed. A series of further simulations were performed with those leaves appropriately closed underneath the jaw to evaluate this effect in detail.

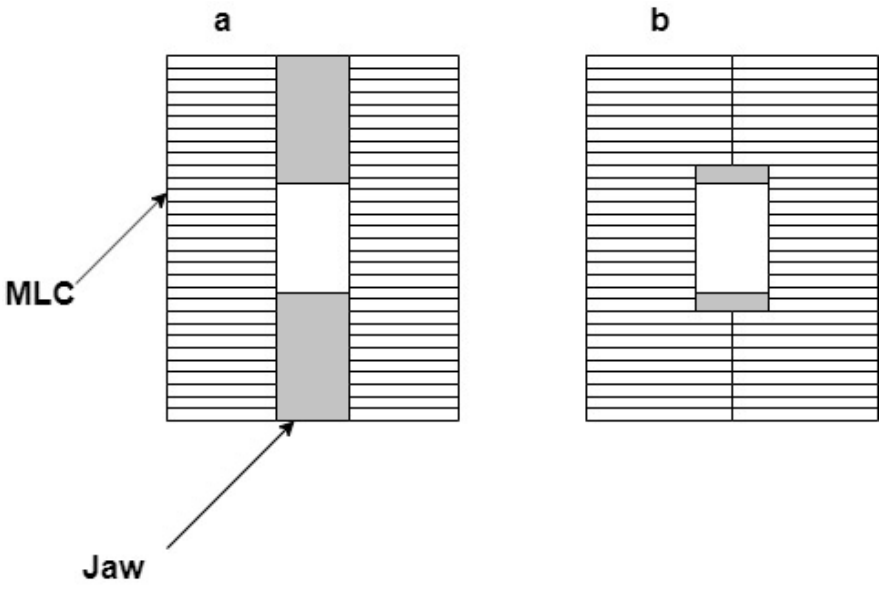

Figure 38: Back-up collimation settings (a) original model (b) corrected model

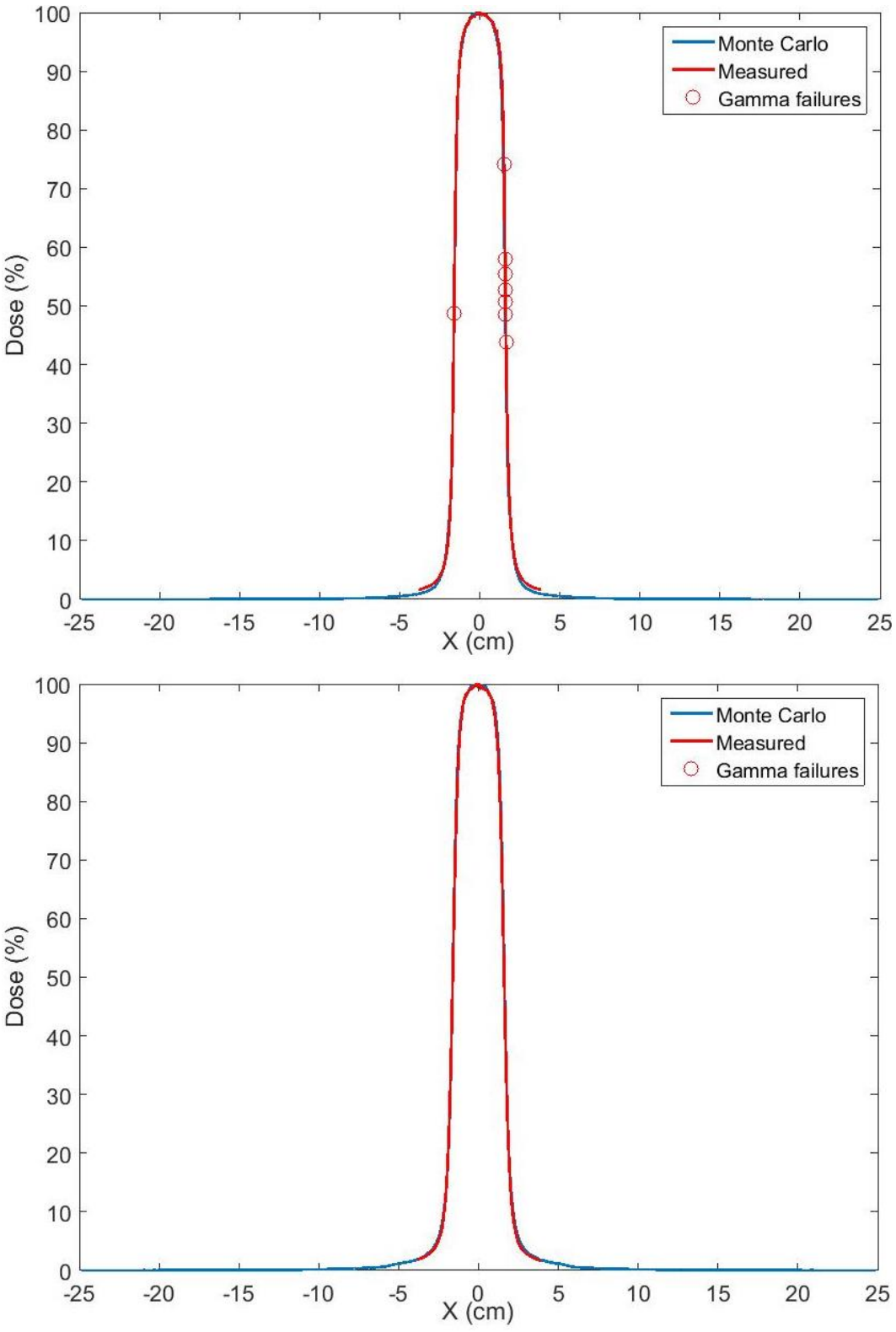

Figure 39: Benchmarking results for the 3cm x 3cm Monte Carlo calculated profiles (blue) against measured data profiles (red) at 100cm SSD. The red circles mark where the difference between the profiles are greater than a global 1%/1mm gamma tolerance. The displayed profiles are (above) at a depth of 10cm in water collimated by the jaws (below) at a depth of 10cm in water collimated by the MLC.

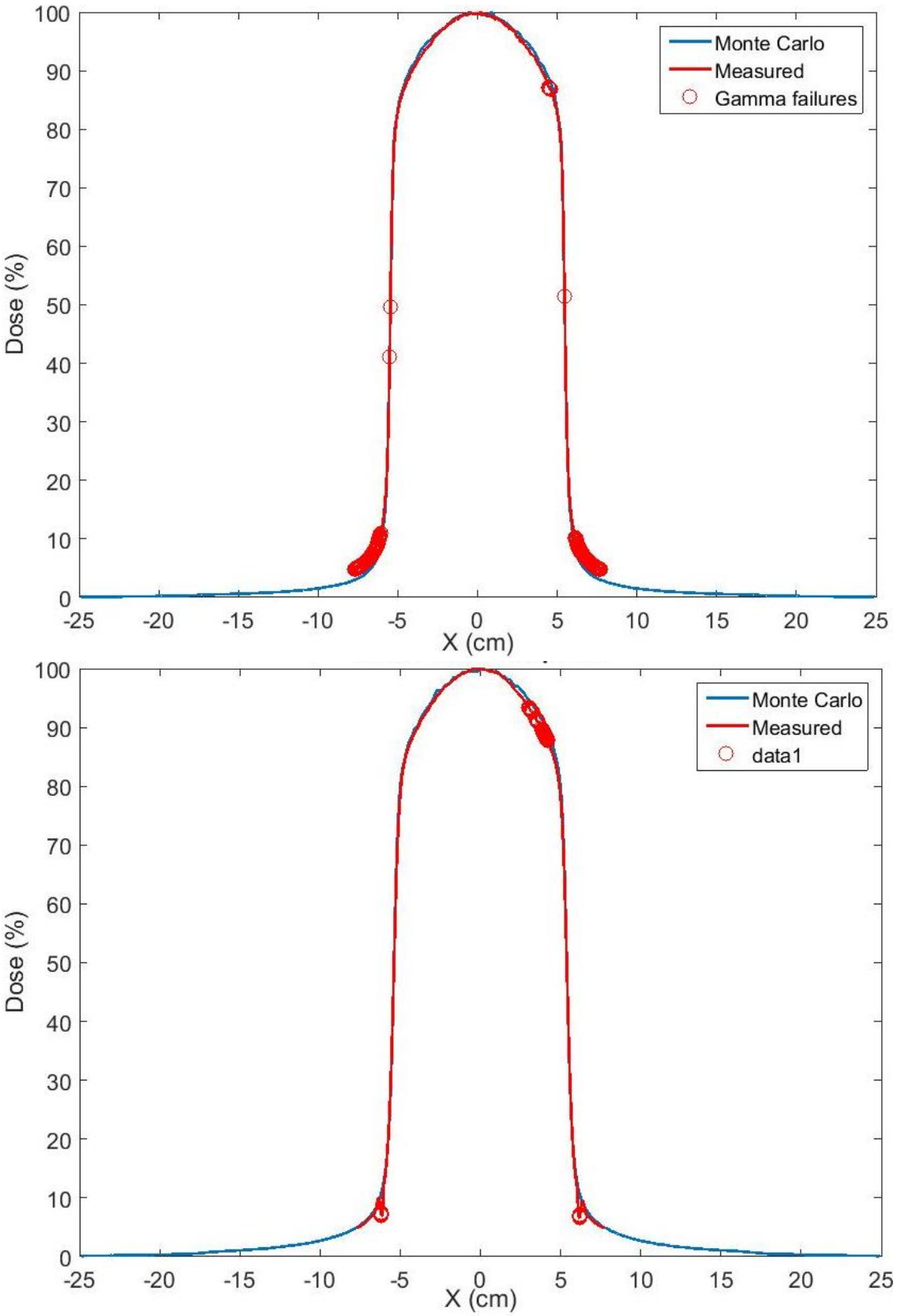

Figure 40: Benchmarking results for the 10cm x 10cm Monte Carlo calculated profiles (blue) against measured data profiles (red) at 100cm SSD. The red circles mark where the difference between the profiles are greater than a global 1%/1mm gamma tolerance. The displayed profiles are (above) at a depth of 10cm in water collimated by the jaws (below) at a depth of 10cm in water collimated by the MLC.

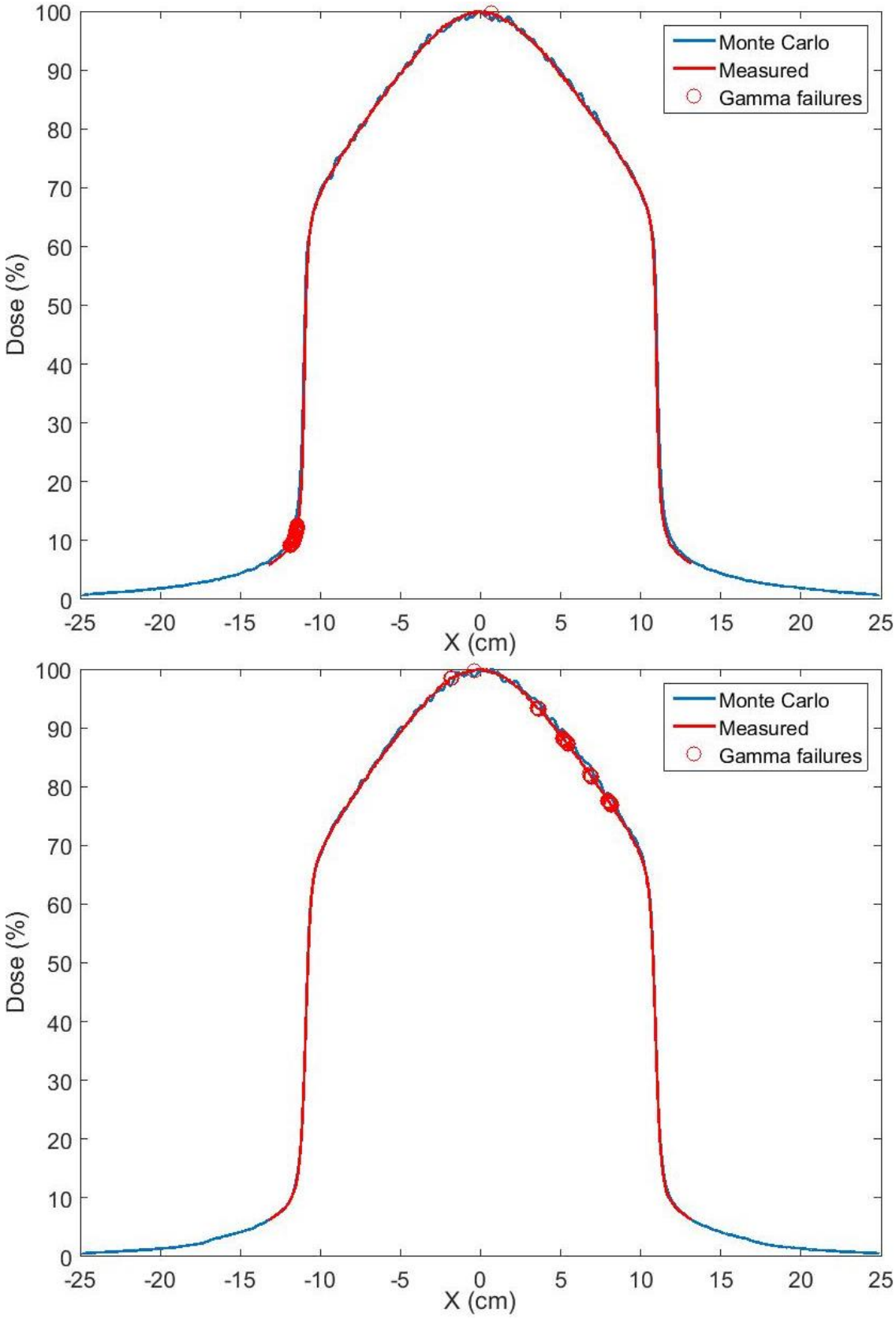

Figure 41: Benchmarking results for the 20cm x 20cm Monte Carlo calculated profiles (blue) against measured data profiles (red) at 100cm SSD. The red circles mark where the difference between the profiles are greater than a global 1%/1mm gamma tolerance. The displayed profiles are (above) at a depth of 10cm in water collimated by the jaws (below) at a depth of 10cm in water collimated by the MLC.

Figure 39 shows that for the 3cm x 3cm field the new Monte Carlo simulation slightly underestimates the dose in the direction collimated by the jaws with excellent agreement with the measured data in the MLC direction. There are no significant areas where the Monte Carlo fails the gamma analysis criteria of 1%/1mm.

Figure 40 shows that for the 10cm x 10cm field the updated Monte Carlo simulations underestimates the out of field dose in the jaw direction, by around 1.5% at the limits of the measured profile and has good agreement in the MLC direction. The failures present in the out of fields in the MLC direction are not significant as they are caused by an interpolation error in the analysis software.

Figure 41 shows that for the 20cm x 20cm field the Monte Carlo simulations show good agreement with the measurements in both the jaw and MLC collimated directions.

5.4. Discussion

The change in shape of the profiles with respect to energy is a result of the conservation of momentum increasing the forward bias of the bremsstrahlung when moving to higher energies. However, by changing the divergence of the beam on the target this forward bias can also be modified so that it is distributed more evenly around the central axis, resulting in a profile shape that is comparable to that of a lower energy beam. A beam divergence on the target of 1.3° was found to best match the measured profile data across the range of clinical field sizes. Reducing the energy to match the profile would reduce in a larger discrepancy to the match in the PDD. From Figure 26 it can be seen that this angular divergence does not have a significant effect on the out of field dose. Conversely previous studies on Monte Carlo simulations of cFF beams have shown insignificant impact of the electron beam divergence on profile shapes and so this parameter is often neglected when modelling MV beams (Sheikh-Bagheri and Rogers, 2002). One previous study postulated that by producing a beam with an extremely large divergence a fully flat beam could be produced (Tsiamas et al., 2011).

The beam divergence parameter is analogous to the bending currents that are used in practice to adjust the beam steering (Paynter et al., 2017). In this work, the bending coarse value of the bending magnet system was found to affect the energy selection of the incident electron beam. However, the bending fine current affects the position that the beam strikes the target. By altering the ratio of these values, the divergence of the electron beam striking the target can be altered. This can be used to broaden or narrow the forward bias of the bremsstrahlung, having the effect of producing a flatter (lower energy) or more peaked (higher energy) profile whilst having a minimal impact on the PDD.

The size of electron spot on the target was determined to be elliptical with dimensions of 0.08cm by 0.17cm; this size provided the best matching of the penumbra for the range of field sizes from 3cm x 3cm to 20cm x 20cm. These dimensions are comparable to the range of dimensions reported by other authors (Sham et al., 2008) with the elliptical shape reported by previous Monte Carlo models of Elekta machines (Almberg et al., 2012).

The fitting of the plots for the field-size calibration in the Monte Carlo model is such that the predicted movement of the leaves and jaws in the Monte Carlo model produces a field size that matches the measured data within 0.2mm for the MLCs and within 0.4mm for the jaws. This matching meets the required gamma analysis criteria for the benchmarking performed in this work and would meet the recommendations for radiotherapy planning system performance tolerances as defined in IPEM81 (IPEM, 2018).

The out of field doses in the Monte Carlo calculations were initially observed to be higher than the measured doses for field-sizes less than 20cm x 20cm. A number of parameters were investigated to attempt to locate the source of this difference. As the dose increase was observed in both the inplane direction (collimated by the jaws) and the cross-plane (collimated by the MLCs, the investigations focussed on geometric parameters that were independent of the jaws and MLCs such as the thickness of the primary collimation system and of the filter plate that replaces the flattening filter in FFF machines. These investigations showed that the thickness had an insignificant effect on the out of field dose in the Monte Carlo calculations. These parameters were investigated as they would alter the amount of scatter radiation within the treatment head that could lead to increased leakage radiation as demonstrated by the reduction of out of field dose when the flattening filter is removed (Murray et al., 2015; Paynter et al., 2014).

The cut-off energy for the electron transport in the Monte Carlo was also investigated to determine if the error was caused by the Monte Carlo calculation properties rather than the geometry. By reducing the cut-off energy from 700keV to 512keV lower energy electrons would be modelled reaching the phantom, as FFF beams have a wider spectrum of energy as a result of the removal of the hardening effect of the flattening filter. The reduction in this cut-off energy showed an improvement in the out of field dose but the reduction was not significant enough to remove the discrepancy from the measured dose. The mechanism for this improvement is that the lower energy electrons would reach the open portion of the beam and increase the infield dose proportionally more than the out of field dose having the effect of reducing the relative out of field dose in comparison to the infield dose.

Following later discussions, additional modelling was performed as in section 5.3.3.2. In the original model (results discussed in section 5.3.3.1) the out of field MLC leaves were positioned at the nominal separation for the required field size across the full leaf bank. It was not originally thought that this would have a significant impact on the out of field dose when investigating profiles in the MLC direction, as the reduction in transmission through the jaw would have been of the order of 0.24% more (Thompson et al., 2014) with the MLCs fully closed over the jaw. However, the results of the newer full simulations with the MLCs closed behind the jaws show excellent agreement with the measured data and reduce the out of field dose by more than the expected amount. By further collimating the beam in these simulations the scattered radiation in the treatment head is reduced and can no longer contribute to the out of field dose. With the leaves fully closed the out of field dose in the jaw direction is reduced more than required resulting in some small gamma failures (at the 1%/1mm level) in that direction. The differences between the original model and the new model in this out of field region increase as the field size decreases. This is due to the measured profiles of larger field sizes receiving a greater contribution from head scatter than smaller field sizes. This explains why the change in the 20cm x 20cm profile is not as significant as the 3cm x 3cm profile. With the majority of the benchmarking showing that the Monte Carlo profile matches the measured profile using the 1%/1mm gamma criteria, the model is now considered accurate enough for further Monte Carlo investigations.

5.5. Conclusion

The modelling of FFF beams with Monte Carlo in EGS/BEAMnrc is possible with the appropriate technical information provided by the vendor. The relationship between the field size and the movement of the jaws and MLCs is not linear and therefore needs to be characterised in order to be able to model more complex field shapes. When modelling FFF beams in Monte Carlo, the divergence of the electron beam at the point of striking the target is a useful parameter to help achieve a realistic model of the incident electron beam on the x-ray target, with a match for both PDD and beam profile distributions. The divergence of the electron beam on the target has minimal impact on the PDD, so once a Gaussian distributed beam energy has been found to produce appropriate PDDs for the clinical range of field sizes, the profile shapes can be further optimised using the divergence parameter. The out of field doses in the original model were not in agreement with measurements for the smaller field sizes and this was investigated by changing a series of model parameters. Further investigations into the model located a discrepancy in the modelled positions of the MLC leaves outside of the field. Running additional simulations with these positions corrected improved the model so that it could now be used for further investigations. The completed model will be used to investigate the out of field dose for

matched FFF beams as previously investigated by Kry et al. (2010) for unmatched FFF beams. The full Monte Carlo simulation will also be compared to the fast Monte Carlo algorithms used in clinically available treatment planning systems in order to benchmark them. The model can also be used to further investigate the out of field doses at a distance to investigate additional treatment sites to the prostate as investigated by Murray et al. (2015).

6. Pre-Clinical evaluation of matched FFF treatments on Elekta Linacs

6.1. Introduction

FFF beams have been proposed as a method of external beam radiotherapy treatment delivery that could decrease the time for hypofractionated treatments, particularly stereotactic ablative body radiotherapy (SABR). The smaller field-sizes generally required for the PTVs encountered for this type of treatment (Consortium, 2016) results in the FFF beam profiles closely matching those of cFF beams, with the advantage of an increased doserate over the target and reduced dose outside of the treated area (Murray et al., 2015). Also, in general, PTV volumes are often not that irregular in shape, therefore, low levels of beam modulation are only likely to be required, leading to fast, efficient treatment deliveries.

The work contained in this chapter was novel at the time of completion and was presented as a poster presentation at ESTRO (Paynter et al., 2013) and also as an oral presentation at the IPEM FFF meeting (Paynter, 2014).

6.2. FFF beams for hypofractionated SABR treatments for lung and other sites

6.2.1. SABR lung fractionations

The hypofractionated regimes investigated for this work are 54Gy in 3 fractions, 55Gy and 5 fractions and 60Gy in 8 fractions. The fractionation regimen is determined by the location of the GTV within the lung. The 54Gy in 3 fraction regimen with the highest dose per fraction is used for GTVs that are not attached to the chest wall or in close proximity to any other OARs. The 55Gy in 5 fractions is used for when the GTV is attached to the chest wall. The 60Gy in 8 fraction regimen is used for when there are OARs in close proximity to the GTV.

6.2.2. Method

To determine whether there are efficiency or dosimetric advantages when using FFF beams for SABR lung treatments, FFF VMAT plans were compared to the current standard of care, i.e. 3-dimensional conformal radiotherapy (3DCRT), as well as cFF VMAT plans. Five lung radiotherapy patients who had previously received 55Gy in 5 fractions SABR treatments were selected. Patients were selected to cover a range of PTV sizes and locations within the lung. They were originally, planned on CMS Xio v4.33 with 7-beam 3DCRT treatments on an Elekta Synergy™ linear accelerator equipped with an MLCi2 head. Each of these patients was planned on a 2mm

dose grid with the superposition algorithm (Miften et al., 2000). The 3DCRT plans were planned with a midline isocentre with 7 beams typically equally spaced around the patient. A midline isocentre places the treatment isocentre at the centre of the patient both left-right and anteriorly-posteriorly treating the target volume off axis. This minimises the risk of collisions between the Linac head and/or XVI imaging system and the patient or treatment couch.

3DCRT beam orientations could be adjusted, if required, to facilitate OAR sparing. In cases where OAR sparing is difficult to achieve with this arrangement non-coplanar beams could be added (Hallemeier et al., 2013).

These patients were re-planned in Monaco v3.2 using a 2mm dose grid and a 1% Monte Carlo variance per plan, on an Elekta Synergy linear accelerator equipped with an Agility head using a VMAT technique with a cFF 6MV beam. Further plans were produced in Monaco v3.3 using the same VMAT technique but with a 6MV FFF beam.

The VMAT plans used a 200° arc, also with a midline isocentre. Some specific details as to how the plans were defined within the Monaco planning system are as follows. For the fluence optimisation, VMAT arcs were calculated with angle increments of 5°. The minimum segment width was set at 1cm. The VMAT plans consisted of an IMRT prescription using the target penalty cost function, set to cover 95% of the PTV with 55Gy.To constrain hot spots within the PTV, a quadratic overdose cost function was used on the PTV with a reference level of 65Gy and a Root Mean Squared (RMS) excess over this value allowed of 1Gy. The dose was kept conformal by using the 'conformality cost function', acting on the patient and with two quadratic overdose functions. These functions were set at 54Gy, with an RMS of 0.1Gy, with a 0cm 'shrink margin' and a 24Gy quadratic overdose cost function with an RMS of 0.25Gy and a shrink margin of 2cm. A shrink margin within the Monaco TPS restricts the area that the cost function applies to a user specified distance from any higher priority target structure. For example, the patient cost function with a 2cm shrink margin applies 2cm away from the PTV. When planning the patients, the RMS values and conformity iso-constraint were iteratively reduced or increased in order to produce the most optimum plan. However, the reference levels, which are the point from which the RMS is calculated, were left unchanged as is the practice at this centre.

The plan quality was compared using dose constraint criteria from the UK SABR consortium guidelines (Consortium, 2016), based on constraints from the ROSEL trial (Hurkmans et al., 2009). Treatment delivery times were also compared. The consortium guidelines contain constraints to control the conformality of the treatment plans that change depending on the size of the target volume; these are described in Table 11.

Table 11: Description of conformality constraints for lung SABR treatments.

Constraint	Description	Effect on constraint of increasing target volume
R100	The ratio of the volume covered by the 100% isodose to the volume of PTV	As the volume of the PTV increases the constraint decreases
R50	The ratio of the volume covered by the 50% isodose to the volume of the PTV	As the volume of the PTV increases the constraint decreases
D2cm	The maximum dose 2cm away from the PTV	As the volume of the PTV increases the constraint increases
L_V20	The volume of lung minus the volume of GTV receiving 20Gy expressed as a percentage	As the volume of the PTV increases the constraint increases

A further 3 lung patients were retrospectively re-planned using a 54Gy in 3 fraction treatment regimen. The IMRT prescription cost function reference levels and starting iso-constraint values for these patients were: target penalty set to 54Gy, with the quadratic overdose, to constrain hotspots, set with a reference level of 67.5Gy and an RMS of 1Gy. The quadratic overdoses used to maintain conformality were 44Gy with an RMS of 0.2Gy and 23Gy with an RMS of 0.2Gy.

The most technically challenging lung SABR plans are planned with a fractionation of 60Gy in 8 fractions. Due to the variability of these plans, 8 patients were retrospectively planned for this work. Patients were selected to cover a range of PTV positions with different OARs in proximity to the PTV. The PTV quadratic overdose was set with a reference level of 75Gy and an RMS of 1Gy, the conformality overdoses were set at 50Gy with an RMS of 0.4Gy and 25Gy with an RMS of 0.4Gy.Where maintaining a conformal dose distribution was not sufficient to meet OAR constraints, additional cost functions were added to the IMRT prescription as a serial cost function with a ‘k’ value of 14 and a reference dose of 65% of the maximum dose allowed to the OAR or 85% of the maximum dose allowed to 0.5 or 1cc of the OAR. The ‘k’ value determines at which points along the Dose volume histogram (DVH) curve the cost function works to reduce the dose. A high ‘k’ value works more on the high doses of the DVH whereas a lower ‘k’ value works more evenly along the DVH curve. The range of ‘k’ values available are from 1 to 20. The ‘k’ values selected for this cost function allow the maximum dose to be controlled whilst providing a suitable dose gradient to achieve coverage and ease of setup during treatments. These reference doses were then iteratively changed to produce the desired dose distribution.

These plans were compared against the 3DCRT plans produced for the patient treatment in terms of plan quality and delivery efficiency.

In addition to lung SABR treatments, commissioning through evaluation (CTE) SABR for oligometastases in the bone and lymph nodes contained in the pelvis were investigated. Commissioning through evaluation (CTE) is a programme that allows patients to access treatment options that a not funded as part of the NHS. The programme aims to provide treatments that show significant promise whilst collecting data so that these treatments can be evaluated by the National Institute of Healthcare Excellence (NICE). The treatments in this programme are for oligometastatic disease where cells from the primary tumour have travelled in the body to form small tumours in other organs.

This was performed to evaluate whether target coverage and OAR constraints could be achieved with FFF beams. As this was a new treatment site, and the SABR lung investigation had already demonstrated that FFF VMAT could produce clinically acceptable plans, no comparison to 3DCRT or cFF beam VMAT was made.

A total of seven patients were planned, including a patient with two metastases in the pelvic region. The plans covered a range of PTV sizes with differing levels of overlap with OARs. The plans could be produced with three different dose fractionations. If the PTV was distal to the primary treatment site the plans were planned at 40Gy in 3 fractions. If it was not possible to meet OAR constraints at this fractionation, they were planned as 30Gy in 3 fractions. For PTVs that were considered as re-irradiation due to the proximity to the original treatment site the dose fractionation was reduced to 30Gy in 5 fractions.

The VMAT prescription used for planning these patients contained the target penalty cost function on the PTV set to cover 95% of the volume with the prescribed dose. A quadratic overdose cost function was used with the reference level set 1Gy above the prescription dose and an RMS dose excess of 2Gy. Should the conformality of the dose to the PTV not be sufficient to spare the OARs, such as when they overlap with the PTV, additional cost functions are added to the prescription. For the bladder and large bowel, a quadratic overdose with a reference level of 27Gy and an RMS of 0.1Gy was used. For the small bowel a quadratic overdose of 24Gy was used with an RMS of 0.1Gy.

6.2.3. Results

6.2.3.1. 55Gy in 5# lung SABR

Table 12: Average results for the five patients planned for the FFF planning comparison. Stated VMAT delivery times are reported by the treatment planning system, 3DCRT times are delivery times as reported by the record and verify system.

				3DCRT plan 6MV cFF		VMAT plan 6MV cFF		VMAT plan 6MV FFF	
Parameter	Units		Aim	Average	SD	Average	SD	Average	SD
V_PTV	cc		N/A	28.42	10.69	28.42	10.69	28.42	10.69
D to 95% of PTV	Gy	≥	55.00	55.26	0.36	55.08	0.05	55.18	0.08
D to 99% of PTV	Gy	≥	49.50	52.42	0.69	53.37	0.41	53.18	0.68
R100		≤	1.15	1.11	0.04	1.11	0.04	1.08	0.05
R50		≤	9.00	4.67	0.61	5.04	0.70	5.03	1.00
D2cm	Gy	≤	38.50	29.56	3.32	31.63	1.53	28.44	2.28
Dlung mean	Gy		N/A	3.20	1.28	3.13	1.14	3.27	1.27
V_L 30	%		N/A	1.82	0.79	1.82	0.73	1.90	0.86
V_L 20	%	≤	6.00	3.52	1.56	3.41	1.37	3.57	1.54
V_L 12.5	%		N/A	7.54	3.22	6.65	2.54	6.92	2.83
V_L 10	%		N/A	10.13	4.29	8.49	3.14	8.97	3.63
V_L 5	%		N/A	18.10	7.48	14.47	6.09	15.97	6.91
Dptv max	Gy		60.5 - 77	69.53	0.50	69.28	2.50	68.21	1.64
Dptv min	Gy		N/A	47.77	2.16	51.29	1.34	50.71	1.36
Dptv mean	Gy		N/A	62.34	0.90	60.20	0.69	61.01	1.04
Dmax CORD (pt)	Gy	≤	25.00	8.24	0.78	8.53	1.02	5.90	3.05
Dmax HEART (1cc)	Gy	≤	27.00	12.66	7.80	11.94	7.05	9.04	6.34
Dmax OESOPH (1cc)	Gy	≤	27.00	9.35	0.67	7.42	0.93	7.31	2.05
Dmax AIRWAY (1cc)	Gy	≤	32.00	9.43	3.60	9.46	4.06	8.85	4.97
Dmax PLEXUS (1cc)	Gy	≤	27.00	3.70	7.27	4.48	8.55	3.62	6.88
Total MU				1868.46	78.62	1685.64	191.14	1925.03	172.42
Delivery time				≈12min		182.80s	20.11s	106.39s	9.08s

The average results across the five patients planned for this comparison are shown in Table 12. The 95% PTV coverages across all three treatment techniques were comparable. Both the VMAT techniques indicated an improved minimum dose to the PTV and 99% coverage of the PTV with the minimum dose improving from approximately 48Gy for the 3DCRT technique to 51Gy for the VMAT technique. The dose received by 99% of the PTV increasing from approximately 52.5Gy to 53Gy. The sample sizes for this study were not large enough to determine statistical significance. The conformality indices of R100, R50 and D2cm were within tolerance despite the improved coverage of the PTVs. The R100 and R50 refer to the relative volume encompassed by the 100% isodose and the 50% isodose lines compared to the volume of the PTV. The D2cm dose constraint refers to the maximum dose at a distance greater than 2cm away from the PTV. The dose received by the lung is assessed by looking at what volume of the lung receives specific doses, as shown in the table as the volumes of lung receiving 30Gy, 20Gy, 12.5Gy 10Gy and 5Gy. All the OAR doses were within tolerance for the three treatment techniques. The VMAT technique used does not have dose entering through the contralateral lung. Therefore, the contralateral lung doses were lower for the VMAT techniques when compared to the 3DCRT techniques. In order to adequately separate the 3DCRT beams out around the patient, beams entering through the contralateral lung are necessary. The VMAT techniques, therefore, reduce the volume of contralateral lung receiving 5Gy from 8% to 1-2%.

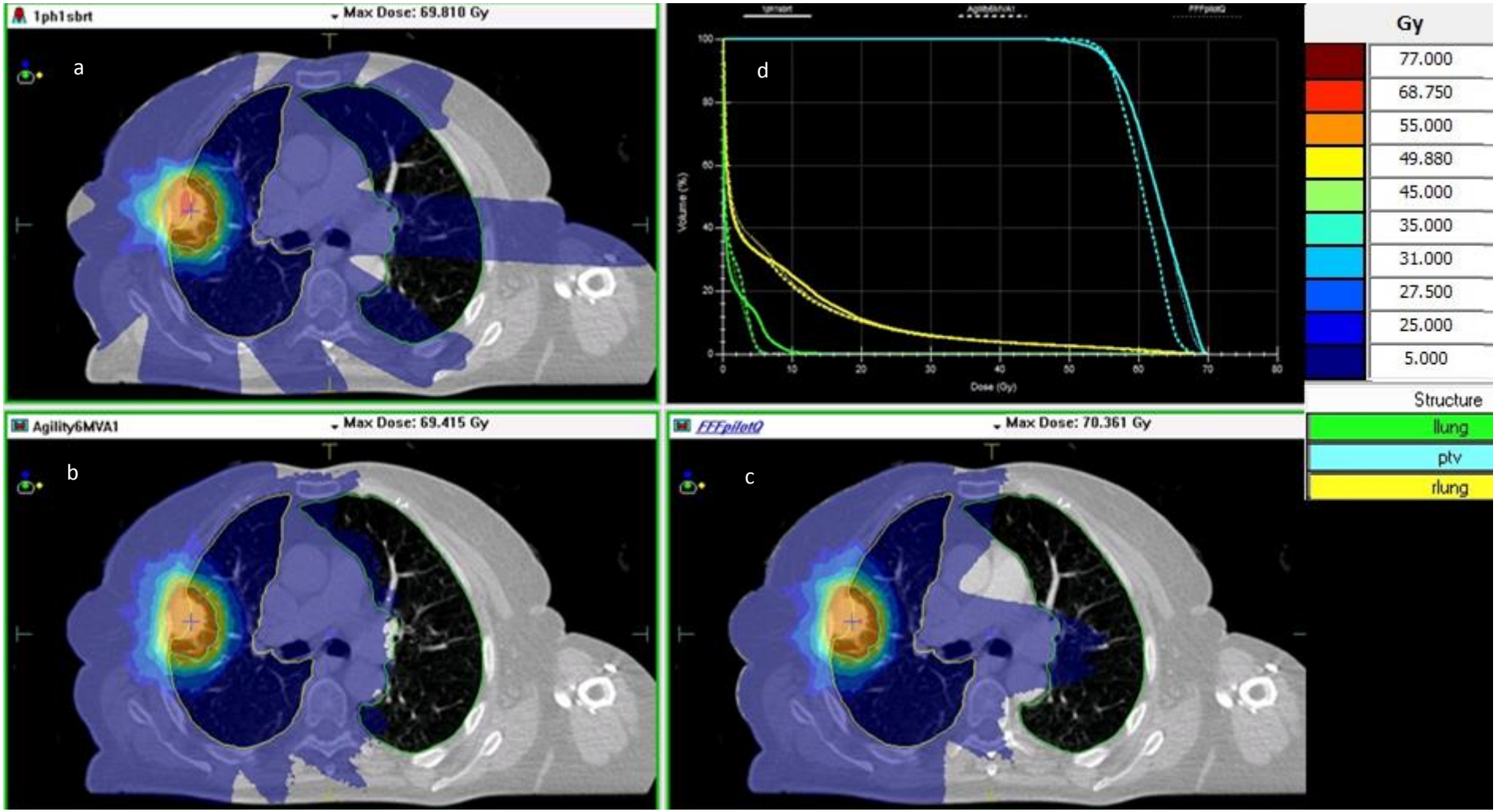

Figure 42: Transaxial slices of the three different techniques for one of the patients investigated. (a) 3DCRT treatment plan, (b) cFF VMAT plan, (c) FFF VMAT plan, (d) DVHs for PTV (blue), right lung (yellow), left lung (green) for each of the treatment techniques (a)solid line (b) dashed line (c) dotted line.

The R100, R50, D2cm and V_L_20 tolerances are dependent on the volume of the PTV treated. Because of the beam matching, the selection of beam energy from a cFF 6MV beam to an FFF 6MV beam does not impact on overall plan quality. However, the difference in dose rate between cFF and FFF beams, 600MUmin^{-1} and 1350MUmin^{-1} respectively, reduces treatment time by approximately a third. Transaxial images of the different plans are displayed in Figure 42. The dose from the 3DCRT beams through the contralateral lung is apparent.

6.2.3.2. 54Gy in 3# lung SABR

Table 13: Average results for the three patients planned for the FFF planning comparison. Stated delivery times are reported by the treatment planning system.

				3DCRT plan 6MV cFF		VMAT plan 6MV FFF	
Parameter	Units		Aim	Average	SD	Average	SD
V_PTV	Cc		N/A	10.5	3.1	10.4	2.9
D to 95% of PTV	Gy	≥	54.0	53.3	0.6	54.2	0.2
D to 99% of PTV	Gy	≥	48.6	52.1	0.7	52.5	0.2
R100		≤	1.25	1.0	0.0	1.2	0.0
R50		≤	12.00	10.5	2.7	10.3	1.0
D2cm	Gy	≤	35.1	28.8	1.3	34.0	2.6
Dcontra_mean	Gy			1.3	0.0	1.1	0.1
VcontraL_5	%			8.9	0.7	3.0	1.4
Dlung mean	Gy		N/A	3.4	0.3	3.3	0.4
V_L 30	%		N/A	1.8	0.3	1.8	0.6
V_L 20	%	≤	5.0	4.1	0.6	3.8	0.9
V_L 12.5	%		N/A	8.1	1.1	7.4	0.9
V_L 10	%		N/A	10.7	1.2	9.2	0.9
V_L 5	%		N/A	18.9	0.9	15.3	1.0
Dptv max	Gy		59.4 -	68.0	0.4	74.2	1.3
Dptv min	Gy		N/A	50.4	0.6	49.8	0.5
Dptv mean	Gy		N/A	57.7	0.7	60.0	0.2
Dmax CORD (pt)	Gy	≤	18.0	10.5	2.6	8.5	2.5
Dmax HEART (1cc)	Gy	≤	24.0	15.0	3.4	14.9	3.0
Dmax OESOPH (1cc)	Gy	≤	24.0	9.7	0.7	8.1	1.4
Dmax AIRWAY (1cc)	Gy	≤	30.0	7.0	4.5	8.4	6.3
Dmax PLEXUS (1cc)	Gy	≤	24.0	0.1	0.1	0.2	0.0
Delivery time				≈12min		204.4s	20.6s

The results of the comparison of the 55Gy in 5 fraction regime demonstrated that VMAT plans produced with FFF were comparable to those produced with cFF beams but with a reduced treatment delivery time. Table 13 shows the average results for the highest dose per fraction regime used for lung SABR treatments, 54Gy in 3 fractions. The FFF VMAT plans were able to achieve improved coverage of the PTV increasing the dose received by 95% of the PTV to the

prescribed dose of 54Gy whilst the 3DCRT technique achieved 53.3Gy. Given the small sample size it is not possible to determine if this improved coverage is statistically significant. The maximum doses received in the VMAT plans were higher with an average maximum dose of 74.2Gy compared to 68Gy for the 3DCRT plan. This increased maximum dose was within tolerance parameter and is not considered clinically significant due to the ablative nature of these planned treatments. The conformality tolerances of the VMAT plans were still within tolerance for the R100, R50 and D2cm.The R50 were equivalent at 10.5 despite the improved coverage. The D2cm showed an increase to 34Gy from 28.8Gy when compared to the 3DCRT plan, but this is likely due to the improved coverage of the VMAT plan. The other OAR doses were within tolerance for both techniques, with the FFF VMAT technique having improved contralateral lung doses, reducing from 8.9% for the 3DCRT technique to 3% for the VMAT technique. Transaxial images of one of the plans where improved coverage was achieved is shown in Figure 43.

6.2.3.3. 60Gy in 8# lung SABR

Due to the variability of SABR plans for individual patients, particularly with respect to proximity to OARs, it is not helpful to produce a table of average results for the 60Gy in 8-fraction plans.

Table 14 shows results for 7 patients with the PTV in close proximity to a range of OARs, planned with both the 3DCRT technique and with FFF VMAT. The cells of the table are highlighted as either yellow or red to draw attention to when a DVH objective has not been met, yellow corresponds to a minor deviation from the clinical protocol and red corresponds to a major deviation from the clinical protocol. An objective value is considered a minor deviation if it breaches the optimal constraint and a major deviation if it breaches a mandatory constraint. Treatment plans can still be accepted if breaching a mandatory constraint with clinician approval.

Patient 1 is an example of a treatment at the anterior apex of the lung abutting the brachial plexus. The PTV coverage of both plans was acceptable with the VMAT plan having better dose conformality. The R100 value for the 3DCRT technique was over the objective value but was classified as a minor deviation from protocol. The D2cm for the 3DCRT technique was classified as a major deviation from protocol at over 50Gy. It was not possible to get the D2cm within the objective value with the VMAT technique but the dose was reduced to a minor deviation. The brachial plexus doses in both techniques were below the tolerance but the VMAT technique was able to produce better sparing for the brachial plexus with a 1cc dose of 24.9Gy compared to 26.7Gy for the 3DCRT technique.

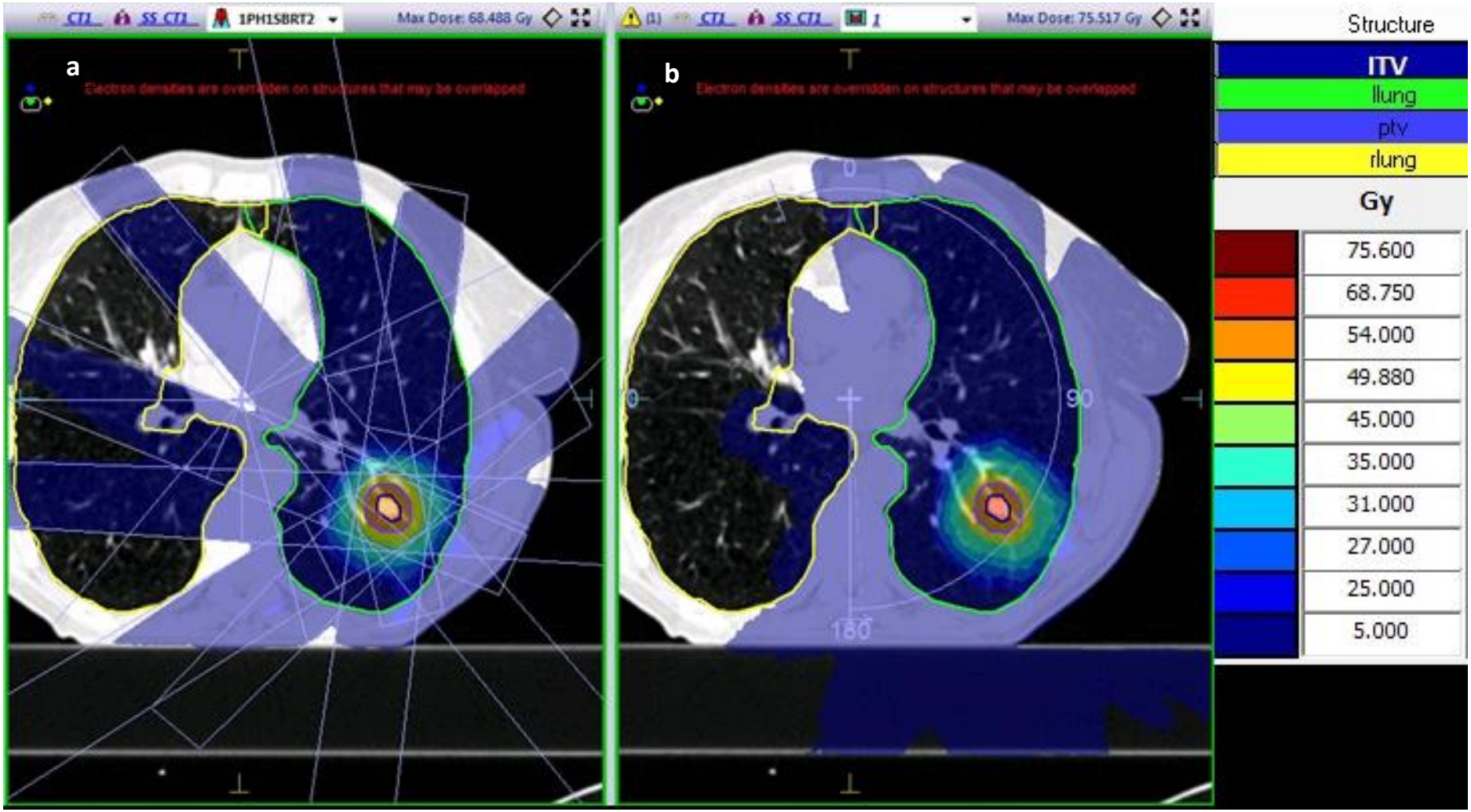

Figure 43: Transaxial slices of the two different with FFF VMAT (b) compared to 3DCRT (a).

Patient 2 has a PTV located close to the spinal cord and oesophagus. Both techniques meet the target coverage objectives (Consortium, 2016). The VMAT plan has better conformality, with the D2cm value considered a minor deviation rather than the major deviation in the 3DCRT plan. The 3DCRT plan also has a minor deviation on the volume of lung receiving 20Gy, whereas, the VMAT plan is within tolerance for this parameter. In order to reduce these deviations the VMAT plan has a higher dose to the oesophagus but this is within tolerance. Both plans keep the dose to the spinal cord below tolerance.

Patient 3 has a PTV located close to the aorta. This is the only example where the VMAT plan had lower PTV coverage than the 3DCRT technique. This was a consequence of the VMAT plan achieving the aorta tolerances when compared to the 3DCRT plan. The D2cm was also reduced from a major deviation to a minor deviation. All other OAR tolerances were met with both of the techniques.

Patient 4 is another example of a PTV in close proximity to spinal cord. Both plans have major deviations on R100 with the 3DCRT plan having an improved value of 1.23 compared to 1.29 for the VMAT plan. For the VMAT plan the D2cm is reduced from a major deviation to a minor deviation.

Patient 5 has the PTV abutting the cardiac wall. Both techniques have minor deviations on the cardiac OAR tolerances and lung V20Gy.

Patient 6 has a PTV close to both spinal cord and the airways. Both techniques fail to achieve the objective coverage in order to meet the OAR constraints. The VMAT plan has a slightly improved D2cm and lung V20Gy, although still a major and minor deviation respectively. The VMAT plan does improve on the 1cc dose constraint on the airway reducing the value to being in tolerance compared to the minor deviation with the 3DCRT technique.

Patient 7 is a case where the PTV is close to the major vessels. The VMAT plan kept the OAR constraints for the vessels within the OAR tolerance and also reduced the D2cm from a minor deviation to being within objective levels. Figure 44 shows transaxial slices comparing the plans produced.

			Patient 1			Patient 2			Patient 3		
				6MV cFF	6MV FFF		6MV cFF	6MV FFF		6MV cFF	6MV FFF
Parameter	Units		Aim	Value	Value	Aim	Value	Value	Aim	Value	Value
V_PTV	cc		N/A	81.6	81.4	N/A	114.6	114.2	N/A	56.9	57.0
D to 95% of PTV	Gy	≥	60.0	60.1	60.1	60.0	60.3	60.0	60.0	58.7	55.2
D to 99% of PTV	Gy	≥	54.0	54.7	56.1	54.0	56.0	56.7	54.0	50.0	44.1
R100		≤	1.10	1.15	1.04	1.10	1.08	1.00	1.10	1.19	0.95
R50		≤	5.00	4.81	4.48	4.50	3.89	3.71	6.00	5.90	5.86
D2cm	Gy	≤	38.5	52.2	39.1	38.5	45.4	41.1	38.5	48.5	41.5
Dcontralung mean	Gy		N/A	2.4	2.6		2.4	2.8		1.5	2.1
Vcontralung_5	%		N/A	18.2	23.5		19.9	23.0		12.8	18.2
Dlung mean	Gy		N/A	7.6	7.5	N/A	6.8	6.9	N/A	4.5	5.2
V_L 30	%		N/A	9.2	8.4	N/A	5.5	4.0	N/A	4.9	5.4
V_L 20	%	≤	10.0	13.1	13.5	10.0	10.3	8.8	10.0	7.1	8.9
V_L 12.5	%		N/A	18.8	16.5	N/A	18.4	18.2	N/A	10.4	11.2
V_L 10	%		N/A	21.6	17.9	N/A	22.1	21.1	N/A	12.3	13.6
V_L 5	%		N/A	28.1	29.8	N/A	33.9	36.7	N/A	19.3	22.6
Dptv max	Gy		66 - 84	76.6	83.6	66 - 84	79.7	82.7	66 - 84	75.2	82.8
Dptv min	Gy		N/A	41.3	38.7	N/A	46.4	51.1	N/A	29.5	25.0
Dptv mean	Gy		N/A	69.2	70.7	N/A	70.3	70.8	N/A	68.2	67.4
Dmax CORD (pt)	Gy	≤	25.0	6.4	17.0	25.0	24.9	24.7	25.0	12.0	20.2
Dmax HEART (1cc)	Gy	≤	50.0	10.6	16.7	50.0	28.4	27.8	50.0	1.9	1.5
Dmax OESOPH (1cc)	Gy	≤	27.0	16.9	19.1	27.0	19.5	26.5	27.0	26.2	26.8
Dmax AIRWAY (1cc)	Gy	≤	32.0	18.3	22.3	32.0	28.8	25.8	32.0	29.0	26.1
Dmax PLEXUS (1cc)	Gy	≤	27.0	26.7	24.9	27.0	0.2	0.2	27.0	25.5	23.5
Dmax Aorta (pt)	Gy	≤							66.0	71.6	64.7
Dmax Aorta (1cc)	Gy	≤							60.0	64.1	54.9
Dmax Aorta (10cc)	Gy	≤							49.0	41.3	41.6

Table 14 continues on next page

			Patient 4			Patient 5			Patient 6			Patient 7		
				6MV cFF	6MV FFF		6MV cFF	6MV FFF		6MV cFF	6MV FFF		6MV cFF	6MV FFF
Parameter	Units		Aim	Value	Value	Aim	Value	Value	Aim	Value	Value	Aim	Value	Value
V_PTV	cc		N/A	60.0	60.0	N/A	36.1	35.83	N/A	77.0	76.8	N/A	41.0	40.8
D to 95% of PTV	Gy	≥	60.0	60.0	60.0	60.0	60.0	60.0	60.0	58.5	58.7	60.0	60.7	60.2
D to 99% of PTV	Gy	≥	54.0	57.2	56.6	54.0	58.8	58.3	54.0	54.1	54.9	54.0	58.1	56.7
R100		≤	1.10	1.23	1.29	1.15	1.00	1.09	1.10	1.08	1.06	1.10	1.10	1.08
R50		≤	6.00	5.87	5.96	9.00	5.13	5.84	5.00	4.45	4.84	6.00	4.87	5.23
D2cm	Gy	≤	38.5	46.6	41.1	38.5	31.6	32.7	38.5	49.8	45.8	38.5	39.3	37.7
Dcontralung mean	Gy		N/A	2.1	2.0	N/A	1.8	1.5		2.7	3.1	N/A	1.8	1.9
Vcontralung_5	%		N/A	18.2	15.3	N/A	14.8	5.6		18.4	30.9	N/A	15.4	12.4
Dlung mean	Gy		N/A	4.4	4.5	N/A	5.1	5.3	N/A	6.9	6.8	N/A	5.1	5.3
V_L 30	%		N/A	3.8	4.0	N/A	3.1	3.5	N/A	5.8	5.7	N/A	4.1	4.4
V_L 20	%	≤	10.0	6.6	6.4	6.0	7.7	7.7	10.0	11.7	10.3	10.0	7.5	8.3
V_L 12.5	%		N/A	9.8	9.5	N/A	14.3	15.2	N/A	20.4	16.1	N/A	12.2	11.4
V_L 10	%		N/A	12.2	11.5	N/A	17.3	17.1	N/A	23.0	19.3	N/A	15.8	13.3
V_L 5	%		N/A	20.5	19.4	N/A	26.7	22.8	N/A	31.2	34.4	N/A	25.9	24.3
Dptv max	Gy		66 - 84	75.3	82.1	66 - 84	75.2	77.6	66 - 84	76.0	83.9	66 - 84	75.3	82.0
Dptv min	Gy		N/A	53.8	51.1	N/A	54.6	55.7	N/A	47.3	47.3	N/A	53.5	49.1
Dptv mean	Gy		N/A	67.6	67.9	N/A	65.9	66.2	N/A	67.7	69.2	N/A	67.6	69.8
Dmax CORD (pt)	Gy	≤	25.0	22.3	24.7	25.0	12.2	11.8	25.0	25.0	23.0	25.0	12.1	13.8
Dmax HEART (1cc)	Gy	≤	50.0	1.3	1.2	50.0	57.5	56.8	50.0	23.5	26.1	50.0	20.1	18.7
Dmax OESOPH (1cc)	Gy	≤	27.0	26.8	20.3	27.0	18.0	15.7	27.0	22.4	23.9	27.0	18.6	16.7
Dmax AIRWAY (1cc)	Gy	≤	32.0	24.5	17.8	32.0	2.3	2.3	32.0	32.2	31.6	32.0	14.4	14.2
Dmax PLEXUS (1cc)	Gy	≤	27.0	12.2	22.5	27.0	N/A	N/A	27.0	17.4	4.0	27.0	0.7	0.9
Dmax Aorta (pt)	Gy	≤										68.0	69.3	67.6
Dmax Aorta (1cc)	Gy	≤										60.0	48.3	45.8
Dmax Aorta (10cc)	Gy	≤										10.0	3.0	2.7

Table 14: DVH prameters for 7 patients with PTV in close proximity to OARs, planned with FFFcompared to the parameters obtained using a 3DCRT technique with a cFF beam. Stated delivery times are reported by the treatment planning system.

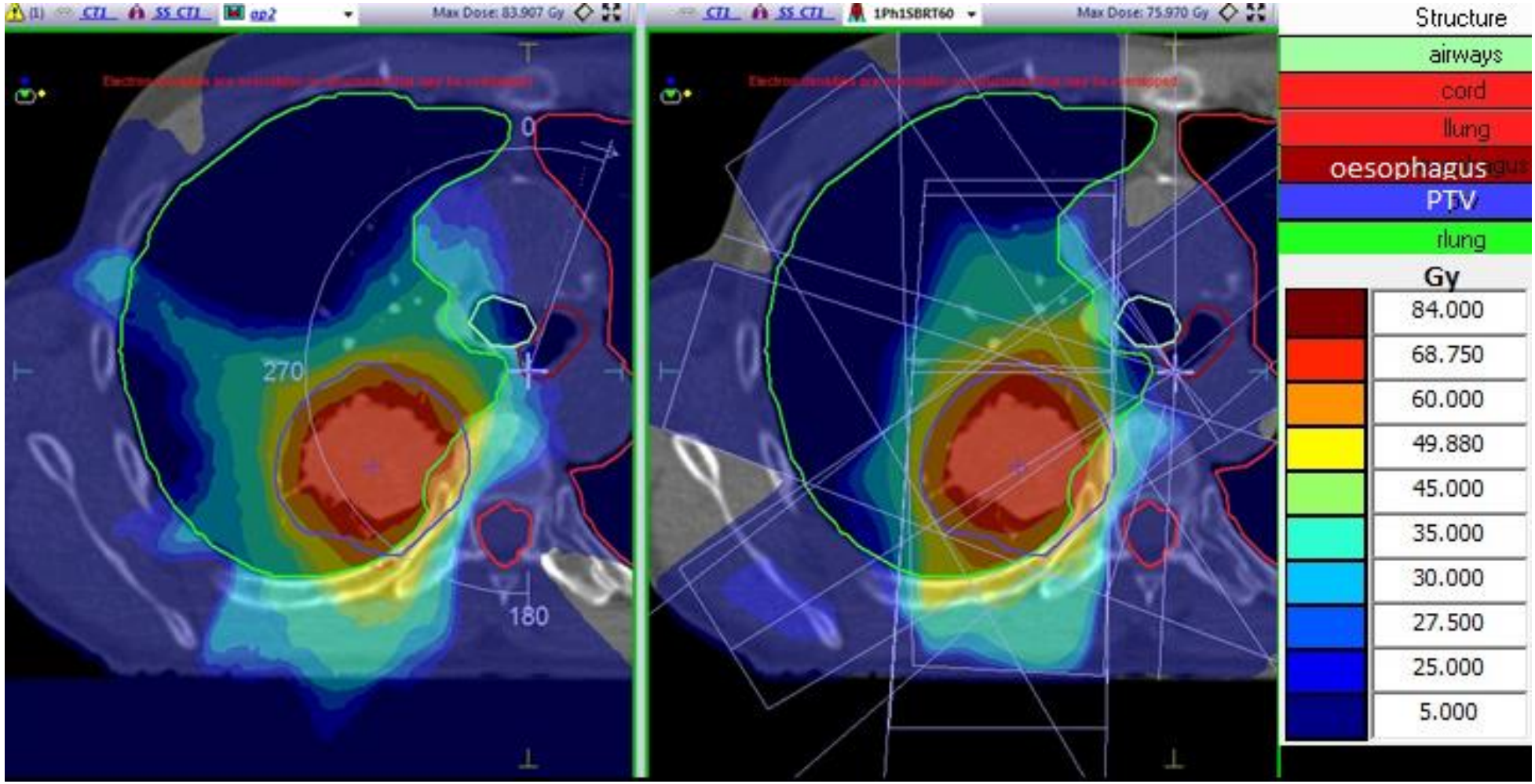

Figure 44: Transaxial slice for the two techniques of one 60in8# plan sparing the spinal cord for patient 7.

6.2.3.4. Commissioning through evaluation (CTE) for pelvic lymph node and bone SABR

Clinically acceptable plans were produced for all the patient plans, with coverage only failing to meet 95% objective when significant OAR overlap was present. Coverage details and OAR doses are shown in Table 15.

Figure 45 shows how the plans avoid OARs and the areas where coverage of PTVs are not met for the patient with the dual site SABR. The white OAR located between the two PTVs was the 'bowel bag', a volume defined to enclose the mobile small bowel. This structure was assigned the OAR constraints of the colon and therefore the prescription dose was not allowed to enter this region.

Patient		PelvLN1	PelvLN2	PelvLN3	PelvLN4	Pelvbone1	Pelvbone2	CTE_PNodesPPTVR	CTE_PNodesPPTVL
Plan		3	newPTV3	30in5	30in5	1	40Gy	2ssoQO40s	2ssoQO40s
Fractionation		30/3#	30/3#	30/5#	30/5#	30/3#	40/3#	30/3#	30/3#
	Aim	Achieved	Achieved	Achieved	Achieved	Achieved	Achieved	Achieved	Achieved
PTV (95%)	Px	30.3	25.5	31.1	31.5	29.8	40.2	27.3	30.6
PTV (mean)		34	31.6	32.6	33.3	33.2	42.4	33	34.8
PTV (min)		25.5	14.8	30.4	28.9	25.3	37.3	25.5	26.2
PTV (0.5cc)	39/40	38.2	37.4	34.4	35.5	38.3	47.9	39.5	39
Small Bowel (0.5cc)	25.2	25.1	23.9	-	-	23.7	14.5	-	-
Small bowel (5cc)	17.7	11.7	17.6	-	-	8.9	11.8	-	-
Large bowel (0.5cc)	28.2	6.8	16.3	-	-	28.1	16.7	28.1	28.1
Bladder (0.5cc)	28.2	13.06	28	-	-	-	15.5	-	-
Bladder (15cc)	16.8	7.9	14	-	-	-	8.9	-	-
Large bowel 5# (0.5cc)	32	-	-	7.4	4.8	-	-	-	-
Bladder 5# (0.5cc)	38	-	-	10.4	18.8	-	-	-	-
Bladder 5# (15cc)	18.3	-	-	6.7	8	-	-	-	-

Table 15: DVH parameters for 7 patients with metastatic disease in the pelvis planned with FFF SABR against the OAR constraints, including one patient with two PTVs to be treated concurrently

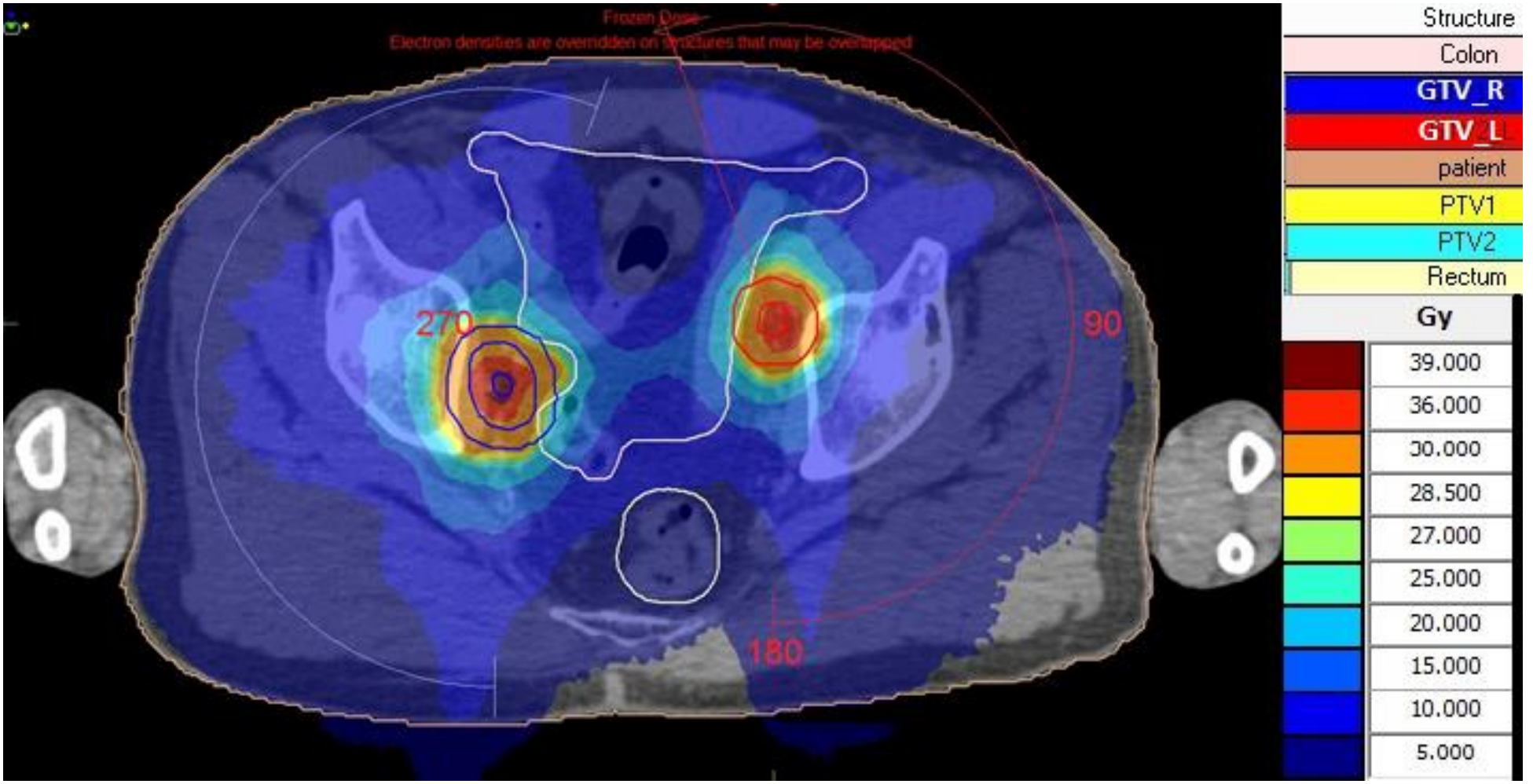

Figure 45: Transaxial slice of the plan treating two PTVs concurrently

6.2.4. Discussion

6.2.4.1. Plan quality

With the investigation into 55Gy in 5 fraction SABR treatments, the change in planning system and modality was first investigated by re-planning patients that had received treatment with 7 beam 3DCRT radiotherapy with VMAT and a cFF beam. Due to limitations within the planning systems used it was not possible to plan 3DCRT using Monaco v3.2 or v3.3, neither was it possible to plan VMAT using CMS Xio. Each system has been appropriately benchmarked and therefore the differences in plan DVHs will be the result of the treatment technique rather than dose calculation algorithm. Benchmarking is performed by comparing calculated and measured PDDs and dose distributions to ensure that beam models used for planning match the delivered dose distributions (Lopez-Tarjuelo et al., 2014; Luo et al., 2013). Plan benchmarking is performed by comparing the delivered plan doses to measurements performed with ion chambers, film and Delta4 (Calvo et al., 2009).

The plan qualities in terms of PTV coverage and OAR doses was comparable between the 7 beam 3DCRT technique and VMAT plans with the exception of the doses to the contralateral lung. An improvement is seen with the VMAT technique as it uses a 200degree partial arc that does not enter through the contralateral lung. With the 7 beam 3DCRT technique this is not possible without reducing the high dose conformality around the PTV. No clinically significant differences in plan quality were identified between the FFF VMAT technique and cFF VMAT technique, that cannot be accounted for with the variation of running multiple optimisations on an inverse planning system that uses a Monte Carlo dose algorithm. The 1% statistical uncertainty in the Monte Carlo calculation results in identical input parameters, obtaining slightly different results when repeat optimisations are performed.

The results of the 55Gy in 5 fraction treatment techniques investigations showed that the differences between planning VMAT with a cFF beam and FFF beam were not significant. Comparable plan quality for cFF and FFF VMAT has been previously reported for SABR treatments on Varian TrueBeam Linacs using ‘unmatched’ FFF beams (Gasic et al., 2014; Hrbacek et al., 2014; Scorsetti et al., 2011), with some authors stating improved OAR sparing with FFF beams compared to cFF beams (Tambe et al., 2016; Lu et al., 2015; Navarria et al., 2013). Therefore, further studies only compare the plan quality between the 7 field 3DCRT technique and FFF VMAT technique. In order for a patient to be prescribed a treatment of 54Gy in 3 fractions the target volume must not be attached to the chest wall and must not be in close proximity to OARs. Therefore, only 3 different patients were investigated as the variability in

plan geometries are small. The VMAT plans produced had improved PTV coverage with a lower dose conformality. This reduction in dose conformality is due to the 3DCRT plans not covering 95% of the PTV with the prescription dose. The conformality index of the VMAT plans was within clinically acceptable limits for all of the plans produced.

The most complex lung SABR plans are planned with the lowest dose per fraction in order to improve OAR sparing. The majority of plans produced with FFF VMAT had improved coverage and OAR sparing when compared to the 7 field 3DCRT plans. The two plans with reduced coverage when planned with FFF were planned so that the vessels or aorta OAR doses resulted in lower risk of side effects, these additional constraints were not achievable with the 3DCRT technique. In order to produce clinically acceptable plans, the 3DCRT plans for these patients had non-coplanar beams added. This resulted in additional dose superior and inferior to the target region when compared to the VMAT FFF plans.

For all of the VMAT SABR plans, the maximum doses within the PTV were higher. With 3DCRT planning the plan is normalised at a point to calculate the required monitor units, which results in plans having a more consistent maximum dose based on this normalisation. The VMAT plans apply no normalisation to the plans and therefore the maximum dose can be higher. The maximum dose is instead constrained using a cost function to keep the maximum dose within 140% of the prescription dose. As these doses are for ablative treatments the increased doses in the PTVs were clinically acceptable. The doses could have been further reduced with the VMAT technique but this would have increased the plan complexity and may have resulted in interplay issues during delivery. These interplay issues and how they have been resolved will be discussed in a following section.

For SABR plans in the pelvis there is a wide range of OARs that could be in close proximity to or overlapping with PTVs. The cases that were planned ranged from PTVs with no overlap and without any OARs in proximity, to PTVs where large amounts of overlap required compromise to the coverage. The case ‘pelvbone2’ had no overlap, with the closest OAR (small bowel), which was far enough away from the PTV for a conformal dose distribution to allow the dose to be escalated to 40Gy in 3 fractions. The plans where it was not possible to cover 95% of the PTV with the prescription dose had volumes of the PTV that overlapped with the OARs. The right-hand volume of the case ‘CTE P’ had a large portion of the PTV that overlapped with the colon (Figure 45). The relationship between the overlap of the OAR and the PTV is shown in Figure 46. For volumes of overlap under 1.5cc it was still possible to achieve coverage of the prescription dose to 95% of the PTV. This is due to the overlapping OAR being a parallel organ; rather than a maximum point dose constraint an area of 0.5cc was able to receive over the stated maximum dose. In order to achieve the OAR doses for the case with two PTVs, both PTVs needed to be

treated in the same plan, so that the optimiser could account for the doses delivered as a result of treating the second PTV whilst minimising the contribution from the beam treating the opposing PTV. This was achieved by using two beams with different isocentres each only optimised to treat one of the PTVs. The isocentre for each beam was positioned in the centre of the associated PTV and constrained to allow the leaves only a margin of 5mm around the PTV. This resulted in both beams contributing doses to the OAR, but the contribution from the second beam being dose from the low dose transmission of the opposing PTV. By planning in this way, if the PTVs migrated relative to each other the dosimetric impact would be low.

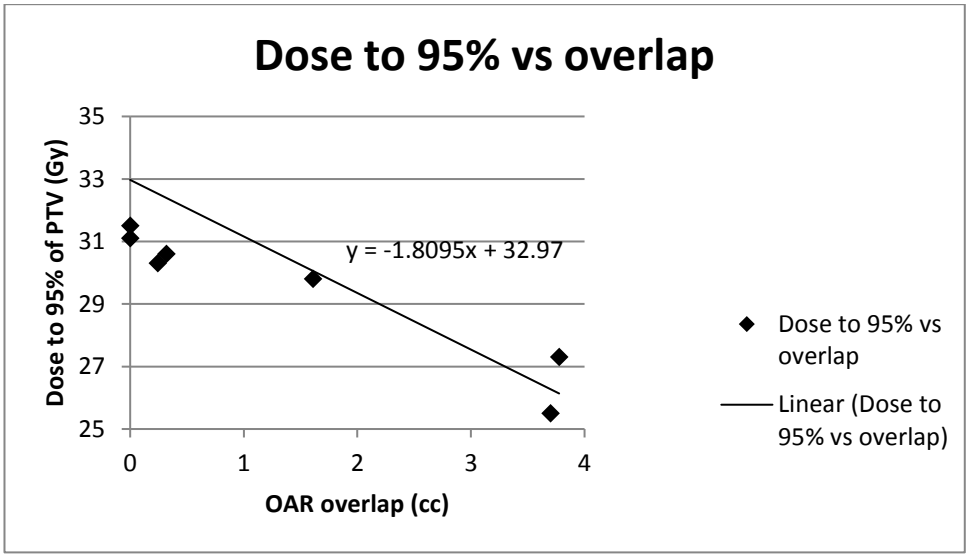

Figure 46: The relationship between OAR overlap and the dose to 95% of the PTV

6.2.4.2. Delivery efficiency

The primary drive for the use of FFF beams in radiotherapy is to reduce treatment times and therefore improve the efficiency of machine use. With the projected increase in demand for radiotherapy (CRUK, 2015) services it is desirable to improve treatment efficiency to increase treatment capacity. Plans that require large MU settings to deliver high doses per fraction are where this increased dose-rate is likely to have the largest impact on treatment times. Table 12 shows that treating with an FFF beam compared to a cFF beam reduces the beam-on time for these lung SBRT treatments from 180seconds to 106seconds, a reduction of 42%, other studies have reported reduction in treatment times of 59% (Hrbacek et al., 2014) and 61% (Tambe et al., 2016), both these studies used an isocentre placed at the centre of the PTV allowing the maximum doserate to be utilised more effectively.. The reduction in beam on time observed in this study is less than the ratio of the dose-rates available for each beam (600MU/min for cFF, 1400MU/min for FFF), which implies the expected reduction would be 57% if this ratio was the

only factor in the delivery. However, the plans with FFF beams required almost 15% more MU than the cFF beams. This is the same as the efficiency loss when comparing the dose-rates of the two modalities. The increase in MU required for FFF beams when compared to cFF beams has been reported by other authors as 34% (Lechner et al., 2013) and 25% (Hrbacek et al., 2014). This increase is greater than that found in this study, as possible cause is that in this work the energy of the FFF beam was matched to the cFF beam resulting in greater penetration.

The energy matching performed on the Elekta implementation of FFF beams means that a reduction in beam penetration does not explain why more MUs are required for the FFF plan. The profile shapes of cFF and FFF beams for field sizes less than 5cm x 5cm are comparable for FFF beams therefore additional modulation is also unlikely to be the cause.

The reason for this reduction in efficiency is a result of the method of planning SABRs at this institute. For these treatments, a 'mid-line' isocentre technique is used. This is where the isocentre is placed in the middle of the patient on a plane that bisects the PTV. The advantage of placing the isocentre in this location is that it is less likely that the location of the isocentre will cause a collision between the patient or couch and the touch guard on the linear accelerator head during cone beam CT image acquisitions. In some situations, particularly for a laterally located PTV, placing the isocentre within the PTV risks causing a collision during the cone beam CT scan, or requires the reduction of the scan acquisition to a 180degree arc, resulting in reduced image quality of the scans. The disadvantage of the mid-line isocentre technique with respect to FFF beams is that a portion of the beam is not delivered on the central axis and due to the profile shape of FFF beams the output off axis is not 1cGy per MU and therefore more MU are required to deliver the same dose (Figure 47).

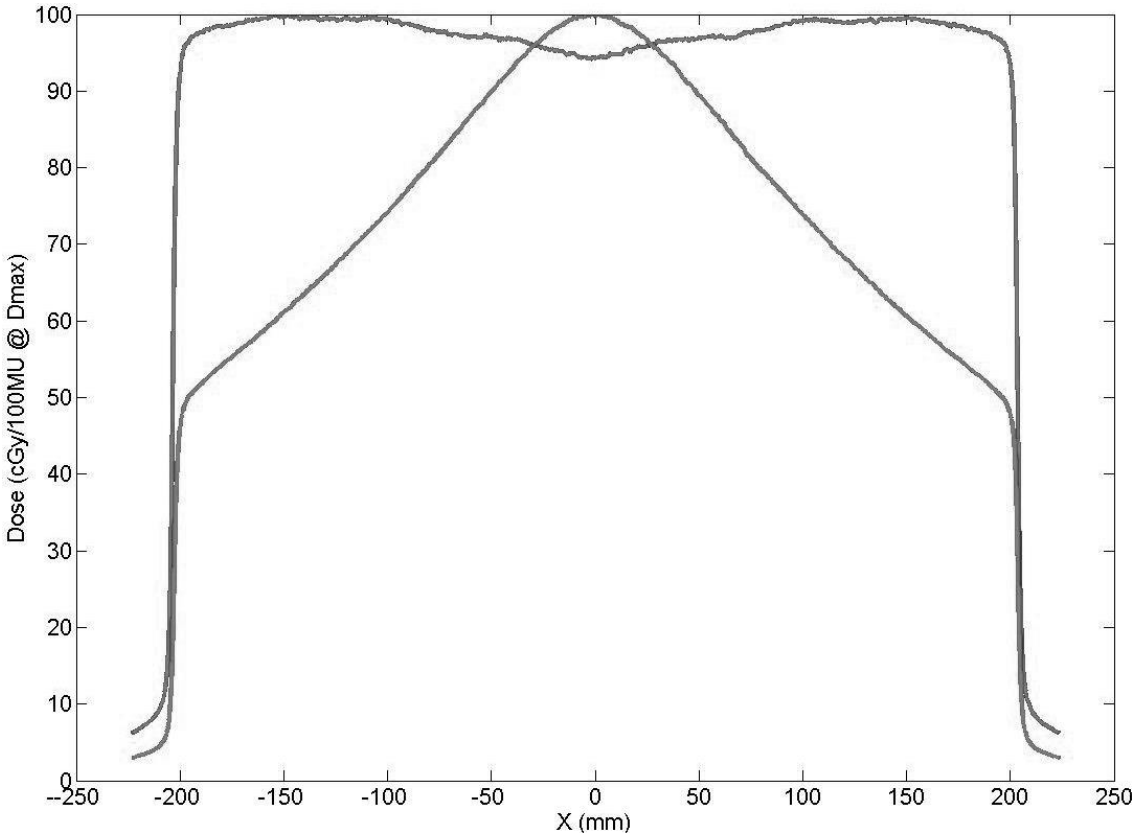

Figure 47: Dose in cGy/MU with respect to off axis distance for 40cm x 40cm 6MV FFF and cFF beams taken at 100cm SSD at a depth of maximum dose

6.2.4.3. Interplay effects

Section 6.2.4.1 concluded that plan quality may have been improved further if the impact of interplay had not been a concern. Interplay is the relationship between the segments used to deliver the treatment field and the motion of the target within the PTV (Shepherd et al., 2018). For lung SABR treatments, the motion due to breathing can be large: up to 2cm (Edvardsson et al., 2018; Kubo et al., 2018)) and the size of the GTV compared to the PTV can be small as a result of breathing motion (Figure 48).

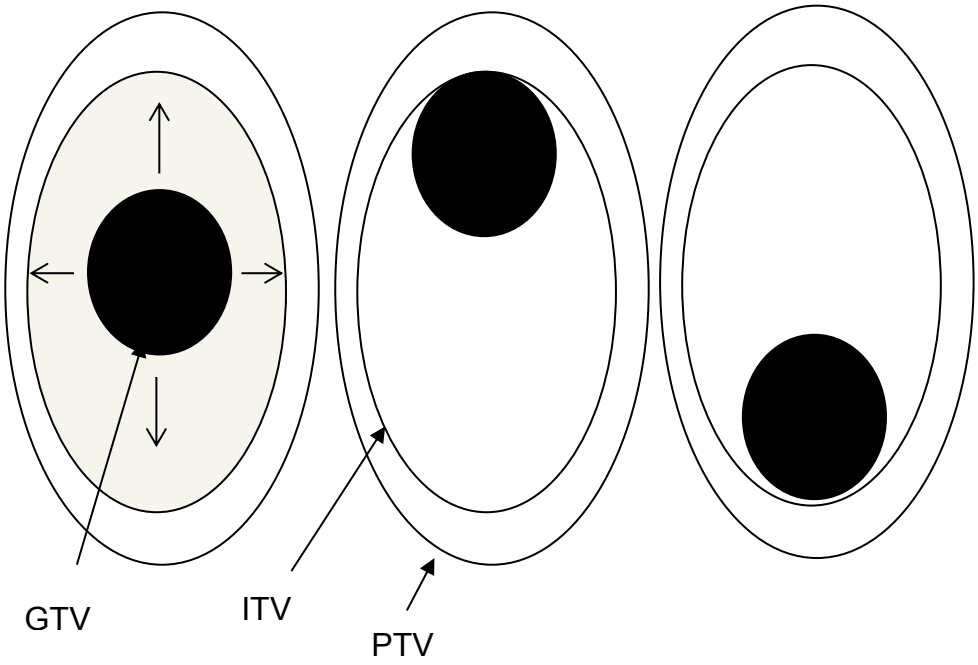

Figure 48: Three of the possible GTV locations within one respiratory cycle

This is of a greater concern for FFF beams as, due to the efficiency of the delivery, the treatments are delivered in a shorter time-frame and therefore over fewer respiratory cycles. As the number of respiratory cycles decreases, the impact of interplay increases (Kubo et al., 2018). In order to minimise this effect, the plans were produced with 'uncomplicated' segments, which results in higher doses to the GTV because the planning system is unable to modulate the beam to cool down these hot areas (Figure 49). The complication of the segments was reduced by setting the minimum segment width to 1cm as well as having a small fluence increment. The small fluence increment means that the leaves travel quickly from one side of the field to the other, thereby reducing the opportunities to produce complicated modulation. This results in higher doses to the GTV because the planning system is unable to modulate the beam to reduce the dose delivered to these 'hot' areas (Figure 49). The plans were also produced with segment shape optimisation set to 'off'. With this function setting the segment shapes were not changed multiple times during the optimisation. A study by Boda-Heggemann et al. (2013) looked at the use of FFF beams for breath hold treatments to mitigate the impact of interplay. The study found that with FFF and 3DCRT treatments for lung SABR that the plans could be delivered in a 15minute timeslot compared to a 30min timeslot for cFF beams. This demonstrates a time efficiency improvement in comparison to cFF beams but not to VMAT deliveries.

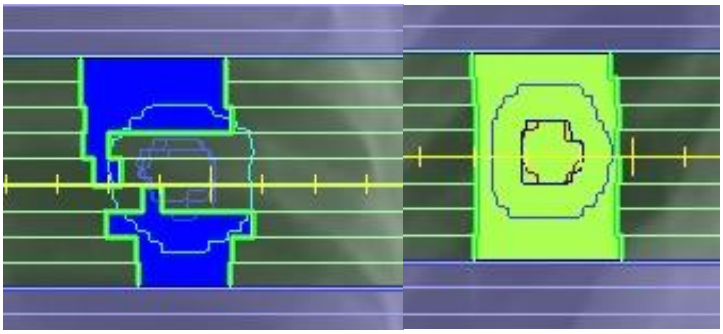

Figure 49: Example of a modulated segment and an open segment, the outer contour represents the PTV and the inner contours represent the ITV and GTV. The shaded areas show the beam aperture.

6.3. Standard fractionated treatments

With the increased dose-rate of FFF beams, most studies have focussed on hypofractionated, high dose per fraction treatments, as the increased dose-rate can produce significant reduction in treatment times (Hrbacek et al., 2014; Lang et al., 2013; Tambe et al., 2016). The potential issues with using FFF beams for standard (2Gy per fraction) fractionated treatments are that additional modulation may be required to produce a uniform dose within the PTVs due to the profile shape of FFF beams. This additional modulation would result in more MU being required relative to cFF beams. However, other efficiencies can be achieved if FFF beams are also used for standard applications. For example, using fewer beam energies for clinical applications means planning system and linear accelerator quality assurance can be reduced. Chapter 4 has discussed how an FFF beam can be quality assured without the need for a clinical cFF beam. Here treatment planning studies have been performed in order to determine if plans with lower doses per fraction can be produced with FFF beams.

6.3.1. Head and Neck 2Gy/#

6.3.1.1. Method

In order to determine the feasibility of using FFF beams for treating head and neck cancers, four patients were planned on Monaco v3.3 with both a cFF 6MV beam with an MLCi2 head and an FFF 6MV beam on an Agility head. The aim was to identify if differences in plan quality or delivery efficiency were observed when planning with FFF. The plans were produced on the two different heads for the different modalities because an appropriately benchmarked and verified cFF model was not available on Monaco for the Agility treatment head.

The beam arrangement used was two 180degree arcs starting at gantry 0 and going clockwise or counter clockwise then returning to gantry 0. This produced a total arc length used for the

optimisation of 720°. This arrangement provides the same arc length as two 360degree arcs with the advantage of double to MLC start positions. The advantage of this is that it allows a break in the treatment delivery so that the MLCs can be moved to start in more optimal positions for the return portion of the arc. In addition to this it also results in the plan finishing with the gantry starting and ending at 0° improving the efficiency of getting the patient on and off the treatment couch. Each case was produced using a 3mm dose grid and a Monte Carlo variance of 1% per plan, this grid size is comparable to those used in other published studies such as Lechner et al. (2013) that used a grid size of 4mm for H&N treatments (Lechner et al., 2013). The increased number of OARs and PTV dose levels in head and neck treatments, along with the non-ablative nature of the treatment, results in IMRT prescriptions that are more complex than for the SABRs previously described. The primary PTV uses a target penalty cost function set at the prescription dose, which was not altered during optimisation. A quadratic overdose with a reference level set at the prescription dose with an RMS of 1.5Gy.The RMS was adjusted to prevent hotspots within the PTV. Elective PTVs were planned with a target penalty cost function set at the elective prescription dose. To control the fall-off of dose from the higher dose PTVs into the elective PTV, a quadratic overdose with a 0cm shrink margin set at the elective dose with an RMS of 2Gy was used. This shrink margin means that the constraint works up to the edge of the PTV. To control the dose received by 50% of the volume (D50%) of the elective PTV, a second quadratic overdose that acts on areas of the PTV 0.9cm away from higher dose PTVs was used, set at the elective prescription with an RMS of 0.8Gy. Elective PTVs cover at risk regional areas that are treated with a lower target dose to the primary PTV.

To prevent having any areas of 110% of the prescription dose, a maximum dose constraint is applied to the entire patient volume set at 110% of the prescription dose minus 0.5Gy. This patient structure also has a conformality cost function that constrains dose outside the PTVs and has a higher dose penalty the further dose is from the PTV. Organs at risk are positioned below the patient cost functions in the IMRT constraints, with the cost functions applied to them set to optimise over all voxels in the structure. Serial cost functions are applied to the cord plus 3mm structure and brainstem with ‘k’ values of 20; the reference level for these is set to 38Gy and 38.5Gy respectively, this ‘k’ value determines where on the DVH curve the constraint works, a ‘k’ value of 20 means that the constraint works at the higher end of the DVH curve and acts more like a maximum dose. Larynx and midline structures use the conformality cost function to reduce the dose spill into these organs where they do not overlap with a PTV. The parotids use a conformality cost function and a serial cost function with a reference dose of 95% of the prescription dose to reduce the dose in the parotid outside of the PTV and prevent hotspots in the OAR that overlaps with the PTV. The plans were compared in terms of plan quality and delivery time.

6.3.1.2. Results

Clinically acceptable plans were achieved for each of the planning cases investigated for both delivery modalities. Trans-axial slices showing the dose distribution achieved on two of the cases are shown in Figure 50.

The DVH values obtained for the same two planning cases are shown in Table 16. Case 1 has comparable coverage of the target when comparing FFF to cFF with 95% of the PTV being covered by 68.4Gy for the cFF plan and 68.0Gy for the FFF plan. The maximum dose to 5% of the PTV and maximum dose to 2% of the PTV are identical in both the cFF and FFF plans. The coverage of the elective PTV is also comparable with 95% coverage of 56.3Gy for the cFF plan and 56.4Gy for the FFF plan. Organ at risk doses were comparable for each plan. The OAR doses for each plan were comparable, with neither technique resulting in a significant change in OAR dose that would cause an OAR to be in or out of tolerance with respect to the other technique.

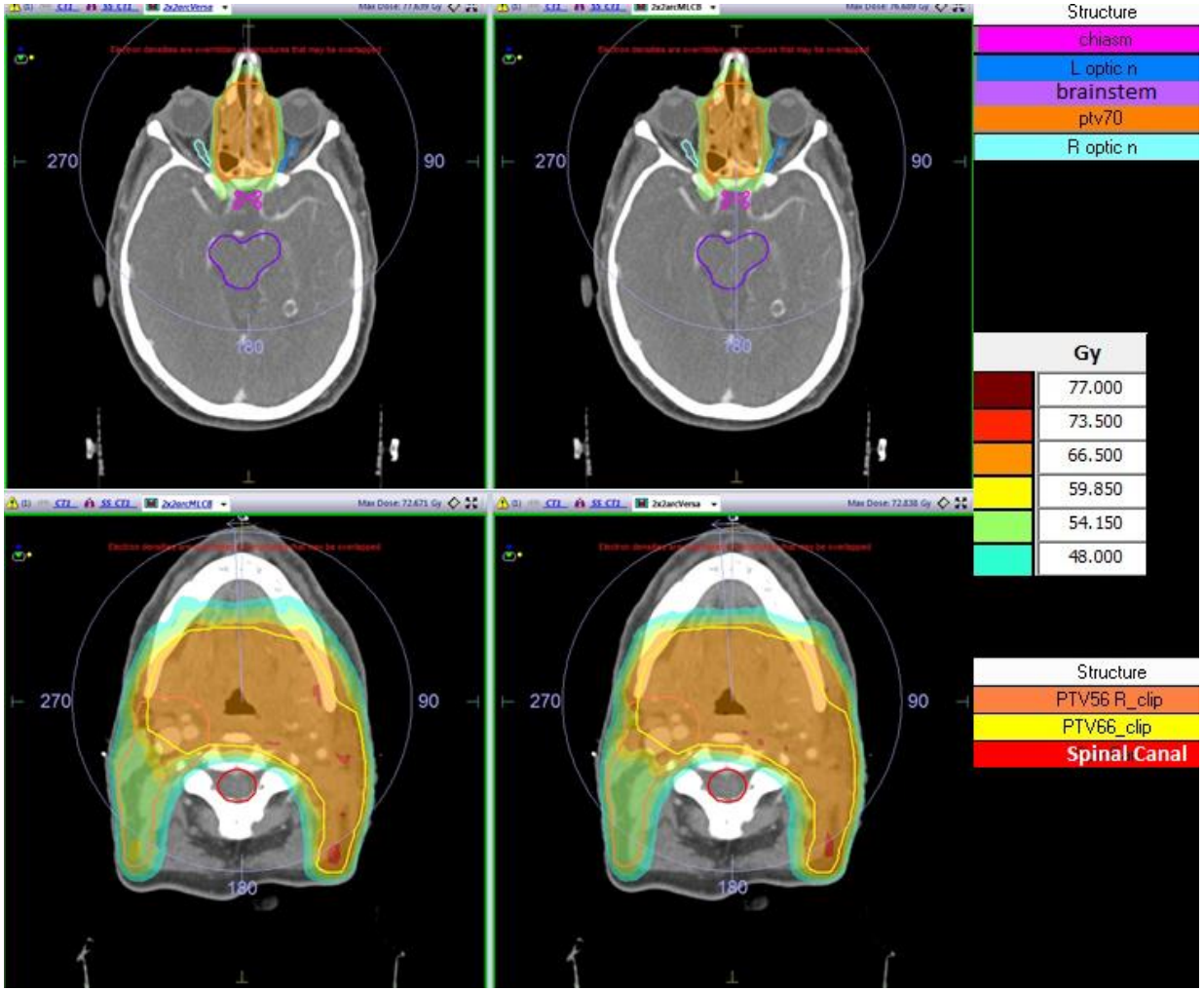

Figure 50: Transaxial slices from two of the planning cases comparing the dose distribution between the two modes of delivery. Upper left FFF, Upper right cFF, Lower left cFF, lower right FFF. Above: a plan with a 70Gy PTV close to optical OARs. Below: a plan with a large high dose region with lower dose elective region to the right hand side of the patient.

Table 16: DVH values obtained for two patients planned with both cFF and FFF beams. Patient 1 refers to a patient with the high dose region in close proximity to optical OARs, patient 2 refers to a patient with a large high dose region. Red text highlights OAR doses that exceed dosimetric aim.

			Patient 1			Patient 2		
Parameter	Units		Aim	6MV cFF	6MV FFF	Aim	6MV cFF	6MV FFF
PTV - radical target			70.0			66.0		
D99% ≥ 90%	Gy	≥	63.00	66.80	66.80	59.40	62.90	63.40
D95 ≥ 95%	Gy	≥	66.50	68.40	68.00	62.70	64.60	64.70
D5% ≤ 105%	Gy	≤	73.50	73.00	73.00	69.30	69.00	69.00
D2% ≤ 107%	Gy	≤	74.90	73.60	73.60	70.62	69.50	69.50
Elective target 1								
Prescribed dose	Gy	=	57.0			56.0		
D99% ≥ 90%	Gy	≥	51.3	55.00	55.30	50.4	54.90	55.10
D95 ≥ 95%	Gy	≥	54.2	56.30	56.40	53.2	56.00	56.10
Spinal canal Max	Gy	≤	48.0	42.7	43.9	48.0	39.7	42.4
Cord PRV dose to 1cc	Gy	<	48.0	43.7	43.8	48.0	42.9	42.8
Brainstem Max	Gy	≤	54.0	51.9	53.6	54.0		
Mean	Gy	≤	40.0	31.8	29.0	40.0	26.5	24.9
Dose to 1cc	Gy	<	60.0	42.9	42.5	60.0	19.4	16.0
Ipsilateral Parotid mean	Gy	≤	26.0	55.2	55.2	26.0	N/A	N/A
Contralateral Parotid mean	Gy	≤		52.2	52.3	26	23.2	23.9
Larynx mean	Gy	≤	45.0	46.2	47.4	45.0	N/A	N/A
Oral Cavity mean	Gy	≤	45.0			45.0	50.7	47.7
Other OAR								
RT eye mean	Gy	≤	45.0	34.7	33.2		N/A	N/A
LT eye mean	Gy	≤	45.0	39.2	36.4		N/A	N/A
RT retina mean	Gy	≤	45.0	28.4	29.0		N/A	N/A
LT retina mean	Gy	≤	45.0	31.7	29.2		N/A	N/A
RT lens max	Gy	≤	6.0	39.4	33.5		N/A	N/A
LT lens max	Gy	≤	6.0	45.6	40.7		N/A	N/A
RT optic nerve max	Gy	≤	60.0	56.5	57.2		N/A	N/A
LT optic nerve max	Gy	≤	60.0	57.2	57.5		N/A	N/A
Chiasm max	Gy	≤	60.0	55.1	55.9		N/A	N/A

6.3.1.3. Discussion

Clinically acceptable plans were achieved for each of the planning cases investigated. Other studies performed on the Varian TrueBeam linear accelerator have demonstrated that the plan quality comparison can be variable in cases of H&N. Some studies have concluded that PTV coverage is equivalent but with improved OAR sparing for FFF plans (Nicolini et al., 2012; Yan et al., 2016). Other studies have found that FFF plans have poorer homogeneity than cFF plans (Zhuang et al., 2013; Gasic et al., 2014). The same optimisation constraints and beam

arrangement were used for both the cFF MLCi2 and FFF Agility plans. The average number of MUs for the cFF plans was 847MU with a standard deviation of 98MU, the MUs required for the FFF plans was 1081MU with a standard deviation of 158MU, this increase in MU of 30% is most likely due to the reduced cGy/MU off axis distance rather than increased plan complexity. This increased number of MU required per plan for FFF beams have also been found by other authors (Gasic et al., 2014) with values stated as 30% (Yan et al., 2016) and 20% (Nicolini et al., 2012) more. Despite this increase the FFF plans would still deliver lower doses outside of the treatment field, reducing the risk of radiation induced secondary cancers (Murray et al., 2015; Paynter et al., 2014; Cashmore et al., 2011). The average delivery time for the cFF plans was 302.9seconds with a standard deviation of 6.5seconds. The average delivery time for the FFF plans was 206.5seconds with a standard deviation of 4.2seconds. The FFF plans were able to be delivered 32% faster than the cFF plans. This reduction in delivery time is most likely a result of the higher dose rate coupled with a differing maximum leaf speed between the two treatments heads. The Agility head has a maximum leaf speed 43% faster than the MLCi2 treatment head when not employing the dynamic leaf guides which gives an increased speed of 70%. With this taken into account it is assumed that the FFF plans would take 10% longer to deliver than the cFF plans if they were delivered on an Agility head if the increased dynamic leaf guide speed is not fully utilised. Other authors have performed studies on the Varian TrueBeam Linac finding that the delivery speed for cFF and FFF plans is comparable (Zhuang et al., 2013; Nicolini et al., 2012; Gasic et al., 2014). When using FFF beams for this type of treatment the treating centre would need to determine if this 10% increase in delivery time is justified with the reduction of overheads associated with maintaining additional beam models.

6.4. Conclusion

This chapter answers the research question “How can FFF beams be implemented in the clinic and are they suitable for a range of treatment sites?” by performing planning studies on a range of treatment sites with comparison to current standard of care treatments with cFF beams.

The use of FFF beams for treatment planning and delivery has the largest benefits when planning hypofractionated treatments as the increased dose-rate provides significant reduction in treatment delivery times. For treatments with standard dose per fractionation of approximately 2Gy, the increased dose-rate does not improve delivery efficiency as the factor dominating the delivery speed is the leaf speed of the collimating device. The plans produced are of equivalent quality. The treatment centre would need to determine whether maintaining multiple beam models and clinical beam energies on the treatment machines justifies the reduction of delivery efficiency when using FFF beams for all treatment sites. Larger patient studies were not performed as this work was part of a feasibility study to determine if FFF beams could produce

clinically acceptable plans. The work on non-hypofractionated deliveries has resulted in in a policy that all of the VMAT treatments at our centre are to be planned with FFF beams. There are currently 21 clinical sites delivered using VMAT in this way, for which the author has had a significant contribution to the class solution of 7. These are paranasal sinus, breast, bilateral H&N, single sided head and neck, lymphoma, lung SABR and pelvic SABR.

7. Summary and future work

The aim of this thesis was to investigate FFF beams from initial characterisation through to the final implementation in the clinical setting. This was done through the following chapters;

1. A literature review of current publications and their findings with respect to FFF beams.
2. The characterisation of the two implementations of FFF beams by the two main manufacturers of Linacs.
3. The setup and quality assurance of FFF beams and proposed new suitable definitions of beam parameters.
4. The Monte Carlo modelling of FFF beams and how this can be achieved.
5. The implementation of FFF beams in a clinical setting including feasibility studies for different treatment sites and dose fractionations.

The literature review highlighted the need for clarification and comparison of the two different implementations of FFF beams by the two main Linac manufacturers. For a reader without prior knowledge of these differences, conclusions could be drawn that might not be relevant for the implementation from a different manufacturer. In addition, earlier publications on FFF beams where the energy had been matched to the equivalent conventionally flattened (cFF) beam were performed with a match of the beam quality specifier TPR20/10 and not the clinical implementation of percentage depth dose at 10cm depth. Chapter 3 investigated the characteristics of both implementations of FFF beams by performing measurements on FFF beams that had not been energy matched (Varian approach) and those that had their energy matched at a depth of 10cm in water at 100cm SSD in a 10cm x 10cm field (Elekta approach). The matching of a FFF beam to a cFF beam at a depth of 10cm in water by increasing the FFF beam energy does not reduce any of the reported benefits of FFF beams. However, there are a number of benefits resulting from matching the FFF beam, e.g. the depth of maximum dose is located deeper and the beam quality and penetration more closely resemble the cFF beams currently used in clinical practice, making dose distributions in water more alike. Highlighted in this work is the fact that some conventional specifications and methods for measurement of beam parameters, such as penumbra, are not relevant. Further research was identified to address this situation with respect to ‘matched’ FFF beams and to determine methods of measurement that are not reliant on an associated cFF beam. This was investigated in Chapter 4.

The quality assurance (QA) of FFF beams has been discussed by other authors primarily for the implementation of FFF beams without energy matching (Fogliata et al., 2012a) and later subsequently applied to matched beams (Fogliata et al., 2016b). These studies defined new

parameters that are required for the QA of FFF beams in addition to the parameters used for characterising cFF beams. Other national recommendations relied on the acquisition of 'gold' standard data that is used for the subsequent analysis and QA of beams. In Chapter 4, new proposed methods are presented that make it possible to independently carry out characterisation, set up and QA measurements on beam energy, flatness, symmetry and field size of an FFF beam. This is without the requirement for an equivalent cFF beam of the same energy or 'gold' standard data. The methods proposed can also be used to carry out this QA for cFF beams, resulting in universal definitions and methods for MV beams. This is presented for matched FFF beams produced by an Elekta linear accelerator, but is anticipated to equally apply to unmatched FFF beams from other manufacturers'. The above work has contributed to UK national recommendations for FFF beams (see below).

A well-produced and benchmarked Monte Carlo model can be a powerful tool in investigations that may otherwise prove difficult to perform through physical measurements. The majority of the literature relating to Monte Carlo models is on the guidance of producing models for cFF beams. The majority of the literature on FFF beams is through modifications of cFF models on beams that are not energy matched. Chapter 5 investigated the production of an FFF Monte Carlo model from first principles for an energy matched FFF beam, with the aim of producing new guidance on modelling of FFF beams and allowing further investigations in out of field doses, a potential benefit of FFF beams. The modelling of FFF beams with Monte Carlo in EGS/BEAMnrc is possible with the appropriate technical information provided by the vendor. The relationship between the field size and the movement of the jaws and MLCs is not linear and therefore needs to be characterised in order to be able to model more complex field shapes. When modelling FFF beams in Monte Carlo, the divergence of the electron beam at the point of striking the target was shown to be a useful parameter to help achieve a realistic model of the incident electron beam on the x-ray target, with a match for both PDD and beam profile distributions. The divergence of the electron beam on the target has minimal impact on the PDD, so once a Gaussian distributed beam energy has been found to produce appropriate PDDs for the clinical range of field sizes, the profile shapes can be further optimised using the divergence parameter. The modelling produces good agreement with measurements for a wide range of field sizes and can be used for further studies into peripheral doses and secondary cancer induction.

The implementation of IMRT and VMAT in most radiotherapy centres has the potential to remove the requirement of a cFF treatment beam for radiotherapy planning. Previous planning studies in the literature have focussed on hypofractionated treatments as the increased doserate of FFF beams is seen as an advantage for these sites. Also, most of the planning studies in the literature are for the non-matched FFF implementation. Chapter 6 contains feasibility

studies for the use of FFF beams for the planning of both hypofractionated treatment regimens and standard treatment fractionations with the aim of demonstrating that a single FFF beam model is suitable for all IMRT and VMAT treatments. The use of FFF beams for treatment planning and delivery has the largest benefits when planning hypofractionated treatments as the increased doserate provides significant reduction in treatment delivery times. For treatments with standard radical dose fractionations of approximately 2Gy per fraction the increased doserate does not improve delivery efficiency, as the factor dominating the delivery speed is the leaf speed of the collimating device and the gantry rotation speed. The plans produced are of equivalent quality and the treatment centre would need to evaluate whether maintaining multiple beam models and clinical beam energies on the treatment machines justifies the reduction of delivery efficiency when using FFF beams for all treatment sites. Larger patient studies were not performed as this work was part of a feasibility study to determine if FFF beams could produce clinically acceptable plans. The work on non-hypofractionated treatments has resulted in a policy that all of the VMAT plans at our centre are delivered with FFF beams. There are currently 21 clinical sites delivered using VMAT in this way, for which the author has had a significant contribution to the class solution of 7. These are paranasal sinus, breast, bilateral H&N, single sided head and neck, lymphoma, lung SABR and pelvic SABR.

The work presented in this thesis has highlighted further areas of study in relation to FFF beams. These areas are described below.

- There is no consistent definition of FFF beams, with multiple publications proposing new methods for analysing FFF beams and performing QA. A further study is required that compares the proposed methods in this thesis with methods proposed by Fogliata et al. (2016b) and Budgell et al. (2016). This work should be performed using data collected from multiple vendors of FFF to ensure that the final proposed methodology is suitable for all radiotherapy photon beams.
- Monte Carlo models can be used along with a model of a cFF beam from the same linear accelerator to investigate if the use of FFF beams can be utilised to reduce the incidence of radiotherapy induced secondary cancers both distal to and in the near field region of radiotherapy treatments.
- Further larger scale treatment planning studies comparing cFF and FFF beams for more treatment sites and fractionation regimes should be investigated to determine if the use of FFF beams should become the standard of care for IMRT and VMAT treatments.

In summary the work in this thesis has provided information regarding the characterisation of FFF beams with respect to the implementation of both main manufacturers, Elekta and Varian.

The work contained in section 3 has been published in a peer review publication (Paynter et al., 2014) and has already received multiple citations from other authors in the field. The work on the QA and setup of FFF beams in section 4 has been published in a peer review journal (Paynter et al., 2017) and has directly helped to influence the practice at Leeds Teaching Hospitals NHS Trust. The work on the clinical implementation has contributed towards the implementation of FFF within St James's University Hospital, Leeds and currently all VMAT and IMRT treatments are delivered using FFF beams. At the time of writing St James's University Hospital, Leeds is in the process of an equipment refresh, each new accelerator installed will have FFF functionality. Following on from publication and conference talks on the FFF work contained in this thesis I was asked to contribute to the UK national recommendations on FFF beams and this work was published in the journal Physics in Medicine and Biology (Budgell et al., 2016) see Appendix A.

8. References

Adler, J.R., Jr., Chang, S.D., Murphy, M.J., Doty, J., Geis, P. and Hancock, S.L. 1997. The Cyberknife: a frameless robotic system for radiosurgery. *Stereotactic and Functional Neurosurgery.* **69**(1-4 Pt 2), pp.124-128.

Agostinelli, S., Allison, J., Amako, K., Apostolakis, J., Araujo, H., Arce, P., Asai, M., Axen, D., Banerjee, S., Barrand, G., Behner, F., Bellagamba, L., Boudreau, J., Broglia, L., Brunengo, A., Burkhardt, H., Chauvie, S., Chuma, J., Chytracek, R., Cooperman, G., Cosmo, G., Degtyarenko, P., Dell'Acqua, A., Depaola, G., Dietrich, D., Enami, R., Feliciello, A., Ferguson, C., Fesefeldt, H., Folger, G., Foppiano, F., Forti, A., Garelli, S., Giani, S., Giannitrapani, R., Gibin, D., Cadenas, J.J.G., Gonzalez, I., Abril, G.G., Greeniaus, G., Greiner, W., Grichine, V., Grossheim, A., Guatelli, S., Gumplinger, P., Hamatsu, R., Hashimoto, K., Hasui, H., Heikkinen, A., Howard, A., Ivanchenko, V., Johnson, A., Jones, F.W., Kallenbach, J., Kanaya, N., Kawabata, M., Kawabata, Y., Kawaguti, M., Kelner, S., Kent, P., Kimura, A., Kodama, T., Kokoulin, R., Kossov, M., Kurashige, H., Lamanna, E., Lampen, T., Lara, V., Lefebure, V., Lei, F., Liendl, M., Lockman, W., Longo, F., Magni, S., Maire, M., Medernach, E., Minamimoto, K., de Freitas, P.M., Morita, Y., Murakami, K., Nagamatu, M., Nartallo, R., Nieminen, P., Nishimura, T., Ohtsubo, K., Okamura, M., O'Neale, S., Oohata, Y., Paech, K., Perl, J., Pfeiffer, A., Pia, M.G., Ranjard, F., Rybin, A., Sadilov, S., Di Salvo, E., Santin, G., Sasaki, T., Savvas, N., Sawada, Y., Scherer, S., Seil, S., Sirotenko, V., Smith, D., Starkov, N., Stoecker, H., Sulkimo, J., Takahata, M., Tanaka, S., Tcherniaev, E., Tehrani, E.S., Tropeano, M., Truscott, P., Uno, H., Urban, L., Urban, P., Verderi, M., Walkden, A., Wander, W., Weber, H., Wellisch, J.P., Wenaus, T., Williams, D.C., Wright, D., Yamada, T., Yoshida, H. and Zschiesche, D. 2003. GEANT4-a simulation toolkit. *Nuclear Instruments & Methods in Physics Research Section a-Accelerators Spectrometers Detectors and Associated Equipment.* **506**(3), pp.250-303.

Almberg, S.S., Frengen, J. and Lindmo, T. 2012. Monte Carlo study of in-field and out-of-field dose distributions from a linear accelerator operating with and without a flattening-filter. *Medical Physics.* **39**(8), pp.5194-5203.

Almond, P.R., Biggs, P.J., Coursey, B.M., Hanson, W.F., Huq, M.S., Nath, R. and Rogers, D.W.O. 1999. AAPM's TG-51 protocol for clinical reference dosimetry of high-energy photon and electron beams. *Medical Physics.* **26**(9), pp.1847-1870.

Baro, J., Sempau, J., Fernandezvarea, J.M. and Salvat, F. 1995. Penelope - an algorithm for Monte-Carlo simulation of the penetration and energy-loss of electrons and positrons in matter. *Nuclear Instruments & Methods in Physics Research Section B-Beam Interactions with Materials and Atoms.* **100**(1), pp.31-46.

Boda-Heggemann, J., Mai, S., Fleckenstein, J., Siebenlist, K., Simeonova, A., Ehmann, M., Steil, V., Wenz, F., Lohr, F. and Stieler, F. 2013. Flattening-filter-free intensity modulated breath-hold image-guided SABR (Stereotactic ABlative Radiotherapy) can be applied in a 15-min treatment slot. *Radiotherapy and Oncology.* **109**(3), pp.505-509.

Bouchta, B.Y., Goddard, K., Petric, M.P. and Bergman, A.M. 2018. Effects of 10 MV and flattening-filter-free beams on peripheral dose in a cohort of pediatric patients. *International Journal of Radiation, Oncology, Biology & Physics.* **102**(5), pp.1560-1568.

Brahme, A., Roos, J.E. and Lax, I. 1982. Solution of an integral-equation encountered in rotation therapy. *Physics in Medicine and Biology.* **27**(10), pp.1221-1229.

Brenner, D.J., Curtis, R.E., Hall, E.J. and Ron, E. 2000. Second malignancies in prostate carcinoma patients after radiotherapy compared with surgery. *Cancer.* **88**(2), pp.398-406.

Budgell, G., Brown, K., Cashmore, J., Duane, S., Frame, J., Hardy, M., Paynter, D. and Thomas, R. 2016. IPEM topical report 1: guidance on implementing flattening filter free (FFF) radiotherapy. *Physics in Medicine and Biology.* **61**(23), pp.8360-8394.

Bush, K., Gagne, I.M., Zavgorodni, S., Ansbacher, W. and Beckham, W. 2011. Dosimetric validation of Acuros XB with Monte Carlo methods for photon dose calculations. *Medical Physics.* **38**(4), pp.2208-2221.

Calvo, O., Guti, R., A., Stathakis, S., Mavroidis, P., Moral, S., Esquivel, C., Shi, C. and Papanikolaou, N. 2009. Validation of the Delta4 dosimetry phantom against ionometric measurements. *Medical Physics.* **36**(6).

Canny, J. 1986. A computational approach to edge detection. *IEEE Translational Pattern Analysis and Machine Intelligence.* **8**(6), pp.679-698.

Cashmore, J. 2008. The characterization of unflattened photon beams from a 6 MV linear accelerator. *Physics in Medicine and Biology.* **53**(7), pp.1933-1946.

Cashmore, J. 2016. Surface dose variations in 6 and 10 MV flattened and flattening filter-free (FFF) photon beams. *Journal of Applied Clinical Medical Physics.* **17**(5), pp.293-307.

Cashmore, J., Golubev, S., Dumont, J.L., Sikora, M., Alber, M. and Ramtohul, M. 2012. Validation of a virtual source model for Monte Carlo dose calculations of a flattening filter free linac. *Medical Physics.* **39**(6), pp.3262-3269.

Cashmore, J., Ramtohul, M. and Ford, D. 2011. Lowering whole-body radiation doses in pediatric intensity-modulated radiotherapy through the use of unflattened photon beams. *International Journal of Radiation Oncology Biology Physics.* **80**(4), pp.1220-1227.

Ceberg, C., Johnsson, S., Lind, M. and Knoos, T. 2010. Prediction of stopping-power ratios in flattening-filter free beams. *Medical Physics.* **37**(3), pp.1164-1168.

Chofor, N., Harder, D., Ruhmann, A., Willborn, K.C., Wiezorek, T. and Poppe, B. 2010. Experimental study on photon-beam peripheral doses, their components and some possibilities for their reduction. *Physics in Medicine and Biology.* **55**(14), pp.4011-4027.

Clivio, A., Belosi, M.F., Cozzi, L., Nicolini, G., Vanetti, E., Bolard, G., Fenoglietto, P., Krauss, H. and Fogliata, A. 2014. On the determination of reference levels for quality assurance of flattening filter free photon beams in radiation therapy. *Medical Physics.* **41**(2).

Consortium, U.S. 2016. Stereotactic Ablative Body Radiation Therapy (SABR): A resource [Online]. [Accessed 20/09/2018].

Cosgrove, V.P., Thomas, M.D.R., Weston, S.J., Thompson, M.G., Reynaert, N., Evans, C.J., Brown, K.J., De Wagter, C., Thwaites, D.I. and Warrington, A.P. 2009. Physical characterization of a new concept design of an Elekta radiation head with integrated 160-leaf multi-leaf collimator. *International Journal of Radiation Oncology Biology Physics.* **75**(3), pp.S722-S723.

Cranmer-Sargison, G., Weston, S., Evans, J.A., Sidhu, N.P. and Thwaites, D.I. 2012. Monte Carlo modelling of diode detectors for small field MV photon dosimetry: detector model simplification and the sensitivity of correction factors to source parameterization. *Physics in Medicine and Biology.* **57**(16).

CRUK. 2015. *Cancer Research UK.* [Online]. [Accessed 06 November 2018]. Available from: https://www.cancerresearchuk.org/

Dalaryd, M., Kragl, G., Ceberg, C., Georg, D., McClean, B., af Wetterstedt, S., Wieslander, E. and Knoos, T. 2010. A Monte Carlo study of a flattening filter-free linear accelerator verified with measurements. *Physics in Medicine and Biology.* **55**(23), pp.7333-7344.

de Prez, L., de Pooter, J., Jansen, B., Perik, T. and Wittkamper, F. 2018. Comparison of k(Q) factors measured with a water calorimeter in flattening filter free (FFF) and conventional flattening filter (cFF) photon beams. *Physics in Medicine and Biology.* **63**(4).

Dobler, B., Obermeier, T., Hautmann, M.G., Khemissi, A. and Koelbl, O. 2017. Simultaneous integrated boost therapy of carcinoma of the hypopharynx/larynx with and without flattening filter - a treatment planning and dosimetry study. *Radiation Oncology.* **12**(1), p114.

Dorr, W. and Herrmann, T. 2002. Cancer induction by radiotherapy: dose dependence and spatial relationship to irradiated volume. *Journal of Radiolical Protection.* **22**(3A), pp.A117-121.

Edvardsson, A., Nordstrom, F., Ceberg, C. and Ceberg, S. 2018. Motion induced interplay effects for VMAT radiotherapy. *Physics in Medicine and Biology.* **63**(8), p085012.

ELEKTA. 2010. *Flattening Filter Free Customer Forum.* [Leaflet].

Fiorentino, A., Giaj-Levra, N., Tebano, U., Mazzola, R., Ricchetti, F., Fersino, S., Di Paola, G., Aiello, D., Ruggieri, R. and Alongi, F. 2017. Stereotactic ablative radiation therapy for brain metastases with volumetric modulated arc therapy and flattening filter free delivery: feasibility and early clinical results. *Radiological Medicine.* **122**(9), pp.676-682.

Fogliata, A., Fleckenstein, J., Schneider, F., Pachoud, M., Ghandour, S., Krauss, H., Reggiori, G., Stravato, A., Lohr, F., Scorsetti, M. and Cozzi, L. 2016a. Flattening filter free beams from TrueBeam and Versa HD units: Evaluation of the parameters for quality assurance. *Medical Physics.* **43**(1), p205.

Fogliata, A., Fleckenstein, J., Schneider, F., Pachoud, M., Ghandour, S., Krauss, H., Reggiori, G., Stravato, A., Lohr, F., Scorsetti, M. and Cozzi, L. 2016b. Flattening filter free beams from TrueBeam and Versa HD units: Evaluation of the parameters for quality assurance. *Medical Physics.* **43**(1), pp.205-212.

Fogliata, A., Garcia, R., Knoos, T., Nicolini, G., Clivio, A., Vanetti, E., Khamphan, C. and Cozzi, L. 2012a. Definition of parameters for quality assurance of flattening filter free (FFF) photon beams in radiation therapy. *Medical Physics.* **39**(10), pp.6455-6464.

Fogliata, A., Garcia, R., Knoos, T., Nicolini, G., Clivio, A., Vanetti, E., Khamphan, C. and Cozzi, L. 2012b. Definition of parameters for quality assurance of flattening filter free (FFF) photon beams in radiation therapy. *Medical Physics.* **39**(10), pp.6455-6464.

Fu, W.H., Dai, J.R., Hu, Y.M., Han, D.S. and Song, Y.X. 2004. Delivery time comparison for intensity-modulated radiation therapy with/without flattening filter: a planning study. *Physics in Medicine and Biology.* **49**(8), pp.1535-1547.

Gasic, D., Ohlhues, L., Brodin, N.P., Fog, L.S., Pommer, T., Bangsgaard, J.P. and Rosenschold, P.M. 2014. A treatment planning and delivery comparison of volumetric modulated arc therapy with or without flattening filter for gliomas, brain metastases, prostate, head/neck and early stage lung cancer. *Acta Oncologica.* **53**(8), pp.1005-1011.

Georg, D., Knoos, T. and McClean, B. 2011. Current status and future perspective of flattening filter free photon beams. *Medical Physics.* **38**(3), pp.1280-1293.

Georg, D., Kragl, G., Wetterstedt, S., McCavana, P., McClean, B. and Knoos, T. 2010. Photon beam quality variations of a flattening filter free linear accelerator. *Medical Physics.* **37**(1), pp.49-53.

Hall, E.J. 2006. Intensity-modulated radiation therapy, protons, and the risk of second cancers. *International Journal of Radiation Oncology Biology Physics.* **65**(1), pp.1-7.

Hallemeier, C.L., Stauder, M.C., Miller, R.C., Garces, Y.I., Foote, R.L., Sarkaria, J.N., Bauer, H.J., Mayo, C.S. and Olivier, K.R. 2013. Lung stereotactic body radiotherapy using a coplanar versus a non-coplanar beam technique: a comparison of clinical outcomes. *Journal of Radiosurgery SBRT.* **2**(3), pp.225-233.

Health and Safety Executive. 2018. *Work with ionising radiation : Ionising Radiations Regulations 2017 approved code of practice and guidance.* London: HSE Books.

Hrbacek, J., Lang, S., Graydon, S.N., Klock, S. and Riesterer, O. 2014. Dosimetric comparison of flattened and unflattened beams for stereotactic ablative radiotherapy of stage I non-small cell lung cancer. *Medical Physics.* **41**(3).

Hrbacek, J., Lang, S. and Klock, S. 2010. Commissioning of photon beams of a flattening filter-free linear accelerator and the accuracy of beam modeling using an anisotropic analytical algorithm. *International Journal of Radiation Oncology Biology Physics.*

Hurkmans, C.W., Cuijpers, J.P., Lagerwaard, F.J., Widder, J., van der Heide, U.A., Schuring, D. and Senan, S. 2009. Recommendations for implementing stereotactic radiotherapy in peripheral stage IA non-small cell lung cancer: report from the Quality Assurance Working Party of the randomised phase III ROSEL study. *Radiation Oncology.* **4**.

IEC. 1998. *Particular requirements for safety of medical electron accelerators in the range 1MeV to 50MeV.* IEC 60601-2-1.

Independent Cancer Taskforce. 2015. *Achieving world-class cancer outcomes, a strategy for England, 2015-2020.*

IPEM. 2018. *Physics aspects of quality control in radiotherapy* Institute of Physics and Engineering in Medicine.

Jeraj, R., Mackie, T.R., Balog, J., Olivera, G., Pearson, D., Kapatoes, J., Ruchala, K. and Reckwerdt, P. 2004. Radiation characteristics of helical tomotherapy. *Medical Physics.* **31**(2), pp.396-404.

Jia, F., Xu, D., Yue, H., Wu, H. and Li, G. 2018. Comparison of flattening filter and flattening filter-free volumetric modulated arc radiotherapy in patients with locally advanced nasopharyngeal carcinoma. *Medical Science Monitor.* **24**, pp.8500-8505.

Khan, F.M. 2003. *The physics of radiation therapy.* 3rd ed. Philadelphia ; London: Lippincott Williams & Wilkins.

Klein, E.E., Maserang, B., Wood, R. and Mansur, D. 2006. Peripheral doses from pediatric IMRT. *Medical Physics.* **33**(7), pp.2525-2531.

Kragl, G., af Wetterstedt, S., Knausl, B., Lind, M., McCavana, P., Knoos, T., McClean, B. and Georg, D. 2009. Dosimetric characteristics of 6 and 10MV unflattened photon beams. *Radiotherapy Oncology.* **93**(1), pp.141-146.

Kragl, G., Baier, F., Lutz, S., Albrich, D., Dalaryd, M., Kroupa, B., Wiezorek, T., Knoos, T. and Georg, D. 2011. Flattening filter free beams in SBRT and IMRT: Dosimetric assessment of peripheral doses. *Zeitschrift Fur Medizinische Physik.* **21**(2), pp.91-101.

Kry, S.F., Howell, R.M., Polf, J., Mohan, R. and Vassiliev, O.N. 2009. Treatment vault shielding for a flattening filter-free medical linear accelerator. *Physics in Medicine and Biology.* **54**(5), pp.1265-1273.

Kry, S.F., Titt, U., Ponisch, F., Vassiliev, O.N., Salehpour, M., Gillin, M. and Mohan, R. 2007a. Reduced neutron production through use of a flattening-filter-free accelerator. *Int J Radiat Oncol Biol Phys.* **68**(4), pp.1260-1264.

Kry, S.F., Titt, U., Ponisch, F., Vassiliev, O.N., Salehpour, M., Gillin, M. and Mohan, R. 2007b. Reduced neutron production through use of a flattening-filter-free accelerator. *International Journal of Radiation Oncology, Biology, Physics.* **68**(4), pp.1260-1264.

Kry, S.F., Vassiliev, O.N. and Mohan, R. 2010. Out-of-field photon dose following removal of the flattening filter from a medical accelerator. *Physics in Medicine and Biology.* **55**(8), pp.2155-2166.

Kubo, K., Monzen, H., Tamura, M., Hirata, M., Ishii, K., Okada, W., Nakahara, R., Kishimoto, S., Kawamorita, R. and Nishimura, Y. 2018. Minimizing dose variation from the interplay effect in stereotactic radiation therapy using volumetric modulated arc therapy for lung cancer. *Journal of Applied Clinical Medical Physics.* **19**(2), pp.121-127.

Kumar, L., Yadav, G., Samuvel, K.R., Bhushan, M., Kumar, P., Suhail, M. and Pal, M. 2017. Dosimetric influence of filtered and flattening filter free photon beam on rapid arc (RA) radiotherapy planning in case of cervix carcinoma. *Reports of Practical Oncology Radiotherapy.* **22**(1), pp.10-18.

Lang, S., Hrbacek, J., Leong, A. and Klock, S. 2012a. Ion-recombination correction for different ionization chambers in high dose rate flattening-filter-free photon beams. *Physics in Medicine and Biology.* **57**(9).

Lang, S., Hrbacek, J., Leong, A. and Klock, S. 2012b. Ion-recombination correction for different ionization chambers in high dose rate flattening-filter-free photon beams. *Physics in Medicine and Biology.* **57**(9), pp.2819-2827.

Lang, S., Reggiori, G., Vaque, J.P., Calle, C., Hrbacek, J., Klock, S., Scorsetti, M., Cozzi, L. and Mancosu, P. 2012c. Pretreatment quality assurance of flattening filter free beams on 224 patients for intensity modulated plans: A multicentric study. *Medical Physics.* **39**(3), pp.1351-1356.

Lang, S., Shrestha, B., Graydon, S., Cavelaars, F., Linsenmeier, C., Hrbacek, J., Klock, S., Studer, G. and Riesterer, O. 2013. Clinical application of flattening filter free beams for extracranial stereotactic radiotherapy. *Radiotherapy and Oncology.* **106**(2), pp.255-259.

Lechner, W., Kragl, G. and Georg, D. 2013. Evaluation of treatment plan quality of IMRT and VMAT with and without flattening filter using Pareto optimal fronts. *Radiotherapy and Oncology.* **109**(3), pp.437-441.

Lillicrap, S.C., Owen, B., Williams, J.R. and Williams, P.C. 1990. Code of practice for high-energy photon therapy dosimetry based on the NPL absorbed dose calibration service. *Physics in Medicine and Biology.* **35**(10), pp.1355-1360.

Lopez-Tarjuelo, J., Garcia-Molla, R., Juan-Senabre, X.J., Quiros-Higueras, J.D., Santos-Serra, A., de Marco-Blancas, N. and Calzada-Feliu, S. 2014. Acceptance and commissioning of a treatment planning system based on Monte Carlo calculations. *Technology in Cancer Research & Treatment.* **13**(2), pp.129-138.

Low, D.A., Harms, W.B., Mutic, S. and Purdy, J.A. 1998. A technique for the quantitative evaluation of dose distributions. *Medical Physics.* **25**(5), pp.656-661.

Lu, J.Y., Lin, Z., Lin, P.X. and Huang, B.T. 2015. Optimizing the flattening filter free beam selection in RapidArc (R)-based stereotactic body radiotherapy for Stage I lung cancer. *British Journal of Radiology.* **88**(1053).

Luo, W., Meacham, A. and Molloy, J. 2013. A dosimetric comparison between superposition algorithm and Monte Carlo simulation for SBRT. *Medical Physics.* **40**(6).

Lye, J.E., Butler, D.J., Oliver, C.P., Alves, A., Lehmann, J., Gibbons, F.P. and Williams, I.M. 2016. Comparison between the TRS-398 code of practice and the TG-51 dosimetry protocol for flattening filter free beams. *Physics in Medicine and Biology.* **61**(14), pp.N362-N372.

Mancosu, P., Castiglioni, S., Reggiori, G., Catalano, M., Alongi, F., Pellegrini, C., Arcangeli, S., Tozzi, A., Lobefalo, F., Fogliata, A., Navarria, P., Cozzi, L. and Scorsetti, M. 2012. Stereotactic body radiation therapy for liver tumours using flattening filter free beam: dosimetric and technical considerations. *Radiation Oncology.* **7**, p16.

Mansur, D.B., Klein, E.E. and Maserang, B.P. 2007. Measured peripheral dose in pediatric radiation therapy: A comparison of intensity-modulated and conformal techniques. *Radiotherapy and Oncology.* **82**(2), pp.179-184.

Mayles, P., Nahum, A.E. and Rosenwald, J.-C. 2007. *Handbook of radiotherapy physics : theory and practice.* New York: Taylor & Francis.

Mesbahi, A. 2007. Dosimetric characteristics of unflattened 6 MV photon beams of a clinical linear accelerator: a Monte Carlo study. *Appl Radiat Isot.* **65**(9), pp.1029-1036.

Metcalfe, P., Kron, T., Elliott, A., Wong, T. and Hoban, P. 1993. Dosimetry of 6-Mv X-Ray-Beam Penumbra. *Medical Physics.* **20**(5), pp.1439-1445.

Metropolis, N. and Ulam, S. 1949. The Monte Carlo method. *Journal of the American Statistical Association.* **44**(247), pp.335-341.

Miften, M., Wiesmeyer, M., Monthofer, S. and Krippner, K. 2000. Implementation of FFT convolution and multigrid superposition models in the FOCUS RTP system. *Physics in Medicine and Biology.* **45**(4), pp.817-833.

Mohan, R., Jayesh, K., Joshi, R.C., Al-Idrisi, M., Narayanamurthy, P. and Majumdar, S.K. 2008. Dosimetric evaluation of 120-leaf multileaf collimator in a Varian linear accelerator with 6-MV and 18-MV photon beams. *Journal of Medical Physics.* **33**(3), pp.114-118.

Moret, J.A., Obermeier, T., Pohl, F., Loeschel, R., Koelbl, O. and Dobler, B. 2018. Second cancer risk after radiation therapy of ependymoma using the flattening filter free irradiation mode of a linear accelerator. *Journal of Applied Clinical Medical Physics.* **19**(5), pp.632-639.

Muir, B.R., McEwen, M.R. and Rogers, D.W.O. 2011. Measured and Monte Carlo calculated k(Q) factors: Accuracy and comparison. *Medical Physics.* **38**(8), pp.4600-4609.

Murray, L.J., Thompson, C.M., Lilley, J., Cosgrove, V., Franks, K., Sebag-Montefiore, D. and Henry, A.M. 2015. Radiation-induced second primary cancer risks from modern external beam radiotherapy for early prostate cancer: impact of stereotactic ablative radiotherapy (SABR), volumetric modulated arc therapy (VMAT) and flattening filter free (FFF) radiotherapy. *Physics in Medicine and Biology.* **60**(3), pp.1237-1257.

Nakano, H., Minami, K., Yagi, M., Imaizumi, H., Otani, Y., Inoue, S., Takashina, M., Seo, Y., Takahashi, Y., Sumida, I., Ogawa, K. and Koizumi, M. 2018. Radiobiological effects of flattening filter-free photon beams on A549 non-small-cell lung cancer cells. *Journal of Radiation Research.* **59**(4), pp.442-445.

Navarria, P., Ascolese, A.M., Mancosu, P., Alongi, F., Clerici, E., Tozzi, A., Iftode, C., Reggiori, G., Tomatis, S., Infante, M., Alloisio, M., Testori, A., Fogliata, A., Cozzi, L., Morenghi, E. and Scorsetti, M. 2013. Volumetric modulated arc therapy with flattening filter free (FFF) beams for stereotactic body radiation therapy (SBRT) in patients with medically inoperable early stage non small cell lung cancer (NSCLC). *Radiotherapy and Oncology.* **107**(3), pp.414-418.

Nicolini, G., Clivio, A., Vanetti, E., Krauss, H., Fenoglietto, R., Cozzi, L. and Fogliata, A. 2013. Evaluation of an aSi-EPID with flattening filter free beams: Applicability to the GLAaS algorithm for portal dosimetry and first experience for pretreatment QA of RapidArc. *Medical Physics.* **40**(11).

Nicolini, G., Ghosh-Laskar, S., Shrivastava, S.K., Banerjee, S., Chaudhary, S., Agarwal, J.P., Munshi, A., Clivio, A., Fogliata, A., Mancosu, P., Vanetti, E. and Cozzi, L. 2012. Volumetric modulation arc radiotherapy with flattening filter-free beams compared with static gantry IMRT and 3D conformal radiotherapy for advanced esophageal cancer: A feasibility study. *International Journal of Radiation Oncology Biology Physics.* **84**(2), pp.553-560.

Ogata, T., Nishimura, H., Mayahara, H., Uehara, K. and Okayama, T. 2017. Identification of the suitable leaf margin for liver stereotactic body radiotherapy with flattening filter-free beams. *Medical Dosimetry.* **42**(4), pp.268-272.

Palma, D., Vollans, E., James, K., Nakano, S., Moiseenko, V., Shaffer, R., Mckenzie, M., Morris, J. and Otto, K. 2008. Volumetric modulated arc therapy for delivery of prostate radiotherapy: Comparison with intensity-modulated radiotherapy and three-dimensional conformal radiotherapy. *International Journal of Radiation Oncology Biology Physics.* **72**(4), pp.996-1001.

Paynter, D. 2014. The beam characteristics and QA aspects of flattening filter free beams. In: *Flattening Filter Free Photon Beams in Radiotherapy*, *06/03/2014, British Dental Association, London*. IPEM.

Paynter, D., Derbyshire, S.J., Lilley, J., Weston, S.J., Thompson, C.M., Cosgrove, V.P. and Thwaites, D.I. 2013. PO-0827: Elekta AgilityTM FFF for lung VMAT SABR. *Radiotherapy and Oncology.* **106**, pp.S316-S317.

Paynter, D., Weston, S.J., Cosgrove, V.P., Evans, J.A. and Thwaites, D.I. 2014. Beam characteristics of energy-matched flattening filter free beams. *Medical Physics.* **41**(5).

Paynter, D., Weston, S.J., Cosgrove, V.P. and Thwaites, D.I. 2017. Characterisation of flattening filter free (FFF) beam properties for initial beam set-up and routine QA, independent of flattened beams. *Physics in Medicine and Biology.* **63**(1), p015021.

Podgorsak, E.B. and International Atomic Energy Agency. 2005. *Radiation oncology physics : a handbook for teachers and students.* Vienna: International Atomic Energy Agency.

Ponisch, F., Titt, U., Vassiliev, O.N., Kry, S.F. and Mohan, R. 2006. Properties of unflattened photon beams shaped by a multileaf collimator. *Medical Physics.* **33**(6), pp.1738-1746.

Prendergast, B.M., Dobelbower, M.C., Spencer, S.A., Popple, R.A., Minnich, D.J., Bonner, J.A. and Fiveash, J.B. 2012. Stereotactic Body Radiation Therapy (SBRT) for lung malignancies: Preliminary toxicity results using a flattening filter-free linear accelerator operating at 2400 monitor units per minute. *International Journal of Radiation Oncology Biology Physics.* **84**(3), pp.S557-S558.

Reggiori, G., Mancosu, P., Castiglioni, S., Alongi, F., Pellegrini, C., Lobefalo, F., Catalano, M., Fogliata, A., Arcangeli, S., Navarria, P., Cozzi, L. and Scorsetti, M. 2012a. Can volumetric modulated arc therapy with flattening filter free beams play a role in stereotactic body radiotherapy for liver lesions? A volume-based analysis. *Medical Physics.* **39**(2), pp.1112-1118.

Reggiori, G., Mancosu, P., Castiglioni, S., Alongi, F., Pellegrini, C., Lobefalo, F., Catalano, M., Fogliata, A., Arcangeli, S., Navarria, P., Cozzi, L. and Scorsetti, M. 2012b. Can volumetric modulated arc therapy with flattening filter free beams play a role in stereotactic body radiotherapy for liver lesions? A volume-based analysis. *Medical Physics.* **39**(2), pp.1112-1118.

Rogers, D.W., Faddegon, B.A., Ding, G.X., Ma, C.M., We, J. and Mackie, T.R. 1995. BEAM: a Monte Carlo code to simulate radiotherapy treatment units. *Medical Physics.* **22**(5), pp.503-524.

Rogers, D.W.O. and Bielajew, A.F. 1984. The use of EGS for Monte-Carlo calculations in medical physics. *Medical Physics.* **11**(3), pp.417-418.

Rogers, D.W.O., Walters, B. and Kawrakow, I. 2015. *BEAMnrc users manual.* National Research Council of Canada.

Scorsetti, M., Alongi, F., Castiglioni, S., Clivio, A., Fogliata, A., Lobefalo, F., Mancosu, P., Navarria, P., Palumbo, V., Pellegrini, C., Pentimalli, S., Reggiori, G., Ascolese, A.M., Roggio, A., Arcangeli, S., Tozzi, A., Vanetti, E. and Cozzi, L. 2011. Feasibility and early clinical assessment of flattening filter free (FFF) based stereotactic body radiotherapy (SBRT) treatments. *Radiation Oncology.* **6**, p113.

Seco, J. and Verhaegen, F. 2013. *Monte Carlo techniques in radiation therapy.* CRC Press.

Sham, E., Seuntjens, J., Devic, S. and Podgorsak, E.B. 2008. Influence of focal spot on characteristics of very small diameter radiosurgical beams. *Medical Physics.* **35**(7), pp.3317-3330.

Sheikh-Bagheri, D. and Rogers, D.W. 2002. Sensitivity of megavoltage photon beam Monte Carlo simulations to electron beam and other parameters. *Medical Physics.* **29**(3), pp.379-390.

Shepherd, A., James, S.S. and Rengan, R. 2018. The practicality of ICRU and considerations for future ICRU definitions. *Seminars in Radiation Oncology.* **28**(3), pp.201-206.

Sievinen, J., Waldemar, U. and Wolfgang, K. 2005. *AAA photon dose calculation model in Eclipse.* Palo Alto (CA): Varian Medical Systems.

Smit, K., Kok, J.G., Lagendijk, J.J. and Raaymakers, B.W. 2014. Performance of a multi-axis ionization chamber array in a 1.5 T magnetic field. *Physics in Medicine and Biology.* **59**(7), pp.1845-1855.

Spruijt, K.H., Dahele, M., Cuijpers, J.P., Jeulink, M., Rietveld, D., Slotman, B.J. and Verbakel, W.F. 2013a. Flattening filter free vs flattened beams for breast irradiation. *International Journal of Radiation Oncology Biology Physics.* **85**(2), pp.506-513.

Spruijt, K.H., Dahele, M., Cuijpers, J.P., Jeulink, M., Rietveld, D., Slotman, B.J. and Verbakel, W.F. 2013b. Flattening filter free vs flattened beams for breast irradiation. *International Journal of Radiation Oncology, Biology, Physics.* **85**(2), pp.506-513.

Stathakis, S., Esquivel, C., Gutierrez, A., Buckey, C.R. and Papanikolaou, N. 2009. Treatment planning and delivery of IMRT using 6 and 18 MV photon beams without flattening filter. *Applied Radiation and Isotopes.* **67**(9), pp.1629-1637.

Tambe, N.S., Fryer, A., Marsden, J.E., Moore, C. and Beavis, A.W. 2016. Determination of clinically appropriate flattening filter free (FFF) energy for treating lung SABR using treatment plans and delivery measurements. *Biomedical Physics & Engineering Express.* **2**(6).

Teoh, M., Clark, C.H., Wood, K., Whitaker, S. and Nisbet, A. 2011. Volumetric modulated arc therapy: a review of current literature and clinical use in practice. *British Journal of Radiology.* **84**(1007), pp.967-996.

Thompson, C.M., Weston, S.J., Cosgrove, V.C. and Thwaites, D.I. 2014. A dosimetric characterization of a novel linear accelerator collimator. *Medical Physics.* **41**(3).

Titt, U., Vassiliev, O.N., Ponisch, F., Dong, L., Liu, H. and Mohan, R. 2006a. A flattening filter free photon treatment concept evaluation with Monte Carlo. *Med Phys.* **33**(6), pp.1595-1602.

Titt, U., Vassiliev, O.N., Ponisch, F., Kry, S.F. and Mohan, R. 2006b. Monte Carlo study of backscatter in a flattening filter free clinical accelerator. *Medical Physics.* **33**(9), pp.3270-3273.

Titt, U., Vassiliev, O.N., Ponisch, F., Kry, S.F. and Mohan, R. 2006c. Monte Carlo study of backscatter in a flattening filter free clinical accelerator. *Med Phys.* **33**(9), pp.3270-3273.

Treutwein, M., Hipp, M., Koelbl, O. and Dobler, B. 2017. Volumetric-modulated arc therapy and intensity-modulated radiation therapy treatment planning for prostate cancer with flattened beam and flattening filter free linear accelerators. *Journal of Applied Clinical Medical Physics.* **18**(5), pp.307-314.

Tsiamas, P., Seco, J., Han, Z., Bhagwat, M., Maddox, J., Kappas, C., Theodorou, K., Makrigiorgos, M., Marcus, K. and Zygmanski, P. 2011. A modification of flattening filter free linac for IMRT. *Medical Physics.* **38**(5), pp.2342-2352.

Tubiana, M. 2009. Can we reduce the incidence of second primary malignancies occurring after radiotherapy? A critical review. *Radiotherapy Oncology.* **91**(1), pp.4-15; discussion 11-13.

Tyler, M. and Dowdell, S. 2018. Delivery efficiency and susceptibility to setup uncertainties of flattening filter free lung SBRT: influence of isocentre geometry and treatment modality. *Physics in Medicine and Biology.* **63**(20), p205017.

Tyner, E., McClean, B., McCavana, P. and af Wetterstedt, S. 2009. Experimental investigation of the response of an a-Si EPID to an unflattened photon beam from an Elekta Precise linear accelerator. *Med Phys.* **36**(4), pp.1318-1329.

University of Leeds. *MARC1 - Advanced research computing.* [Online]. [Accessed 22/11/2018].

Vassiliev, O.N., Kry, S.F., Kuban, D.A., Salehpour, M., Mohan, R. and Titt, U. 2007. Treatment-planning study of prostate cancer intensity-modulated radiotherapy with a Varian Clinac operated without a flattening filter. *International Journal of Radiation Oncology, Biology, Physics.* **68**(5), pp.1567-1571.

Vassiliev, O.N., Kry, S.F., Wang, H.C., Peterson, C.B., Chang, J.Y. and Mohan, R. 2018. Radiotherapy of lung cancers: FFF beams improve dose coverage at tumor periphery compromised by electronic disequilibrium. *Physics in Medicine and Biology.* **63**(19).

Vassiliev, O.N., Titt, U., Kry, S.F., Ponisch, F., Gillin, M.T. and Mohan, R. 2006a. Monte Carlo study of photon fields from a flattening filter-free clinical accelerator. *Med Phys.* **33**(4), pp.820-827.

Vassiliev, O.N., Titt, U., Ponisch, F., Kry, S.F., Mohan, R. and Gillin, M.T. 2006b. Dosimetric properties of photon beams from a flattening filter free clinical accelerator. *Physics in Medicine and Biology.* **51**(7), pp.1907-1917.

Walters, B., Kawrakov, I. and Rogers, D.W.O. 2015. *DOSXYZnrc users manual.* [Online].

Waters, L.S., McKinney, G.W., Durkee, J.W., Fensin, M.L., Hendricks, J.S., James, M.R., Johns, R.C. and Pelowitz, D.B. 2007. The MCNPX Monte Carlo radiation transport code. *Hadronic Shower Simulation Workshop.* **896**, pp.81-+.

Xiao, Y., Kry, S.F., Popple, R., Yorke, E., Papanikolaou, N., Stathakis, S., Xia, P., Huq, S., Bayouth, J., Galvin, J. and Yin, F.F. 2015. Flattening filter-free accelerators: a report from the AAPM therapy emerging technology assessment work group. *Journal of Applied Clinical Medical Physics.* **16**(3), pp.12-29.

Xiong, G. and Rogers, D.W. 2008. Relationship between %dd(10)x and stopping-power ratios for flattening filter free accelerators: a Monte Carlo study. *Med Phys.* **35**(5), pp.2104-2109.

Yan, Y., Yadav, P., Bassetti, M., Du, K.F., Saenz, D., Harari, P. and Paliwal, B.R. 2016. Dosimetric differences in flattened and flattening filter-free beam treatment plans. *Journal of Medical Physics.* **41**(2), pp.92-99.

Zavgorodni, S. 2013. Monte Carlo investigation into feasibility and dosimetry of flat flattening filter free beams. *Physics in Medicine and Biology.* **58**(21), pp.7699-7713.

Zhu, X.R., Kang, Y. and Gillin, M.T. 2006. Measurements of in-air output ratios for a linear accelerator with and without the flattening filter. *Med Phys.* **33**(10), pp.3723-3733.

Zhuang, M.Z., Zhang, T.D., Chen, Z.J., Lin, Z.X., Li, D.R., Peng, X., Qiu, Q.C. and Wu, R.H. 2013. Advanced nasopharyngeal carcinoma radiotherapy with volumetric modulated arcs and the potential role of flattening filter-free beams. *Radiation Oncology.* **8**.

Appendix A

IOP Publishing | Institute of Physics and Engineering in Medicine Physics in Medicine & Biology
Phys. Med. Biol. **61** (2016) 8360–8394 doi:10.1088/0031-9155/61/23/8360

IPEM topical report 1: guidance on implementing flattening filter free (FFF) radiotherapy

Geoff Budgell[1,6], Kirstie Brown[2,6], Jason Cashmore[3,6], Simon Duane[4,6], John Frame[2,6], Mark Hardy[1], David Paynter[5,6] and Russell Thomas[4,6]

[1] Christie Medical Physics and Engineering, The Christie NHS Foundation Trust, Wilmslow Road, Manchester M20 4BX, UK
[2] Department of Clinical Physics and Bioengineering, Beatson West of Scotland Cancer Centre, 1053 Great Western Road, Glasgow G12 0YN, UK
[3] Hall-Edwards Radiotherapy Research Group, University Hospital Birmingham NHS Foundation Trust, Birmingham B15 2TH, UK
[4] National Physical Laboratory, Hampton Road, Teddington, Middlesex TW11 0LW, UK
[5] Medical Physics & Engineering Department, St James's University Hospital, Leeds LS9 7TF, UK
[6] IPEM Radiotherapy Special Interest Group, Flattening Filter Free Working Party

E-mail: geoff.budgell@christie.nhs.uk

Received 1 July 2016, revised 28 July 2016
Accepted for publication 5 August 2016
Published 7 November 2016

Abstract

Flattening filter free (FFF) beams are now commonly available with new standard linear accelerators. These beams have recognised clinical advantages in certain circumstances, most notably the reduced beam-on times for high dose per fraction stereotactic treatments. Therefore FFF techniques are quickly being introduced into clinical use. The purpose of this report is to provide practical implementation advice and references for centres implementing FFF beams clinically. In particular UK-specific guidance is given for reference dosimetry and radiation protection.

Keywords: FFF, guidance, UK

(Some figures may appear in colour only in the online journal)

0031-9155/16/238360+35$33.00

Appendix B

IOP Publishing Phys. Med. Biol. 63 (2018) 015021 (8pp) https://doi.org/10.1088/1361-6560/aa9a1f

Physics in Medicine & Biology

IPEM Institute of Physics and Engineering in Medicine

PAPER

Characterisation of flattening filter free (FFF) beam properties for initial beam set-up and routine QA, independent of flattened beams

RECEIVED
8 August 2017

REVISED
26 October 2017

ACCEPTED FOR PUBLICATION
13 November 2017

PUBLISHED
19 December 2017

D Paynter[1], S J Weston[1], V P Cosgrove[1] and D I Thwaites[2,3]

[1] Medical Physics and Engineering, Leeds Cancer Centre, Leeds Teaching Hospitals NHS Trust, Leeds, LS9 7TF, United Kingdom
[2] Division of Medical Physics, LIGHT Institute, University of Leeds, Leeds, LS2 9JT, United Kingdom
[3] School of Physics, Institute of Medical Physics, University of Sydney, Sydney, NSW 2006, Australia

E-mail: david.paynter@nhs.net

Keywords: quality assurance, flattening filter free, radiotherapy

Abstract

Flattening filter free (FFF) beams have reached widespread use for clinical treatment deliveries. The usual methods for FFF beam characterisation for their quality assurance (QA) require the use of associated conventional flattened beams (cFF). Methods for QA of FFF without the need to use associated cFF beams are presented and evaluated against current methods for both FFF and cFF beams. Inflection point normalisation is evaluated against conventional methods for the determination of field size and penumbra for field sizes from 3 cm × 3 cm to 40 cm × 40cm at depths from dmax to 20 cm in water for matched and unmatched FFF beams and for cFF beams. A method for measuring symmetry in the cross plane direction is suggested and evaluated as FFF beams are insensitive to symmetry changes in this direction. Methods for characterising beam energy are evaluated and the impact of beam energy on profile shape compared to that of cFF beams. In-plane symmetry can be measured, as can cFF beams, using observed changes in profile, whereas cross-plane symmetry can be measured by acquiring profiles at collimator angles 0 and 180. Beam energy and 'unflatness' can be measured as with cFF beams from observed shifts in profile with changing beam energy. Normalising the inflection points of FFF beams to 55% results in an equivalent penumbra and field size measurement within 0.5 mm of conventional methods with the exception of 40 cm × 40 cm fields at a depth of 20 cm. New proposed methods are presented that make it possible to independently carry out set up and QA measurements on beam energy, flatness, symmetry and field size of an FFF beam without the need to reference to an equivalent flattened beam of the same energy. The methods proposed can also be used to carry out this QA for flattened beams, resulting in universal definitions and methods for MV beams. This is presented for beams produced by an Elekta linear accelerator, but is anticipated to also apply to other manufacturers' beams.

Introduction

The use of flattening filter free (FFF) beams has become more prevalent in clinical treatment delivery following the commercial availability of Linear accelerators (Linacs) fitted with both conventional flattened (cFF) and FFF beam energies. For the VersaHD FFF implementation (Elekta AB, Sweden), the beam energy is retuned so that the percentage depth dose (PDD) at 10 cm deep in water, for a 10 cm × 10 cm beam, is matched to that of the associated flattened beam energy (matched flattening filter free beam or MFFF) (Paynter *et al* 2014). This ability to adjust the PDD means that it is possible to both energy match the FFF beam to the cFF beam and also match the beams across a group of linacs. This can improve service continuity and patient management in the event of planned or unplanned equipment down-time in a centre with multiple FFF enabled linacs.

In order to use a single beam energy model for multiple linacs, a process to match beam data across the linacs is required; in addition, regular quality assurance (QA) will be required to ensure that the energies remain matched. Previous authors have used a system of empirically derived values to characterise and QA unflattened

Appendix C

Beam characteristics of energy-matched flattening filter free beams

D. Paynter, S. J. Weston, and V. P. Cosgrove
St James Institute of Oncology The Leeds Teaching Hospitals NHS Trust, Medical Physics, Leeds LS9 7TF, United Kingdom

J. A. Evans
LIGHT Institute University of Leeds Leeds LS2 9JT, Division of Medical Physics, Leeds, United Kingdom

D. I. Thwaites
LIGHT Institute University of Leeds Leeds LS2 9JT, Division of Medical Physics, Leeds, United Kingdom and Institute of Medical Physics, School of Physics, University of Sydney, Australia

(Received 30 September 2013; revised 18 March 2014; accepted for publication 23 March 2014; published 25 April 2014)

Purpose: Flattening filter free (FFF) linear accelerators can increase treatment efficiency and plan quality. There are multiple methods of defining a FFF beam. The Elekta control system supports tuning of the delivered FFF beam energy to enable matching of the percentage depth-dose (PDD) of the flattened beam at 10 cm depth. This is compared to FFF beams where the linac control parameters are identical to those for the flattened beam. All beams were delivered on an Elekta Synergy accelerator with an Agility multi-leaf collimator installed and compared to the standard, flattened beam. The aim of this study is to compare "matched" FFF beams to both "unmatched" FFF beams and flattened beams to determine the benefits of matching beams.
Methods: For the three modes of operation 6 MV flattened, 6 MV matched FFF, 6 MV unmatched FFF, 10 MV flattened, 10 MV matched FFF, and 10 MV unmatched FFF beam profiles were obtained using a plotting tank and were measured in steps of 0.1 mm in the penumbral region. Beam penumbra was defined as the distance between the 80% and 20% of the normalized dose when the inflection points of the unflattened and flattened profiles were normalized with the central axis dose of the flattened field set as 100%. PDD data was obtained at field sizes ranging from 3 cm × 3 cm to 40 cm × 40 cm. Radiation protection measurements were additionally performed to determine the head leakage and environmental monitoring through the maze and primary barriers.
Results: No significant change is made to the beam penumbra for FFF beams with and without PDD matching, the maximum change in penumbra for a 10 cm × 10 cm field was within the experimental error of the study. The changes in the profile shape with increasing field size are most significant for the matched FFF beam, and both FFF beams showed less profile shape variation with increasing depth when compared to flattened beams, due to consistency in beam energy spectra across the radiation field. The PDDs of the FFF beams showed less variation with field size, the d_{max} value was deeper for the matched FFF beam than the FFF beam and deeper than the flattened beam for field sizes greater than 5 cm × 5 cm. The head leakage when using the machine in FFF mode is less than half that for a flattened beam, but comparable for both FFF modes. The radiation protection dose-rate measurements show an increase of instantaneous dose-rates when operating the machines in FFF mode but that increase is less than the ratio of MU/min produced by the machine.
Conclusions: The matching of a FFF beam to a flattened beam at a depth of 10 cm in water by increasing the FFF beam energy does not reduce any of the reported benefits of FFF beams. Conversely, there are a number of potential benefits resulting from matching the FFF beam; the depth of maximum dose is deeper, the out of field dose is potentially reduced, and the beam quality and penetration more closely resembles the flattened beams currently used in clinical practice, making dose distributions in water more alike. Highlighted in this work is the fact that some conventional specifications and methods for measurement of beam parameters such as penumbra are not relevant and further work is required to address this situation with respect to "matched" FFF beams and to determine methods of measurement that are not reliant on an associated flattened beam. [http://dx.doi.org/10.1118/1.4871615]

Key words: radiotherapy, flattening filter free, beam characteristics

1. INTRODUCTION

With the increase in intensity modulated radiotherapy (IMRT) treatments in radiotherapy there has been both an improvement in treatment plan quality but often with an increase in the treatment delivery time.[1] This is due to the segmented treatment deliveries requiring more monitor units relative to conventional conformal planning techniques. The use of IMRT